THE UNIVERSITY OF ALABAMA IN HUNTSVILLE

FINAL REPORT ON NASA CONTRACT

NAS8-38609 Delivery Order No. 34

UAH MATHEMATICAL MODEL OF THE VARIABLE POLARITY PLASMA ARC WELDING SYSTEM CALCULATION

Prepared by

R. J. Hung, Ph.D., P.E.

Professor of Mechanical and Aerospace Engineering

The University of Alabama in Huntsville

Huntsville, Alabama 35899, USA

January, 1994

(NASA-CR-193926) UAH MATHEMATICAL MODEL OF THE VARIABLE POLARITY PLASMA ARC WELDING SYSTEM CALCULATION Final Report (Alabama Univ.) 197 p

N94-27221

Unclas

G3/37 0209835

ABSTRACT

Significant advantages of Variable Polarity Plasma Arc (VPPA) welding process include faster welding, fewer repairs, less joint preparation, reduced weldment distortion, and absence of porosity. In this report, a mathematical model is presented to analyze the VPPA welding process. Results of the mathematical model have been compared with the experimental observation accomplished by the GDI team.

I. INTRODUCTION

The plasma arc is a concentrated energy source commonly used in welding and cutting processes. It is composed of a partially ionized gas stream produced by forcing an inert gas to flow through an electric arc and emerge from a constricting nozzle. With its high energy density and velocity, the plasma arc, when impinging on the workpiece, can create a hole in the molten pool generated by its heat and can penetrate through the workpiece. Depending on the operating parameters employed, this hole may either become self-healing or remain open as the arc transverses along the workpiece. A "keyhole" welding process occurs in the self-healing case, in which the molten metal in front of the arc flows around the arc column and resolidifies behind the arc. On the other hand, a cutting operation is achieved if the hole remains open (O'Brien, 1968).

The plasma welding process is essentially an extension of gas tungsten-arc welding (GTAW); however, constraining the arc to flow through a nozzle produces much higher energy density in the arc and much higher gas velocity and momentum. The process produces deep penetration welds by forming a keyhole in the workpiece by the pressure of the gas flow. The metal melted in front of the advancing keyhole flows around to the rear where it solidifies to form the weld bead. This is distinct from the essentially surface melting produced by the GTAW process (which cannot normally penetrate to a depth equal to the width of a weld pool).

In 1955 Linde Air Products introduced a plasma arc torch for metal cutting applications, and by 1965 Linde had developed an automatic plasma arc welding facility for Westinghouse Electric Corporation to fabricate a 120 in. diameter, 3/8 in. thick D6AC steel rocket motor case for the Titan III-C booster assembly (Miller and Filipski, 1966; Privoznik and Miller, 1966). The plasma arc welding process was reported to halve the welding time required. Then in 1965 Thermal Dynamics Corporation reported the use of direct current reversed polarity (workpiece negative) plasma arc to join 1/4 in. thick aluminum plate (Cooper et al., 1965). At the end of the 1960's, Van Cleave at the Boeing Company began his efforts to combine the plasma arc process with a variable polarity feature in which the electrode polarity was periodically reversed. Alternating electrode potential for aluminum welding had been investigated as early as 1947 (Herbst, 1947). Difficulties with welding power supplies in this application were evident early-on. In addition, when variable polarity plasma arc (VPPA) welding was used in the U.S. Army Roland Missile Production Program, development problems such as arc pressure pulsation were noted (Nunes et al., 1981; 1983). As a result of Van Cleave's promising work at Boeing, a VPPA research and development project was initiated in 1978 at the NASA Marshall Space Flight Center, to determine the potential for replacing the GTAW system used in the fabrication of the Space Shuttle External Tank (ET). After the original used in the fabrication and process were

improved, VPPA welding finally exceeded the expectations (Nunes et al., 1984a; 1984b).

The Space Shuttle ET (diameter 28.6 ft., length 154 ft.) is the largest known "drop tank," carrying 140,000 gallons of liquid oxygen and 380,000 gallons of liquid hydrogen. From the outset of ET production, the conventional GTAW system operating in the direct current electrode negative mode was used. With the GTAW system, in spite of the requisite careful joint preparation, weld porosity and defects had been ever-present problems since the fabrication of the Saturn lunar rocket first stage. Therefore, the decision was made at the outset to use 100% radiographic inspection. Weld porosity and defects had to be ground out and repaired systematically.

The VPPA process significantly reduced porosity and defects with less stringent joint preparation and, in addition, reduced weldment distortion, and speeded up the welding process.

In this study, the power distribution for an argon plasma gas has been analyzed along its course through the VPPA welding system. The study includes the following sections:

(1) Electric potential distribution of straight and reverse polarities, and potential intensities for the VPPA welding system;

(2) VPPA welding system electric power input at the electrode, within orifice, in the free plasma jet column and in the keyhole of workpiece;

(3) Power loss at electrode, within the gap between electrode and within orifice, standoff column and the workpiece;

(4) Determination of plasma arc enthalpy;

(5) Determination of crown and root bead widths;

(6) Determination of crown and root heights;

(7) Determination of leading edge angle of keyhole.

(8) Comparison between molding and experimental measurements

II. VARIABLE POLARITY PLASMA ARC WELDING SYSTEM ELECTRIC POTENTIAL CALCULATION

The significant current carriers in a welding arc are electrons and positive ions. Electrons carry the bulk of the current, moving rapidly from negative cathode to positive anode. The positive ions drift more slowly through the interelectrode space. In a fixed polarity arrangement, the differential drift rate results in an asymmetrical heating of the welding arc's ends. The cathode receives less heat and the anode more heat. The straight polarity mode of operation entails a negative electrode (cathode) and a positive workpiece (anode). Where the primary object of the weld process is to deliver the maximum heat to the workpiece with minimum deterioration of the electrode, straight polarity is used.

Reverse polarity, which entails positive electrode and negative workpiece, has the advantage that the workpiece is subjected to a cleaning process (cathodic cleaning) by the impingement of positive ions on the workpiece surface. Recent work suggests that heavy positive ion weight is irrelevant to the cleaning process which seems to be more like capacitor breakdown than hammer impact. In the case of plasma arc welding, reverse polarity action appears to condition the surface of the aluminum alloy so that the molten metal flows easily and controllably under the arc. It is conjectured that this fluid control is accomplished through breaking up of surface oxide films. Cutoff of reverse

polarity during VPPA welding transforms a weld metal flow which closes smoothly and soundly behind the keyhold to an irregular, intermittent, globular flow. This process leaves a rough, lumpy bead sunken below the parent metal surface and protruding jaggedly from the root of the weld. However, continuous reverse polarity is not necessary to provide adequate cathodic cleaning action.

The variable polarity square-wave with unequal straight and reverse polarity time intervals offered a combination of the high heating capability of straight polarity with the cleaning feature of reverse polarity. Adequate cleaning is obtained by incorporating a relatively short (1/10 to 1/5 the duration of the straight polarity current) pulse of reverse polarity current into the welding current waveform.

Figure 1 show the VPPA electric power system. During the straight polarity mode of operation, it employs a negative electrode (cathode) and a positive workpiece (anode); during the reverse polarity mode of operation it employs a positive electrode and a negative workpiece. Figure 1 at left illustrates the straight polarity mode; at right, reverse polarity mode.

Calculation of electric potential can be obtained from the following formulations:

(A) For Straight Polarity

$$V_E = V_F - \Delta V_a - \phi_w$$

$$V_G = V_E - \sum_i \left(\frac{dV}{dL}\right)_{3,i} \Delta L_{3,i}$$

$$V_C = V_G - \sum_i \left(\frac{dV}{dL}\right)_{2,i} \Delta L_{2,i}$$

$$V_D = V_C + \Delta V_a + \phi_N$$

$$V_B = V_C - \sum_i \left(\frac{dV}{dL}\right)_{1,i} \Delta L_{1,i}$$

$$V_A = V_B - \Delta V_c + \phi_E$$

$$\Delta V_m^+ = \Delta V_{FA} = V_F - V_A = -V_A$$

$$\Delta V_p^+ = \Delta V_{DA} = V_D - V_A$$

where ϕ_E = Electrode Work Function

ϕ_N = Orifice Work Function

ϕ_w = Workpiece Work Function

ΔV_a = Anode Drop

ΔV_C = Cathode Drop

$\left(\frac{dV}{dL}\right)_{1,i}, \left(\frac{dV}{dL}\right)_{2,i}, \left(\frac{dV}{dL}\right)_{3,i}$ = Electric Potential Intensities in segment i of L_1, L_2 and L_3, respectively

$\Delta L_{1,i}$, $\Delta L_{2,i}$, $\Delta L_{3,i}$ = Length of segment i in L_1, L_2, and L_3, respectively

(B) For Reverse Polarity

$$V_E' = V_F' + \Delta V_C - \phi_w + \epsilon_R$$

$$V_G' = V_E' + \sum_i \left(\frac{dV}{dL}\right)_{3,i} \Delta L_{3,i}$$

$$V_C' = V_G' + \sum_i \left(\frac{dV}{dL}\right)_{2,i} \Delta L_{2,i}$$

$$V_D' = V_C' - \sum_i \left(\frac{dV}{dL}\right)_{2,i} \Delta L_{2,i} + \Delta V_a + \phi_N$$

$$V_B' = V_C' + \sum_i \left(\frac{dV}{dL}\right)_{1,i} \Delta L_{1,i}$$

$$V_A' = V_B' + \Delta V_a + \phi_E$$

$$\epsilon_R = \text{Reverse Polarity Rise} = A + B \frac{t_-}{t_+ + t_-}$$

where A, B = constant varying with workpiece materials

t_+ = Straight Polarity Time Period

t_- = Reverse Polarity Time Period

$\Delta V_m^- = \Delta V_{A',F'} = V_{A'} - V_{F'} = V_{A'}$

$\Delta V_p^- = \Delta V_{A',D'} = V_{D'} - V_{A'}$

(C) For Potential Intensities

Electric potential intensities of the plasma fluid in the plasma column can be calculated from the electric conductivity, σ_E, of plasma fluid at the location of interest. The value of electric conductivity at the location of interest is determined by the local plasma jet pressure and temperature. By using the data provided by Devoto (1973), Lancaster (1986) has calculated the electrical conductivity of argon plasma gas as it varies with temperature at one atmosphere pressure. Figure 2 shows the variation of argon gas electrical conductivity with temperature at one atmospheric pressure. In this model

calculation, we have divided the lengths of plasma column along the axial direction into several segments with ΔL_i as the length of segment i. Joule heating, and radiative and convective heat transfer losses at the segment i are calculated with the assumed value of electric potential intensity of that segment, $(\Delta V/\Delta L)_i'$, and the given inlet values of power and enthalpy of plasma fluid at that segment. Outlet values of power and enthalpy of plasma fluid at that segment are then calculated based on these parameters. The value of electric conductivity $\sigma_{E,i}$ at segment i is thus determined from the average fluid temperature at that segment. The value of average temperature is obtained from the corresponding average value of plasma fluid enthalpy at that segment which is calculated from the average value of inlet and outlet plasma fluid enthalpys at that segment. Electrical resistance, R_i; electric potential difference, ΔV_i; and electric field intensity, $(\Delta V/\Delta L)_i$, at segment i can be determined from the computed value of electric conductivity $\sigma_{E,i}$ at that segment. Convergent solution is obtained through the trial and error compuations between the computed value of $(\Delta V/\Delta L)_i$ and the assumed value of $(\Delta V/\Delta L)_i'$ at segment i. From these calculations, it is clearly shown that the values of electric potential of the plasma fluid and heat transfer computations are mutually coupled together. Furthermore, the values of plasma

electrical conductivity fluctuate with local variations of temperature. The physical parameters affecting the plasma temperature, such as plasma and shielding gas flow rates, radiative and convective heat transfer losses, values of main and pilot electric currents, standoff distance, etc., all influence the values of electric potential and electric field intensity in the plasma fluid.

The effect of shielding gas flow rate occurs through shielding gas mixing into the plasma standoff column L_3 and vice versa. The continuous mixing between plasma gas and shielding gas induced by the plasma jet stream in plasma column results in local variations of species constituent concentration and temperature along the axial direction. Thus, the effect of jet mixing in column streams between plasma and shielding gases must be taken into consideration in addition to heat transfer losses in computing electric potential along the plasma jet. Figure 3 shows the variation of electrical resistance with temperature for various argon-helium mixtures.

III. VPPA WELDING SYSTEM ELECTRIC POWER INPUT

VPPA Electric Power Input can be calculated as follows:

$$P_{total} = \frac{I_m^+ \Delta V_m^+ t_+ + I_p^+ \Delta V_p^+ t_+ + I_m^- \Delta V_m^- t_- + I_p^- \Delta V_p^- t_-}{t_+ + t_-} \quad (3\text{-}1)$$

where I_m^+ = Straight Polarity Main Current

I_p^+ = Straight Polarity Pilot Current

I_m^- = Reverse Polarity Main Current

I_p^- = Reverse Polarity Pilot Current

Equation (3-1) is the total electric power input of the system which is the summation of power input for the plasma arc jet in the gap between electrode and orifice, power input within orifice, power input in free jet column (standoff), and power input within keyhole of workpiece. The power input can be itemized, and calculated as follows:

(III-A) Power Input at the Electrode

$$P_E = \frac{(I_m^+ + I_p^+)(\Delta V_C - \phi_E) t_+ + (I_m^- - I_p^-)(\Delta V_A + \phi_E) t_-}{t_+ + t_-} \quad (3\text{-}2)$$

(III-B) Power Input in the Gap Between Electrode and Orifice (Joule Heating)

$$P_{J,1} = \frac{(I_m^+ + I_p^+)\left[\sum_i \left(\frac{dV}{dL}\right)_{1,i} \Delta L_{1,i}\right] t_+ + (I_m^- - I_p^-)\left[\sum_i \left(\frac{dV}{dL}\right)_{1,i} \Delta L_{1,i}\right] t_-}{t_+ + t_-} \quad (3\text{-}3)$$

(III-C) Power Input Within Orifice

This includes power input through the work function of metal

$$P_{N,1} = \frac{I_p^{+}\phi_N t_+ + I_p^{-}\phi_N t_-}{t_+ + t_-} \qquad (3\text{-}4)$$

Power input through anode drop,

$$P_{N,2} = \frac{I_p^{+}\Delta V_a t_+ + I_p^{-}\Delta V_a t_-}{t_+ + t_-} \qquad (3\text{-}5)$$

and power input through Joule heating within the orifice

$$P_{J,2} = \frac{I_m^{+}\left[\sum_i \left(\frac{dV}{dL}\right)_{2,i} \Delta L_{2,i}\right] t_+ + (I_m^{-} - I_p^{-})\left[\sum_i \left(\frac{dV}{dL}\right)_{2,i} \Delta L_{2,i}\right] t_-}{t_+ + t_-} \qquad (3\text{-}6)$$

(III-D) Power Input in the Free Plasma Jet Column (Standoff) (Joule Heating)

$$P_{J,3} = \frac{I_m^{+}\left[\sum_i \left(\frac{dV}{dL}\right)_{3,i} \Delta L_{3,i}\right] t_+ + I_m^{-}\left[\sum_i \left(\frac{dV}{dL}\right)_{3,i} \Delta L_{3,i}\right] t_-}{t_+ + t_-} \qquad (3\text{-}7)$$

It is important to note that shielding gas surrounding the plasma jet, is induced into the plasma jet column due to the flow generated by the plasma jet stream. Power of shielding gas introduced into the plasma jet, P_{sd}, shown in Equation (4-29), shall be included as a part of the plasma jet power input, in addition to the power input shown in Equation (3-7).

(III-E) Power Input in the Keyhole of Workpiece

This includes power input through the work function of metal and reverse polarity potential rise

$$P_{W,1} = \frac{I_m^{+}\phi_W t_+ + I_m^{-}(\epsilon_R - \phi_W) t_-}{t_+ + t_-} \qquad (3\text{-}8a)$$

and power input through anode and cathode drops

$$P_{w,2} = \frac{I_m^{+}\Delta V_a t_+ + I_m^{-}\Delta V_c t_-}{t_+ + t_-} \qquad (3\text{-}8b)$$

(III-F) Total Power Input to the VPPA Welding System

Total power input of VPPA welding system, shown in Equation (3-1) shall be equal to the summation of power input shown in Equation (3-2) to (3-8) and plasma jet induced shielding gas power input, P_{sd}, namely

$$P_{total} = P_E+P_{J,1}+P_{N,1}+P_{N,2}+P_{J,2}+P_{J,3}+P_{w,1}+P_{w,2}+P_{sd} \qquad (3\text{-}9)$$

IV. POWER LOSS CALCULATION OF VPPA WELDING SYSTEM

(IV-A) Electrode Heat Conduction Loss

A one-dimensional formulation of the electrode heat conduction loss is given by

$$Q_E = k_E \cdot A_E \frac{(T_E - T_0)}{L_E} \qquad (4\text{-}1)$$

where

Q_E = Electrode Heat Conduction Loss

k_E = Thermal Conductivity Coefficient of Electrode

A_E = Cross-sectional Area of Electrode

L_E = Length of Electrode (from tip to water-cooled collet)

$T_E - T_0$ = Temperature Difference of Electrode Between Tip and Collet Position

(IV-B) Radiation Heat Loss Between Electrode and Orifice

Plasma arc heat radiation loss within the gap between electrode and orifice can be computed from the following equation (Evans and Tankin, 1967; Cram, 1985):

$$Q_G(W) = V_G(m^3)(4 \times 10^{10})\left[\frac{T(^0K)}{15000}\right]^{16} \Big/ \left\{1 + \left[\frac{T(^0K)}{15000}\right]^{16}\right\} \qquad (4\text{-}2)$$

where

Q_G = Heat Radiation Loss Within the Gap Between Electrode and Orifice (W)

V_G = Plasma Arc Jet Volume Within Gap Between Electrode and Orifice (m^3)

T = Absolute Temperature (^0K)

(IV-C) Power Loss Within the Orifice

Power Loss within the orifice is comprised of the following items:

(IV-C-1) Heat Convection Loss Within the Orifice

Heat convection loss within the orifice can be computed from the following formulation of convective heat transfer model (Hsu and Rubinsky, 1987):

$$Nu = 0.2233(X^{+})^{-0.7455} + 3.66 \qquad (4-3)$$

where

$$X^{+} = \frac{X}{R_0} \cdot \frac{1}{(Re \cdot Pr)_m}$$

Here

X = Axial Distance, (Distance from the entrance of orifice to the half distance of the segment of interest)

R_0 = Radius of Orifice

Re = Reynolds Number of Plasma Arc Fluids

Pr = Prandtl Number of Plasma Arc Fluids

Nu = Nusselt Number of Plasma Arc Fluids

Subscript m = mean values

Heat convection loss within the orifice, thus, can be computed from the Nusselt number obtained from Equation (4-3), namely,

$$Q_{N,c} = Nu \cdot A_N \cdot \frac{k}{D} \cdot \frac{(h_{plasma} - h_N)}{c_p} \qquad (4-4)$$

where

$Q_{N,c}$ = Heat Convection Loss within the Orifice

A_N = Heat Transfer Area of Segment of Interests

D = Diameter of Orifice = 2 R_o

k = Thermal Conductivity of Plasma Arc

c_p = Constant Pressure Specific Heat of Plasma Arc

h_{plasma} = Average Enthalpy of Plasma Arc through the Orifice

h_N = Average Enthalpy of plasma in Orifice corresponding to the Orifice Wall Temperature

All thermal properties used in this model are determined at the temperature corresponding to the average enthalpy of plasma arc.

(IV-C-2) Direct Power Loss to Surface of Orifice

Direct power loss to the orifice surface includes $P_{N,1}$, orifice work function induced power input; and part of $P_{N,2}$, orifice anode drop induced power input, namely

$$Q_{N,G} = P_{N,1} + \phi P_{N,2} \qquad (4-5)$$

where,

$Q_{N,G}$ = Direct power loss from the orifice surface

ϕ = Fraction power generated by anode drop lost to orifice

$(1-\phi)P_{N,2}$ = Plasma arc power input from power generated at orifice anode drop

(IV-C-3) Electron Collision Power Loss Within Orifice

Power loss due to free electrons entering the surface of orifice can be calculated from the following equation:

$$Q_{N,e} = \frac{I}{e}\left(\frac{3}{2}KT\right) \qquad (4-6)$$

where

$Q_{N,e}$ = Free electron power loss to the orifice

e = Electron charge = 1.602×10^{-19} coulomb/mole

K = Boltzman constant = 1.38×10^{-16} $^{erg}/_{mol \cdot K}$

T = Plasma arc temperature;

and I is the electric current which can be computed as follows:

$$I = \frac{I_p^{+} t_{+} + I_p^{-} t_{-}}{t_{+} + t_{-}} \qquad (4\text{-}7)$$

Total power loss in orifice, Q_N, is the summation of Equations (4-4), (4-5), and (4-6), namely,

$$Q_N = Q_{N,c} + Q_{N,G} + Q_{N,e} \qquad (4\text{-}8)$$

(IV-D) Power Loss from Standoff Column

Power loss from the standoff column includes radiative heat loss, $Q_{s,r}$, and convective heat loss, $Q_{s,c}$.

Calculation of radiative heat loss is similar to Equation (4-2) for that in the gap between electrode and orifice, namely

$$Q_{s,r}(W) = V_s(m^3)(4 \times 10^{10}) \left[\frac{T(^\circ K)}{15000}\right]^{16} \Big/ \left\{1 + \left[\frac{T(^\circ K)}{15000}\right]^{16}\right\} \qquad (4\text{-}9)$$

where V_s denotes plasma arc volume within the standoff column; and T is the absolute temperature corresponding to the average value of plasma arc enthalpy.

Radiative heat loss is strongly dependent on fluid temperature. This and what follows require trial and error computations.

To compute the convective heat loss, $Q_{s,c}$, from the standoff column, jet stream mixing theory is employed. Turbulent mixing between plasma jet and the surrounding shielding gas is shown schematically in Figure 4a. r_1 stands for the inner boundary of jet boundary layer, and r_2 expresses the outer boundary of jet boundary

layer. Both are functions of axial distance x from the outlet end of the orifice. The inner jet core region, surrounded by $r_1(x)$ is a non-perturbed zone of jet core. The jet boundary layer lies between $r_2(x)$ and $r_1(x)$. Jet stream parameters in the jet boundary layer, including velocity, temperature and species concentration, vary from original (pure plasma gas jet) parameters at $r = r_1$ to ambient (pure shielding gas) parameters at $r = r_2$. The jet core extends to $x = x_H$. As $x > x_H$, the jet core disappears and the jet boundary layer occupies the entire extent from $r = 0$ to $r = r_2$. The initial region from $x = 0$ to $x = x_H$ is the region of jet mixing. Boundary thickness at transition $x = x_H$ is $r_{2,H}$.

Based on the formulations of Abramovich (1963), the boundary layer within the initial region of jet mixing is governed by the following equations:

$$\frac{R_0 - r_1}{cx} = \frac{1 - m}{1 + m}\left[0.416 + 0.134m + 0.021\,\frac{cx}{R_0}\left(\frac{1 - m}{1 + m}\right)\cdot(1 + 0.8m - 0.45m^2)\right] \tag{4-10}$$

$$\frac{R_0 - r_1}{r_2 - r_1} = 0.416 + 0.134m + 0.021\,\frac{(r_2 - r_1)}{R_0}(1 + 0.8m - 0.45m^2) \tag{4-11}$$

where R_0 denotes the radius of orifice; r_1, the radius of inner boundary of jet boundary layer; r_2, the radius of outer boundary of jet boundary layer; and x, the axial distance from the outlet end of orifice to the point of interest. $m = u_H/u_0$, where u_H is ambient fluid velocity; ;and u_0, the original jet flow velocity inside jet core. c is empirical constant which is 0.27 when $u_0 >> u_H$.

Substituting the values of m = 0 and c = 0.27 in Equations (4-10) and (4-11), we have

$$\frac{R_0 - r_1}{x} = 0.27 \left(0.416 + 0.00567 \frac{x}{R_0}\right) \tag{4-12}$$

$$\frac{R_0 - r_1}{r_2 - r_1} = 0.416 + 0.021 \left(\frac{r_2 - r_1}{R_0}\right) \tag{4-13}$$

From equation (4-12) , we can solve for the jet inner boundary r_1 in term of the axial distance x which is given by

$$\frac{r_1}{R_0} = 1 - 0.1123 \frac{x}{R_0} - 0.0015 \left(\frac{x}{R_0}\right)^2 \tag{4-14}$$

Similarly, from Equation (4-13), we can determine the boundary layer thickness, $r_2 - r_1$, i.e.,

$$r_2 - r_1 = \frac{1}{2} \{-19.81R_0 + [392.44R_0^2 + 190.48 (R_0 - r_1) R_0]^{1/2}\} \tag{4-15}$$

To determine the axial distance of jet initial region x_H, we can solve Equation (4-14) by substituting $r_1 = 0$, i.e.,

$$\frac{x_H}{R_0} = 8 \tag{4-16}$$

In our case, the radius of orifice $R_0 = 1.5875$ mm, and the axial distance of the jet initial region $x_H = 8(1.5875) = 12.7$ mm. In the present study, the range of standoff distance considered is between 1 to 10 mm, so that all standoff values considered in the present study lie within the range of the initial region of jet mixing. Let us consider velocity, temperature and species concentration profiles within the range of jet initial region as follows:

$$\frac{u_0 - u}{u_0 - u_H} = (1 - \eta^{1.5})^2 \tag{4-17}$$

$$\frac{T_0 - T}{T_0 - T_H} = 1 - \eta \tag{4-18}$$

$$\frac{\rho_{pl}}{\rho_{pl} + \rho_{sd}} = \eta \tag{4-19}$$

where u_0 and T_0 denote original velocity and temperature of jet core, respectively; and u_H and T_H, the ambient velocity and temperature at the outer layer of jet boundary layer, respectively. Dimensionless coordinate parameter $\eta = (r_2 - r)/(r_2 - r_1)$. ρ_{sd} and ρ_{pl} denote masses of shielding gas and plasma gas per unit of volume within the jet boundary layer, respectively.

In the present model, the effect of the mole fraction of shielding gas induced by jet mixing into the plasma column has been fully taken into consideration.

It is convenient to employ partial pressure P_{pl} and P_{sd}, rather than density in the calculation. By using equation of state, Equation (4-19) can be rewritten as

$$\frac{P_{sd}}{P_{pl}} = \frac{M_{pl}}{M_{sd}} \left(\frac{1}{\eta} - 1\right) \tag{4-20}$$

Since

$$P_{pl} + P_{sd} = P_H \tag{4-21}$$

We can solve partial pressure P_{pl} and P_{sd} from Equations (4-20) and (4-21) as follows:

$$P_{pl} = \frac{P_H}{\left[1 + \frac{M_{pl}}{M_{sd}}\left(\frac{1}{\eta} - 1\right)\right]} \tag{4-22}$$

and

$$P_{sd} = P_H - P_{pl} \tag{4-23}$$

where P_{pl} and P_{sd} denote partial pressures of plasma and shielding gases, respectively; and M_{pl} and M_{sd} stand for molecular weights of plasma and shielding gases, respectively. For example, M_{pl} = 39.95 kg/k-mol for argon gas, and M_{sd} = 4.003 kg/k-mol for helium gas. Also, P_H is ambient pressure of gases.

Plasma and shielding gas density, ρ_{pl} and ρ_{sd}, can be determined from Equation (4-18) for temperature profile and Equations (4-22) and (4-23) for partial pressure of plasma and shielding gases, i.e.,

$$\rho_{pl} = \frac{P_{pl}M_{pl}}{R\ T} \tag{4-24}$$

$$\rho_{sd} = \frac{P_{sd}M_{sd}}{R\ T} \tag{4-25}$$

where R denotes the universal gas constant which is 8315 J/kmol·K. Furthermore, plasma and shielding gas enthalpies can be obtained from the table at their corresponding values of temperature. Finally, jet stream power P_{Jet} can be calculated from the following integration.

$$P_{Jet} = \int_0^{r_2} 2\pi ru\ (\rho_{pl}h_{pl} + \rho_{sd}h_{sd})dr \tag{4-26}$$

It is noted that $\rho_{pl} = (\rho_{pl})_0$, $(\rho_{sd})_0 = 0$, $h_{pl} = (h_{pl})_0$, and $u = u_0$ within the region of jet core. Thus, Equation (4-26) can

be rewritten as follows:

$$P_{Jet} = \pi r_1^2 u_0 \ (\rho_{pl})_0 (h_{pl})_0 + \\ + \int_{r_1}^{r_2} 2\pi r u \ (\rho_{pl} h_{pl} + \rho_{sd} h_{sd}) dr \qquad (4\text{-}27)$$

At the outlet end of standoff column, the total power of plasma jet can be expressed as

$$P'_{3,0} = P_{3,1} + P_{J,3} - Q_{s,r} + P_{sd} \qquad (4\text{-}28)$$

where $P_{3,1}$ denotes the plasma jet power at the inlet end of standoff column (or at the outlet end of orifice); $P_{J,3}$, the plasma jet power due to Joule heating within the standoff column; $Q_{s,r}$, the radiative heat power loss from the standoff column; and P_{sd}, the induced power from surrounding shielding gas into plasma jet boundary layer, namely,

$$P_{sd} = \dot{m}_{sd} \, h_{sd,H} \qquad (4\text{-}29)$$

Here, $h_{sd,H}$ denotes shielding gas enthalpy corresponding to the ambient temperature of shielding gas; $\dot{m}_{sd}$, mass flow rate of shielding gas

$$\dot{m}_{sd} = \int_{r_1}^{r_2} 2\pi r u \ \rho_{sd} \ dr \qquad (4\text{-}30)$$

In this calculation, total power of plasma jet $P'_{3,0}$ shown in Equation (4-28), contains the power within the whole cross section of jet boundary layer where temperature varies radially from more than 10^4 K at the inner layer of jet boundary layer to ambient temperature (say 298 ^{0}K) at the outer layer of jet boundary layer. The welding process requires sufficiently high temperature difference to maintain heat conduction and to promote sufficient heat flow to melt

the workpiece metal. More important than promoting heat flow by convection is the maintenance of a conducting plasma path for current. Spot welding electrodes do not have to be hot at all to provide a molten weld nugget by resistance heating. Resistance heating due to plasma sheath voltage drop and work function drop are more important (Eckert and Pfender, 1967).

Let R_c be a half size of the crown width. This is also equivalent to the radius of the inlet end of keyhole (See Figure 4b). As $R_c \leq r_2$,

$$P_{3,0} = \int_0^{R_c} 2\pi r u \, (\rho_{\rho 1} h_{\rho 1} + \rho_{sd} h_{sd}) dr \qquad (4\text{-}31)$$

and as $R_c > r_2$,

$$P_{3,0} = \int_0^{r_2} 2\pi r u \, (\rho_{\rho 1} h_{\rho 1} + \rho_{sd} h_{sd}) dr + \pi (R_c^2 - r_2^2) \, u_H \, \rho_{sd} \qquad (4\text{-}32)$$

The difference between $P'_{3,0}$, calculated from Equation (4-28), and $P_{3,0}$, calculated from Equations (4-31) or (4-32), is the convective heat loss or power increment due to injecting shielding gas $Q_{s,c}$, within the standoff column, i.e.,

$$Q_{s,c} = P'_{3,0} - P_{3,0} \qquad (4\text{-}33)$$

In short, workpiece heating is mainly contributed by the plasma jet, comprising a mixture of plasma and shielding gases, with the power of $P_{3,0}$. Throughout the keyhole all plasma gas properties used in heat transfer calculations are based upon the mixture of plasma and shielding gas established at the inlet of the keyhole.

A detalied descritption of how to determine radius R_c will be disscussed in Section VI of this report.

(IV-E) Total Workpiece Power Loss

Total power loss in the workpiece is comprised of the following items:

(IV-E-1) Convective Heat Loss in Workpiece

Local power loss to the workpiece from heat conduction can be computed from Equation (4-34), namely,

$$Q_{W,c_z} = Nu_z \cdot A_w \cdot \frac{k}{D} \frac{(h_{plasma} - h_w)}{c_p} \qquad (4\text{-}34)$$

where Nu_z is the Nusselt number along the axial direction; A_w stands for heat transfer area per unit length along the axial direction of the workpiece ($A_w = \pi R,$) i.e. the plasma contact area in the keyhole taken to resemble a finger ring comprimising somewhat more than one half of the circumferencial area of the keyhole; R is the radius of plasma contact area in the keyhole which varies with respect to axial distance z and is determined by the calculation; and D is the diameter of the keyhole equal to twice the effective radius of plasma contact area (2 R). The rest of symbols are the same as used in the orifice.

The Nusselt number is computed as in Equation (4-3), used in orifice, which is

$$Nu_z = 0.2233(z^+)^{-0.7455} + 3.66 \qquad (4\text{-}35)$$

where

$$z^+ = \frac{z}{R} \frac{1}{(Re \cdot Pr)_m}$$

Here R denotes effective radius of plasma contact area in the keyhole at the axial location of z. z is the distance between the entrance of keyhole to the half thickness of the section of interest in the workpiece considered. The rest of the symbols stand for the same

definition used in the orifice.

Total convective heat loss in the workpiece is

$$Q_{w,c} = \int_0^{L_4} Q_{w,c_z}\, dz = \int_0^{L_4} Nu_z\, A_w \cdot \frac{k}{D} \frac{(h_{plasma} - h_w)}{c_p}\, dz \qquad (4\text{-}36)$$

(IV-E-2) Direct Power Loss from the Surface of Keyhole

Direct power loss to the keyhole surface includes $P_{w,1}$, the power generated by the workpiece work function; and part of $P_{w,2}$, the power generated at the workpiece anode and cathode drops, namely,

$$Q_{w,G} = P_{w,1} + \psi P_{w,2} \qquad (4\text{-}37)$$

where

$Q_{w,G}$ = Direct power loss to the keyhole surface

ψ = Fraction of power generated by anode and cathode drops that is transmitted to the keyhole surface

$(1-\psi)P_{w,2}$ = Power transmitted to the plasma from that generated at anode and cathode drops

(IV-E-3) Electron Collision Power Loss in Keyhole

Power carried by free electrons into the surface of the keyhole can be calculated from the following equation:

$$Q_{w,e} = \frac{I}{e}\left(\frac{3}{2} KT\right) \qquad (4\text{-}38)$$

where $Q_{w,e}$ denotes power carried by free electrons in to the keyhole wall; T, the mean electron temperature entering the wall taken as the average temperature between plasma arc and wall of keyhole; and I, the straight polarity component of the transmitted current, which can be computed from the following equation:

$$I = \frac{I_m^{+} t_+}{t_+ + t_-} \qquad (4\text{-}39)$$

Thus, total power loss to the workpiece, Q_w, is the summation of losses computed by Equations (4-36), (4-37), and (4-38), namely

$$Q_w = Q_{w,c} + Q_{w,G} + Q_{w,e} \qquad (4\text{-}40)$$

(IV-F) Power Discharge Loss

The power carried away by the plasma jet discharge from the exit end of keyhole, Q_{dis}, can be computed from the plasma arc enthalpy and mass flow rate, i.e.,

$$Q_{dis} = (h_{pl}\,\dot{m}_{pl} + h_{sd}\dot{m}_{sd})_{dis} \qquad (4\text{-}41)$$

where the values of $h_{pl}\dot{m}_{pl}$ and $h_{sd}\dot{m}_{sd}$ are the results of integration over the cross-section of the outlet end of the keyhole from r = 0 to r = R_r. R_r is the radius of the outlet end of the keyhole. A detailed description of how to determine R_r will be discussed in Section VI of this report.

Obviously, summation of power loss throughout the entire VPPA welding system is equivalent to the total power input of the system, P_{total}, namely

$$P_{total} = Q_E + Q_G + Q_N + Q_s + Q_W + Q_{dis} \qquad (4\text{-}42)$$

Calculation of power loss at each part of VPPA welding system will be illustrated in Section VII of this report.

V. CALCULATION OF PLASMA ARC ENTHALPY

To give an example, the density of argon gas at a pressure of 1 atmosphere and a temperature of 298 °K is

$$\rho_{pl} = \frac{PM_{Ar}}{R\,T} = \frac{101320\ (N/m^2)\ \cdot\ 39.95\ (kg/kmol)}{8315\ (N\cdot m/kmol\ ^\circ K)\ \cdot\ 298\ (^\circ K)}$$

$$= 1.6336\ (kg/m^3)$$

where

P = Atmospheric pressure

M_{Ar} = Molecular weight of argon

R = Universal gas constant

T = Absolute Temperature

The mass flow rate of argon gas in terms of volumetric flow rate can be computed as

$$\dot{m} = (\dot{V}\ ft^3/hr)\left(\frac{1}{3600}\ hr/s\right)\left(\frac{1}{35.3147}\ m^3/ft^3\right)\rho_{Ar}$$

$$= \frac{1.6336}{(3600)(35.3147)}\ (\dot{V}\ ft^3/hr)$$

$$= 1.285 \cdot 10^{-5}\ (\dot{V}\ ft^3/hr) \qquad (kg/s)$$

$$= 1.285 \cdot 10^{-2}\ (\dot{V}\ ft^3/hr) \qquad (g/s)$$

(V-A) Plasma Arc Enthalpy Within the Gap Between Electrode and Orifice

Let us assume that entrance and exit ends of plasma arc enthalpy in the gap between electrode and orifice are $h_{1,1}$ and $h_{1,2}$, respectively.

The plasma arc power entering the gap, $P_{1,1}$, is the power

generated at the electrode, P_E, minus the power loss by electrode heat conduction, Q_E, namely

$$P_{1,i} = P_E - Q_E \tag{5-1}$$

Plasma arc enthalpy at the entrance end of the gap, thus, can be calculated as

$$h_{1,i} = \frac{P_{1,i}}{\dot{m}} \tag{5-2}$$

The plasma arc power at the exit end of the gap, $P_{1,o}$, has been augmented through Joule heating, $P_{J,1}$, and diminished through radiative heat loss, Q_G. It is

$$P_{1,o} = P_{1,i} + P_{J,1} - Q_G \tag{5-3}$$

Thus, plasma arc enthalpy at the exit end of the gap can be calculated from the expression

$$h_{1,o} = \frac{P_{1,o}}{\dot{m}} \tag{5-4}$$

(V-B) Plasma Arc Enthalpy Within Orifice

Let us assume that the enthalpy of the plasma at the entrance and exit ends of the orifice are $h_{2,i}$ and $h_{2,o}$, respectively.

The power, $P_{2,i}$, and enthalpy, $h_{2,i}$, of the plasma arc at the entrance end of the orifice are identical to the power, $P_{1,o}$ and enthalpy, $h_{1,o}$, respectively, of the plasma arc at the exit end of the gap between electrode and orifice. Thus,

$$\left.\begin{aligned} P_{2,i} &= P_{1,o} \\ h_{2,i} &= h_{1,o} \end{aligned}\right\} \tag{5-5}$$

The plasma arc power at the exit end of orifice, $P_{2,o}$, is increased by part of the power generated at the orifice anode drop, (1-

$\psi)P_{N,2}$, and by all the power generated by Joule heating within orifice, $P_{J,2}$, and is reduced by convective heat loss to the orifice, $Q_{N,c}$, and free electron power loss to the orifice, $Q_{N,e}$. Thus,

$$P_{2,o} = P_{2,i} + (1-\psi)P_{N,2} + P_{J,2} - Q_{N,c} - Q_{N,e} \qquad (5-6)$$

The corresponding plasma arc enthalpy at the exit end of orifice is

$$h_{2,o} = \frac{P_{2,o}}{\dot{m}} \qquad (5-7)$$

(V-C) Plasma Arc Enthalpy Within Standoff Column

Let us assume that the plasma enthalpies sat at the entrance and exit ends of the standoff column are $h_{3,i}$ and $h_{3,o}$, respectively.

The plasma arc power, $P_{3,i}$, and enthalpy, $h_{3,i}$, at the entrance end of standoff column are identical to the plasma arc power, $P_{2,o}$, and enthalpy, $h_{2,o}$, respectively, at the exit end of orifice. Thus,

$$\left.\begin{aligned} P_{3,i} &= P_{2,o} \\ h_{3,i} &= h_{2,o} \end{aligned}\right\} \qquad (5-8)$$

Plasma arc power at the exit end of standoff column, $P_{3,o}$, is increased by Joule heating in standoff column, $P_{J,3}$, and increased by shielding gas mixing power, P_{sd}, and reduced by radiative heat loss, $Q_{s,r}$, and convective heat loss, $Q_{s,c}$, from the same column. Thus,

$$P_{3,o} = P_{3,i} + P_{J,3} + P_{sd} - Q_{s,r} - Q_{s,c} \qquad (5-9)$$

The corresponding plasma arc enthalpy at the exit end of standoff column is

$$h_{3,o} = \frac{\dot{m}_{pl}h_{pl} + \dot{m}_{sd}h_{sd}}{\dot{m}_{pl} + \dot{m}_{sd}} \qquad (5-10)$$

where the values of $\dot{m}_{pl}$, $\dot{m}_{sd}$, $\dot{m}_{pl}h_{pl}$, and $\dot{m}_{sd}h_{sd}$ are the results of integration at the cross-section of outlet end of standoff column from

$r = 0$ to $r = R_c$ where R_c is the half crown width.

(V-D) Plasma Arc Enthalpy Within Keyhole of Workpiece

Let us assume that the plasma enthalpy at the entrance and exit ends of the keyhole of the workpiece are $h_{4,i}$ and $h_{4,o}$, respectively.

The plasma arc power, $P_{4,i}$, and enthalpy, $h_{4,i}$, at the entrance end of the keyhole of workpiece are identical to the plasma arc power, $P_{3,o}$, and enthalpy, $h_{3,o}$, respectively, at the exit end of standoff column. Thus,

$$\left.\begin{aligned} P_{4,i} &= P_{3,o} \\ h_{4,i} &= h_{3,o} \end{aligned}\right\} \qquad (5\text{-}11)$$

Plasma arc power at the exit end of the keyhole of workpiece, $P_{4,o}$, is increased by a portion of the power generated at the workpiece anode and cathode drops, $(1-\psi)P_{w,2}$, and is reduced by convective heat loss to the keyhole surface, $Q_{w,c}$ and the loss of hot electrons to the keyhole, $Q_{w,e}$. Thus,

$$P_{4,o} = P_{4,i} + (1-\psi)P_{w,2} - Q_{w,c} - Q_{w,e} \qquad (5\text{-}12)$$

The corresponding plasma arc enthalpy at the exit end of the keyhole of the workpiece is

$$h_{4,o} = \frac{\dot{m}_{pl}h_{pl} + \dot{m}_{sd}h_{sd}}{\dot{m}_{pl} + \dot{m}_{sd}} \qquad (5\text{-}13)$$

where the values of $\dot{m}_{pl}$, $\dot{m}_{sd}$, $\dot{m}_{pl}h_{pl}$, and $\dot{m}_{sd}h_{sd}$ are the results of integration at the cross-section of outlet end of keyhole from $r = 0$ to $r = R_r$.

(V-E) Plasma Arc Enthalpy Discharged from the Workpiece

Plasma arc power, Q_{dis}, and enthalpy, h_{dis} discharged from the keyhole of workpiece is identical to the plasma arc power, $P_{4,o}$, and enthalpy, $h_{4,o}$, at the exit end of keyhole, namely

$$\left.\begin{aligned} Q_{dis} &= P_{4,o} \\ h_{dis} &= h_{4,o} \end{aligned}\right\} \qquad (5\text{-}14)$$

Calculation of plasma arc enthalpy at each part of VPPA welding system will be illustrated in Section VII of this report.

VI. CALCULATION OF CROWN AND ROOT BEAD WIDTHS

Bead width is calculated from the heat absorbed in the workpiece, Q_W. As shown in Equation (4-40) Q_W is the summation of convection heating (the empirical relation actually includes radiation.) from the plasma, "direct" heating of the surface by current passing through localized surface voltage drops, and heat carried into the surface by hot electrons from the plasma.

The heat input source in the keyhole during the actual welding process is neither a point source nor a line source along the axial direction in which the input energy is not uniformly distributed. To make a calculation closer to the actual situation, we adopted a calculated result at various locations of z along the axial direction as a heat source distribution. As the magnitude of the heat source per unit length along the z axis is closely related to the area of heat trandfer (radius of keyhole at various locations of z), both heat absorbed by the keyhole per unit lenth along the axial direction and the radius of the keyhole at various locations of the z-axis shall be solved by simultaneous iteration.

The temperature field within the confined space between the two surfaces (assumed nonconducting) of the workpiece is constructed out of moving heat sources in an infinite continuum. "Image" sources are added outside the workpiece space so as to produce planes of symmetry across which no heat flows at the location of the workpiece surfaces. Given coordinate z zeroed at the top of the workpiece and extending down into the workpiece body and locating the heat source $Q_{W,z}$ at location z, then an image heat source above the top of the plate of

strength $Q_{W,z}$ located at -z creates a plane of zero heat flow at z = 0, the location of the top surface of the workpiece. The latter plane will remain and a further plane of zero heat flow at the site of the bottom surface of the workpiece will be created if an infinite array of image heat source pairs is constructed along the z-axis, each heat source pair of strength $Q_{W,z}$ spaced at ± z about an infinite array of points spaced at $2L_4$ and including z = 0. See Figure 5 for illustration.

The temperature T_c at location (x_c, y_c, z_c) within the workpiece due to the welding power input to the workpiece is then:

$$T_c - T_0 = \sum_{i=-\infty}^{\infty} \frac{Q'_{W,z}\, dz}{4\pi K R_i} \exp\left(-\frac{u(R_i + x_c)}{2\alpha}\right) \qquad (6\text{-}1)$$

where

T_0 = Ambient temperature of workpiece

K = Thermal conductivity of workpiece

u = Weld speed (in the x-direction)

α = Thermal diffusivity of workpiece

R_i = Distance between the i^{th} point heat source and the point of interest

R_i is computed as follows:

$$R_i = \sqrt{x_c^2 + y_c^2 + (z_i - z_c)^2} \qquad (6\text{-}2)$$

$$z_i = \left[i + \frac{1 + (-1)^{i+1}}{2}\right] L_4 + (-1)^i z \qquad (6\text{-}3)$$

Weld bead width is determined by locating the largest value of y_c for which $T_c = T_m$, the melting temperature of the workpiece, at z = 0

(crown) and $z_c = L_4$ (root). The weld widths are twice the values of these y_c's. A converging computer search routine is used to make the computation.

One approximation is used in the computations. The summation is truncated. 35 source points are used, 17 image sources on each side of the weld heat source. The values of z_i are generated by a recurrence relation:

$$z_i = z_{i-2} + 2L_4 \tag{6-3}$$

where the starting values are:

$$z_0 = z \tag{6-4}$$

$$z_1 = 2L_4 - z \tag{6-5}$$

where $0 \leq z \leq L_4$

z_o (=z) is the weld heat source position located in the workpiece.

After truncation, Equation (6-1) becomes

$$T_c - T_o = \sum_{i=-17}^{17} \frac{Q'_{w,z}dz}{4\pi k R_i} \exp\left[-u\left(\frac{R_i + x_c}{2\alpha}\right)\right] \tag{6-6}$$

As we indicated earlier for the computation of heat source distribution along the z-axis, the temperature distribution within the workpiece can be obtained by integrating Equation (6-6) which is

$$T_c - T_o = \int_0^{L_4} \sum_{i=-17}^{17} \frac{Q'_{w,z}dz}{4\pi k R_i} \exp\left[-u\frac{(R_i + x_c)}{2\alpha}\right]$$

$$= \sum_{i=-17}^{17} \int_0^{L_4} \frac{Q'_{w,z}dz}{4\pi k R_i} \exp\left[-u\frac{(R_i + x_c)}{2\alpha}\right] \tag{6-7}$$

Adopting temperature T_c to be the melting temperature T_m, one can

compute the melting isotherm surface from Equation (6-7). The geometric distribution of the keyhole can also be obtained for the maximum radius of the melting widths at various locations of z. Crown and root widths, $2R_c$ and $2R_r$, at the upper and lower ends of the workpiece can be calculated by a similar method.

Equation (6-7) is used to compute the temperature distribution within the workpiece in which $Q'_{w,z}$, denotes the power conducted away through the workpiece, or the strength of heat source per unit length at location z. This strength of the heat source in the workpiece is the heat absorption $Q_{w,z}$ contributed from the plasma jet, minus a power loss due to the radiative heat transfer from the surfaces of the workpiece Q_R. In the actual numerical integration of Equation (6-7), Q_R is included in $Q'_{w,z}$ at various locations of z by a method of weighing.

Since the distributions of $Q_{w,G}$ from Equation (4-37) and $Q_{w,e}$ from Equation (4-38) inside the keyhole are hard to determine, we assume the parabolic type of square approximation (see Figure 6 for schematic expression of the workpiece power distribution),

$$Q_z = a\left(1 - \frac{z}{L_4}\right)^2 Q \qquad (6\text{-}8)$$

where Q denotes either $Q_{w,G}$ or $Q_{w,e}$. a is a constant which will be determined from the integration of Equation (6-8) based on the value of Q in which the total value of either $Q_{w,G}$ or $Q_{w,e}$ shall be conserved. This is

$$Q = \int_0^{L_4} Q_z dz = \int_0^{L_4} a(1 - \frac{z}{L_4})^2 Q dz$$

which leads to $a = 3/L_4$, and Equation (6-8) becomes

$$Q_z = \frac{3}{L_4}(1 - \frac{z}{L_4})^2 Q \qquad (6\text{-}9)$$

Radiation losses from both sides of the workpiece surfaces are computed. The radiative heat transfer loss can be computed as

$$Q_R = \Sigma A_i e \sigma T_i^4 \qquad (6\text{-}10)$$

where A_i denotes a small element i of surface area; ϵ_i is emissivity of the workpiece; T_i stands for the average temperature (°K) of the surface area element A_i; and σ is Stefan-Boltzman constant (= 5.67 x 10^{-8} $W/m^2 \cdot k^4$).

Workpiece power absorption per unit length along the z-axis due to melting heat can be computed from the following relation:

$$Q_{m,z} = u \rho_w Q_f d_z \qquad (6\text{-}11)$$

where

u = Traveling speed of welding

ρ_w = Density of workpiece

Q_f = Melting heat of workpiece

d_z = Bead width at position z

Based on this analysis, power transfer per unit length in workpiece $Q'_{w,z}$ can be computed as follows:

$$Q'_{w,z} = Q_{w,c_z} + \frac{3}{L_4}(1 - \frac{z}{L_4})^2 (Q_{w,G} + Q_{w,e}) - Q_{m,z} - Q_R(\frac{Q_{w,z}}{Q_w}) \qquad (6\text{-}12)$$

The total net power absorbed by workpiece is then

$$Q'_w = \int_0^{L_4} Q'_{w,z} dz \qquad (6\text{-}13)$$

Substituting Equations (6-12) in (6-13), we have

$$Q'_w = Q_w - Q_R - Q_m \qquad (6\text{-}14)$$

where

$$Q_w = \int_0^{L_4} Q_{w,c_z} dz + Q_{w,G} + Q_{w,e}$$

$$= Q_{w,c} + Q_{W,G} + Q_{w,e}$$

is similar to Equation (4-40), and Q_R is from Equation (6-10). Here,

$$Q_m = \int_0^{L_4} Q_{m,z} dz$$

is the total melting power.

VII. CALCULATION OF PARTIAL PENETRATION OF THE WORKPIECE

In Section VI, we have discussed the weld widths and power loss in the workpiece. An estimation of full penetration or partial penetration shall be made before we can proceed the calculation of Section VI. Before the keyhole is formed for partial penetration, the plasma jet impinges perpendicularly on the surface of the weld pool, and is deflected across the weld surface radially away from the stagnation area. Thus, the heat transfer from the plasma jet to the surface of the weld pool and the model of the heat source used to calculate the temperature field of the workpiece are different from those of the weld process in which keyhole has been formed in the workpiece.

(VII-A) Weld Pool Convective Heat Transfer

For the case of partial penetration, a concave shape melting puddle is formed while the plasma jet impinges on the surface of the workpiece. At this moment, there is a very complicated flow pattern developed within the melting puddle of the molten liquid metal. It is anticipated that heat transfer process, which causes the convective heat flow from the plasma jet to the workpiece, is also very complicated. It is hard to adopt a very suitable mathematical formulation to describe convective heat loss from the plasma jet to the workpiece. In this study in the determination of partial and full penetration of the workpiece, an axial symmetry circular plasma jet, which impinges perpendicularly on the surface of the weld pool of the workpiece, is assumed to compute the convective heat loss problem.

The power transferred to the workpiece by convection from the plasma arc jet can be written as:

$$Q_{w,c} = h \cdot A_w \cdot (H_{plasma} - H_w) / C_{pm} \qquad (7\text{-}1)$$

where

A_w = Plasma arc jet impingement surface area

$= \pi R_2^2$

R_2 = Outer boundary radius produced by plasma arc jet on the surface of the workpiece (see Figure 4b)

H_{plasma} = Average enthalpy of the plasma arc jet on the stagnation area A_w

H_w = Enthalpy of the plasma arc jet at the temperature of the weld pool

C_{pm} = Specific heat of the plasma corresponding to a temperature T_m at which the enthalpy of plasma is equal to the mean enthalpy at the temperature of the arc jet and the weld pool

h = Convective heat transfer coefficient

h can be computed from the following relation (Metcalfe and Quigley, 1975):

$$N_u = 0.78\ R_e^{0.5} P_r^{0.33} \qquad (7\text{-}2)$$

where the dimensionless parameters are defined as follows:

$$N_u = \frac{h(2R_2)}{k}$$

$$R_e = \frac{\rho v (2R_2)}{\mu}$$

$$P_r = \frac{C_p \mu}{k}$$

Here, v is the average velocity of the plasma arc jet within the outer boundary on the surface of the workpiece. The rest of the parameters are the same as that defined earlier. In this calculation, the parameters of the plasma are determined based on the average enthalpy within the cross sectional area of radius R_2.

Total power absorbed by the weld pool or the workpiece, Q_w, shall be the summation of Equations (7-1), (4-37) and (4-38), i.e.,

$$Q_w = Q_{w,c} + Q_{w,G} + Q_{w,e} \qquad (7-3)$$

(VII-B) The Model of Temperature Field and Partial Penetration

In the determination of the formation of keyhole from the plasma arc jet impingement on the surface of the workpiece, it is assumed that there is a point source with an intensity of Q_w which moves with a speed of u acting on the surface of the workpiece. Point source model, proposed by Rosenthal, is adopted to compute the temperature field of the workpiece created by this moving point source. The depth of the weld pool, z_m, created by the moving point source can be computed by the constant temperature surface of the workpiece molten temperature which is the solid-molten pool interface of the workpiece weld pool. The impingement of the high speed plasma jet creates an intensive disturbance on the molten liquid of the workpiece and forms a concave hole on the surface of the workpiece. It may create a distributed heat source from the surface of the workpiece to the depth of the weld pool if the impingement of the plasma jet can reach the bottom of the molten

pool. To simplify the calculation , we may assume that there is a uniformly distributed heat source moving with a speed of u, and with an intensity of Q_w/Z_m (See Figure 7). The temperature field of the workpiece can be computed based on the effect of the moving uniformly distributed heat source. Determination of the depth of the partial penetration and the formation of the keyhole can be resulted from the distribution of the constant temperature surface of the workpiece molten temperature.

The temperature field produced by the point source at the surface of the workpiece moving with uniform velocity of u along the a moving coordinate with a speed u moved with a point Location of the point source is at the origin) is

$$T_c - T_o = \sum_{i=-\infty}^{\infty} \frac{Q_w'}{4\pi k R_i} \exp\left[-\frac{u}{2\alpha}(R_i + x_c)\right] \qquad (7-4)$$

where

k = Heat conductivity of the workpiece

α = Thermal diffusivity of the workpiece

u = Moving speed of the point source

$R_i = [x_c^2 + y_c^2 + (z_c - z_i)^2]^{1/2}$

x, y, z = Location of the point of interests

$z_i = \left[i + \frac{1 + (-1)^{i+1}}{2}\right] \cdot L_4$

L_4 = Thickness of the workpiece

Here,

$Q_w' = Q_w - Q_m$

Q_w can be computed from Equation (7-3), and

Q_m = Latent power of the workpiece

$$= \int_o^{z_m} Q_f u \rho d_z dz$$

where

Q_f = Latent heat of the workpiece

ρ = Density of the workpiece

d_z = Width of the molten liquid of the workpiece at the corresponding location of z

Put $T_c = T_m$ (molten temperature of the workpiece) in Equation (7-4), one can solve the constant molten temperature surface of the workpiece. The depth of the workpiece molten pool under the effect of the heat source, thus, can be determined.

The temperature field created by the moving uniformly distributed heat source with intensity of Q_w'/Z_m located from z = 0 to Z_m is

$$T_c - T_o = \sum_{i=-\infty}^{\infty} \int_0^{Z_m} \frac{(Q_w'/Z_m)}{4\pi k R_i} \exp\left[-\frac{u}{2\alpha}(R_i + x_c)\right] dz \qquad (7\text{-}5)$$

where

$$R_i = [x_c^2 + y_c^2 + (z_i - z_c)^2]^{1/2}$$

$$z_i = \left[i + \frac{1 + (-1)^{i+1}}{2}\right] \cdot L_4 + (-1)^i z$$

$$0 \le Z \le Z_m$$

$$Q_w' = Q_w - Q_m$$

$$Q_m = \int_0^{z_1} Q_t u \rho d_z dz$$

z_1 = Molten metal depth of the workpiece under the effect of uniformly distributed heat source

The determination of full penetration or the formation of the keyhole is dependent upon whether z_1 is equal to the workpiece thickness L_4. In the realistic calculation, adoption of 35 terms of series summation in Equation (7-5) is good enough to assure the series convergence accuracy of the temperature field determination. In other words, the adoption of $-17 \leq i \leq 17$ together with solving simultaneous equations of Equation (7-5) and the computation of T_m with iteration of related variables are required to solve the temperature filed distribution.

It is due to the fact that there is no experimental data available for the variation of the depth of partial penetration with respect to control parameters of the welding processes. There is no way to compare the model results with the all of the stages of penetration processes during the plasma arc jet welding. In this study, model comparison with the experimental results of partial penetration and the possibility of the formation of the keyhole are made.

Equation (7-5) is used to calculate the probability of full penetration as the lower surface of the workpiece reaches the molten temperature. For the case of partial penetration, it may be due to the fact that the power supply is too small and/or the weld speed is too high. So long as the keyhole is formed, Section VI

will be used to compute the power absorbed by the workpiece in the keyhole, the weld widths, etc.

VIII. CALCULAITON OF CROWN AND ROOT HEIGHTS

(VIII-A) Volume Conservation Equation of Materials

Assuming that reinforcement profiles of crown and root beads are paraboloid, as shown in Figure 8. These paraboloid profile can be expressed in the following equation:

$$Z = h_c \left[1 - \left(\frac{2y}{d_c} \right)^n \right] \tag{8-1}$$

where

h_c = Crown height

d_c = Crown bead width

n = Numerical value greater than 1

The cross-sectional area of the crown reinforcement is

$$A_c = 2 \int_0^{d_c/2} \left\{ h_c \left[1 - \left(\frac{2y}{d_c} \right)^n \right] \right\} dy$$

$$= \frac{n}{n+1} h_c d_c$$

Similarly, cross-sectional area of the root reinforcement is

$$A_r = \frac{n}{n+1} h_r d_r$$

where

h_r = Root height

d_r = Root bead width

Volume conservation requires the equation of the material volume provided by welding wire to the reinforcement volume crown and root beads plus any gaps of holes in the weld site prior to welding:

$$\frac{n}{n+1} d_c h_c + \frac{n}{n+1} d_r h_r = \frac{\pi}{4} d_w^2 \frac{V_w}{u} - L_4 \cdot W_g \qquad (8\text{-}2)$$

where

d_w = Diameter of wire

V_w = Feeding speed of wire

u = Welding speed

W_g = Initial gap at the weld seam

L_4 = Thickness of workpiece

(VIII-B) Force Equilibrium Equation

It should be noted that for the sake of tractability the force-equilibrium analysis has been greatly simplified. Longitudinal curvature of the weld puddle surface has been neglected as have the effects of Marangoni circulations and thermal variation of surface tension. There is a great deal of room for improvement of this first, very rough analysis. The cross-sectional areas a, b, and c, defined in Figure 9 which are given by

$$A_a = 2 \int_0^{d_r/2} \left\{ h_c \left[1 - \left(\frac{2y}{d_c} \right)^n \right] \right\} dy$$

$$= h_c d_r - \frac{1}{n+1} h_c d_c \left(\frac{d_r}{d_c} \right)^{n+1} \qquad (8\text{-}3)$$

$$A_b = d_r \cdot L_4 \qquad (8\text{-}4)$$

$$A_c = A_r = \frac{n}{n+1} h_r d_r \qquad (8\text{-}5)$$

The slopes of the reinforcement surfaces at points B (crown) and D (root), shown in Figure 9, are given by

$$\tan \theta_c = \left.\frac{dz}{dy}\right|_{y=d_r/2} = -\frac{2nh_c}{d_c}\left(\frac{d_r}{d_c}\right)^{n-1}$$

and

$$\tan \theta_r = \left.\frac{dz}{dy}\right|_{y=d_r/2} = \frac{2nh_r}{d_r}$$

It is due to the fact that both θ_c and θ_r are relatively small, and we can assume $\sin\theta_c \simeq \tan\theta_c$ and $\sin\theta_r \simeq \tan\theta_r$.

With reference to the free-body diagram shown in Figure 9, the force equilibrium equation for the body comprising areas a, b, and c is given by

$$\left[h_c d_r - \frac{1}{n+1} h_c d_c \left(\frac{d_r}{d_c}\right)^{n+1} + d_r \cdot L_4 + \frac{n}{n+1} d_r h_r\right] \rho g = 4n\left[\frac{h_r}{d_r} - \frac{h_c}{d_c}\left(\frac{d_r}{d_c}\right)^{n-1}\right] \sigma - \bar{p} d_r \qquad (8\text{-}6)$$

where the first term represents a gravitational force, g being the gravitational acceleration component perpendicular to the workpiece surface and directed from crown to root. The second term represents a surface tension force, σ being the molten weld puddle surface tension. The third term represents a pressure force, $\bar{p}$ being the mean pressure acting on the weld crown surface.

(VIII-C) Calculation of Crown and Root Heights in Horizontal Welding (with Consideration of Gravity Force)

Experience suggests that the effect of external pressure $\bar{p}$ is

much smaller than that of the surface tension. Therefore, the $\bar{p}$ term will be deleted from the force equilibrium equation (8-6). Crown and root heights, thus, can be found by simultaneously solving Equations (8-2) and (8-6) which yield the following expressions:

$$h_c = \frac{-\left[1 - \frac{4}{d_r^2}(n+1)\frac{\sigma}{\rho g}\right]\left[\frac{\pi}{4} d_w^2 \frac{V_w}{u} - L_4 \cdot W_g\right] - d_r \cdot L_4}{d_r - \frac{n}{n+1} d_c + \frac{4n\sigma}{\rho g}\left[\frac{1}{d_c}\left(\frac{d_r}{d_c}\right) + \frac{d_c}{d_r^2}\right] - \frac{1}{n+1} d_c \left(\frac{d_r}{d_c}\right)^{n+1}} \tag{8-7}$$

$$h_r = \frac{\frac{\pi}{4} d_w^2 \frac{V_w}{u} - L_4 \cdot W_g - \frac{n}{n+1} d_c h_c}{\frac{n}{n+1} d_r} \tag{8-8}$$

(VIII-D) Calculation of Crown and Root Heights in Vertical Welding (Without Gravity Effect)

The gravity force component g perpendicular to the workpiece vanishes for the case of vertical welding and also for welding carried out in space. Ignoring both gravity force and external pressure in Equation (8-6) one obtains

$$h_r = h_c \left(\frac{d_r}{d_c}\right)^n \tag{8-9}$$

and substituting this equation to Equation (8-2),

$$h_c = \frac{\frac{\pi}{4} d_w^2 \frac{V_w}{u} - L_4 \cdot W_g}{\frac{n}{n+1}\left[d_c + d_r \left(\frac{d_r}{d_c}\right)^n\right]} \tag{8-10}$$

(VIII-E) Depression of Crown Height During Solidification

Figure 10 shows the configuration of the cross-section of puddle during the process of solidification. The solid-liquid interface lies along the melting temperature isotherm, which generally expand toward the hotter crown and contract towad the colder root. They come together, thus, first at the root as in Figure 10(B). This leaves a sector of molten metal which shrinks upon solidification. The height of the solidified crown must fall to accomodate the shrinkage volume reduction as shown in Figure 10(C). The cross-sectional area of the molten sector in Figure 10(B) can be approximated as

$$A_c \simeq \frac{1}{2} L_4 \cdot d_c' \tag{8-11}$$

where L_4 stands for the thickness of the workpiece; and d_c', the crown width in a state of molten metal. Given a volumetric shrinkage, $\Delta v/v$, a material property, the reduction in area ΔA_c of the molten material during solidification is

$$\Delta A_c = A_c \left(\frac{\Delta V}{V}\right) = \frac{1}{2} L_4 \cdot d_c' \left(\frac{\Delta V}{V}\right) \tag{8-12}$$

From Equation (8-5) for the cross-sectional area of the crown reinforcement, the reduction in the area can be related to the change in the crown reinforcement height $\Delta h_c'$

$$\Delta A_c = \Delta \left(\frac{n}{n+1} d_c' h_c'\right) = \frac{n}{n+1} d_c' \Delta h_c' \tag{8-13}$$

Equating Equations (8-12) and (8-13), leads to

$$\frac{1}{2} L_4 \cdot d_c' \left(\frac{\Delta V}{V}\right) = \frac{n}{n+1} d_c' \Delta h_c'$$

which gives upon simplification

$$\Delta h_c' = \frac{n+1}{2n} L_4 \left(\frac{\Delta v}{v}\right) \qquad (8\text{-}14)$$

Using King's (1987), value for specific volumetric shrinkage for aluminum during the solidfication, $\Delta v/v$, is 6.7%. Therefore, crown height shrinkage for solidification of aluminum Equation (8-14) becomes

$$\Delta h_c' = 0.067 \frac{n+1}{2n} L_4 \qquad (8\text{-}15)$$

Detailed calculation results of crown and root heights are illustrated in Section IX of this report.

IX. LEADING EDGE ANGLE COMPUTATION

The leading edge angle of the keyhole of workpiece can be computed from thermal power equilibrium requirements as follows:

$$\tan\theta = \frac{\rho v[\mathcal{L} + c_s(T_m - T_o) + c_\ell (T_s - T_m)]}{P_w / \pi D L_4} \qquad (9\text{-}1)$$

where

ρ = Density of workpiece ($^{kg}/_{m^3}$)

v = weld speed (m/s)

$\mathcal{L}$ = Melting latent heat of workpiece ($^{kJ}/_{kg}$)

c_s = Specific heat of solid workpiece (Kj/kg·K)

c_ℓ = Specific heat of liquid workpiece (Kj/kg·K)

T_m = Melting temperature of workpiece (K)

T_o = Original temperature (room temperature) of workpiece (K)

T_s = Temperature of superheated molten fluid at leading edge (K)

P_w = Thermal power absorbed by workpiece (Kw)

D = Keyhole diameter (m) or orifice diameter (m)

L_4 = Thickness of workpiece (m)

θ = Leading edge angle

Theoretical computations and experimental measurements from rubber molds of keyholes (Nichols Research, 1992) are found to be in good agreement, at least with respect to velocity dependence except for four measurements at low plasma flow rates, which show experimental leading edge angles of $\theta > \text{or} = 30°$. In other words, Equation (9-1) may hold only above some threshold value of plasma flow rate. Above the threshold value, for reasons not yet understood a "beam absorption" model may allow computation of the

leading edge angle of the VPPA keyhole; while another concept appears to be required to deal with this problem when the plasma flow rate is below the threshold value.

X. RESULTS OF COMPUTATION AND COMPARISON WITH MEASUREMENTS MADE BY THE GDI TEAM

A computer implementation of the proposed mathematical model for VPPA modeling computation is included in the Appendix A; and for VPPA partial penetration to the formation of the keyhole is included in the Appendix B. Input data for the computer program is provided for in Appendix C for aluminum; and Appendix D for mild steel. Nomenclature are listed in Appendix E.

For the purpose to explain VPPA modeling computation, and VPPA partial penetration computation listed in Appendices A and B, two block diagrams and corresponding explanations are included in Appendices F and G to explain the structures of VPPA partial penetration and VPPA modeling computation, respectively.

Model computations have been made and compared with the experimental measurements accomplished by Nichols Research Corporation (1992). These comparisons are included in Appendix H of this report.

ACKNOWLEDGEMENT

The author and his team member would like to express their gratitude to Dr. Arthur C. Numes of the Material and Processes Laboratory, NASA Marshall Space Flight Center for stimulating discussions during the course of the present study. They also acknowledge the support of the present work through NASA Contract NAS8-38609/Delivery Order No. 34.

REFERENCES

Abramovich, G. N., "The Theory of Turbulent Jets", pp. 671, MIT Press, MA, 1963.

American Society for Metals Handbook Commitee, "Metals Handbook", 9th Edition, Vol. 2, pp. 855, American Society for Metals, Metals Park, OH, 1979.

Cram, L. E., "Statistical Evaluation of Radiative Power Losses from Thermal Plasma due to Spectral Lines", Jounal of Physics, D: Applied Physics 18, 1985.

Drellishak, K. S., Knopp, C. F., and Cambel, A. B., "Partition Function and Thermodynamic Properties of Argon Plasma", AEDC-TDR-63-146, pp. 238, Arnold Engineering Development Center, TN, 1963.

Eckert, E. R. G., and Pfender, E., "Plasma Energy Transfer to Surface With and Without Electric Current," Welding Journal Research Supplement, Vol. 46, No. 10, 471-s to 480-s, 1967.

Evans, D. L. and Tankin, R. S., "Measurement of Emmission and Absorption Radiation by an Argon Plasma", Physics of Fluids, 10 (6), 1137-1144, 1967.

Hsu, Y. T., and Rubinsky, B., "Transient Melting of a Metal Plate by a Penetrating Plasma Arc", Journal of Heat Transfer, 109, 463-469, 1987.

Hunn, B. D., and Moffat, R. J., "Radiative Heat Transfer from a Plasma in Tube Flow", International Journal of Heat and Mass Transfer, 17, 1319-1328, 1974.

Ibele, W., "Modern Developments in Heat Transfer", pp. 443, Academic

Press, New York, 1963.

King, F., "Aluminum and Its Alloys", pp. 313, The Camelot Press, Southampton, United Kingdom, 1987.

Lancaster, J. F., "The Physics of Welding", 2nd Edition, pp. 340, Pergamon Press, Oxford, England, 1986.

Metcalfe, J. C., and Quigley, A. B. C., "Heat Transfer in Plasma Arc Welding", Welding Journal, 54, 995-1035, 1975.

Miller, H. R., and Filipski, S. P., "Automated Plasma Arc Welding for Aerospace and Cryogenic Fabrication", Welding Journal, 45, 493-501, 1966.

Nichols Research Corporation, "VPPA Weld Model Evaluation," NASA Contract NAS8- 38812 Final Report, 1992.

Nunes, A. C., Jr., Novak, H. L., and McIlwain, M. C., "Weld Geometry Strength Effect in 2219-T87 Aluminum", NASA Technical Memorandum TM-82404, 1981.

Nunes, A. C., Jr., Bayless, O. E., Jr., Jones, C. S., III, Munafo, P. M., Biddle, A. P., and Wilson, W. A., "The Variable Polarity Plasma Arc Welding Process: Its Application to the Space Shuttle External Tank-First Interim Report", NASA Technical Memorandum TM-82532, 1983.

Nunes, A. C., Jr., Bayless, O. E., Jr., Jones, C. S., III, Munafo, P. M., Biddle, A. P., and Wilson, W. A., "Variable Polarity Plasma Arc Welding on the Space Shuttle External Tank", Welding Journal, 63, 27-35, 1984a.

Nunes, A. C., Jr., Bayless, O. E., Jr., Jones, C. S., III, Munafo, P. M., Biddle, A. P., and Wilson, W. A., "Variable Polarity Plasma

Arc Welding Process: Its Application to the Space Shuttle External Tank-Second Interim Report", NASA Technical Memorandum TM-86482, 1984b.

O'Brien, R. L., "Arc Plasma for Joining, Cutting and Surfacing", Welding Research Council, No. 131, 1968.

Privozhik, L. J., and Miller, H. R., "Evaluation of Plasma Arc Welding for 120 inch Diameter Rocket Motor Cases", Welding Journal, 45, 717-725, 1966.

Robert, S. W., and Melvin, J. A., "CRC Handbook of Chemistry and Physics", 61st Edition, CRC Press, NY, 1981.

Rosenthal, D., Welding Journal, 20, 220, 1941.

Solomon, H. D., and Levy, S., "HAZ Temperatures and Cooling Rates as Determined by a Simple Computer Program", in Trends in Welding Research in the United States, Proceeding a Conference Sponsored by the Joining Division of American Society for Metals, New Orleans, LA, pp. 173-205, Nov. 1981.

Tsai, C. L., "Modeling of Thermal Behaviors of Metal During Welding", in Trends in Welding Research in the Unites States, Edited by S. A. David, American Society for Metals, pp. 91-108, 1982.

Wilkinson, J. B., and Milner, D. R., British Welding Journal, Vol. 7, 115-128, 1960.

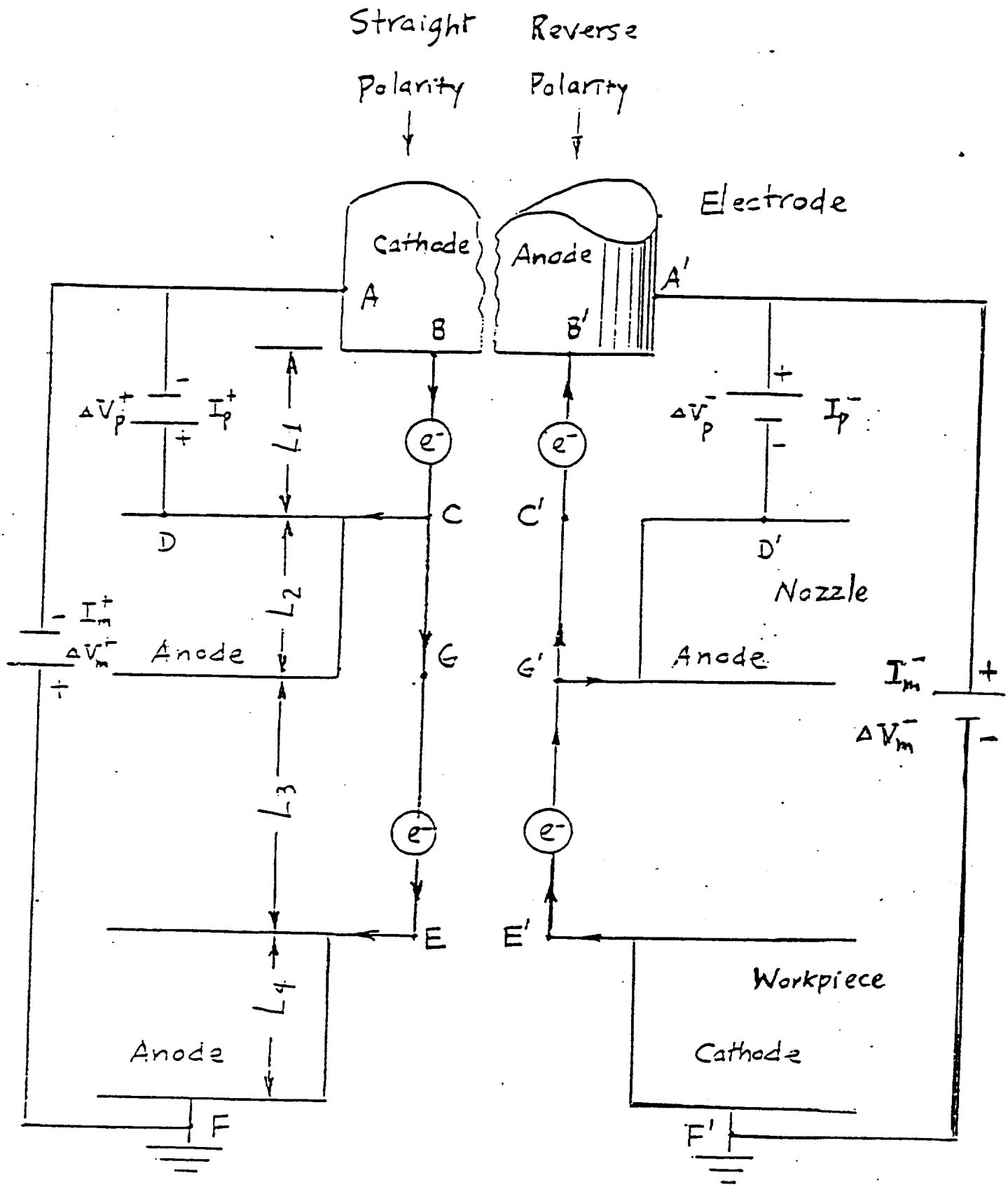
Straight Polarity
Reverse Polarity
Electrode
Cathode
Anode
A
B
A'
B'
ΔV_p^+
I_p^+
L_1
e^-
C
C'
D
D'
Nozzle
I_m^+
ΔV_m^+
Anode
L_2
G
G'
Anode
I_m^-
ΔV_m^-
L_3
E
E'
Workpiece
L_4
Anode
Cathode
F
F'

Fig. 1

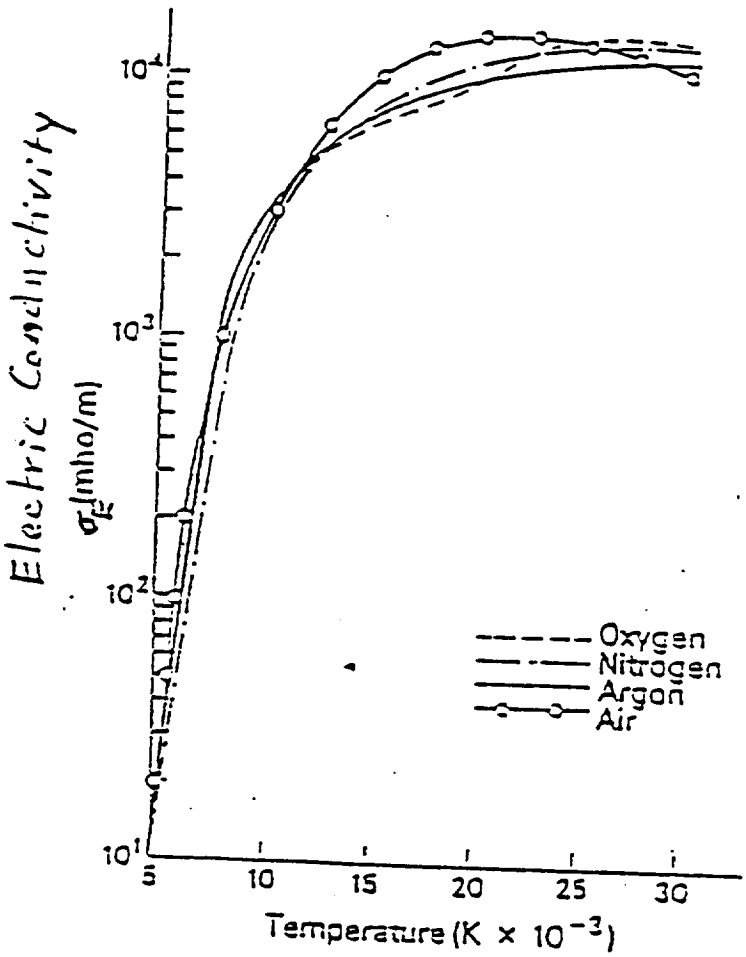
Electric Conductivity
σ_e(mho/m)
10^4
10^3
10^2
10^1
5
10
15
20
25
30
Temperature (K x 10^{-3})
Oxygen
Nitrogen
Argon
Air

Fig. 2

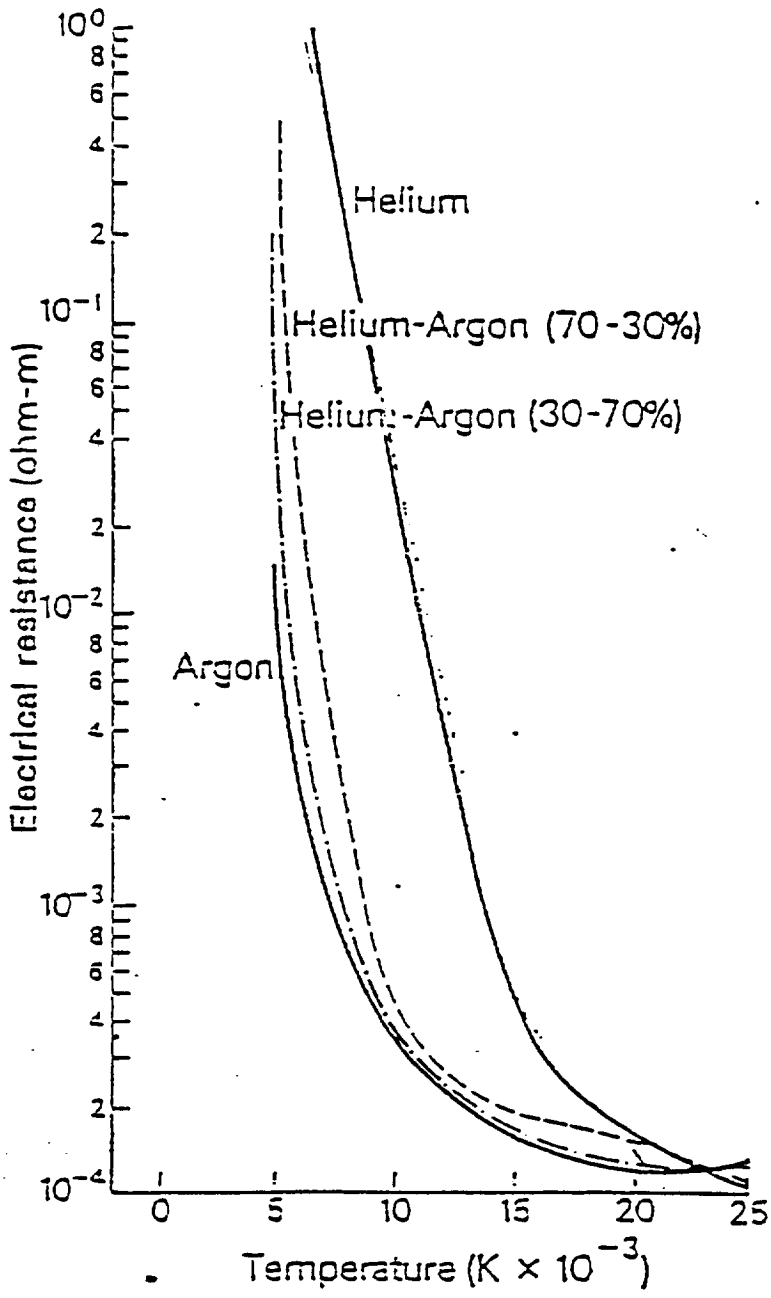
Helium
Helium-Argon (70-30%)
Helium-Argon (30-70%)
Argon
Electrical resistance (ohm-m)
Temperature (K × 10⁻³)
10⁰
10⁻¹
10⁻²
10⁻³
10⁻⁴
0
5
10
15
20
25

Fig. 3

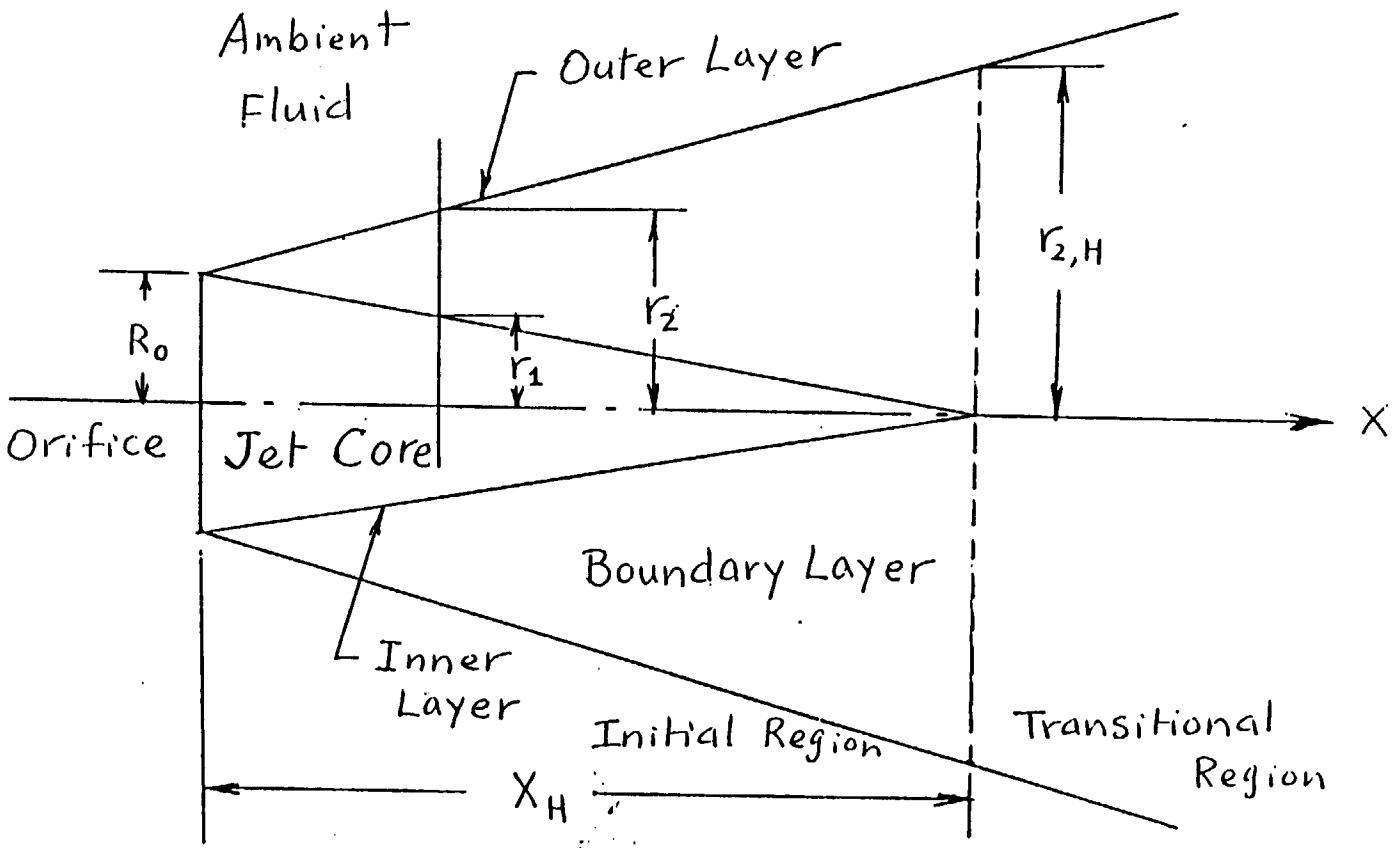
Ambient
Fluid
Outer Layer
$r_{2,H}$
r_2
R_o
r_1
Orifice
Jet Core
X
Boundary Layer
Inner
Layer
Initial Region
Transitional
Region
X_H

Fig. 4a

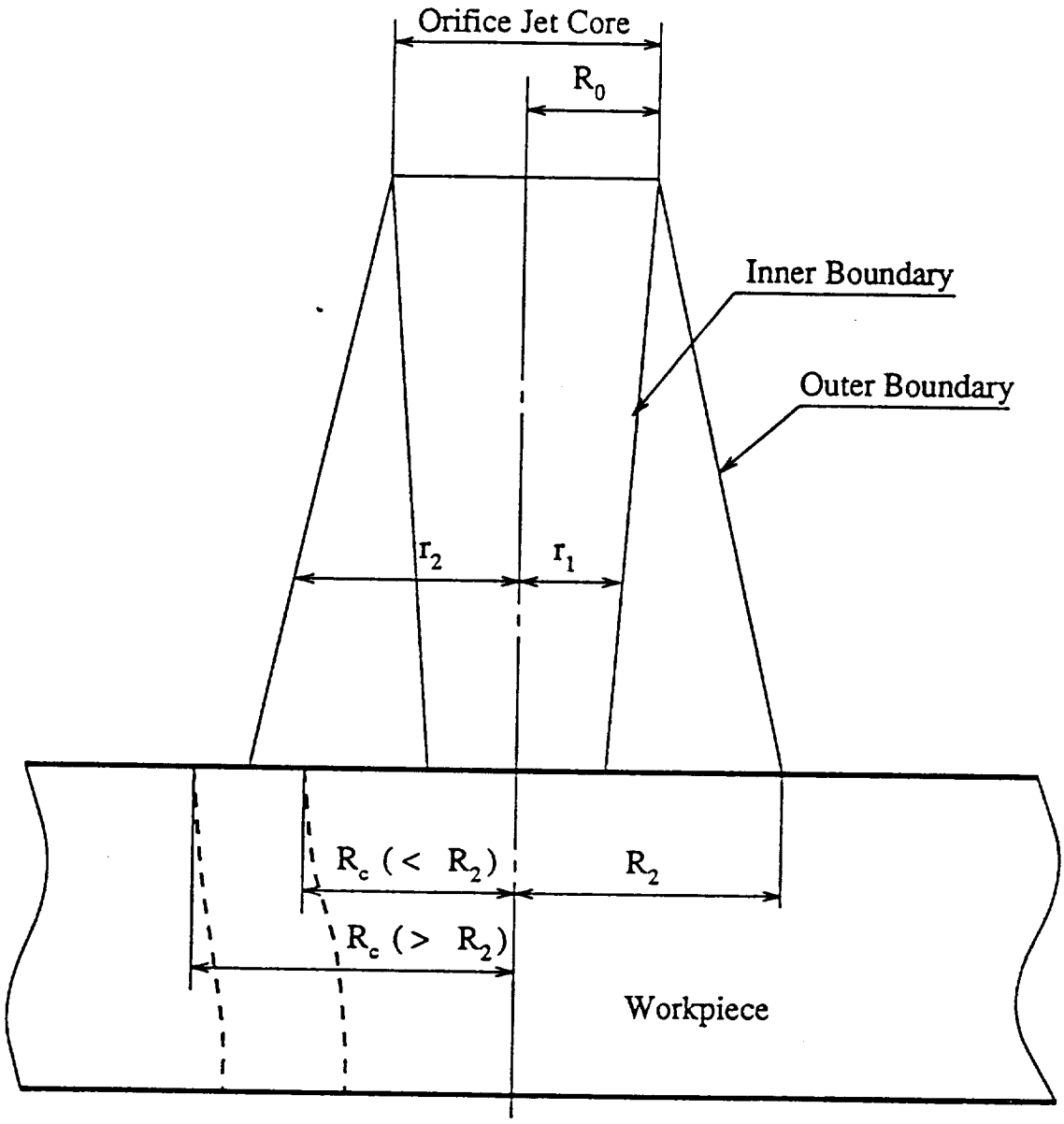

Fig. 4b Acting Range of Plasma Jet on Workpiece Surface

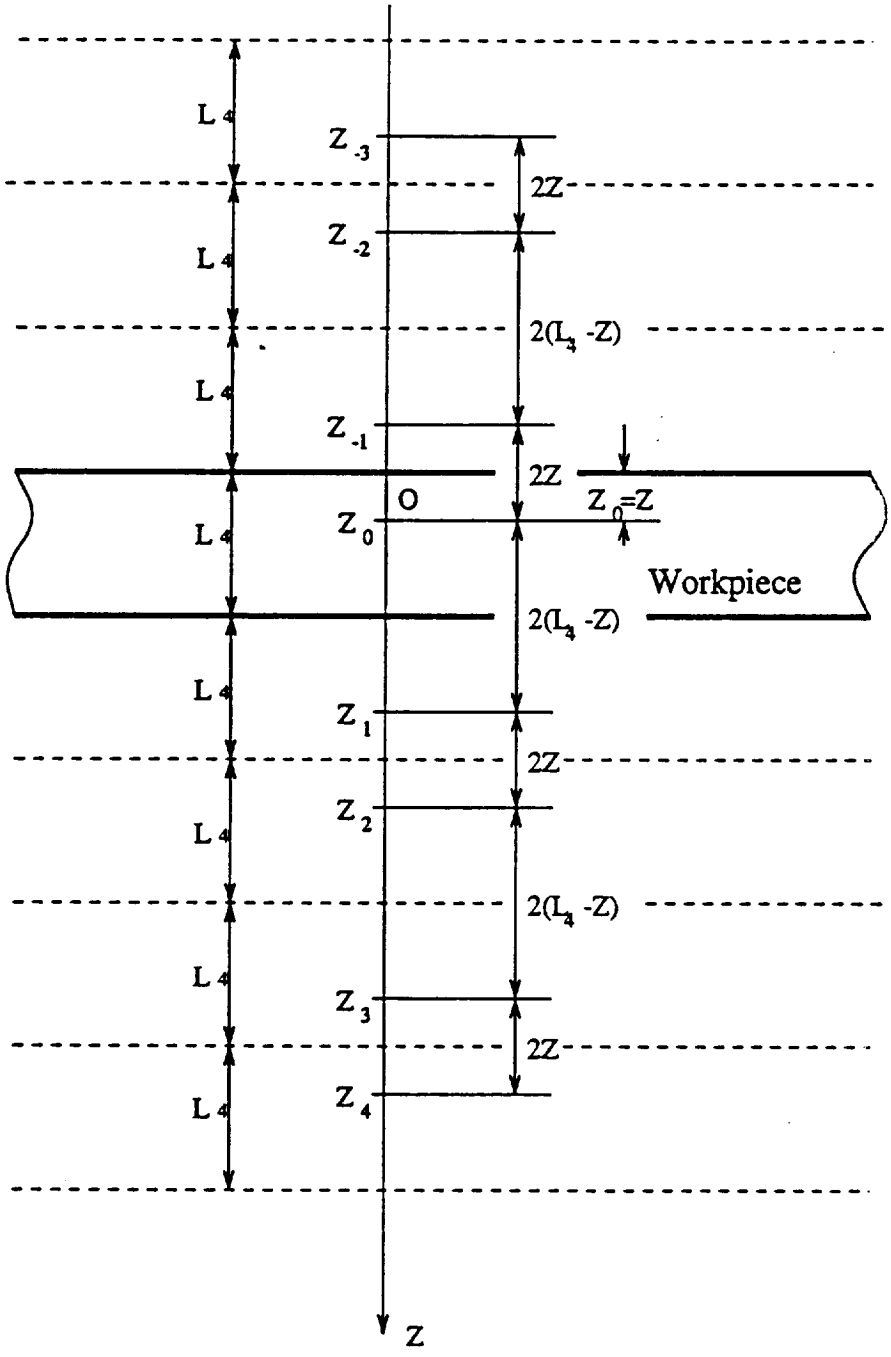
L4
L4
L4
L4
L4
L4
L4
Z-3
Z-2
Z-1
Z0
Z1
Z2
Z3
Z4
2Z
2Z
2(L4 -Z)
2Z
2(L4 -Z)
2Z
2(L4 -Z)
2Z
O
Z0=Z
Workpiece
Z

Fig. 5

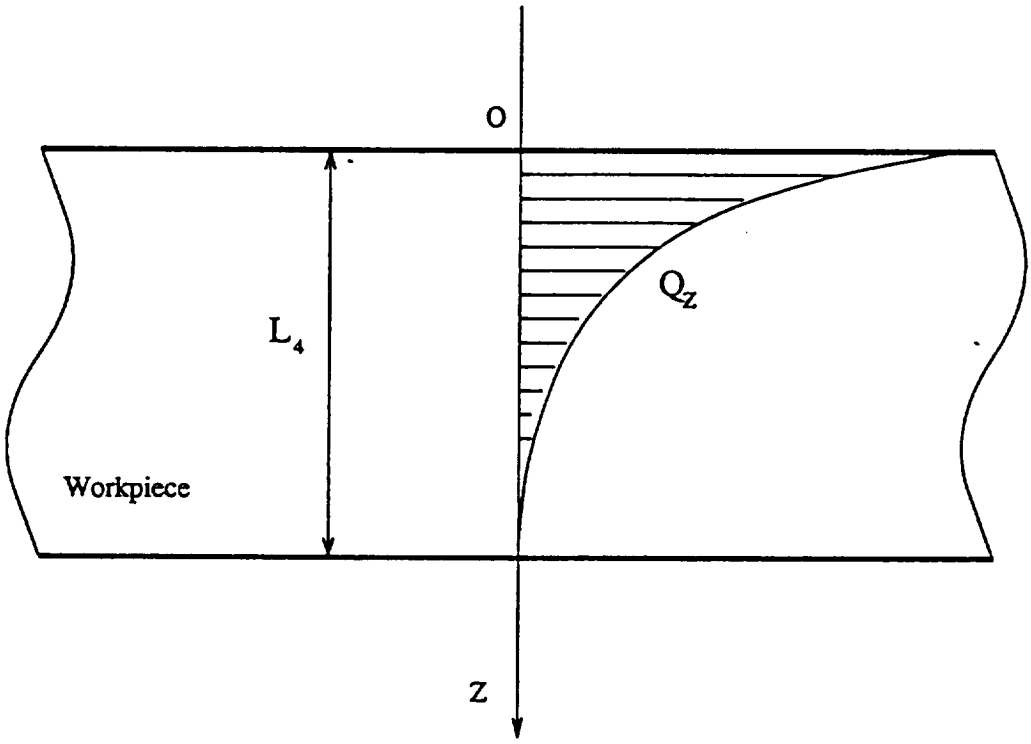

Fig. 6 Workpiece Heat Power Distribution

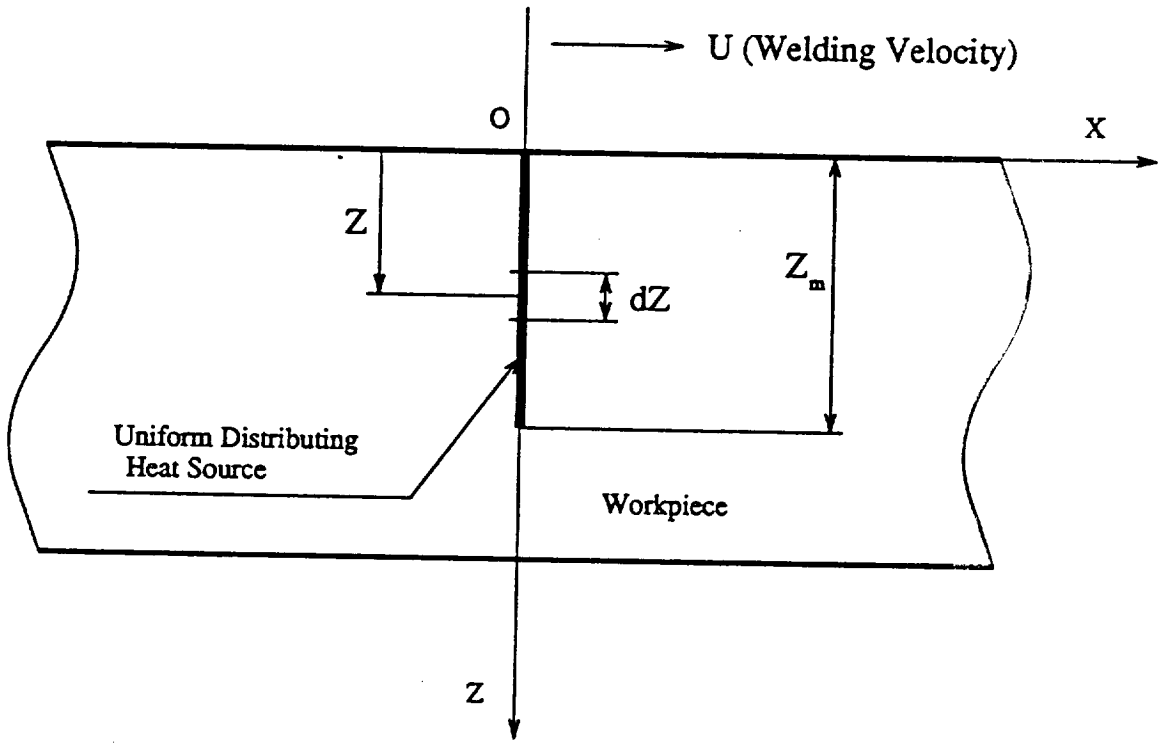

Fig. 7 Uniformly Distributed Heat Source

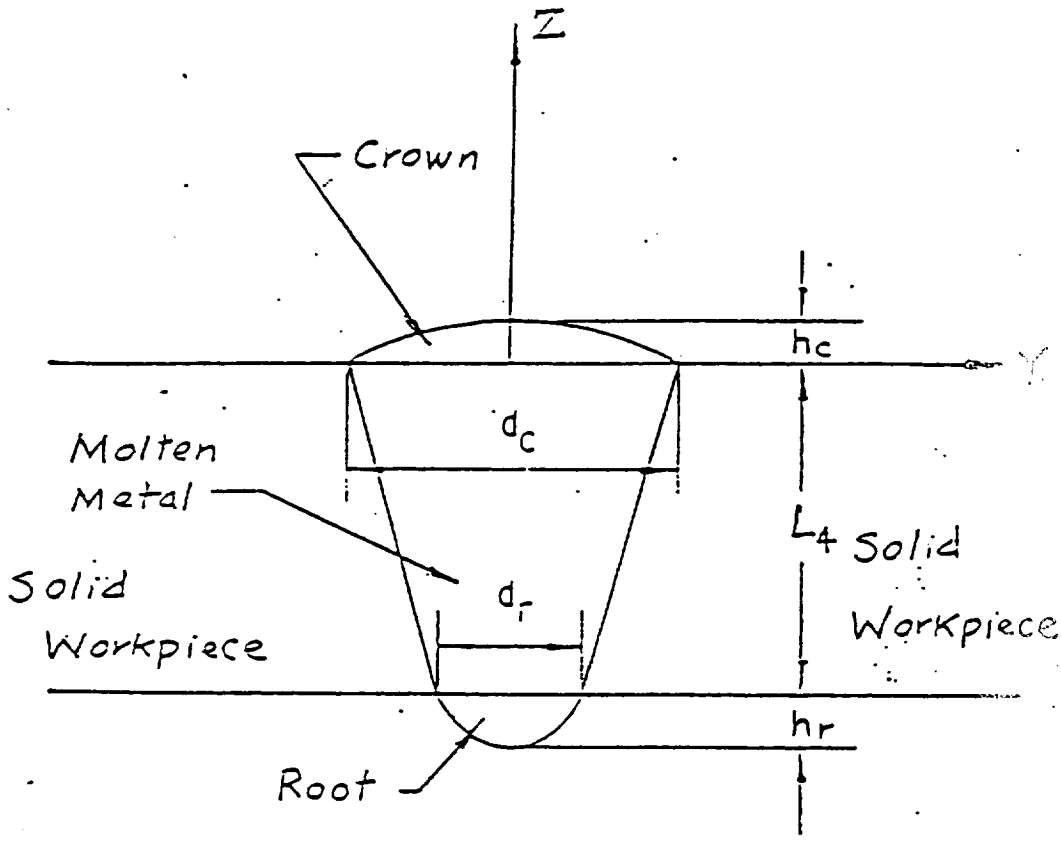
Z
Crown
hc
dc
Molten
Metal
L4 Solid
Workpiece
Solid
Workpiece
dr
hr
Root

Fig. 8

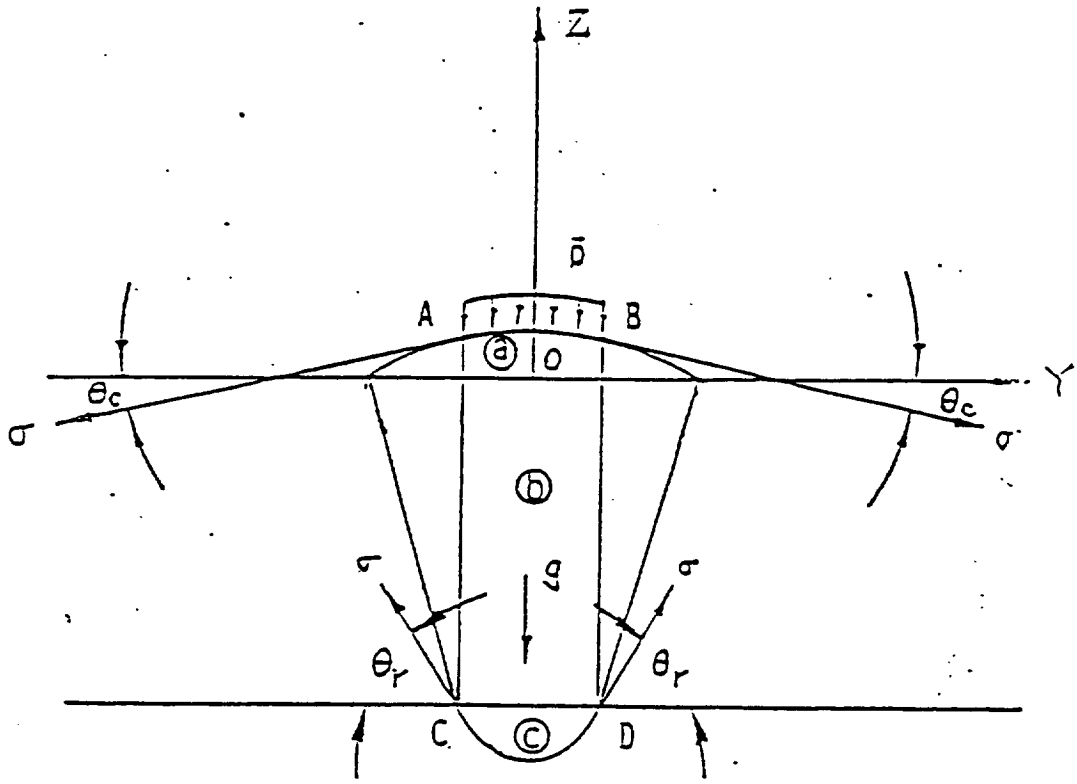

Fig. 9

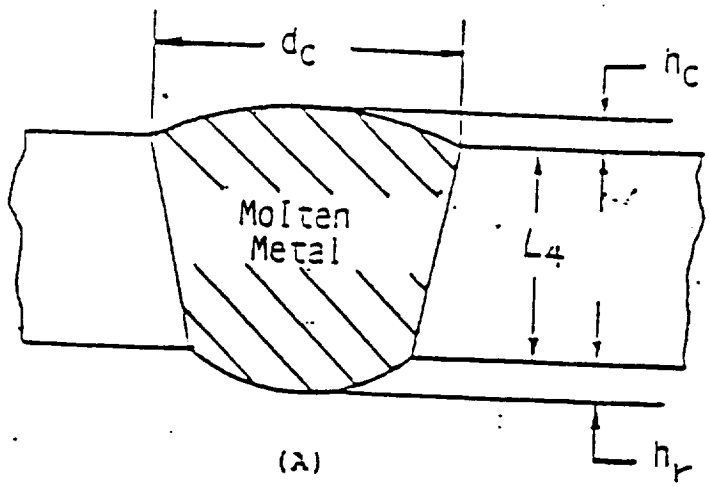

(A)

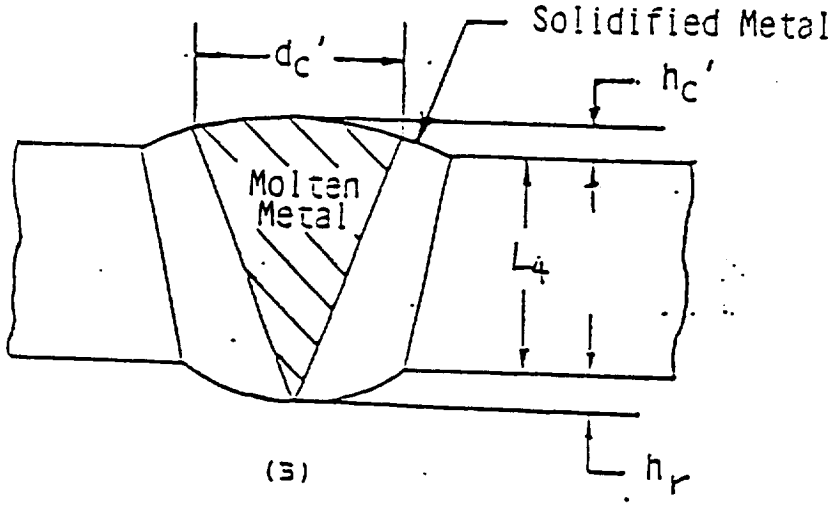

(B)

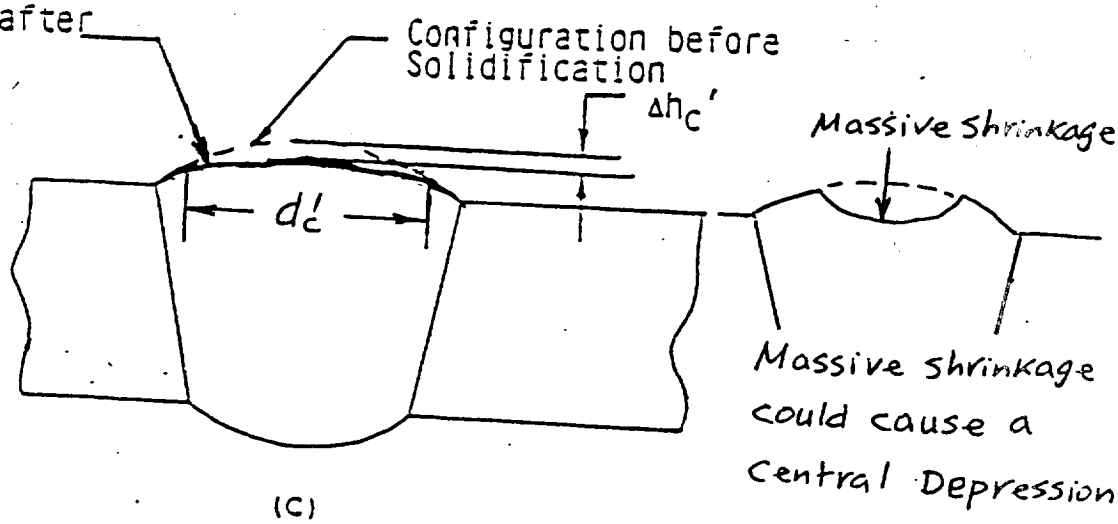

Fall in crown height occurs only over d_c' and not over already solid borders.

(C)

Figure 10 (A, B, C)

Appendix A

********** COMPUTER PROGRAM FOR VPPA MODELING **********

```
C-----------------------------------------------------------------------
C       PROGRAM WELDBOTH.FOR,COMPILED ON FEB. 26,1993
C
C         Line source , keyhole diameter is variable along the axis
C         of keyhole
c
      DIMENSION POW1(11),POW2(11),POW3(11),POW4(11)
      DIMENSION ENT1(11),ENT2(11),ENT3(11),ENT4(11),TABMPL(26)
      DIMENSION QLOS1(10),QLOS2(10),QLOS3(10),QLOS4(10),TABMSD(26)
      DIMENSION TEMP1(11),TEMP2(11),TEMP3(11),TEMP4(11),BHOLE(10)
      DIMENSION ELOS2(10),ELOS4(10),QSEGM(10),XSOUR(10),BHOLE0(10)
      DIMENSION AREA(10),DUDL1(10),DUDL2(10),DUDL3(10),QSOUR(10)
      DIMENSION R1(11),R2(11),FLWPL(11),FLWSD(11),ENERG(11)
      COMMON/DAT10/NX,NY,NZ,X(25),Y(20),TM,T0,THK,EPSL,DENS,HFUSI
      COMMON MMM
      COMMON TABTEM(26),TABIPL(26),TABCPL(26),TABKPL(26),TABISD(26)
      COMMON ITMAX,DHMAX,DTMAX
      COMMON TAMBI,DNOZL,FMPL
      COMMON TABCSD(26),TABKSD(26)
      COMMON TW4,MREG4,NREG4
      COMMON PLM,SDM
      OPEN(5,FILE='C:WELDTAB.USE')
      OPEN(6,FILE='C:WELDIN.USE')
      OPEN(7,FILE='C:WELDOU.USE')
      READ(5,*) MMM
      READ(5,*) (TABTEM(I),I=1,MMM)
      READ(5,*) (TABIPL(I),I=1,MMM)
      READ(5,*) (TABCPL(I),I=1,MMM)
      READ(5,*) (TABKPL(I),I=1,MMM)
      READ(5,*) (TABISD(I),I=1,MMM)
      READ(5,*) (TABCSD(I),I=1,MMM)
      READ(5,*) (TABKSD(I),I=1,MMM)
      READ(5,*) (TABMPL(I),I=1,MMM)
      READ(5,*) (TABMSD(I),I=1,MMM)
      READ(6,*) NREG1,NREG2,NREG3,NREG4
      READ(6,*) VA,VC
      READ(6,*) FIA1,FIA2,FIA3
      READ(6,*) TIME,TIMER
      READ(6,*) DISL1,DISL2,DISL3,DISL4
      READ(6,*) VVE,VVK
      READ(6,*) APIL,APILR,AMAI,AMAIR
      READ(6,*) DNOZL,DSHID,VPL,VSD
      READ(6,*) PLMOL,SDMOL,UR
      READ(6,*) ITMAX,DHMAX,DTMAX
      READ(6,*) TW1,TW2,TW4,HSUR2,HSUR4
      READ(6,*) DXW,TAMBI,DPOLAR,AMDW
      READ(6,*) PSIA,PAMBI,CPSD
      READ(6,*) ALFA,VWELD
      READ(6,*) NX,NY
      READ(6,*) X(1),X(NX)
      READ(6,*) Y(1),Y(NY)
```

```
      READ(6,*) TM,TO
      READ(6,*) THK,EPSL
      READ(6,*) DENS,HFUSI
      VOLPL=VPL/1.27133/1.E5
      VOLSD=VSD/1.27133/1.E5
      FMPL=VOLPL*PAMBI*PLMOL/8315./TAMBI
      FMSD=VOLSD*PAMBI*SDMOL/8315./TAMBI
      UH=VOLSD*4./3.14159/(DSHID**2-DNOZL**2)
      AREAW=3.14159*DPOLAR**2/4.
      WRITE(7,1030) DISL1,DISL2,DISL3,DISL4
      WRITE(7,1040) APIL,APILR,AMAI,AMAIR
      WRITE(7,1060) FIA1,FIA2,FIA3
      WRITE(7,1070) VA,VC
      WRITE(7,1130) PLMOL,SDMOL,UR
      ELOS=1.5*VVK/VVE/1.E10
      GHW=((AMAI+APIL)*(VC-FIA1)*TIME+(AMAIR-APILR)*(VA+FIA1)*
     $     TIMER)/(TIME+TIMER)/1000.
      CONDW=AMDW*AREAW*(TW1-TAMBI)/DXW
      POW1(1)=GHW-CONDW
      ENT1(1)=POW1(1)/FMPL
      CALL INSEP(TABIPL,TABTEM,ENT1(1),TEMP1(1))
      ELOS1=ELOS*TEMP1(1)*(AMAIR-APILR)*TIMER/(TIME+TIMER)
      AMPCP1=((AMAI+APIL)*TIME+(AMAIR-APILR)*TIMER)/(TIME+TIMER)
      DX1=DISL1/FLOAT(NREG1)
      GEOL1=3.14159*((DPOLAR+DNOZL)/2.)**2/4./DX1
      VOLUM1=3.14159*((DNOZL+DPOLAR)/2.)**2/4.*DX1
      MREG1=NREG1+1
      SUMQ1=0.
      DUBC=0.
      DO 40 M=2,MREG1
      N=M-1
      DUDL1(N)=2000.
      QLOS1(N)=0.
      NN1=0
10    CONTINUE
      NN1=NN1+1
      IF(NN1.GT.200) THEN
        WRITE(*,*)'       NN1.GT.200.  Erro stop'
        STOP
      ENDIF
      DP1=DUDL1(N)*DX1*AMPCP1/1000.-QLOS1(N)
      POW1(M)=POW1(N)+DP1
      ENT1(M)=POW1(M)/FMPL
      ENTCP1=(ENT1(N)+ENT1(M))/2.
      CALL INSEP(TABIPL,TABTEM,ENTCP1,TEMCP1)
      QLOS1(N)=VOLUM1*4.*1.E7*(TEMCP1/15000.)**16/
     $          (1.+(TEMCP1/15000.)**16)
      CALL INSEP(TABTEM,TABMPL,TEMCP1,PLMHO)
      OHM1=1./PLMHO/GEOL1
      DUDL=AMPCP1*OHM1/DX1
      DIFU=1.-DUDL/DUDL1(N)
      IF(ABS(DIFU).GE.0.005) THEN
        DUDL1(N)=(DUDL+DUDL1(N))/2.
        GO TO 10
```

```
          ENDIF
          DUBC=DUBC+DUDL1(N)*DX1
          SUMQ1=SUMQ1+QLOS1(N)
          CALL INSEP(TABIPL,TABTEM,ENT1(M),TEMP1(M))
   40   CONTINUE
C         WRITE(7,1170) (POW1(I),I=1,MREG1)
C         WRITE(7,1180) (ENT1(I),I=1,MREG1)
C         WRITE(7,1190) (QLOS1(I),I=1,NREG1)
C         WRITE(7,1200) (TEMP1(I),I=1,MREG1)
C         WRITE(7,1220) (DUDL1(I),I=1,NREG1)
C         WRITE(7,1210) SUMQ1,DUBC
C-----------------------------------------------------------------
        POW2(1)=POW1(MREG1)
        ENT2(1)=ENT1(MREG1)
        TEMP2(1)=TEMP1(MREG1)
        AMPCP2=(AMAI*TIME+(AMAIR-APILR)*TIMER)/(TIME+TIMER)
        DX2=DISL2/FLOAT(NREG2)
        AREA2=3.14159*DNOZL*DX2
        GEOL2=3.14159*DNOZL**2/4./DX2
        MREG2=NREG2+1
C       WRITE(7,1230)
        GHN1=(APIL*FIA2*TIME+APILR*FIA2*TIMER)/(TIME+TIMER)/1000.
        GHN2=(APIL*VA*TIME+APILR*VA*TIMER)/(TIME+TIMER)/1000.
        SUMQ2=GHN1+PSIA*GHN2
        DUCG=0.
        DO 80 M=2,MREG2
          N=M-1
          XM=FLOAT(N)*DX2-DX2/2.
          DUDL2(N)=2000.
          QLOS2(N)=0.
          NN2=0
   50     CONTINUE
          NN2=NN2+1
          IF(NN2.GT.200)THEN
            WRITE(*,*)'    Erro Stop      ENT3=',ENT3
            STOP
          ENDIF
          IF(NREG2.EQ.1)THEN
            ELOS2(N)=ELOS*TEMP2(N)*(APIL*TIME+APILR*TIMER)/(TIME+TIMER)
           ELSE IF(NREG2.NE.1.AND.N.EQ.1)THEN
            ELOS2(N)=ELOS*TEMP2(N)*APIL*TIME/(TIME+TIMER)
             ELSE IF(NREG2.NE.1.AND.N.EQ.NREG2)THEN
            ELOS2(N)=ELOS*TEMP2(N)*APILR*TIMER/(TIME+TIMER)
          ENDIF
          DP2=DUDL2(N)*DX2*AMPCP2/1000.+(1.-PSIA)*GHN2/FLOAT(NREG2)
     $       -ELOS2(N)-QLOS2(N)
          POW2(M)=POW2(N)+DP2
          ENT2(M)=POW2(M)/FMPL
          ENTCP=(ENT2(N)+ENT2(M))/2.
          CALL INSEP(TABIPL,TABTEM,ENTCP,TEMCP)
          CALL INSEP(TABTEM,TABKPL,TEMCP,AMD)
          CALL INSEP(TABTEM,TABCPL,TEMCP,CP)
          CALL INSEP(TABTEM,TABMPL,TEMCP,PLMHO)
          COEFC=2.*FMPL*CP/3.14159/AMD
```

```
          XPLUS=COEFC/XM
          VNUX=0.2233*XPLUS**0.7455+3.66
          ALFAX=VNUX*AMD/DNOZL
          QLOS2(N)=ALFAX*AREA2*(ENTCP-HSUR2)/CP
          OHM2=1./PLMHO/GEOL2
          DUDL=AMPCP2*OHM2/DX2
          DIFU=1.-DUDL/DUDL2(N)
          IF(ABS(DIFU).GE.0.005) THEN
            DUDL2(N)=(DUDL+DUDL2(N))/2.
            GO TO 50
          ENDIF
          DUCG=DUCG+DUDL2(N)*DX2
          SUMQ2=SUMQ2+QLOS2(N)+ELOS2(N)
          CALL INSEP(TABIPL,TABTEM,ENT2(M),TEMP2(M))
   80   CONTINUE
C         WRITE(7,1250) (POW2(I),I=1,MREG2)
C         WRITE(7,1260) (ENT2(I),I=1,MREG2)
C         WRITE(7,1270) (QLOS2(I),I=1,NREG2)
C         WRITE(7,1280) (TEMP2(I),I=1,MREG2)
C         WRITE(7,1290) (ELOS2(I),I=1,NREG2)
C         WRITE(7,1300) (DUDL2(I),I=1,NREG2)
C         WRITE(7,1310) SUMQ2,DUCG
C         WRITE(7,1320)
C-----------------------------------------------------------------
        RO=DNOZL/2.
        POW3(1)=POW2(MREG2)
        MITER=0
   90   CONTINUE
          MITER=MITER+1
          IF(MITER.GT.200) THEN
            WRITE(*,*)'    Erro Stop     MITER.GT.200,DPP=',DPP
            STOP
          ENDIF
          ENT3(1)=POW3(1)/FMPL
          CALL INSEP(TABIPL,TABTEM,ENT3(1),TEMP3(1))
          DENSO=PAMBI*PLMOL/8315./TEMP3(1)
          UO=FMPL/DENSO/3.14159/RO**2
          ENERG(1)=FMPL*UO**2/2./1000.
          PPP=POW2(MREG2)-ENERG(1)
          DPP=ABS(1.-PPP/POW3(1))
          POW3(1)=PPP
        IF(DPP.GE.0.005) GO TO 90
        COEFM=UH/UO
C        WRITE(7,1340) UH,UO,COEFM
        VMID1=(1.-COEFM)/(1.+COEFM)
        VMID3=1.+0.8*COEFM-0.45*COEFM**2
        DX3=DISL3/FLOAT(NREG3)
        MREG3=NREG3+1
        SUMQ3=0.
        DUGE=0.
        R1(1)=RO
        R2(1)=RO
        FLWPL(1)=FMPL
        FLWSD(1)=0.
```

```
      AMPCP3=(AMAI*TIME+AMAIR*TIMER)/(TIME+TIMER)
      DO 190 M=2,MREG3
        N=M-1
        X3=FLOAT(N)*DX3
        VMID2=0.27*X3
        VMID4=VMID1*(0.416+0.134*COEFM+0.021*VMID2*VMID1*VMID3/R0)
        R1(M)=R0-VMID2*VMID4
        VMIDA=0.021*VMID3/R0
        VMIDB=0.416+0.134*COEFM
        VMIDC=R1(M)-R0
        VMIDD=(-VMIDB+SQRT(VMIDB**2-4.*VMIDA*VMIDC))/2./VMIDA
        R2(M)=R1(M)+VMIDD
        NOM=0
        TBEGI=TEMP3(1)
        DENBEG=DENS0
        DR=(R2(M)-R1(M))/10.
        DUDL2(N)=2000.
        GEOL3=3.14159*R2(M)**2/DX3
120     CONTINUE
        NOM=NOM+1
        IF(NOM.GT.200) THEN
          WRITE(*,*)'     Erro Stop     ITER.IN STANDOFF EXCEED 200'
          STOP
        ENDIF
        FLWPL(M)=3.14159*R1(M)**2*U0*DENBEG
        FLWSD(M)=0.
        ENERG(M)=FLWPL(M)*U0**2/2./1000.
        CALL INSEP(TABTEM,TABIPL,TBEGI,EBEGI)
        POWER=FLWPL(M)*EBEGI
        DO 150 K=1,10
          RMID=FLOAT(K)*DR-DR/2.+R1(M)
          ATA=(R2(M)-RMID)/(R2(M)-R1(M))
          UMID=U0-(U0-UH)*(1.-ATA**1.5)**2
          TMID=TBEGI-(TBEGI-TAMBI)*(1.-ATA)
          PGPL=PAMBI/(1.+(1./ATA-1.)*PLMOL/SDMOL)
          PGSD=PAMBI-PGPL
          DENPL=PGPL*PLMOL/8315./TMID
          DENSD=PGSD*SDMOL/8315./TMID
          VOLUM=2.*3.14159*RMID*DR*UMID
          FLWPL(M)=FLWPL(M)+VOLUM*DENPL
          FLWSD(M)=FLWSD(M)+VOLUM*DENSD
          ENERG(M)=ENERG(M)+(DENPL+DENSD)*VOLUM*UMID**2/2./1000.
          IF(TMID.GE.3000.) THEN
            CALL INSEP(TABTEM,TABIPL,TMID,ENTPL)
            CALL INSEP(TABTEM,TABISD,TMID,ENTSD)
           ELSE
            ENTPL=TABCPL(1)*TMID
            ENTSD=TABCSD(1)*TMID
          ENDIF
          POWER=POWER+VOLUM*(DENPL*ENTPL+DENSD*ENTSD)
150     CONTINUE
        POWRCP=(POWER+POW3(N))/2.
        PLCP=(FLWPL(M)+FLWPL(N))/2.
        SDCP=(FLWSD(M)+FLWSD(N))/2.
```

```
      CALL AVERT(PLCP,SDCP,POWRCP,TABTEM,TABIPL,TABISD,TCP)
      VRADI=3.14159*(R2(M)+R2(N))**2/4.*DX3
      QLOS3(N)=VRADI*4.*1.E7*(TCP/15000.)**16/(1.+(TCP/15000.)**16)
      CALL INSEP(TABTEM,TABMPL,TCP,PLMHO)
      CALL INSEP(TABTEM,TABMSD,TCP,SDMHO)
      CPMHO=((FLWPL(M)+FLWPL(N))*PLMHO+(FLWSD(M)+FLWSD(N))*SDMHO)/
     $          (FLWPL(M)+FLWPL(N)+FLWSD(M)+FLWSD(N))
      OHM3=1./CPMHO/GEOL3
      DUDL3(N)=OHM3*AMPCP3/DX3
      DP3=OHM3*AMPCP3**2/1000.
      POW3(M)=POW3(N)+DP3-QLOS3(N)+(FLWSD(M)-FLWSD(N))*CPSD*TAMBI-
     $           (ENERG(M)-ENERG(N))
      PMP=1.-POWER/POW3(M)
      IF(ABS(PMP).GE.0.010) THEN
        TBEGI=TBEGI*(1.+PMP/10.)
        DENBEG=PAMBI*PLMOL/8315./TBEGI
        UO=UO*FMPL/FLWPL(M)
        GO TO 120
      ENDIF
      WRITE(*,1390) N,NOM,PMP
      SUMQ3=SUMQ3+QLOS3(N)
      CALL AVERT(FLWPL(M),FLWSD(M),POWER,TABTEM,TABIPL,TABISD,
     $               TEMP3(M))
      ENT3(M)=POW3(M)/(FLWPL(M)+FLWSD(M))
      DUGE=DUGE+DUDL3(N)*DX3
  190 CONTINUE
      WRITE(*,1480) (FLWPL(I),I=1,MREG3)
      WRITE(7,1480) (FLWPL(I),I=1,MREG3)
      WRITE(7,1490) (FLWSD(I),I=1,MREG3)
      PAID=FLWSD(MREG3)*CPSD*TAMBI
C-----------------------------------------------------------------------
      RBOUND=RO
      ITWID=1
      DO 191 N=1,NREG4
        BHOLE(N)=RBOUND
  191 CONTINUE
  195 CONTINUE
      ATARB=(R2(MREG3)-RBOUND)/(R2(MREG3)-R1(MREG3))
      TBOUND=TBEGI-(1.-ATARB)*(TBEGI-TAMBI)
      WRITE(7,1540) TBOUND
      DR=(R2(MREG3)-RBOUND)/10.
      PLLOS=0.
      SDLOS=0.
      QLOSJ=0.
      QGETJ=0.0
      SDGET=0.0
      DO 220 K=1,10
        RMID=FLOAT(K)*DR-DR/2.+RBOUND
        ATA=(R2(MREG3)-RMID)/(R2(MREG3)-R1(MREG3))
        UMID=UO-(UO-UH)*(1.-ATA**1.5)**2
        TMID=TBEGI-(TBEGI-TAMBI)*(1.-ATA)
        PGPL=PAMBI/(1.+(1./ATA-1.)*PLMOL/SDMOL)
        PGSD=PAMBI-PGPL
        DENPL=PGPL*PLMOL/8315./TMID
```

```
          DENSD=PGSD*SDMOL/8315./TMID
          VOLUM=2.*3.14159*RMID*DR*UMID
          PLLOS=PLLOS+VOLUM*DENPL
          SDLOS=SDLOS+VOLUM*DENSD
          IF(TMID.GE.3000.) THEN
            CALL INSEP(TABTEM,TABIPL,TMID,ENTPL)
            CALL INSEP(TABTEM,TABISD,TMID,ENTSD)
           ELSE
            ENTPL=TABCPL(1)*TMID
            ENTSD=TABCSD(1)*TMID
          ENDIF
          QLOSJ=QLOSJ+VOLUM*(DENPL*ENTPL+DENSD*ENTSD)
  220 CONTINUE
C-----------------------------------------------------------------
      GHK1=(AMAI*FIA3*TIME+AMAIR*(UR-FIA3)*TIMER)/(TIME+TIMER)/1000.
      GHK2=(AMAI*VA*TIME+AMAIR*VC*TIMER)/(TIME+TIMER)/1000.
C-----------------------------------------------------------------
  225 CONTINUE
      POWER=POW3(MREG3)-QLOSJ+QGETJ
      PLM=FMPL-PLLOS
      SDM=FLWSD(MREG3)-SDLOS+SDGET
      POW4(1)=POWER+(1.-PSIA)*GHK2
      ENT4(1)=POW4(1)/(PLM+SDM)
      CALL AVERT(PLM,SDM,POW4(1),TABTEM,TABIPL,TABISD,TEMP4(1))
      SUMQ4=0.
      DP4=0.
      ELOSS=ELOS*TEMP4(1)*AMAI*TIME/(TIME+TIMER)
      GHK12=GHK1+PSIA*GHK2
C      WRITE(7,1555)
      DL=DISL4/FLOAT(NREG4)
      MREG4=NREG4+1
      DO 230 I=2,MREG4
        J=I-1
        XSOUR(J)=FLOAT(J)*DL-DL/2.
        AREA(J)=3.14159*BHOLE(J)*DL
  230 CONTINUE
C     WRITE(7,1560) (XSOUR(K),K=1,NREG4)
C     WRITE(7,1570) RBOUND
C     WRITE(7,1580) (AREA(K),K=1,NREG4)
      WRITE(7,1590) PLM,SDM,TEMP4(1)
      DO 240 M=2,MREG4
        N=M-1
        QSEGM(N)=3.*GHK12*(1.-XSOUR(N)/DISL4)**2*DL/DISL4
        ELOS4(N)=3.*ELOSS*(1.-XSOUR(N)/DISL4)**2*DL/DISL4
        CALL CONV4(XSOUR(N),AREA(N),DP4,POW4(N),POW4(M),ENT4(M),
     $                    QLOS4(N),HSUR4,ELOS4(N),BHOLE(N))
        CALL AVERT(PLM,SDM,POW4(M),TABTEM,TABIPL,TABISD,TEMP4(M))
        QSOUR(N)=QLOS4(N)+ELOS4(N)+QSEGM(N)
        SUMQ4=SUMQ4+QSOUR(N)
  240 CONTINUE
        CALL WIDTH(SUMQ4,QSOUR,XSOUR,NREG4,DISL4,ALFA,VWELD,BHOLE0,ITWID)
        ITWID=ITWID+1
        WRITE(*,*)'R0=',R0,' RBOUND=',RBOUND,'  R2(MREG3)=',R2(MREG3)
      DRB=0.0
```

```
      DO 250 J=1,NREG4
        DRB=AMAX1(DRB,ABS(BHOLE0(J)-BHOLE(J))/BHOLE(J))
  250 CONTINUE
      IF(DRB.GE.0.002)THEN
        DO 260 J=1,NREG4
          BHOLE(J)=BHOLE(J)+.5*(BHOLE0(J)-BHOLE(J))
  260   CONTINUE
        RBOUND=BHOLE(1)
        IF(RBOUND.GE.R2(MREG3))THEN
          DENSD=PAMBI*SDMOL/8315./TAMBI
          QLOSJ=0.0
          PLLOS=0.0
          SDLOS=0.0
          SDGET=3.14159*(RBOUND**2-R2(MREG3)**2)*UH*DENSD
          QGETJ=SDGET*TAMBI*CPSD
          GO TO 225
         ELSE
          GO TO 195
        ENDIF
      ENDIF
C       WRITE(7,1600) QIMPIN
C       WRITE(7,1610) (POW4(I),I=1,MREG4)
C       WRITE(7,1620) (ENT4(I),I=1,MREG4)
C       WRITE(7,1630) (TEMP4(I),I=1,MREG4)
C       WRITE(7,1640) (QLOS4(I),I=1,NREG4)
C       WRITE(7,1650) (ELOS4(I),I=1,NREG4)
C       WRITE(7,1660) (QSEGM(I),I=1,NREG4)
C       WRITE(7,1670) (QSOUR(I),I=1,NREG4)
      WRITE(7,1680) SUMQ4
      PTOTOU=CONDW+SUMQ1+SUMQ2+SUMQ3+SUMQ4+POW4(MREG4)
     $       +QLOSJ+ENERG(MREG3)
        PTOTIN=GHW+(AMPCP1*DUBC+AMPCP2*DUCG+AMPCP3*DUGE)/1000.
     $       +GHN1+GHN2+GHK1+GHK2+PAID
      WRITE(7,1690) PTOTIN,PTOTOU
      PERCQW=CONDW/PTOTIN
      PERQG=SUMQ1/PTOTIN
      PERQN=SUMQ2/PTOTIN
      PERQSR=SUMQ3/PTOTIN
      PERQSC=QLOSJ/PTOTIN
      PERQW=SUMQ4/PTOTIN
      PERQD=POW4(MREG4)/PTOTIN
      PERSUM=PERCQW+PERQG+PERQN+PERQSR+PERQSC+PERQW+PERQD
      WRITE(7,1700) CONDW,PERCQW
      WRITE(7,1710) SUMQ1,PERQG
      WRITE(7,1720) SUMQ2,PERQN
      WRITE(7,1730) SUMQ3,PERQSR
      WRITE(7,1740) QLOSJ,PERQSC
      WRITE(7,1750) SUMQ4,PERQW
      WRITE(7,1760) POW4(MREG4),PERQD
      WRITE(7,1770) PERSUM
      WRITE(7,1780)  AMPCP1,AMPCP2,AMPCP3
      DUBE=DUBC+DUCG+DUGE
      DUAF=DUBE+VA+VC+FIA3-FIA1
      DUAFR=DUBE+VA+VC-FIA3+FIA1+UR
```

```
      WRITE(7,1790) DUBE,DUAF,DUAFR
      DUPF=DUBC+VA+VC+FIA2-FIA1
      DUPR=FIA2-FIA1-DUBC-DUCG
      PTOTAL=((AMAI*DUAF+APIL*DUPF)*TIME+(AMAIR*DUAFR+APILR*DUPR)*
     $       TIMER)/(TIME+TIMER)/1000.
C     PTOTAL=(AMAI*DUAF*TIME+AMAIR*DUAFR*TIMER)/(TIME+TIMER)/1000.
      ATAQ4=SUMQ4/PTOTAL
      WRITE(7,1800) DUPF,DUPR
      WRITE(7,1810) PTOTAL,SUMQ4,ATAQ4
      WRITE(7,*)'  CROWN WIDTH=',2.*BHOLE(1),'(mm)'
      WRITE(7,*)'   ROOT WIDTH=',2.*BHOLE(NREG4),'(mm)'
        STOP
C-----------------------------------------------------------------------
 1000   FORMAT(///5X,'INPUT DATA:')
 1010   FORMAT(/2X,'PLSMA (kg/s)',E12.5,2X,'SHIELD (kg/s)',E12.5)
 1020   FORMAT(/5X,'TW OF W,NOZZLE,HOLE,INITIAL SOLID',3F8.1,/
     $         5X,'ENT. OF ARC IN TW OF NOZZLE,HOLE',2E12.5)
 1030 FORMAT(/5X,'L1,L2,L3,L4 (m)',2X,4F10.8)
 1040 FORMAT(/5X,'PILOT I(+)=',F8.2,5X,'PILOT I(-)=',F8.2,/
     $         5X,'MAIN I(+)=',F8.2,5X,'MAIN I(-)=',F8.2)
 1050   FORMAT(/5X,'t(+)=',E11.4,5X,'t(-)=',E11.4)
 1060   FORMAT(/5X,'WORK FUNCTION 1,2,3 =',3F5.2)
 1070   FORMAT(/5X,'ANODE DROP=',F5.2,
     $         2X,'CATHOD DROP=',F5.2)
 1080   FORMAT(/5X,'e=',E12.5,5X,'k=',E12.5)
 1090 FORMAT(/5X,'NREG1=',I3,2X,'NREG2=',I3,2X,'NREG3=',I3,
     $         2X,'NREG4=',I3)
 1100 FORMAT(/5X,'NOZZLE DIAM.(m)',F8.6,2X,'SHIELD DIAM.(m)',F8.6)
 1110 FORMAT(/5X,'LENGTH OF POLARITY W =',E12.5,
     $        /5X,'ENVIROMENT TEMP. =',F6.1,2X,'AREA OF W POLARITY',
     $           E12.5,/5X,'AMD OF POLARITY W =',E12.5)
 1120 FORMAT(/5X,'ITMAX,DHMAX,DTMAX=',I4,E12.5,F6.4)
 1125 FORMAT(/5X,'PSIA=',F6.4,2X,'PAMBI(N/m**2)=',F10.1,/
     $         2X,'CP. OF HE IN AMBIENT (kJ/kg)=',E12.5,
     $         2X,' (m/s)',E12.5)
 1130 FORMAT(/5X,'PLASMA MOL.WEIGHT (kg/kmol)=',F8.4,2X,
     $        /5X,'SHIELD MOL.WEIGHT (kg/kmol)=',F8.4,
     $        /5X,'UR=',F5.1)
 1140 FORMAT(/2X,'GHW,CONDW,ELOS1(kw)',3E12.5)
 1150 FORMAT(//5X,'BEGINING OF SEGMENT ONE')
 1170 FORMAT(/2X,'POW1=',4E12.5,/7X,4E12.5)
 1180 FORMAT(/2X,'ENT1=',4E12.5,/7X,4E12.5)
 1190 FORMAT(/1X,'QLOS1=',4E12.5,/7X,4E12.5)
 1200 FORMAT(/2X,'TEMP1=',4E12.5,/8X,4E12.5)
 1210 FORMAT(/2X,'TOTAL LOSS IN GAP I',E12.5,2X,'DUBC(v)',F6.2)
 1220 FORMAT(/2X,'DUDL1',4E12.5,/7X,4E12.5)
 1230 FORMAT(//5X,'NOZZLE COMPUTATION')
 1240 FORMAT(/5X,'NN2.GT.100')
 1250 FORMAT(/5X,'POW2=',4E12.5/10X,4E12.5)
 1260 FORMAT(/5X,'ENT2=',4E12.5/10X,4E12.5)
 1270 FORMAT(/4X,'QLOS2=',4E12.5/10X,4E12.5)
 1280 FORMAT(/2X,'TEMP2',4E12.5,/7X,4E12.5)
 1290 FORMAT(/2X,'ELOS2',4E12.5,/7X,4E12.5)
 1300 FORMAT(/2X,'DUDL2',4E12.5,/7X,4E12.5)
```

```
 1310 FORMAT(/5X,'TOTAL LOSS IN NOZZLE =',E12.5,2X,'DUCG(v)',F6.2)
 1320 FORMAT(//5X,'STANDOFF COMPUTATION')
 1340 FORMAT(/5X,'UH,UO,COEFM',3E12.5)
 1350 FORMAT(/2X,'LINE 285 TBEGI',E12.4)
 1370 FORMAT(/1X,'ATA,TBEGI,TAMBI,TMID',4E11.4)
C1360 FORMAT(1X,'M,R1,R2,DR,RMID,ATA',I2,2E12.5,/5X,3E12.5)
 1380 FORMAT(/2X,'IN MAIN,NOM,MAR,MHE,POWER',I4,2X,3E10.3)
 1390 FORMAT(/2X,'ITER.IN STANDOFF,SEG.=',I2,2X,'NOM=',I4,
     $        2X,'PMP=',F10.6)
 1450 FORMAT(/2X,'TOTAL LOSS IN STANDOFF =',E12.5,2X,'DUGE(v)',F6.2)
 1410 FORMAT(/5X,'POW3=',4E12.5,/10X,4E12.5)
 1430 FORMAT(/4X,'QLOS3=',4E12.5,/10X,4E12.5)
 1440 FORMAT(/4X,'TEMP3=',4E12.5,/10X,4E12.5)
 1460 FORMAT(/5X,'R1(m)=',4F10.8,/11X,4F10.8)
 1470 FORMAT(/5X,'R2(m)=',4F10.8,/11X,4F10.8)
 1480 FORMAT(/5X,'FLWPL=',4E12.5,/11X,4E12.5)
 1490 FORMAT(/5X,'FLWSD=',4E12.5,/11X,4E12.5)
 1500 FORMAT(/5X,'ENERG=',4E12.5,/11X,4E12.5)
 1510 FORMAT(/2X,'DUDL3',4E12.5,/7X,4E12.5)
 1520 FORMAT(/5X,'POWER AID FROM SHIELD, PAID(kW)=',E12.5)
 1530 FORMAT(/2X,'VELOC.,TEMP.IN CORE AT LAST',2E12.5)
 1540 FORMAT(/5X,'T OF BOUNDARY, TBOUND=',E12.5)
 1550 FORMAT(/5X,'CONVECTIVE LOSS OF JET (kW)',E12.5)
 1555 FORMAT(//10X,'WORKPIECE COMPUTATION')
 1560 FORMAT(/2X,'XSOUR',2X,5F8.6)
 1570 FORMAT(/5X,'RADIUS OF KEYHOLE (m)=',E12.5)
 1580 FORMAT(/2X,'AREA(m**2)',4E12.5,/12X,4E12.5)
 1590 FORMAT(/4X,'PLM,SDM,TEMP4(1)',3E14.5)
 1600 FORMAT(/5X,'IMPINGE LOSS (kw)',F8.5)
 1610 FORMAT(/2X,'POW4=',4E12.5,/7X,4E12.5)
 1620 FORMAT(/2X,'ENT4=',4E12.5,/7X,4E12.5)
 1630 FORMAT(/2X,'TEMP4=',4E12.5,/8X,4E12.5)
 1640 FORMAT(/2X,'QLOS4=',4E12.5,/8X,4E12.5)
 1650 FORMAT(/2X,'ELOS4=',4E12.5,/8X,4E12.5)
 1660 FORMAT(/2X,'QSEGM=',4E12.5,/8X,4E12.5)
 1670 FORMAT(/2X,'QSOUR=',4E12.5,/8X,4E12.5)
 1680 FORMAT(/5X,'TOTAL LOSS IN WORKPIECE =',E12.5)
 1690 FORMAT(5X,'TOTAL POWER INCLUDING HELIUM, PTOTIN=',E12.5,/
     $       5X,'TOTAL POWER FROM LOSS, PTOTOU=',E12.5)
 1700 FORMAT(/2X,'POLARITY CONDUC. LOSS AND PERCENT.',2E12.5)
 1710 FORMAT(/2X,'GAP LOSS AND PERCENTAGE',2E12.5)
 1720 FORMAT(/2X,'NOZZLE LOSS AND PERCENTAGE',2E12.5)
 1730 FORMAT(/2X,'RADIAT.IN STANDOFF AND PERCENTAGE',2E12.5)
 1740 FORMAT(/2X,'CONVEC.IN STANDOFF AND PERCENTAGE',2E12.5)
 1750 FORMAT(/2X,'WORKPIECE LOSS AND PERCENTAGE',2E12.5)
 1760 FORMAT(/2X,'DISCHARGE LOSS AND PERCENTAGE',2E12.5)
 1770 FORMAT(/5X,'SUM. PERCENTAGE',F8.5)
 1780 FORMAT(/5X,'AMPCP1,2,3',3E12.5)
 1790 FORMAT(/5X,'DUBE,DUAF,DUAFR',3E12.5)
 1800 FORMAT(/4X,'DUPF=',E12.4,4X,'DUPR=',E12.4)
 1810 FORMAT(/2X,'POWER,Q4,ATAQ4=', 3E14.5)
       END
C
C-----------------------------------------------------------------
```

```
C
      SUBROUTINE CONV4(XMID,AMID,DP,PA,PB,HB,PCONV,HW,QELOS,RHOLE)
      COMMON MMM
      COMMON TABTEM(26),TABIPL(26),TABCPL(26),TABKPL(26),TABISD(26)
      COMMON ITMAX,DHMAX,DTMAX
      COMMON TAMBI,DNOZL,FMPL
      COMMON TABCSD(26),TABKSD(26)
      COMMON TW4,MREG4,NREG4
      COMMON PLM,SDM
      PB=PA
      NOM=0
200   CONTINUE
      NOM=NOM+1
      IF(NOM.GT.ITMAX) THEN
      WRITE(*,*)'   Erro Stop   ITERATIONS EXCEED ITMAX IN CONV4'
      STOP
      ENDIF
      PCP=(PA+PB)/2.
      HCP=PCP/(PLM+SDM)
      CALL AVERT(PLM,SDM,PCP,TABTEM,TABIPL,TABISD,TCP)
      CALL INSEP(TABTEM,TABKPL,TCP,PLAMD)
      CALL INSEP(TABTEM,TABKSD,TCP,SDAMD)
      AMD=(PLAMD*PLM+SDAMD*SDM)/(PLM+SDM)
      CALL INSEP(TABTEM,TABCPL,TCP,PLCP)
      CALL INSEP(TABTEM,TABCSD,TCP,SDCP)
      CP=(PLCP*PLM+SDCP*SDM)/(PLM+SDM)
      COEFC=2.*(PLM+SDM)*CP/3.14159/AMD
      XPLUS=COEFC/XMID
      VNUX=0.2233*XPLUS**0.7455+3.66
      ALFAX=VNUX*AMD/RHOLE/2.
      PCONV=ALFAX*AMID*(HCP-HW)/CP
      POU=PA-PCONV+DP-QELOS
      HB=POU/(PLM+SDM)
      DIFP=ABS(POU-PB)/PB
      PB=POU
      IF(DIFP.GE.DHMAX) GO TO 200
      END
C
C-----------------------------------------------------------------------
C
      SUBROUTINE AVERT(FLOPL,FLOSD,PSUM,TABT,TABPL,TABSD,TVERA)
      DIMENSION TABT(26),TABPL(26),TABSD(26)
      COMMON MMM
C     WRITE(7,3000) FLOPL,FLOSD,PSUM
      NN=0
      TVERA=10000.
10    CONTINUE
      NN=NN+1
      IF(NN.GT.200) THEN
      WRITE(*,*)'  Erro Stop    ITER.EXCEED 200 IN AVERT, THEN STOP'
      STOP
      ENDIF
      CALL INSEP(TABT,TABPL,TVERA,EPL)
      CALL INSEP(TABT,TABSD,TVERA,ESD)
```

```
      PCOMP=FLOPL*EPL+FLOSD*ESD
      DPOWR=1.-PCOMP/PSUM
      IF(ABS(DPOWR).GE.0.010) THEN
      TVERA=TVERA*(1.+DPOWR/10.)
      GO TO 10
      ENDIF
      RETURN
      END
C
C-----------------------------------------------------------------------
C
      SUBROUTINE INSEP(A,B,C,D)
      DIMENSION A(26),B(26)
      COMMON MMM
      IF(C.LT.A(1).OR.C.GT.A(MMM)) THEN
      WRITE(*,*)'    Erro Stop      INDEP. IS BEYOND SCOPE'
      WRITE(*,*)'  C=',C,'A(1)=',A(1),'A(MMM)=',A(MMM)
      STOP
      ENDIF
     DO 30 K=2,MMM
        IF((C.LE.A(K).AND.C.GE.A(K-1)).OR.
     $    (C.GE.A(K).AND.C.LE.A(K-1)))THEN
        D=B(K-1)+(B(K)-B(K-1))/(A(K)-A(K-1))*(C-A(K-1))
        GO TO 40
      ENDIF
 30   CONTINUE
 40   CONTINUE
      RETURN
 4010 FORMAT(/5X,'INDEP. C=',E12.4,5X,'DEPEND. D=',E12.4)
      END
C
C-----------------------------------------------------------------------
C
      SUBROUTINE WIDTH(QORIG,QSOUR,HH,NHH,H,ALPHA,VWELD,RMAX,ITWID)
      DIMENSION ZZ(34),TEMP(25,15,11),TEMP0(10,25,15,11)
      DIMENSION BEAD(30,10),QSOUR(10),QMOLT(10),HH(10),Q4K(10),QS(10),
     $          Z(11),RMAX0(11),RMAX(11)
      COMMON/DAT10/NX,NY,NZ,X(25),Y(20),TM,TO,THK,EPSL,DENS,HFUSI
      IF(ITWID.GT.1) GO TO 66
     IF(NX.GT.1)THEN
      DO 1 I=1,NX
        X(I)=X(1)+FLOAT(I-1)*(X(NX)-X(1))/FLOAT(NX-1)
1     CONTINUE
     ENDIF
     IF(NY.GT.1)THEN
      DO 5 J=1,NY
        Y(J)=Y(1)+FLOAT(J-1)*(Y(NY)-Y(1))/FLOAT(NY-1)
5     CONTINUE
      ENDIF
     NZ=NHH
     IF(NZ.GT.1)THEN
      DO 6 K=1,NZ
        Z(K)=FLOAT(K-1)*H/FLOAT(NZ-1)
6     CONTINUE
```

```
      ENDIF
      NOM=1
      DO 8 L=1,NHH
        HH(L)=FLOAT(L-1)*H/FLOAT(NHH-1)
    8 CONTINUE
C-----------------------------------------------------------------
        TMOLT=TM-TO
        V=VWELD*0.0254/60.
        V2A=-V/(2.*ALPHA)
        NITER=0
        NZ=NHH+1
        QTOTAL=QORIG
      DO 10 I=1,NZ
        RMAX(I)=0.0
        Z(I)=FLOAT(I-1)*H/FLOAT(NZ-1)
   10 CONTINUE
        DO 40 N=1,NHH
          QS(N)=QSOUR(N)
          DO 30 L=1,NZ
            DO 25 K=1,NY
                DO 20 J=1,NX
                  TEMPO(N,J,K,L)=0.
   20         CONTINUE
   25       CONTINUE
   30     CONTINUE
   40 CONTINUE
      DO 65 N=1,NHH
        HHH=HH(N)
        ZZ(1)=-16.*H-HHH
        ZZ(2)=-16.*H+HHH
        DO 50 K=3,34,2
          ZZ(K)=ZZ(K-2)+2.*H
          ZZ(K+1)=ZZ(K-1)+2.*H
   50   CONTINUE
        DO 64 K=1,NX
         DO 63 L=1,NY
          DO 62 J=1,NZ
           DO 60 M=1,34
            ZZZ=Z(J)-ZZ(M)
            XXX=X(K)
            YYY=Y(L)
            R=SQRT(XXX**2+YYY**2+ZZZ**2)
            RX=R+XXX
            RX=V2A*RX
            TEMPO(N,K,L,J)=TEMPO(N,K,L,J)+EXP(RX)/R
   60       CONTINUE
   62      CONTINUE
   63     CONTINUE
   64   CONTINUE
   65 CONTINUE
C-----------------------------------------------------------------
   66 CONTINUE
      NITER=NITER+1
      IF(NITER.GT.200) THEN
```

```
        WRITE(*,*)'  Erro Stop       NITER.GT.200 IN WIDTH, THEN STOP'
        STOP
      ENDIF
      DO 68 N=1,NHH
C       Q4K(N)=QS(N)/(4.*3.14159*THK)
        QMOLT(N)=(RMAX(N)+RMAX(N+1))*H/FLOAT(NHH)*V*DENS*HFUSI
        Q4K(N)=(QS(N)-QMOLT(N))/(4.*3.14159*THK)
   68 CONTINUE
        DO 75 K=1,NX
          DO 74 L=1,NY
            DO 73 J=1,NZ
              TEMP(K,L,J)=0.0
              DO 72 N=1,NHH
                TEMP(K,L,J)=TEMP(K,L,J)+Q4K(N)*TEMPO(N,K,L,J)
   72         CONTINUE
   73       CONTINUE
   74     CONTINUE
   75 CONTINUE
      DO 95 K=1,NZ
        RMAXO(K)=0.0
        DO 90 I=1,NX
          DO 80 J=2,NY
            L=J-1
            IF((TEMP(I,L,K).LT.TMOLT.AND.TEMP(I,J,K).GE.TMOLT).OR.
     $         (TEMP(I,L,K).GT.TMOLT.AND.TEMP(I,J,K).LE.TMOLT))THEN
              YMOLT=Y(L)+(Y(J)-Y(L))/(TEMP(I,J,K)-TEMP(I,L,K))*
     $              (TMOLT-TEMP(I,L,K))
              GO TO 85
            ENDIF
   80       CONTINUE
   85       RMAXO(K)=AMAX1(RMAXO(K),YMOLT)
   90     CONTINUE
   95 CONTINUE
      DRMAX=0
        DO 100 N=1,NZ
        DRMAX=AMAX1(DRMAX,ABS(RMAX(N)-RMAXO(N)))
        WRITE(*,*)'N=',N,' 2*RMAX(N)=',2.*RMAX(N),
     $              '  2*RMAXO(N)=',2.*RMAXO(N)
  100 CONTINUE
        WIDTHC=2.*RMAXO(1)
        WIDTHR=2.*RMAXO(NZ)
        write(*,*)' ROOT WIDTH=',WIDTHR,'  CROWN WIDTH=',WIDTHC
        write(7,*)' ROOT WIDTH=',WIDTHR,'  CROWN WIDTH=',WIDTHC
        QRCRO=0.
        QRROO=0.
        DO 120 I=2,NX
          I1=I-1
          DO 110 J=2,NY
            J1=J-1
            TRMID=(TEMP(I1,J,1)+TEMP(I1,J1,1)+TEMP(I,J1,1)
     $           +TEMP(I,J,1))/4.
            TCMID=(TEMP(I1,J,NZ)+TEMP(I1,J1,NZ)+TEMP(I,J1,NZ)
     $           +TEMP(I,J,NZ))/4.
            DX=X(I1)-X(I)
```

```
            DY=Y(J)-Y(J1)
            DAREA=2.*ABS(DX*DY)
            QRCRO=QRCRO+ABS(DAREA)*EPSL*0.00567*((TCMID+T0)/100.)**4
            QRROO=QRROO+ABS(DAREA)*EPSL*0.00567*((TRMID+T0)/100.)**4
  110     CONTINUE
  120   CONTINUE
        QSQS=QORIG-QRCRO-QRROO
C         QSQS=QORIG
          DQS=1.-QSQS/QTOTAL
        DB=DRMAX/WIDTHC
          IF(ABS(DQS).GE.0.005.OR.DB.GE.0.002)THEN
          WRITE(*,*)'  DQS=',DQS,'  DB=',DB
          QTOTAL=0.0
          DO 130 N=1,NHH
            QS(N)=QS(N)*(1.-DQS/QORIG)
              QTOTAL=QTOTAL+QS(N)
  130     CONTINUE
          DO 140 N=1,NZ
            RMAX(N)=RMAX(N)+.5*(RMAXO(N)-RMAX(N))
  140     CONTINUE
            GO TO 66
          ENDIF
        RETURN
          END
```

Appendix B

********** COMPUTER PROGRAM FOR VPPA PENETRATION **********

```
C-----------------------------------------------------------------------
C         PROGRAM WELDO.FOR,COMPILED ON MARCH 16,1993
C
C         Point and Line Source Models are Combined to Estimate Whether
C         a Keyhole Can be Formed.
C
C         Impinging Convective Heat Transfer on the Surface of Workpiece
C         Is Taken as Convection before Keyhole Formed.
C
        DIMENSION POW1(5),POW2(5),POW3(5),POW4(10)
        DIMENSION ENT1(5),ENT2(5),ENT3(5),ENT4(10),TABMPL(20)
        DIMENSION QLOS1(10),QLOS2(10),QLOS3(10),QLOS4(10),TABMSD(20)
        DIMENSION TEMP1(5),TEMP2(5),TEMP3(5),TEMP4(10)
        DIMENSION ELOS2(10),ELOS4(10),QSEGM(10),XSOUR(10)
        DIMENSION AREA(10),TEMPG(11),DUDL1(10),DUDL2(10),DUDL3(10)
        DIMENSION QSOUR(5),QNET(5)
        DIMENSION R1(11),R2(11),FLWPL(11),FLWSD(11),ENERG(11)
      common/dat10/NX,NY,X(25),Y(15),TM,TO,THK,EPSL,DENS,HFUSI
        COMMON MMM
        COMMON TABTEM(20),TABIPL(20),TABCPL(20),TABKPL(20),TABISD(20)
        COMMON ITMAX,DHMAX,DTMAX
        COMMON TAMBI,DNOZL,FMPL
        COMMON TABCSD(20),TABKSD(20),TABNPL(20),TABNSD(20)
        COMMON TW4,MREG4,NREG4
        COMMON PLM,SDM
        OPEN(5,FILE='C:WELDTAB.DAT')
        OPEN(6,FILE='C:WELDIN.USE')
        OPEN(7,FILE='C:WELDOU.USE')
        READ(5,*) MMM
        READ(5,*) (TABTEM(I),I=1,MMM)
        READ(5,*) (TABIPL(I),I=1,MMM)
        READ(5,*) (TABCPL(I),I=1,MMM)
        READ(5,*) (TABKPL(I),I=1,MMM)
        READ(5,*) (TABISD(I),I=1,MMM)
        READ(5,*) (TABCSD(I),I=1,MMM)
        READ(5,*) (TABKSD(I),I=1,MMM)
        READ(5,*) (TABMPL(I),I=1,MMM)
        READ(5,*) (TABMSD(I),I=1,MMM)
        READ(5,*) (TABNPL(I),I=1,MMM)
        READ(5,*) (TABNSD(I),I=1,MMM)
        READ(6,*) NREG1,NREG2,NREG3,NREG4
        READ(6,*) VA,VC
        READ(6,*) FIA1,FIA2,FIA3
        READ(6,*) TIME,TIMER
        READ(6,*) DISL1,DISL2,DISL3,DISL4
        READ(6,*) VVE,VVK
        READ(6,*) APIL,APILR,AMAI,AMAIR
        READ(6,*) DNOZL,DSHID,VPL,VSD
        READ(6,*) PLMOL,SDMOL,UR
        READ(6,*) ITMAX,DHMAX,DTMAX
        READ(6,*) TW1,TW2,TW4,HSUR2,HSUR4
```

```
      READ(6,*) DXW,TAMBI,DPOLAR,AMDW
      READ(6,*) PSIA,PAMBI,CPSD
      READ(6,*) ALFA,VWELD
      READ(6,*) NX,NY
      READ(6,*) X(1),X(NX)
      READ(6,*) Y(1),Y(NY)
      READ(6,*) TM,TO
      READ(6,*) THK,EPSL
      READ(6,*) DENS,HFUSI
C-----------------------------------------------------------------------
      WRITE(7,1000)
      WRITE(7,1001)MMM
      WRITE(7,1002)
      WRITE(7,1003)
      WRITE(7,1004)
      WRITE(7,1005)
      WRITE(7,1006)
      WRITE(7,1007)
      WRITE(7,1008)
      WRITE(7,1009)
      WRITE(7,1010)
      WRITE(7,1011)
      WRITE(7,1012)
      WRITE(7,1013)NREG1
      WRITE(7,1014)NREG2
      WRITE(7,1015)NREG3
      WRITE(7,1016)NREG4
      WRITE(7,1017)VA
      WRITE(7,1018)VC
      WRITE(7,1019)FIA1
      WRITE(7,1020)FIA2
      WRITE(7,1021)FIA3
      WRITE(7,1022)TIME
      WRITE(7,1023)TIMER
      WRITE(7,1024)DISL1
      WRITE(7,1025)DISL2
      WRITE(7,1026)DISL3
      WRITE(7,1027)DISL4
      WRITE(7,1028)VVE
      WRITE(7,1029)VVK
      WRITE(7,1030)APIL
      WRITE(7,1031)APILR
      WRITE(7,1032)AMAI
      WRITE(7,1033)AMAIR
      WRITE(7,1034)DNOZL
      WRITE(7,1035)DSHID
      WRITE(7,1036)VPL
      WRITE(7,1037)VSD
      WRITE(7,1038)PLMOL
      WRITE(7,1039)SDMOL
      WRITE(7,1040)UR
      WRITE(7,1041)ITMAX
      WRITE(7,1042)DHMAX
      WRITE(7,1043)DTMAX
```

```
      WRITE(7,1044)TW1
      WRITE(7,1045)TW2
      WRITE(7,1046)TW4
      WRITE(7,1047)HSUR2
      WRITE(7,1048)HSUR4
      WRITE(7,1049)DXW
      WRITE(7,1050)TAMBI
      WRITE(7,1051)DPOLAR
      WRITE(7,1052)AMDW
      WRITE(7,1053)PSIA
      WRITE(7,1054)PAMBI
      WRITE(7,1055)CPSD
      WRITE(7,1056)ALFA
      WRITE(7,1057)VWELD
      WRITE(7,1058)NX
      WRITE(7,1059)NY
      WRITE(7,1060)X(1)
      WRITE(7,1061)X(NX)
      WRITE(7,1062)Y(1)
      WRITE(7,1063)Y(NY)
      WRITE(7,1064)TM
      WRITE(7,1065)TO
      WRITE(7,1066)THK
      WRITE(7,1067)EPSL
      WRITE(7,1068)DENS
      WRITE(7,1069)HFUSI
C-----------------------------------------------------------------
      VOLPL=VPL/1.27133/1.E5
      VOLSD=VSD/1.27133/1.E5
        FMPL=VOLPL*PAMBI*PLMOL/8315./TAMBI
        FMSD=VOLSD*PAMBI*SDMOL/8315./TAMBI
        UH=VOLSD*4./3.14159/(DSHID**2-DNOZL**2)
C
C---------- FIRST SEGMENT CALCULATION ---------------------
C
        AREAW=3.14159*DPOLAR**2/4.
        ELOS=1.5*VVK/VVE/1.E10
        GHW=((AMAI+APIL)*(VC-FIA1)*TIME+(AMAIR-APILR)*(VA+FIA1)*
     $      TIMER)/(TIME+TIMER)/1000.
        CONDW=AMDW*AREAW*(TW1-TAMBI)/DXW
        POW1(1)=GHW-CONDW
        ENT1(1)=POW1(1)/FMPL
        CALL  INSEP(TABIPL,TABTEM,ENT1(1),TEMP1(1))
        ELOS1=ELOS*TEMP1(1)*(AMAIR-APILR)*TIMER/(TIME+TIMER)
        AMPCP1=((AMAI+APIL)*TIME+(AMAIR-APILR)*TIMER)/(TIME+TIMER)
        DX1=DISL1/FLOAT(NREG1)
        GEOL1=3.14159*((DPOLAR+DNOZL)/2.)**2/4./DX1
        VOLUM1=3.14159*((DNOZL+DPOLAR)/2.)**2/4.*DX1
        MREG1=NREG1+1
        SUMQ1=0.
        DUBC=0.
       DO 40 M=2,MREG1
        N=M-1
        DUDL1(N)=2000.
```

```
        QLOS1(N)=0.
        NN1=0
   10 CONTINUE
      NN1=NN1+1
        IF(NN1.GT.200) THEN
          WRITE(*,*)'       NN1.GT.200.  Erro stop'
          STOP
        ENDIF
        DP1=DUDL1(N)*DX1*AMPCP1/1000.-QLOS1(N)
        POW1(M)=POW1(N)+DP1
        ENT1(M)=POW1(M)/FMPL
        ENTCP1=(ENT1(N)+ENT1(M))/2.
        CALL INSEP(TABIPL,TABTEM,ENTCP1,TEMCP1)
        QLOS1(N)=VOLUM1*4.*1.E7*(TEMCP1/15000.)**16/
     $  (1.+(TEMCP1/15000.)**16)
        CALL INSEP(TABTEM,TABMPL,TEMCP1,PLMHO)
        OHM1=1./PLMHO/GEOL1
        DUDL=AMPCP1*OHM1/DX1
        DIFU=1.-DUDL/DUDL1(N)
        IF(ABS(DIFU).GE.0.005) THEN
          DUDL1(N)=(DUDL+DUDL1(N))/2.
          GO TO 10
        ENDIF
        DUBC=DUBC+DUDL1(N)*DX1
        SUMQ1=SUMQ1+QLOS1(N)
        CALL INSEP(TABIPL,TABTEM,ENT1(M),TEMP1(M))
   40 CONTINUE
C       WRITE(7,1170) (POW1(I),I=1,MREG1)
C       WRITE(7,1180) (ENT1(I),I=1,MREG1)
C       WRITE(7,1190) (QLOS1(I),I=1,NREG1)
C       WRITE(7,1200) (TEMP1(I),I=1,MREG1)
C       WRITE(7,1220) (DUDL1(I),I=1,NREG1)
C       WRITE(7,1210) SUMQ1,DUBC
C
C------------- SECOND SEGMENT CLCULATION --------------------------
C
      POW2(1)=POW1(MREG1)
      ENT2(1)=ENT1(MREG1)
      TEMP2(1)=TEMP1(MREG1)
      AMPCP2=(AMAI*TIME+(AMAIR-APILR)*TIMER)/(TIME+TIMER)
      DX2=DISL2/FLOAT(NREG2)
      AREA2=3.14159*DNOZL*DX2
      GEOL2=3.14159*DNOZL**2/4./DX2
      MREG2=NREG2+1
C      WRITE(7,1230)
      GHN1=(APIL*FIA2*TIME+APILR*FIA2*TIMER)/(TIME+TIMER)/1000.
      GHN2=(APIL*VA*TIME+APILR*VA*TIMER)/(TIME+TIMER)/1000.
      SUMQ2=GHN1+PSIA*GHN2
      DUCG=0.
      DO 80 M=2,MREG2
        N=M-1
        XM=FLOAT(N)*DX2-DX2/2.
        DUDL2(N)=2000.
        QLOS2(N)=0.
```

```
      NN2=0
   50 CONTINUE
      NN2=NN2+1
      IF(NN2.GT.200)THEN
        WRITE(*,*)'    Erro Stop      ENT3=',ENT3
        STOP
      ENDIF
      IF(NREG2.EQ.1)then
        ELOS2(N)=ELOS*TEMP2(N)*(APIL*TIME+APILR*TIMER)/(TIME+TIMER)
      else IF(NREG2.NE.1.AND.N.EQ.1)then
        ELOS2(N)=ELOS*TEMP2(N)*APIL*TIME/(TIME+TIMER)
      else IF(NREG2.NE.1.AND.N.EQ.NREG2)then
        ELOS2(N)=ELOS*TEMP2(N)*APILR*TIMER/(TIME+TIMER)
      endif
      DP2=DUDL2(N)*DX2*AMPCP2/1000.+(1.-PSIA)*GHN2/FLOAT(NREG2)
     $     -ELOS2(N)-QLOS2(N)
      POW2(M)=POW2(N)+DP2
      ENT2(M)=POW2(M)/FMPL
      ENTCP=(ENT2(N)+ENT2(M))/2.
      CALL INSEP(TABIPL,TABTEM,ENTCP,TEMCP)
      CALL INSEP(TABTEM,TABKPL,TEMCP,AMD)
      CALL INSEP(TABTEM,TABCPL,TEMCP,CP)
      CALL INSEP(TABTEM,TABMPL,TEMCP,PLMHO)
      COEFC=2.*FMPL*CP/3.14159/AMD
      XPLUS=COEFC/XM
      VNUX=0.2233*XPLUS**0.7455+3.66
      ALFAX=VNUX*AMD/DNOZL
      QLOS2(N)=ALFAX*AREA2*(ENTCP-HSUR2)/CP
      OHM2=1./PLMHO/GEOL2
      DUDL=AMPCP2*OHM2/DX2
      DIFU=1.-DUDL/DUDL2(N)
      IF(ABS(DIFU).GE.0.005) THEN
         DUDL2(N)=(DUDL+DUDL2(N))/2.
         GO TO 50
      ENDIF
      DUCG=DUCG+DUDL2(N)*DX2
      SUMQ2=SUMQ2+QLOS2(N)+ELOS2(N)
      CALL INSEP(TABIPL,TABTEM,ENT2(M),TEMP2(M))
   80 CONTINUE
C       WRITE(7,1250) (POW2(I),I=1,MREG2)
C       WRITE(7,1260) (ENT2(I),I=1,MREG2)
C       WRITE(7,1270) (QLOS2(I),I=1,NREG2)
C       WRITE(7,1280) (TEMP2(I),I=1,MREG2)
C       WRITE(7,1290) (ELOS2(I),I=1,NREG2)
C       WRITE(7,1300) (DUDL2(I),I=1,NREG2)
C       WRITE(7,1310) SUMQ2,DUCG
C       WRITE(7,1320)
C
C------------- THIRD SEGMENT CLCULATION -------------------------
C
      RO=DNOZL/2.
      POW3(1)=POW2(MREG2)
      MITER=0
   90 CONTINUE
```

```
      MITER=MITER+1
      IF(MITER.GT.200) THEN
        WRITE(*,*)'    Erro Stop     MITER.GT.200,DPP=',DPP
        STOP
      ENDIF
      ENT3(1)=POW3(1)/FMPL
      CALL INSEP(TABIPL,TABTEM,ENT3(1),TEMP3(1))
      DENSO=PAMBI*PLMOL/8315./TEMP3(1)
      UO=FMPL/DENSO/3.14159/RO**2
      ENERG(1)=FMPL*UO**2/2./1000.
      PPP=POW2(MREG2)-ENERG(1)
      DPP=ABS(1.-PPP/POW3(1))
      POW3(1)=PPP
      IF(DPP.GE.0.005) GO TO 90
      COEFM=UH/UO
      VMID1=(1.-COEFM)/(1.+COEFM)
      VMID3=1.+0.8*COEFM-0.45*COEFM**2
      DX3=DISL3/FLOAT(NREG3)
      MREG3=NREG3+1
      SUMQ3=0.
      DUGE=0.
      R1(1)=RO
      R2(1)=RO
      FLWPL(1)=FMPL
      FLWSD(1)=0.
      AMPCP3=(AMAI*TIME+AMAIR*TIMER)/(TIME+TIMER)
      DO 190 M=2,MREG3
        N=M-1
        X3=FLOAT(N)*DX3
        VMID2=0.27*X3
        VMID4=VMID1*(0.416+0.134*COEFM+0.021*VMID2*VMID1*VMID3/RO)
        R1(M)=RO-VMID2*VMID4
        VMIDA=0.021*VMID3/RO
        VMIDB=0.416+0.134*COEFM
        VMIDC=R1(M)-RO
        VMIDD=(-VMIDB+SQRT(VMIDB**2-4.*VMIDA*VMIDC))/2./VMIDA
        R2(M)=R1(M)+VMIDD
        NOM=0
        TBEGI=TEMP3(1)
        DENBEG=DENSO
        DR=(R2(M)-R1(M))/10.
        DUDL2(N)=2000.
        GEOL3=3.14159*R2(M)**2/DX3
120     CONTINUE
        NOM=NOM+1
        IF(NOM.GT.200) THEN
          WRITE(*,*)'     Erro Stop     ITER.IN STANDOFF EXCEED 200'
          STOP
        ENDIF
        FLWPL(M)=3.14159*R1(M)**2*UO*DENBEG
        FLWSD(M)=0.
        ENERG(M)=FLWPL(M)*UO**2/2./1000.
        CALL INSEP(TABTEM,TABIPL,TBEGI,EBEGI)
        POWER=FLWPL(M)*EBEGI
```

```
      DO 150 K=1,10
        RMID=FLOAT(K)*DR-DR/2.+R1(M)
        ATA=(R2(M)-RMID)/(R2(M)-R1(M))
        UMID=UO-(UO-UH)*(1.-ATA**1.5)**2
        TMID=TBEGI-(TBEGI-TAMBI)*(1.-ATA)
        PGPL=PAMBI/(1.+(1./ATA-1.)*PLMOL/SDMOL)
        PGSD=PAMBI-PGPL
        DENPL=PGPL*PLMOL/8315./TMID
        DENSD=PGSD*SDMOL/8315./TMID
        VOLUM=2.*3.14159*RMID*DR*UMID
        FLWPL(M)=FLWPL(M)+VOLUM*DENPL
        FLWSD(M)=FLWSD(M)+VOLUM*DENSD
        ENERG(M)=ENERG(M)+(DENPL+DENSD)*VOLUM*UMID**2/2./1000.
        IF(TMID.GE.3000.) THEN
          CALL INSEP(TABTEM,TABIPL,TMID,ENTPL)
          CALL INSEP(TABTEM,TABISD,TMID,ENTSD)
         ELSE
          ENTPL=TABCPL(1)*TMID
          ENTSD=TABCSD(1)*TMID
        ENDIF
        POWER=POWER+VOLUM*(DENPL*ENTPL+DENSD*ENTSD)
150   CONTINUE
      POWRCP=(POWER+POW3(N))/2.
      PLCP=(FLWPL(M)+FLWPL(N))/2.
      SDCP=(FLWSD(M)+FLWSD(N))/2.
      CALL AVERT(PLCP,SDCP,POWRCP,TABTEM,TABIPL,TABISD,TCP)
      VRADI=3.14159*(R2(M)+R2(N))**2/4.*DX3
      QLOS3(N)=VRADI*4.*1.E7*(TCP/15000.)**16/(1.+(TCP/15000.)**16)
      CALL INSEP(TABTEM,TABMPL,TCP,PLMHO)
      CALL INSEP(TABTEM,TABMSD,TCP,SDMHO)
      CPMHO=((FLWPL(M)+FLWPL(N))*PLMHO+(FLWSD(M)+FLWSD(N))*SDMHO)/
     $        (FLWPL(M)+FLWPL(N)+FLWSD(M)+FLWSD(N))
      OHM3=1./CPMHO/GEOL3
      DUDL3(N)=OHM3*AMPCP3/DX3
      DP3=OHM3*AMPCP3**2/1000.
      POW3(M)=POW3(N)+DP3-QLOS3(N)+(FLWSD(M)-FLWSD(N))*CPSD*TAMBI-
     $         (ENERG(M)-ENERG(N))
      PMP=1.-POWER/POW3(M)
      IF(ABS(PMP).GE.0.010) THEN
        TBEGI=TBEGI*(1.+PMP/10.)
        DENBEG=PAMBI*PLMOL/8315./TBEGI
        UO=UO*PMPL/FLWPL(M)
        GO TO 120
      ENDIF
      WRITE(*,1390) N,NOM,PMP
      SUMQ3=SUMQ3+QLOS3(N)
      CALL AVERT(FLWPL(M),FLWSD(M),POWER,TABTEM,TABIPL,TABISD,
     $             TEMP3(M))
      ENT3(M)=POW3(M)/(FLWPL(M)+FLWSD(M))
      DUGE=DUGE+DUDL3(N)*DX3
190 CONTINUE
    PAID=FLWSD(MREG3)*CPSD*TAMBI
C
C-----------------------------------------------------------------
```

```
        GHK1=(AMAI*FIA3*TIME+AMAIR*(UR-FIA3)*TIMER)/(TIME+TIMER)/1000.
        GHK2=(AMAI*VA*TIME+AMAIR*VC*TIMER)/(TIME+TIMER)/1000.
C       GHK1=(AMAI*FIA3*TIME-AMAIR*FIA3*TIMER)/(TIME+TIMER)/1000.
C       GHK2=(AMAI*VA*TIME+AMAIR*(UR+VC)*TIMER)/(TIME+TIMER)/1000.
C-----------------------------------------------------------------------
      POWER=POW3(MREG3)
      PLM=FMPL
      SDM=FLWSD(MREG3)
      POW4(1)=POWER+(1.-PSIA)*GHK2
      ENT4(1)=POW4(1)/(PLM+SDM)
      CALL AVERT(PLM,SDM,POW4(1),TABTEM,TABIPL,TABISD,TEMP4(1))
      ELOSS=ELOS*TEMP4(1)*AMAI*TIME/(TIME+TIMER)
      GHK12=GHK1+PSIA*GHK2
      CALL CONVO(R2(MREG3),ENT4(1),TEMP4(1),PLM,SDM,HSUR4,QCONV)
        SUMQ4=QCONV+ELOSS+GHK12
      WRITE(*,*)'  SUMQ4=',SUMQ4,'  VWELD=',VWELD
      CALL DEPTH(SUMQ4,DISL4,NREG4,ALFA,VWELD)
C=======================================================================
       STOP
C+++++++++++++++++++++++++++++++++++++++++++++++++++++++++++++++++++++++
 1000 FORMAT(/3X,'SYMBOL  UNIT     DESCRIPTION                          ',
     $'      DATA'/)
 1001 FORMAT(/3X,'MMM              Number of point in table             ',
     $I5)
 1002 FORMAT(/3X,'TABTEM  K        Temperaeture table                   ',
     $'    Table attached')
 1003 FORMAT(/3X,'TABIPL  kJ/kg    Enthalpy of plasma gas               ',
     $'    Table attached')
 1004 FORMAT(/3X,'TABCPL  kJ/kg.K  Specific heat of plasma gas          ',
     $'    Table attached')
 1005 FORMAT(/3X,'TABKPL  kW/M.K   Thermal conductivity of plasma gas   ',
     $'    Table attached')
 1006 FORMAT(/3X,'TABISD  kJ/kg    Enthalpy of shield gas               ',
     $'    Table attached')
 1007 FORMAT(/3X,'TABCSD  kJ/kg.K  Specific heat of shield gas          ',
     $'    Table attached')
 1008 FORMAT(/3X,'TABKSD  kW/M.K   Thermal conductivity of shield gas   ',
     $'    Table attached')
 1009 FORMAT(/3X,'TABMPL  MHO/M    Elictric conductivity of plasma gas',
     $'    Table attached')
 1010 FORMAT(/3X,'TABMSD  MHO/M    Electric conductivity of shield gas',
     $'    Table attached')
 1011 FORMAT(/3X,'TABNPL  kg/M.S   Viscosity of plasma gas              ',
     $'    Table attached')
 1012 FORMAT(/3X,'TABNSD  kg/M.S   Viscosity of shield gas              ',
     $'    Table attached')
 1013 FORMAT(/3X,'NREG1            Segment number between electrode    ',
     $ /3X,'                  and orifice                          ',I5)
 1014 FORMAT(/3X,'NREG2            Segment number of orifice           ',
     $I5)
 1015 FORMAT(/3X,'NREG3            Segment number of standoff          ',
     $I5)
 1016 FORMAT(/3X,'NREG4            Segment number of workpiece         ',
     $I5)
```

```
1017 FORMAT(/3X,'VA       V          Anode potential drop                  ',
     $e12.5)
1018 FORMAT(/3X,'VC       V          Cathode potential drop                ',
     $e12.5)
1019 FORMAT(/3X,'FIA1     V          Electrode work function               ',
     $e12.5)
1020 FORMAT(/3X,'FIA2     V          Orifice work function                 ',
     $e12.5)
1021 FORMAT(/3X,'FIA3     V          Workpiece work function               ',
     $e12.5)
1022 FORMAT(/3X,'TIME     mS         Time duration for straight polarity',
     $e12.5)
1023 FORMAT(/3X,'TIMER    mS         Time duration for reverse polarity ',
     $e12.5)
1024 FORMAT(/3X,'DISL1    M          Distance betwteen electrode and    ',
     $/3X,'                 orifice                                  ',E12.5)
1025 FORMAT(/3X,'DISL2    M          Axial length of orifice            ',
     $e12.5)
1026 FORMAT(/3X,'DISL3    M          Distance of standoff               ',
     $e12.5)
1027 FORMAT(/3X,'DISL4    M          Thickness of workpiece             ',
     $e12.5)
1028 FORMAT(/3X,'VVE      Coulomb    Electron charge                    ',
     $e12.5)
1029 FORMAT(/3X,'VVK      erg/K      Boltzman constant                  ',
     $e12.5)
1030 FORMAT(/3X,'APIL     A          Pilot electric current in straight ',
     $/3x,'                 polarity                                 ',e12.5)
1031 FORMAT(/3X,'APILR    A          Pilot electric current in reverse  ',
     $/3x,'                 polarity                                 ',e12.5)
1032 FORMAT(/3X,'AMAI     A          Main electric current in straight  ',
     $/3x,'                 polarity                                 ',e12.5)
1033 FORMAT(/3X,'AMAIR    A          Main electric current in reverse   ',
     $/3x,'                 polarity                                 ',e12.5)
1034 FORMAT(/3X,'DNOZL    M          Orifice diameter                   ',
     $e12.5)
1035 FORMAT(/3X,'DSHID    M          External diameter of shield        ',
     $e12.5)
1036 FORMAT(/3X,'VPL      scfh       Plasma gas flow rate               ',
     $e12.5)
1037 FORMAT(/3X,'VSD      scfh       Shield gas flow rate               ',
     $e12.5)
1038 FORMAT(/3X,'PLMOL    kg/kmol    Molecular weight of plasma gas     ',
     $e12.5)
1039 FORMAT(/3X,'SDMOL    kg/kmol    Molecular weight of shield gas     ',
     $e12.5)
1040 FORMAT(/3X,'UR       V          Reverse polarity voltage rise      ',
     $e12.5)
1041 FORMAT(/3X,'ITMAX               Maximum number of iteration        ',
     $I5)
1042 FORMAT(/3X,'DHMAX               Maximum relative error of enthalpy ',
     $e12.5)
1043 FORMAT(/3X,'DTMAX    K          Maximum error of temperature       ',
     $e12.5)
```

```
 1044 FORMAT(/3X,'TW1      K         Electrode wall temperature          ',
     $e12.5)
 1045 FORMAT(/3X,'TW2      K         Orifice wall temperature            ',
     $e12.5)
 1046 FORMAT(/3X,'TW4      K         Workpiece wall temperature          ',
     $e12.5)
 1047 FORMAT(/3X,'HSUR2    kJ/kg     Plasma enthalpy correponding to TW2',
     $e12.5)
 1048 FORMAT(/3X,'HSUR4    kJ/kg     Jet enthalpy correponding to TW4    ',
     $e12.5)
 1049 FORMAT(/3X,'DXW      M         Electrode length                    ',
     $e12.5)
 1050 FORMAT(/3X,'TAMBI    K         Enviromental temperature            ',
     $e12.5)
 1051 FORMAT(/3X,'DPOLAR   M         Electrode diameter                  ',
     $e12.5)
 1052 FORMAT(/3X,'AMDW     kW/M.K    Thermal conductivity of electrode   ',
     $e12.5)
 1053 FORMAT(/3X,'PSIA               Fraction power loss due to anode    ',
     $/3x,'                  and cathode drop                    ',e12.5)
 1054 FORMAT(/3X,'PAMBI    N/M2      Environmental pressure              ',
     $e12.5)
 1055 FORMAT(/3X,'CPSD     kJ/kg.K   Specific heat of shield gas with    ',
     $/3x,'                  environmental temperature           ',e12.5)
 1056 FORMAT(/3X,'ALFA     kW/M.K    Thermal diffusivity of workpiece    ',
     $e12.5)
 1057 FORMAT(/3X,'VWELD    ipm       Welding speed                       ',
     $e12.5)
 1058 FORMAT(/3X,'NX                 Number of computing nodal in X      ',
     $/3x,'                  coordinate                          ',I5)
 1059 FORMAT(/3X,'NY                 Number of computing nodal in Y      ',
     $/3x,'                  coordinate                          ',I5)
 1060 FORMAT(/3X,'X(1)     M         Beginning position of computed      ',
     $/3x,'                  nodal in X coordinate               ',e12.5)
 1061 FORMAT(/3X,'X(NX)    M         Ending position of computed         ',
     $/3x,'                  nodal in X coordinate               ',e12.5)
 1062 FORMAT(/3X,'Y(1)     M         Beginning position of computed      ',
     $/3x,'                  nodal in Y coordinate               ',e12.5)
 1063 FORMAT(/3X,'Y(NY)    M         Ending position of computed         ',
     $/3x,'                  nodal in Y coordinate               ',e12.5)
 1064 FORMAT(/3X,'TM       K         Melting temperature of workpiece    ',
     $e12.5)
 1065 FORMAT(/3X,'TO       K         Initial temperature of workpiece    ',
     $e12.5)
 1066 FORMAT(/3X,'THK      kW/M.K    Thermal conductivity of workpiece   ',
     $e12.5)
 1067 FORMAT(/3X,'EPSL               Emissivity of workpiece             ',
     $e12.5)
 1068 FORMAT(/3X,'DENS     kg/M3     Density of workpiece                ',
     $e12.5)
 1069 FORMAT(/3X,'HFUSI    kJ/kg     Melting latent heat of workpiece    ',
     $e12.5)
C+++++++++++++++++++++++++++++++++++++++++++++++++++++++++++++++++++++++++
 1170 FORMAT(/2X,'POW1=',4E12.5,/7X,4E12.5)
```

```
1180 FORMAT(/2X,'ENT1=',4E12.5,/7X,4E12.5)
1190 FORMAT(/2X,'QLOS1=',4E12.5,/7X,4E12.5)
1200 FORMAT(/2X,'TEMP1=',4E12.5,/7X,4E12.5)
1210 FORMAT(/2X,'TOTAL LOSS IN GAP I',E12.5,2X,'DUBC(v)',F6.2)
1220 FORMAT(/2X,'DUDL1',4E12.5,/7X,4E12.5)
1300 FORMAT(/2X,'DUDL2',4E12.5,/7X,4E12.5)
1310 FORMAT(/5X,'TOTAL LOSS IN NOZZLE =',E12.5,2X,'DUCG(v)',F6.2)
1250 FORMAT(/5X,'POW2=',4E12.5/10X,4E12.5)
1260 FORMAT(/5X,'ENT2=',4E12.5/10X,4E12.5)
1270 FORMAT(/4X,'QLOS2=',4E12.5/10X,4E12.5)
1280 FORMAT(/2X,'TEMP2',4E12.5,/7X,4E12.5)
1290 FORMAT(/2X,'ELOS2',4E12.5,/7X,4E12.5)
1320 FORMAT(//5X,'STANDOFF COMPUTATION')
1230 FORMAT(//5X,'NOZZLE COMPUTATION')
1240 FORMAT(/5X,'NN2.GT.100')
1340 FORMAT(/5X,'UH,UO,COEFM',3E12.5)
1350 FORMAT(/2X,'LINE 285 TBEGI',E12.4)
1370 FORMAT(/1X,'ATA,TBEGI,TAMBI,TMID',4E11.4)
1360 FORMAT(1X,'M,R1,R2,DR,RMID,ATA',I2,2E12.5,/5X,3E12.5)
1380 FORMAT(/2X,'IN MAIN,NOM,MAR,MHE,POWER',I4,2X,3E10.3)
1390 FORMAT(/2X,'ITER.IN STANDOFF,SEG.=',I2,2X,'NOM=',I4,
    $         2X,'PMP=',F10.6)
1510 FORMAT(/2X,'DUDL3',4E12.5,/7X,4E12.5)
1450 FORMAT(/2X,'TOTAL LOSS IN STANDOFF =',E12.5,2X,'DUGE(v)',F6.2)
1410 FORMAT(/5X,'POW3=',4E12.5,/10X,4E12.5)
1430 FORMAT(/4X,'QLOS3=',4E12.5,/10X,4E12.5)
1440 FORMAT(/4X,'TEMP3=',4E12.5,/10X,4E12.5)
1460 FORMAT(/5X,'R1(m)=',4F10.8,/11X,4F10.8)
1470 FORMAT(/5X,'R2(m)=',4F10.8,/11X,4F10.8)
1480 FORMAT(/5X,'FLWPL=',4E12.5,/11X,4E12.5)
1490 FORMAT(/5X,'FLWSD=',4E12.5,/11X,4E12.5)
1500 FORMAT(/5X,'ENERG=',4E12.5,/11X,4E12.5)
1520 FORMAT(/5X,'POWER AID FROM SHIELD, PAID(kW)=',E12.5)
1530 FORMAT(/2X,'VELOC.,TEMP.IN CORE AT LAST',2E12.5)
1540 FORMAT(/5X,'T OF BOUNDARY, TBOUND=',E12.5)
1550 FORMAT(/5X,'CONVECTIVE LOSS OF JET (kW)',E12.5)
1555 FORMAT(//10X,'WORKPIECE COMPUTATION')
1560 FORMAT(/2X,'XSOUR',2X,5F8.6)
1570 FORMAT(/5X,'RADIUS OF KEYHOLE (m)=',E12.5)
1580 FORMAT(/2X,'AREA(m**2)',4E12.5,/12X,4E12.5)
1590 FORMAT(/4X,'PLM,SDM,TEMP4(1)',3E14.5)
1600 FORMAT(/5X,'IMPINGE LOSS (kw)',F8.5)
1660 FORMAT(/2X,'QSEGM=',4E12.5,/8X,4E12.5)
1680 FORMAT(/5X,'TOTAL LOSS IN WORKPIECE =',E12.5)
1610 FORMAT(/2X,'POW4=',4E12.5,/7X,4E12.5)
1620 FORMAT(/2X,'ENT4=',4E12.5,/7X,4E12.5)
1630 FORMAT(/2X,'TEMP4=',4E12.5,/8X,4E12.5)
1640 FORMAT(/2X,'QLOS4=',4E12.5,/8X,4E12.5)
1650 FORMAT(/2X,'ELOS4=',4E12.5,/8X,4E12.5)
1670 FORMAT(/2X,'QSOUR=',4E12.5,/8X,4E12.5)
1690 FORMAT(5X,'TOTAL POWER INCLUDING HELIUM, PTOTIN=',E12.5,/
    $       5X,'TOTAL POWER FROM LOSS, PTOTOU=',E12.5)
1700 FORMAT(/2X,'POLARITY CONDUC. LOSS AND PERCENT.',2E12.5)
1710 FORMAT(/2X,'GAP LOSS AND PERCENTAGE',2E12.5)
```

```
 1720 FORMAT(/2X,'NOZZLE LOSS AND PERCENTAGE',2E12.5)
 1730 FORMAT(/2X,'RADIAT.IN STANDOFF AND PERCENTAGE',2E12.5)
 1740 FORMAT(/2X,'CONVEC.IN STANDOFF AND PERCENTAGE',2E12.5)
 1750 FORMAT(/2X,'WORKPIECE LOSS AND PERCENTAGE',2E12.5)
 1760 FORMAT(/2X,'DISCHARGE LOSS AND PERCENTAGE',2E12.5)
 1770 FORMAT(/5X,'SUM. PERCENTAGE',F8.5)
 1780 FORMAT(/5X,'AMPCP1,2,3',3E12.5)
 1790 FORMAT(/5X,'DUBE,DUAF,DUAFR',3E12.5)
 1800 FORMAT(/4X,'DUPF=',E12.4,4X,'DUPR=',E12.4)
      END
C
C-----------------------------------------------------------------------
C
      SUBROUTINE AVERT(FLOPL,FLOSD,PSUM,TABT,TABPL,TABSD,TVERA)
      DIMENSION TABT(20),TABPL(20),TABSD(20)
      COMMON MMM
C     WRITE(7,3000) FLOPL,FLOSD,PSUM
      NN=0
      TVERA=10000.
   10 CONTINUE
      NN=NN+1
      IF(NN.GT.200) THEN
       WRITE(*,*)'  Erro Stop    ITER.EXCEED 200 IN AVERT, THEN STOP'
         STOP
      ENDIF
        CALL INSEP(TABT,TABPL,TVERA,EPL)
        CALL INSEP(TABT,TABSD,TVERA,ESD)
        PCOMP=FLOPL*EPL+FLOSD*ESD
        DPOWR=1.-PCOMP/PSUM
        IF(ABS(DPOWR).GE.0.010) THEN
          TVERA=TVERA*(1.+DPOWR/10.)
C       WRITE(*,3020) NN,DPOWR
          GO TO 10
      ENDIF
C       WRITE(7,3030) NN,DPOWR,TVERA
        RETURN
 3000 FORMAT(/2X,'IN AVERT,MPL,MSD,PSUM',3E11.4)
 3020 FORMAT(2X,'NN=',I3,2X,'DPOWR=',E12.5)
 3030 FORMAT(/2X,'SUB.AVERT, NN,DPOWR,TVERA',I4,2E14.5)
      END
C
C-----------------------------------------------------------------------
C
      SUBROUTINE INSEP(A,B,C,D)
      DIMENSION A(26),B(26)
      COMMON MMM
      IF(C.LT.A(1).OR.C.GT.A(MMM)) THEN
      WRITE(*,*)'   Erro Stop     INDEP. IS BEYOND SCOPE'
      WRITE(*,*)'  C=',C,'A(1)=',A(1),'A(MMM)=',A(MMM)
      STOP
      ENDIF
      DO 30 K=2,MMM
      IF((C.LE.A(K).AND.C.GE.A(K-1)).OR.
     $    (C.GE.A(K).AND.C.LE.A(K-1))) THEN
```

```
            D=B(K-1)+(B(K)-B(K-1))/(A(K)-A(K-1))*(C-A(K-1))
C           WRITE(*,4010) C,D
              GO TO 40
            ENDIF
 30       CONTINUE
C       WRITE(*,4020)
 40     CONTINUE
          RETURN
 4020 FORMAT(/5X,'WRITE FROM FORMAT 31 IN SUB. INSEP')
 4010 FORMAT(/5X,'INDEP. C=',E12.4,5X,'DEPEND. D=',E12.4)

          END
C
C-------------------------------------------------------------------
C
       SUBROUTINE DEPTH(QORIG,H,NHH,ALPHA,VWELD)
          DIMENSION Z(20),ZZ(34),HH(15),TEMP(25,10,10)
          DIMENSION XMOLT(50),YMOLT(50),ZMOLT(50),ZMY(50),DZ(15),
      $     DHZ(15),XMOLTO(50),ZMOLTO(50),TEMPO(10,25,10,10)
         common/dat10/NX,NY,X(25),Y(15),TM,TO,THK,EPSL,DENS,HFUSI
          OPEN(8,FILE='C:WEL.OU1')
          OPEN(9,FILE='C:WEL.OU2')
         OPEN(10,FILE='C:WEL.OU3')
         IF(NX.GT.1)THEN
           DO 1 I=1,NX
             X(I)=X(1)+FLOAT(I-1)*(X(NX)-X(1))/FLOAT(NX-1)
     1     CONTINUE
         ENDIF
         IF(NY.GT.1)THEN
           DO 5 J=1,NY
               Y(J)=Y(1)+FLOAT(J-1)*(Y(NY)-Y(1))/FLOAT(NY-1)
     5     CONTINUE
           ENDIF
         NZ=NHH
         IF(NZ.GT.1)THEN
           DO 6 K=1,NZ
             Z(K)=FLOAT(K-1)*H/FLOAT(NZ-1)
     6     CONTINUE
         ENDIF
         NOM=1
         DO 10 L=1,NHH
           HH(L)=FLOAT(L-1)*H/FLOAT(NHH-1)
    10   CONTINUE
C-------------------------------------------------------------
          TMOLT=TM-TO
          V=VWELD*0.0254/60.
          V2A=-V/(2.*ALPHA)
          QS=QORIG
        Q4K=1./(4.*3.14159*THK)
C-------------------------------------------------------------
          DO 70 N=1,NHH
          HHH=HH(N)
            ZZ(1)=-16.*H-HHH
          ZZ(2)=-16.*H+HHH
```

```
      DO 20 K=3,34,2
        ZZ(K)=ZZ(K-2)+2.*H
        ZZ(K+1)=ZZ(K-1)+2.*H
   20 CONTINUE
      DO 60 K=1,NX
        DO 50 L=1,NY
          DO 40 J=1,NZ
            DO 30 M=1,34
              ZZZ=Z(J)-ZZ(M)
              XXX=X(K)
              YYY=Y(L)
              R=SQRT(XXX**2+YYY**2+ZZZ**2)
              RX=R+XXX
C             IF(RX.GT.10.) GO TO 60
              RX=V2A*RX
              EXPAN=EXP(RX)
              TEMPO(N,K,L,J)=TEMPO(N,K,L,J)+Q4k*EXPAN/R
   30       CONTINUE
   40     CONTINUE
   50   CONTINUE
   60 CONTINUE
   70 CONTINUE
      QM=0.0
C-----------------------------------------------------------------------
  110 CONTINUE
      DO 150 K=1,NZ
        DO 140 J=1,NY
          DO 130 I=1,NX
            TEMP(I,J,K)=0.0
  130     CONTINUE
  140   CONTINUE
  150 CONTINUE
      DO 190 I=1,NX
        DO 180 J=1,NY
          DO 170 K=1,NZ
            IF(NOM.GT.1)THEN
              DO 160 N=1,NOH
                TEMP(I,J,K)=TEMP(I,J,K)+QS/ZMAXO*DHZ(N)*TEMPO(N,I,J,K)
  160         CONTINUE
            ELSE
              TEMP(I,J,K)=QS*TEMPO(1,I,J,K)
            ENDIF
  170     CONTINUE
  180   CONTINUE
  190 CONTINUE
      ZMAX=0.0
      M1=0
      M2=0
      M3=0
      DO 220 K=1,NZ
        YMOLT(K)=0.0
        DO 210 I=1,NX-1
          IF(TMOLT.GT.TEMP(I,1,K).AND.TMOLT.LE.TEMP(I+1,1,K))THEN
            XM1=X(I)+(X(I+1)-X(I))*(TMOLT-TEMP(I,1,K))/
```

```
     $            (TEMP(I+1,1,K)-TEMP(I,1,K))
                M1=M1+1
                XMOLT(M1)=-1000*XM1
                ZMOLT(M1)=1000.*Z(K)
                ZMAX=AMAX1(ZMAX,Z(K))
                I1=I+1
              ENDIF
              IF(TMOLT.LE.TEMP(I,1,K).AND.TMOLT.GT.TEMP(I+1,1,K))THEN
                XM2=X(I)+(X(I+1)-X(I))*(TMOLT-TEMP(I,1,K))/
     $            (TEMP(I+1,1,K)-TEMP(I,1,K))
                M2=M2+1
                XMOLTO(M2)=-1000.*XM2
                ZMOLTO(M2)=1000.*Z(K)
                ZMAX=AMAX1(ZMAX,Z(K))
                I2=I
              ENDIF
              DO 200 J=1,NY-1
                IF((TMOLT.GE.TEMP(I,J,K).AND.TMOLT.LT.TEMP(I,J+1,K)).OR.
     $             (TMOLT.LE.TEMP(I,J,K).AND.TMOLT.GT.TEMP(I,J+1,K)))THEN
                  YM=Y(J)+(Y(J+1)-Y(J))/(TEMP(I,J+1,K)-TEMP(I,J,K))*
     $                (TMOLT-TEMP(I,J,K))
                  IF(YMOLT(K).LT.1000.*YM) JY=J
                  YMOLT(K)=AMAX1(YMOLT(K),1000.0*YM)
                  ZMY(K)=1000.0*Z(K)
                  M3=K
                ENDIF
  200         CONTINUE
  210       CONTINUE
  220     CONTINUE
C-----------------------------------------------------------------------
          WRITE(*,*)' M1=',M1,'  I1=',I1,'  I2=',I2
          IF(M1.LT.NZ)THEN
            DO 240 I=I1,I2
              DO 230 IM=2,NZ
                IF(TMOLT.LE.TEMP(I,1,IM-1).AND.TMOLT.GT.TEMP(I,1,IM))THEN
                  ZM1=Z(IM-1)+(Z(IM)-Z(IM-1))*(TMOLT-TEMP(I,1,IM-1))/
     $                (TEMP(I,1,IM)-TEMP(I,1,IM-1))
                  M1=M1+1
                  XMOLT(M1)=-1000.*X(I)
                  ZMOLT(M1)=1000.0*ZM1
                  ZMAX=AMAX1(ZM1,ZMAX)
                  GO TO 240
                ENDIF
  230         CONTINUE
  240       CONTINUE
          ENDIF
C-----------------------------------------------------------------------
          DZ(1)=0.5*(HH(2)-HH(1))
          DZ(M2)=ZMAX-0.5*(HH(M2)+HH(M2-1))
C          WRITE(*,*)'  DZ(1)=',DZ(1),'  DZ(M2)=',DZ(M2)
          DO 248 L=2,M2-1
            DZ(L)=0.5*(HH(L)+HH(L+1))-0.5*(HH(L-1)+HH(L))
C            WRITE(*,*)'  DZ(L)=',DZ(L)
  248     CONTINUE
```

```
      QM=0.0
      DO 250 K=1,M2
        QM=QM+2.*V*DZ(K)*YMOLT(K)*HFUSI*DENS*0.001
  250 CONTINUE
      QSQS=QORIG-QM
      WRITE(*,*)'QSQS=',QSQS,'    QORIG=',QORIG,'    QM=',QM
      DQS=1.-QSQS/QS
      IF(ABS(DQS).GT.0.05) THEN
        QS=QS*(1.-0.2*DQS)
        GO TO 110
      ENDIF
      IF(NOM.EQ.1)THEN
        NOM=NOM+1
        NOH=M2
        ZMAXO=ZMAX
          DO 252 I=1,NOH
          DHZ(I)=DZ(I)
  252   CONTINUE
        GO TO 110
      ENDIF
C-----------------------------------------------------------------------
      WRITE(*,*)'        ZMAX=',ZMAX,'        ZMAXO=',ZMAXO
      WRITE(*,*)'      ZMAX/H=',ZMAX/H
      IF((1.0-ZMAX/H).LT.1.E-6)THEN
        WRITE(*,*)'        A keyhole has been formed !!!'
      ELSE
        WRITE(*,*)'           No keyhole !!!'
      ENDIF
  300 CONTINUE
      MM=M1+M2
      WRITE(8,*)'     MM=',MM
      DO 310 I=1,M2
        XMOLT(I+M1)=XMOLTO(M2-I+1)
        ZMOLT(I+M1)=ZMOLTO(M2-I+1)
  310 CONTINUE
      DO 320 J=1,MM
         WRITE(8,*) XMOLT(J),ZMOLT(J)
  320 CONTINUE
C-----------------------------------------------------------------------
      WRITE(*,*)'      M3=',M3,'        JY=',JY
      IF(M3.LT.NZ)THEN
        DO 333 J=JY,1,-1
         ZM0=0.0
         DO 332 I=1,NX
           DO 331 K=2,NZ
            IF((TMOLT.LE.TEMP(I,J,K-1).AND.TMOLT.GT.TEMP(I,J,K)).OR.
     $         (TMOLT.GE.TEMP(I,J,K-1).AND.TMOLT.LT.TEMP(I,J,K)))THEN
              ZM3=Z(K-1)+(Z(K)-Z(K-1))*(TMOLT-TEMP(I,J,K-1))/
     $             (TEMP(I,J,K)-TEMP(I,J,K-1))
                  ZM0=AMAX1(ZM0,ZM3)
              GO TO 332
            ENDIF
  331       CONTINUE
  332     CONTINUE
```

```
          M3=M3+1
          YMOLT(M3)=1000.0*Y(J)
            ZMY(M3)=1000.0*ZMO
C          WRITE(*,*)'  J=',J,' YM=',YMOLT(M3),'  ZM=',ZMY(M3)
  333   CONTINUE
      ENDIF
      DO 335 J=1,M3
          WRITE(9,*)YMOLT(J),ZMY(J)
  335 CONTINUE
C-----------------------------------------------------------------------
      IF((1.0-ZMAX/H).LT.1.E-6)THEN
        WRITE(10,3000)QSQS,QORIG,QM
      ELSE
        WRITE(10,3005)QSQS,QORIG,QM,100*ZMAX/H
      ENDIF
      RETURN
 3000 FORMAT(/3X,'      QSQS       QORIG       QM             Keyhole(Y/N)?',
     $       //3X,3F10.3,'          Y')
 3005 FORMAT(/3X,'      QSQS       QORIG       QM             Keyhole(Y/N)?',
     $       //3X,3F10.3,'          N',F6.1,' %')
        END
C
C-----------------------------------------------------------------------
C
        SUBROUTINE CONV0(RJ,HJ,TJ,PLM,SDM,HW,PCONV)
        COMMON MMM
        COMMON TABTEM(20),TABIPL(20),TABCPL(20),TABKPL(20),TABISD(20)
        COMMON ITMAX,DHMAX,DTMAX
        COMMON TAMBI,DNOZL,FMPL
        COMMON TABCSD(20),TABKSD(20),TABNPL(20),TABNSD(20)
        COMMON TW4,MREG4,NREG4
        NOM=0
 200    CONTINUE
        NOM=NOM+1
        IF(NOM.GT.ITMAX) THEN
        WRITE(*,*)'   Erro Stop   ITERATIONS EXCEED ITMAX IN CONV4'
          STOP
        ENDIF
        VJM=PLM+SDM
       write(*,*)'  TJ=',TJ
      HM=.5*(HJ+HW)
      POW=VJM*HM
      CALL AVERT(PLM,SDM,POW,TABTEM,TABIPL,TABISD,TM)
        CALL INSEP(TABTEM,TABCPL,TJ,PLCP)
        CALL INSEP(TABTEM,TABCSD,TJ,SDCP)
       CP=(PLCP*PLM+SDCP*SDM)/VJM
        CALL INSEP(TABTEM,TABCPL,Tm,PLCPM)
        CALL INSEP(TABTEM,TABCSD,Tm,SDCPM)
       CPM=(PLCPM*PLM+SDCPM*SDM)/VJM
        CALL INSEP(TABTEM,TABKPL,TJ,PLAMD)
        CALL INSEP(TABTEM,TABKSD,TJ,SDAMD)
       AMD=(PLAMD*PLM+SDAMD*SDM)/VJM
        CALL INSEP(TABTEM,TABNPL,TJ,PLN)
        CALL INSEP(TABTEM,TABNSD,TJ,SDN)
```

```
 VISC=(PLN*PLM+SDN*SDM)/VJM
REN=2.*VJM/RJ/VISC/3.14159
  PRA=CP*VISC/AMD
  VNU=0.78*REN**0.5*PRA**0.33
  ALFAJ=.5*VNU*AMD/RJ
  PCONV=3.14159*RJ*RJ*ALFAJ*(HJ-Hw)/CPM
  RETURN
  END
```

Appendix C

*** INPUT DATA FOR ALUMINUM ***

SYMBOL	UNIT	DESCRIPTION	DATA
MMM		Number of point in table	18
TABTEM	K	Temperaeture table	Table attached
TABIPL	kJ/kg	Enthalpy of plasma gas	Table attached
TABCPL	kJ/kg.K	Specific heat of plasma gas	Table attached
TABKPL	kW/M.K	Thermal conductivity of plasma gas	Table attached
TABISD	kJ/kg	Enthalpy of shield gas	Table attached
TABCSD	kJ/kg.K	Specific heat of shield gas	Table attached
TABKSD	kW/M.K	Thermal conductivity of shield gas	Table attached
TABMPL	MHO/M	Electric conductivity of plasma gas	Table attached
TABMSD	MHO/M	Electric conductivity of shield gas	Table attached
TABNPL	kg/M.S	Viscosity of plasma gas	Table attached
TABNSD	kg/M.S	Viscosity of shield gas	Table attached
NREG1		Segment number between electrode and orifice	1
NREG2		Segment number of orifice	1
NREG3		Segment number of standoff	1
NREG4		Segment number of workpiece	7
VA	V	Anode potential drop	.30000E+01
VC	V	Cathode potential drop	.45000E+01
FIA1	V	Electrode work function	.30000E+01
FIA2	V	Orifice work function	.45000E+01
FIA3	V	Workpiece work function	.38000E+01
TIME	mS	Time duration for straight polarity	Variable
TIMER	mS	Time duration for reverse polarity	Variable
DISL1	M	Distance betwteen electrode and orifice	Variable
DISL2	M	Axial length of orifice	Variable

DISL3	M	Distance of standoff	Variable
DISL4	M	Thickness of workpiece	.63500E-02
VVE	Coulomb	Electron charge	.16020E-18
VVK	erg/K	Boltzman constant	.13800E-15
APIL	A	Pilot electric current in straight polarity	Variable
APILR	A	Pilot electric current in reverse polarity	Variable
AMAI	A	Main electric current in straight polarity	Variable
AMAIR	A	Main electric current in reverse polarity	Variable
DNOZL	M	Orifice diameter	.31800E-02
DSHID	M	External diameter of shield	.18000E-01
VPL	scfh	Plasma gas flow rate	Variable
VSD	scfh	Shield gas flow rate	Variable
PLMOL	kg/kmol	Molecular weight of plasma gas	.39950E+02
SDMOL	kg/kmol	Molecular weight of shield gas	.40030E+01
UR	V	Reverse polarity voltage rise	.11480E+02
ITMAX		Maximum number of iteration	100
DHMAX		Maximum relative error of enthalpy	.50000E-02
DTMAX	K	Maximum error of temperature	.50000E+00
TW1	K	Electrode wall temperature	.25000E+04
TW2	K	Orifice wall temperature	.40000E+03
TW4	K	Workpiece wall temperature	.91600E+03
HSUR2	kJ/kg	Plasma enthalpy correponding to TW2	.20800E+03
HSUR4	kJ/kg	Jet enthalpy correponding to TW4	.47600E+03
DXW	M	Electrode length	Variable
TAMBI	K	Enviromental temperature	.29800E+03
DPOLAR	M	Electrode diameter	.39600E-02
AMDW	kW/M.K	Thermal conductivity of electrode	.23500E-01

PSIA		Fraction power loss due to anode and cathode drop	.20000E+00
PAMBI	N/M2	Environmental pressure	.10132E+06
CPSD	kJ/kg.K	Specific heat of shield gas with environmental temperature	.51930E+01
ALFA	M2/S	Thermal diffusivity of workpiece	.52410E-04
VWELD	ipm	Welding speed	.91000E+01
NX		Number of computing nodal in X coordinate	15
NY		Number of computing nodal in Y coordinate	7
X(1)	M	Beginning position of computed nodal in X coordinate	-.70000E-02
X(NX)	M	Ending position of computed nodal in X coordinate	.70000E-02
Y(1)	M	Beginning position of computed nodal in Y coordinate	.00000E+00
Y(NY)	M	Ending position of computed nodal in Y coordinate	.70000E-02
TM	K	Melting temperature of workpiece	.91600E+03
TO	K	Initial temperature of workpiece	.29800E+03
THK	kW/M.K	Thermal conductivity of workpiece	.12000E+00
EPSL		Emissivity of workpiece	.10000E+00
DENS	kg/M3	Density of workpiece	.26500E+04
HFUSI	kJ/kg	Melting latent heat of workpiece	.38700E+03

Attached Table for Aluminum

Temperaeture (K)

.3000E+04	.6000E+04	.7000E+04	.8000E+04	.9000E+04
.1000E+05	.1100E+05	.1200E+05	.1300E+05	.1400E+05
.1500E+05	.1600E+05	.1700E+05	.1800E+05	.1900E+05
.2000E+05	.2200E+05	.2400E+05		

Enthalpy of Plasma Gas (kJ/kg) (ARGON)

.1562E+04	.3138E+04	.3652E+04	.4229E+04	.4966E+04
.6125E+04	.8164E+04	.1183E+05	.1778E+05	.2613E+05
.3553E+05	.4384E+05	.4957E+05	.5372E+05	.5661E+05
.5945E+05	.6862E+05	.8667E+05		

Specific Heat of Plasma Gas (kJ/kg.K) (ARGON)

.5192E+00	.5192E+00	.5401E+00	.6280E+00	.8918E+00
.1511E+01	.2721E+01	.4677E+01	.7243E+01	.9253E+01
.9253E+01	.7159E+01	.4731E+01	.3211E+01	.2734E+01
.3136E+01	.6573E+01	.1122E+02		

Thermal Conductivitv of Plasma Gas (kW/M.K) (ARGON)

.1440E-03	.1660E-03	.2030E-03	.2720E-03	.4020E-03
.6250E-03	.9610E-03	.1403E-02	.1901E-02	.2297E-02
.2417E-02	.2315E-02	.2252E-02	.2294E-02	.2436E-02
.2644E-02	.3094E-02	.3542E-02		

Enthalpy of Shield Gas (kJ/kg) (HELIUM)

.2597E+05	.3116E+05	.3635E+05	.4154E+05	.4674E+05
.5194E+05	.5728E+05	.6295E+05	.6935E+05	.7718E+05
.8773E+05	.1027E+06	.1245E+06	.1562E+06	.2011E+06
.2624E+06	.4322E+06	.6198E+06		

Specific Heat of Shield Gas (kJ/kg.K) (HELIUM)

.5193E+01	.5193E+01	.5193E+01	.5193E+01	.5229E+01
.5266E+01	.5453E+01	.5924E+01	.6952E+01	.8913E+01
.1232E+02	.1777E+02	.2588E+02	.3720E+02	.5183E+02
.6880E+02	.9526E+02	.8384E+02		

Thermal Conductivity of Shield Gas (kW/M.K) (HELIUM)

.9100E-03	.9300E-03	.9500E-03	.1028E-02	.1164E-02
.1300E-02	.1620E-02	.1940E-02	.3060E-02	.4980E-02
.6900E-02	.1174E-01	.1658E-01	.2260E-01	.2980E-01
.3700E-01	.3860E-01	.3420E-01		

Electric Conductivity of Plasma Gas (MHO/M) (ARGON)

.1030E+02	.1010E+03	.3610E+03	.9230E+03	.1770E+04
.2730E+04	.3730E+04	.4740E+04	.5740E+04	.6670E+04
.7490E+04	.8200E+04	.8810E+04	.9730E+04	.9880E+04
.1040E+05	.1080E+05	.1050E+05		

Electric Conductivity of Shield Gas (MHO/M) (HELIUM)

.4285E-01	.7852E+00	.2070E+01	.5458E+01	.1439E+02
.3793E+02	.1000E+03	.2512E+03	.6310E+03	.1261E+04
.2002E+04	.2887E+04	.3648E+04	.4368E+04	.5137E+04
.5720E+04	.7093E+04	.8794E+04		

Viscosity of Plasma Gas (kg/M.S) (ARGON)

.1290E-03	.2090E-03	.2330E-03	.2560E-03	.2770E-03
.2900E-03	.2840E-03	.2450E-03	.1810E-03	.1170E-03
.7110E-04	.4460E-04	.3150E-04	.2570E-04	.2380E-04
.2300E-04	.2100E-04	.1560E-04		

Viscosity of Shield Gas (kg/M.S) (HELIUM)

.1000E-03	.1400E-03	.1550E-03	.1620E-03	.1700E-03
.1840E-03	.1920E-03	.2000E-03	.2060E-03	.2120E-03
.2180E-03	.2200E-03	.2180E-03	.2110E-03	.2050E-03
.1950E-03	.1600E-03	.1000E-03		

Appendix D: Input Data in Program (I) (Mild Steel)

SYMBOL	DESCRIPTION	DATA
MMM	Number of point in table	26
TABTEM	Temperature table	Table Attached
TABIPL	Enthalpy of plasma gas (Argon)	Table Attached
TABCPL	Specific heat of plasma gas (Argon)	Table Attached
TABKPL	Thermal conductivity of plasma gas (Argon)	Table Attached
TABISD	Enthalpy of shield gas (Argon)	Table Attached
TABCSD	Specific heat of sheild gas (Argon)	Table Attached
TABKSD	Thermal conductivity of sheild gas (Argon)	Table Attached
TABMPL	Electric conductivity of plasma gas (Argon)	Table Attached
TABMSD	Electric conductivity of sheild gas (Argon)	Table Attached
NREG1	Segment number between electrode and orifice	1-5
NREG2	Segment number of orifice	1-5
NREG3	Segment number of standoff	1-5
NREG4	Segment number of workpiece	1-5
VA	Anode potential drop	3V
VC	Cathode potential drop	4.5V
FIA1	Electrode work function	2.6V
FIA2	Orifice work function	4.5V
FIA3	Workpiece work function	4.2V
TIME	Time duration for straight polarity	19ms
TIMER	Time duration for reverse polarity	4ms
DISL1	Distance between electrode and orifice	1.1938mm

D: Input Data in Program (II)

SYMBOL	DESCRIPTION	DATA
DISL2	Vertical length of orifice	3.175mm
DISL3	Distance of standoff	Variable
DISL4	Thichness of workpiece	6.35mm
VVE	Electron charge	1.602×10^{-19} coulomb
VVK	Boltzman constant	1.38×10^{-16} erg/k
APIL	Pilot electric current in straight polarity	Variable
APILR	Pilot electric current in reverse polarity	Variable
AMAI	Main electric current in straight polarity	Variable
AMAIR	Main electric current in reverse polarity	Variable
DNOZL	Orifice diameter	3.175mm
DSHID	External diameter of sheild gas	18mm
VPL	Plasma gas flow rate	Variable
VSD	Shield gas flow rate	Variable
PLMOL	Molecular weight of plasma gas (Argon)	39.5 kg/kmol
SDMOL	Molecular weight of shield gas (Argon)	39.5 kg/kmol
URA	Constant in computation of reverse polarity rise	12.2
URB	Constant in computation of reverse polarity rise	16
ITMAX	Maximum number of iteration	100
DHMAX	Maximum relative error of enthalpy	0.005
DTMAX	Maximum error of temperature	0.5K
TWI	Electrode wall temperature	2500K
TW2	Orifice wall temperature	353K
TW4	Workpiece wall temperature	1727K

D : Input Data in Program (III)

SYMBOL	DESCRIPTION	DATA
HSUR2	Plasma enthalpy corresponding to TW2 (Argon)	190 kJ/kg
HSUR4	Jet enthalpy corresponding to TW4 (Argon)	900 kJ/kg
DXW	Electrode length	68.072mm
TAMBI	Environmental temperature	298K
DPOLAR	Electrode diameter	3.9624mm
AMDW	Thermal conductivity of electrode	23.5 W/m.K
PSIA	Fraction of power loss due to anode and cathode drops	0.
PAMBI	Environmental pressure	101320 N/m^2
CPSD	Specific heat of shield gas with environmental temperature (Argon)	0.5205 kJ/kg.K
NX	Number of computing nodal in X coordinate	10
NY	Number of computing nodal in Y coordinate	20
NZ	Number of computing nodal in Z coordinate	2
NHH	Number of heat source	1
X	Position of computed nodal in X coordinate	Variable
Y	Position of computed nodal in Y coordinate	Variable
Z	Position of computed nodal in Z coordinate	0., 6.35mm
HH	Position of heat source	3.175mm
H	Workpiece thickness	6.35mm
V	Welding speed	Variable
ALPHA	Thermal diffusivity of workpiece	5.45×10^{-6} m^2/s

D : Input Data in Program (IV)

SYMBOL	DESCRIPTION	DATA
THK	Thermal conductivity of workpiece	21.63 W/m.K
DENS	Density of workplace	7900 kg/m^3
HFUSI	Melting latent heat	272 kJ/kg
TMOLT	Temperature rise	1429K

Appendix D: Attached Table for Mild Steel (I)

51,99L

THERMAL CONDUCTIVITY OF PLASMA GAS (kW/m.K) (ARGON)

.1013E-03 .1057E-03 .1174E-03 .1432E-03 .1933E-03

.2820E-03 .4279E-03 .6550E-03 .9916E-03 .1463E-02

.2050E-02 .2563E-02 .2675E-02 .2480E-02 .2348E-02

.2374E-02 .2507E-02 .2697E-02 .3148E-02 .3632E-02

.4126E-02 .4623E-02 .5120E-02 .5618E-02 .6116E-02

.6365E-02

ENTHALPY OF SHIELD GAS (kJ/kg) (ARGON)

.1562E+04 .2082E+04 .2603E+04 .3125E+04 .3654E+04

.4215E+04 .4894E+04 .5931E+04 .7892E+04 .1173E+05

.1823E+05 .2680E+05 .3549E+05 .4287E+05 .4874E+05

.5351E+05 .5762E+05 .6143E+05 .6988E+05 .8590E+05

.1112E+06 .1298E+06 .1441E+06 .1609E+06 .1831E+06

.1956E+06

SPECIFIC HEAT OF SHIELD GAS (kJ/kg.K) (ARGON)

.5205E+00 .5205E+00 .5209E+00 .5238E+00 .5382E+00

.5972E+00 .7971E+00 .1370E+01 .2719E+01 .5115E+01

.7791E+01 .8973E+01 .8163E+01 .6581E+01 .5236E+01

.4370E+01 .3901E+01 .3771E+01 .5252E+01 .1139E+02

.1173E+02 .7515E+01 .7329E+01 .9700E+01 .1229E+02

.1265E+02

*

D: Attached Table for Mild Steel (II)

```
51,99L
   51:
   52:      THERMAL CONDUCTIVITY OF PLASMA GAS (kW/m.K)  (ARGON)
   53:
   54:      .1013E-03   .1057E-03   .1174E-03   .1432E-03   .1933E-03
   55:
   56:      .2820E-03   .4279E-03   .6550E-03   .9916E-03   .1463E-02
   57:
   58:      .2050E-02   .2563E-02   .2875E-02   .2480E-02   .2348E-02
   59:
   60:      .2374E-02   .2507E-02   .2697E-02   .3148E-02   .3632E-02
   61:
   62:      .4126E-02   .4623E-02   .5120E-02   .5618E-02   .6116E-02
   63:
   64:      .6365E-02
   65:
   66:
   67:
   68:      ENTHALPY OF SHIELD GAS (kJ/kg)   (ARGON)
   69:
   70:      .1562E+04   .2082E+04   .2603E+04   .3125E+04   .3654E+04
   71:
   72:      .4215E+04   .4894E+04   .5931E+04   .7892E+04   .1173E+05
   73:
   74:      .1823E+05   .2680E+05   .3549E+05   .4287E+05   .4874E+05
   75:
   76:      .5351E+05   .5762E+05   .6143E+05   .6988E+05   .8590E+05
   77:
   78:      .1112E+06   .1298E+06   .1441E+06   .1609E+06   .1831E+06
   79:
   80:      .1956E+06
   81:
   82:
   83:
   84:      SPECIFIC HEAT OF SHIELD GAS (kJ/kg.K)  (ARGON)
   85:
   86:      .5205E+00   .5205E+00   .5209E+00   .5238E+00   .5382E+00
   87:
   88:      .5972E+00   .7971E+00   .1370E+01   .2719E+01   .5115E+01
   89:
   90:      .7791E+01   .8973E+01   .8163E+01   .6581E+01   .5236E+01
   91:
   92:      .4370E+01   .3901E+01   .3771E+01   .5252E+01   .1139E+02
   93:
   94:      .1173E+02   .7515E+01   .7329E+01   .9700E+01   .1229E+02
   95:
   96:      .1265E+02
   97:
   98:
   99:
```

D: Attached Table for Mild Steel (III)

```
100,147L
  100:      THERMAL CONDUCTIVITY OF SHIELD GAS (KW/m.K)  (ARGON)
  101:
  102:      .1013E-03   .1057E-03   .1174E-03   .1432E-03   .1933E-03
  103:
  104:      .2820E-03   .4279E-03   .6550E-03   .9916E-03   .1463E-02
  105:
  106:      .2050E-02   .2563E-02   .2675E-02   .2480E-02   .2348E-02
  107:
  108:      .2874E-02   .2507E-02   .2697E-02   .3148E-02   .3632E-02
  109:
  110:      .4126E-02   .4623E-02   .5120E-02   .5618E-02   .6116E-02
  111:
  112:      .6365E-02
  113:
  114:
  115:
  116:      ELECTRIC CONDUCTIVITY OF PLASMA GAS (MHO/m)  (ARGON)
  117:
  118:      .5960E-04   .1270E+00   .1030E+02   .1010E+03   .3610E+03
  119:
  120:      .9230E+03   .1770E+04   .2730E-04   .3730E+04   .4740E+04
  121:
  122:      .5740E-04   .6670E+04   .7490E+04   .8200E+04   .8810E+04
  123:
  124:      .9730E+04   .9880E+04   .1040E+05   .1080E+05   .1050E+05
  125:
  126:      .1020E+05   .1040E+05   .1090E+05   .1130E+05   .1160E+05
  127:
  128:      .1170E+05
  129:
  130:
  131:
  132:      ELECTRIC CONDUCTIVITY OF SHIELD GAS (MHO/m)  (ARGON)
  133:
  134:      .5960E-04   .1270E+00   .1030E+02   .1010E+03   .3610E+03
  135:
  136:      .9230E+03   .1770E+04   .2730E+04   .3730E+04   .4740E+04
  137:
  138:      .5740E+04   .6670E+04   .7490E+04   .8200E+04   .8810E+04
  139:
  140:      .9730E+04   .9880E+04   .1040E+05   .1080E+05   .1050E+05
  141:
  142:      .1020E+05   .1040E+05   .1090E+05   .1130E+05   .1160E+05
  143:
  144:      .1170E+05
*
```

Appendix E : Nomenclature

A_C = Crown reinforcement area (m^2)

A_E = Cross-sectional area of electrode (m^2)

A_N = Orifice circumferential area (m^2)

A_r = Root reinforcement area (m^2)

C_p = Constant pressure specific heat (J/kg·k)

D = Orifice diameter (m)

D_E = Electrode diameter (m)

$D_{s,e}$ = External diameter of shielding gas (m)

d_c = Crown bead width (m)

d_r = Root bead width (m)

$\frac{dv}{dL}$ = Voltage drop per unit length (V/m)

d_w = Feed wire diameter (m)

g = Gravitational acceleration (m/s^2)

h_c = Crown height (m)

h_{exit} = Plasma jet enthalpy at the exit of workpiece (J/kg)

h_N = Plasma enthalpy corresponding to the orifice wall temperature (J/kg)

h_{plasma} = Plasma enthalpy (J/kg)

h_r = Root height (m)

$h_{1,i}$, $h_{1,o}$ = Plasma enthalpy at entrance and exit ends, respectively, of gap between electrode and orifice (J/kg)

$h_{2,i}$, $h_{2,o}$ = Plasma enthalpy at entrance and exit ends, respectively, of orifice (J/kg)

$h_{3,i}$, $h_{3,o}$ = Plasma enthalpy at entrance and exit ends, respectively, of standoff column (J/kg)

$h_{4,i}$, $h_{4,o}$ = Plasma enthalpy at entrance and exit ends, respectively, of workpiece keyhole (J/kg)

I_m^+, I_m^- = Main electric current in straight and reverse polarities, respectively (A)

I_p^+, I_p^- = Pilot electric current in straight and reverse polarities, respectively (A)

k = Thermal conductivity of plasma jet (W/m·k)

k_E = Thermal conductivity of electrode (W/m·k)

L_E = Length of electrode (m)

L_1 = Distance between electrode and orifice (m)

L_2 = Axial length of orifice (m)

L_3 = Column distance of standoff (m)

L_4 = Thickness of workpiece (m)

$\dot{m}_{pl}$ = Plasma gas mass flow rate (kg/s)

$\dot{m}_{sd}$ = Shielding gas mass flow rate (kg/s)

M_{pl} = Molecular weight of plasma gas (kg/kmol)

M_{sd} = Molecular weight of shielding gas (kg/kmol)

n = Parabolic exponent of reinforcement shape

$\bar{P}$ = External pressure (N/m^2)

P_{pl} = Partial pressure of plasma gas (N/m^2)

P_E = Power input at electrode (W)

P_H = Environment pressure (N/m^2)

P_{sd} = Partial pressure of shielding gas (N/m^2)

$P_{J,1}$ = Joule heating power input in the gap between electrode and orifice (W)

$P_{J,2}$ = Joule heating power input in the orifice (W)

$P_{J,3}$ = Joule heating power input in the standoff column (W)

$P_{N,1}$ = Orifice work function induced power input (W)

$P_{N,2}$ = Orifice anode drop induced power input (W)

$P_{w,1}$ = Workpiece work function induced power input (W)

$P_{w,2}$ = Workpiece anode and cathode drops induced power input (W)

$P_{1,i}$, $P_{1,o}$ = Plasma arc power at entrance and exit ends respectively, of gap between electrode and orifice (W)

$P_{2,i}$, $P_{2,o}$ = Plasma arc power at entrance and exit ends respectively, of orifice (W)

$P_{3,i}$, $P_{3,o}$ = Plasma arc power at entrance and exit ends respectively, of standoff column (W)

$P_{4,i}$, $P_{4,o}$ = Plasma power at entrance and exit ends, respectively, of workpiece keyhole (W)

Q_{dis} = Plasma arc discharged power loss (at exit end of keyhole) (W)

Q_G = Power loss in the gap between electrode and orifice (W)

Q_N = Total power loss in the orifice (W)

$Q_{N,c}$ = Convective heat transfer power loss in the orifice (W)

$Q_{N,e}$ = Free electron power loss in the orifice (W)

$Q_{N,G}$ = Direct power loss from the surface of the orifice contributed by total power input to work function and part of power input to anode drop at orifice (W)

$Q_{s,r}$ = Standoff column radiative power loss (W)

$Q_{s,c}$ = Standoff columln convective power loss (W)

Q_s = Standoff column total power loss (W)

$Q_{W,c}$ = Convective heat transfer workpiece power loss (W)

$Q_{W,e}$ = Free electron power loss in workpiece (W)

Q_w = Total power loss in workpiece (W)

R = Universal gas constant (J/mol·K)

R_E = Effective radius of plasma jet (m)

R_o = Orifice radius (m)

R_i = Distant between source and point of computation at workpiece (m)

t_+, t_- = Time duration for straight and reverse polarities, respectively (s)

T_E = Effective temperature of plasma jet; Electrode temperature (K)

T_H = Environment temperature (K)

T_m = Melting temperature of workpiece (K)

T_o = Jet core temperature; Initial temperature of workpiece (K)

u = Welding traveling speed; plasma jet velocity (m/s)

u_H = Ambient flow velocity (m/s)

u_o = Jet core velocity (m/s)

V_A, V_B, V_C, V_D, V_E, V_F, V_G = Straight polarity electric voltage, shown in Figure 1, at points A, B, C, D, E, F, and G, respectively (V)

V_A', V_B', V_C', V_D', V_E', V_F', V_G' = Reverse polarity electric voltage, shown in Figure 1, at points A', B', C', D', E', F', and G', respectively (V)

V_G = Plasma volumetric flow rate in the gap between electrode and orifice (m^3/s)

V_s = Plasma volume in the standoff column (m^3/s)

V_w = Wire feeding speed (m/s)

W_g = Initial gap distance between two workpieces (m)

x_H = Distance of Jet Initial Region (m)

Y = Coordinate axis

Y_c = Coordinate to be used for spatial temperature distribution computation (m)

Z = Coordinate axis

Z_c = Coordinate to be used for spatial temperature distribution computation (m)

$Z_{1\ 35}$ = Heat source spatial point of distribution (m)

α = Angle (rad); workpiece thermal diffusivity (m^2/s)

β = Angle (rad)

ΔV_a, ΔV_c = Anode and cathode electric potential drops, respectively (V)

ΔV_m^+, ΔV_m^- = Main electric voltage drops in straight and reverse polarities, respectively (V)

ΔV_p^+, ΔV_p^- = Pilot electric voltage drops in straight and reverse polarities, respectively (V)

ϵ = Emissivity of workpiece

ϵ_R = Reverse polarity voltage rise (V)

σ_s = Surface tension coefficient (N/m)

ϕ = Fraction of heat source distributed in spatial coordinate

ϕ_E = Electrode work function (V)

ϕ_N = Orifice work function (V)

ϕ_w = Workpiece work function (V)

ψ = Fraction of orifice, or workpiece, power loss contributed by anode and cathode drops

η = Dimensionless coordinate

ρ_{pl} = Mass of plasma gas in unit volume of plasma jet (kg/m^3)

ρ_{sd} = Mass of shielding gas in unit volume of plasma jet (kg/m^3)

Basic Input Parameters (I)

(Aluminum #2219-T87)

Symbol	Description	Data Input
L_1	Distance between electrode and nozzle	1.1176 mm
L_2	Vertical length of nozzle	3.2766 mm
L_4	Thickness of workpiece	6.35 mm
L_E	Length of electrode	69.6 mm
D	Nozzle diameter	3.175 mm
D_E	Electrode diameter	3.9624 mm
K_E	Thermal conductivity of electrode	23.0 kW/m·°K
$\dot{m}$	Argon gas mass flow rate	Variable
ϕ_E	Electrode work function	3.0 V
ϕ_N	Nozzle work function	4.5 V
ϕ_w	Workpiece work function	3.8 V
ΔV_a	Anode potential drop	3.0 V
ΔV_c	Cathode potential drop	4.5 V
I_m^+	Main electric current in straight polarity	Variable
I_m^-	Main electric current in reverse polarity	Variable
I_p^+	Pilot electric current in straight polarity	Variable
I_p^-	Pilot electric current in reverse polarity	Variable
t_+	Time duration for straight polarity	19 ms
t_-	Time duration for reverse polarity	4 ms
T_E	Electrode temperature	2500 °K
T_N	Nozzle temperature	400 °K
T_o	Environment temperature; Initial temperature of workpiece	298 °K

Basic Input Parmeters (II)

(Aluminum #2219-T87)

Symbol	Description	Data Input
h_N	Plasma enthalpy corresponding to orifice wall temperature	0.208 $\frac{kJ}{g}$
h_W	Plasma enthalpy corresponding to keyhole temperature	0.476 $\frac{kJ}{g}$
ψ	Fraction of power loss due to anode and cathode drops	0.0
ϕ	Location of welding heat source from back of workpiece in fraction of plate thickness	0.5 - 1.0
u	Welding traveling speed	Variable
k_w	Thermal conductivity of workpiece	0.13 $\frac{kw}{m \cdot {}^{\circ}K}$
α	Thermal diffusivity of workpiece	5.678×10^{-5} $\frac{m^2}{s}$
ρ_W	Density of workpiece	2650 kg/m^3
Q_f	Melting heat of workpiece	387 kJ/kg
ϵ	Emissivity of workpiece	0.1
T_m	Melting temperature of workpiece	916 $^{\circ}K$

Appendix F Block Diagram of Penetration Depth Calculation

Structure Diagram of WELD0 Computer Program
(Computation of penetration depth)

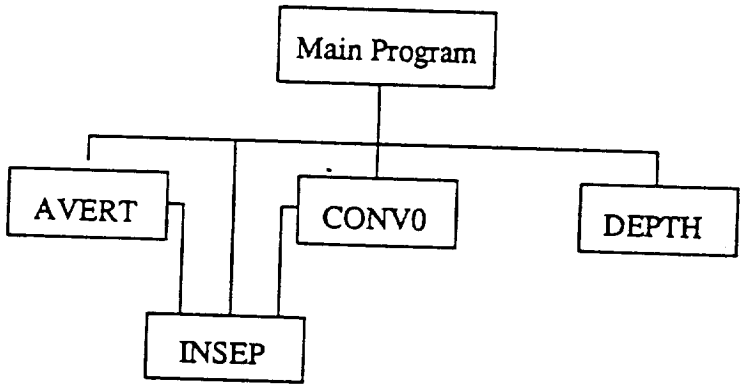

Explanation of WELD0 Program Structure

1. Main Program

   Input physical parameter tables of plasma and shield gas and initial parameters of welding process .
   Compute distribution of related physical parameters of plasma and shield gas , such as electric potential , power , power loss , enthalpy, etc., between torch and workpiece.

2. Subroutine AVERT

   Compute mean temperature of plasma and shield gas mixture with given plasma and shield gas flow rate and power of the mixture.

3. Subroutine INSEP

   Compute interpalatively temperature or enthalpy and their corresponding values of related physical parameters of plasma and shield gas with input values of plasma and shield gas material constants and given temperature or enthalpy of plasma and shield gas.

4. Subroutine CONV0

   Compute power transmission from plasma jet to workpiece through heat process.

5. Subroutine DEPTH

   Compute temperature distribution , geometry of molten pool of workpiece and depth of partial penetration of welding process.

Flow Chart of WELD0 Computation Program

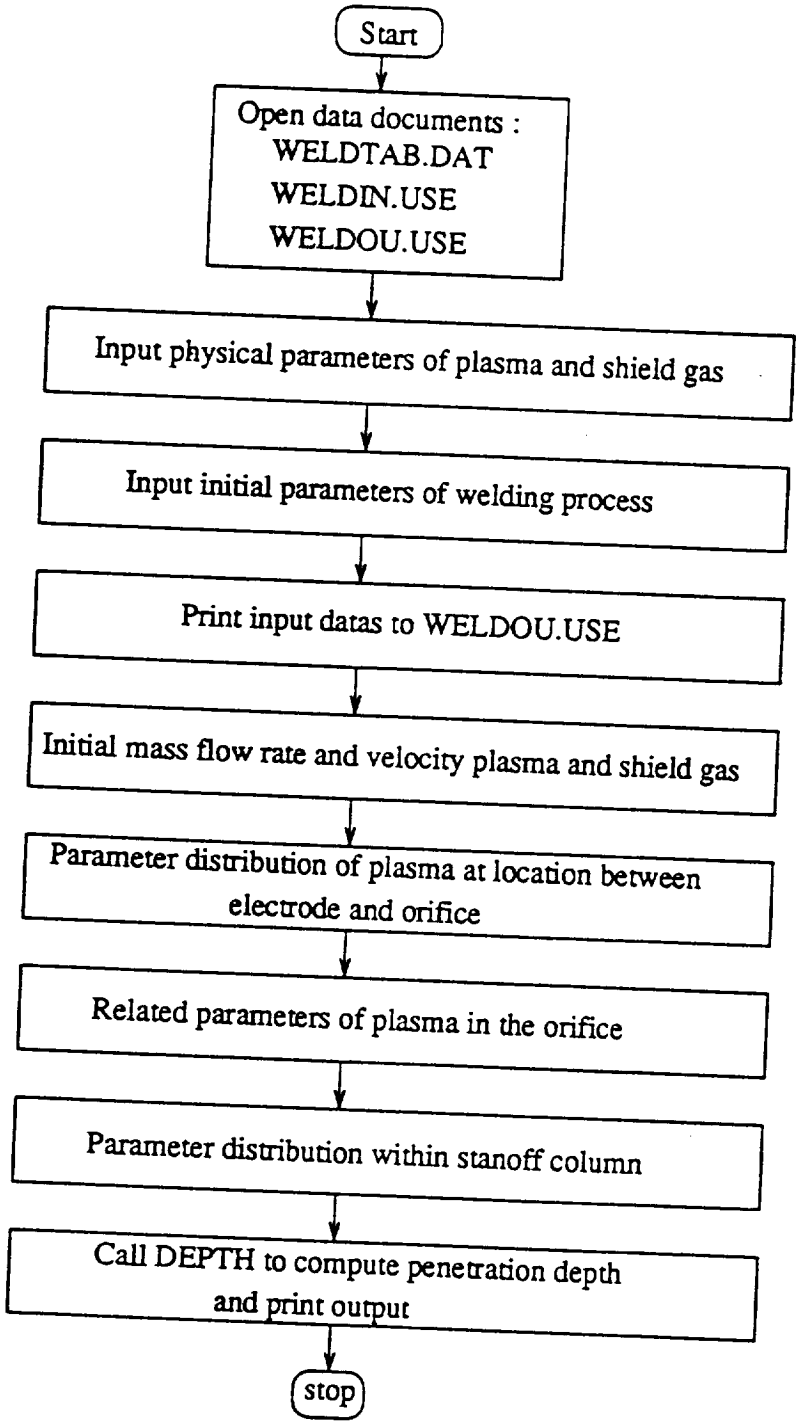

Appendix G Block Diagram of VPPA Modeling Structure

Structure Diagram of Diagram of WELDBOTH
(VPPA Modeling)

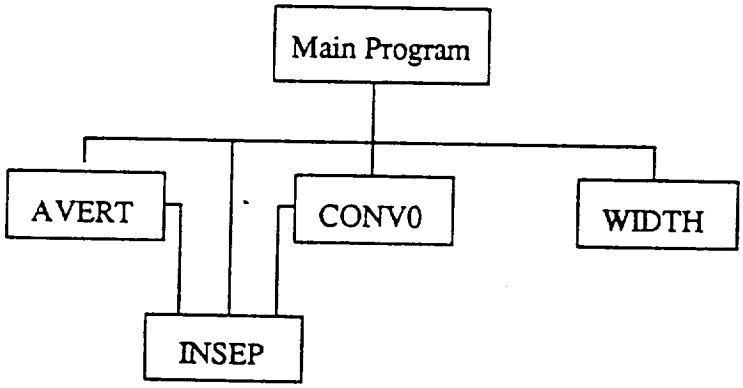

Explanation of WELDBOTH Program Structure

1. Main Program
   Input physical parameter tables of plasma and shield gas and initial parameters of welding process. Compute distribution of related physical parameters of plasma and shield gas ,such as electric potential , power , power loss , enthalpy , etc., between torch and workpiece .
2. Subroutine AVERT
   Compute mean temperature of plasma and shield gas mixture with given plasma and shield gas flow rate and power of the mixture .
3. Subroutine INSEP
   Compute interpalatively temperature or enthalpy and their corresponding values of related physical parameters of plasma and shield gas with input values of plasma and shield gas material constants and given temperature or enthalpy of plasma and shield gas.
4. Subroutine CONV4
   Compute power transmission from plasma jet to the wall of keyhole in workpiece through heat convection process.
5. Subroutine DEPTH
   Compute crown and root widths based on temperature distribution of workpiece and geometry of keyhole.

Flow Chart of WELDBOTH Computation Program

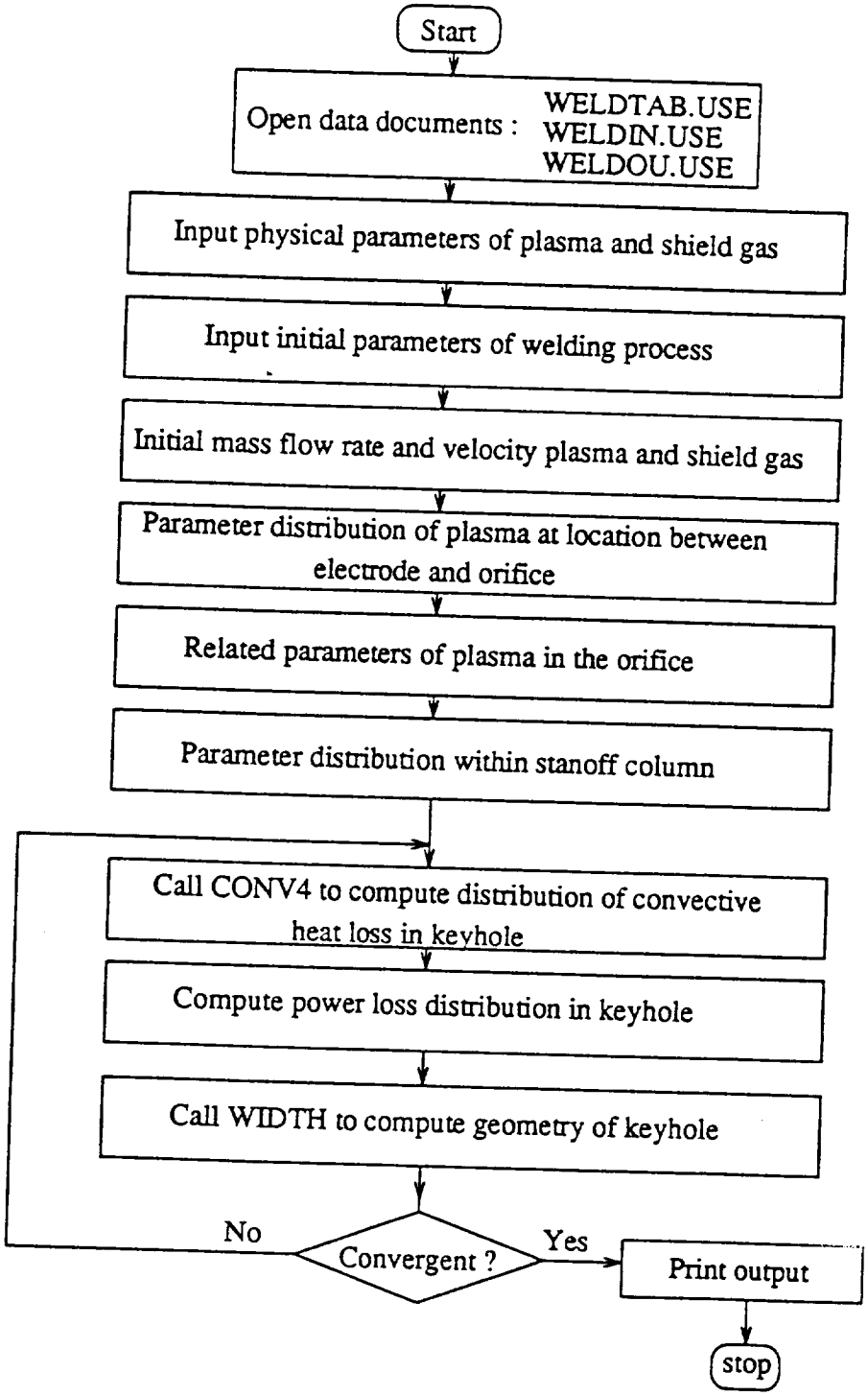

Appendix H

Comparison Between Results of Model Computations and Experimental Measurements

Figures H-1 to H-63 show the comparison between the results of model computations and experimental measurements. Model computations are based on the mathematical formulations illustrated in this report, while experimental measurements are adopted from the experiments accomplished by Nichols Research Corporation (1992).

In Figures H-1 to H-31, comparisons are made between the model computed values of forward electric voltage and reversed electric voltage versus that of the values of experimental measurements. The results show that the tendency and magnitudes of the model computations are very much the same as that of the experimental measurements.

In Figures H-32 to H-38, comparisons are made for leading edge angle between model computated values and that of the values of experimental measurements. There are so many parameters which could be changed in the experimental measurements. It is very hard to choose a series of experimental measurement with one parameter as a variable and with the rest of the parameters unchanged. Comparisons made in Figures H-32 to H-38 follow the order of the sequence of experimental measurement of leading edge angle between model computation and experiment. The results also show that the tendency and magnitudes of the model computations are very much the same as that of the experimental measurements.

Figures H-39 to H-62 show the comparison for crown width and root width between model computed values and that of the values of experimental measurements. The results show that the model computation and the experimental measurement are relatively in good manners of agreement. It is noted that some parameters provide a great influence on the model computation of the crown and root widths. However, within the range of proper control of parameters, it can anticipate to predict a fairly reasonably good values of model computation in crown and root widths agreeable in comparison with the experimental measurements.

As to the problems of abnormal welding, model formulations illustrated in Section VII of this report have been adopted to calculate the probability of the keyhole full and partial penetrations of the welding workpiece. Table H-A shows the results of model computations for keyhole full and partial penetration of the workpiece in comparison to experimental measurements of ID Numbers 7A to 7P listed in the report accomplished by Nichols Research Corporation (1992), while Table H-B illustrates the results of the similar model computations in comparison to experimental measurements of ID Numbers 8A to 8N listed in the same report. It shows that the results of model computation are basically all agreeable with the experimental measurements based on the points of the possibility of keyhole full and partial penetrations of the welding workpiece.

For the purpose of making easier comparison for the possibility of keyhole full and partial penetrations of welding workpiece among so many different controlled parameters of welding

process between model computation and experimental measurements, a set of dimensionless parameters are proposed and illustrated in Figure H-63 with $V \cdot H/(2\alpha)$ as the horizontal coordinate and $Q/[4\pi \cdot H \cdot (k \cdot \Delta T_m + \alpha \rho L_f)]$ as the vertical coordinate. Here,

V = Welding Speed

H = Thickness of workpiece

α = Thermal diffusivity of workpiece

k = Thermal conductivity of workpiece

ΔT_m = Temperature difference between molten and initial temperatures of workpiece

ρ = Density of workpiece

L_f = Latent heat of molten workpiece

Q = Total power absorption of workpiece during the welding process.

Recall that there is no available experimental measurements of Q values because of the difficulty in accurate measurements of Q values experimentally. Q values adopted in Figure H-63 are calculated based on the physical model illustrated in Equation (7-3) of this report.

Figure H-63 shows the critical curve for keyhole full and partial penetrations of welding workpiece from the model computation. In this figure, the left-hand upper region shows the zone of keyhole full penetration while the right-hand lower region illustrates the zone of partial penetration. This curve is computed based on the condition of the bottom portion of the workpiece to attain molten temperature of the metal. Precise locations of each experimental measurements with experimental ID

numbers 7 and 8 from the Nichols report are also plotted. In these experiments, aluminum workpiece with thickness of 1/4" (6.35 mm) are used. The results show that the model computations predict the keyhole full and partial penetrations of welding completely agreeable with that of the experimental measurements.

Table H-A (a)

CALCULATION COMPARED WITH EXPERIMENT

ID#	QSQS (kW)	QORIG (kW)	QM (kW)	Keyhole(Y/N)? Cal.	Exp.
7A1	1.235	1.381	.143	Y	Y
7A2	1.306	1.474	.168	Y	Y
7A3	1.404	1.604	.199	Y	Y
7B1	1.241	1.390	.148	Y	Y
7B2	1.337	1.515	.178	Y	Y
7B3	1.444	1.657	.212	Y	Y
7C1	1.300	1.467	.167	Y	Y
7C2	1.394	1.590	.196	Y	Y
7C3	1.507	1.740	.233	Y	Y
7D1	1.377	1.567	.191	Y	Y
7D2	1.493	1.708	.225	Y	Y
7D3	1.594	1.858	.264	Y	Y
7E1	1.226	1.340	.115	N 51.4 %	N
7E2	1.347	1.479	.132	N 55.6 %	N
7E3	1.456	1.614	.158	N 63.0 %	N
7F1	1.257	1.378	.121	N 51.9 %	N
7F2	1.385	1.526	.141	N 59.3 %	N
7F3	1.502	1.673	.171	N 64.3 %	N
7G1	1.321	1.455	.134	N 53.6 %	N
7G2	1.432	1.585	.135	N 61.7 %	N
7G3	1.563	1.755	.188	N 66.2 %	N

Table H - A (b)

7H1	1.399	1.544	.145	N	60.2 %	N
7H2	1.516	1.691	.174	N	64.8 %	N
7H3	1.665	1.874	.209	N	75.0 %	N
7I1	0.981	1.087	.106	N	77.14%	INTERMIT
7I2	1.098	1.232	.134	Y		INTERMIT
7I3	1.231	1.385	.172	Y		INTERMIT
7J1	1.004	1.111	.107	N		INTERMIT
7J2	1.133	1.284	.151	Y		INTERMIT
7J3	1.246	1.426	.180	Y		INTERMIT
7K1	1.074	1.202	.128	N		INTERMIT
7K2	1.197	1.364	.167	Y		INTERMIT
7K3	1.305	1.501	.196	Y		INTERMIT
7L1	1.137	1.290	.153	Y		INTERMIT
7L2	1.261	1.444	.183	Y		INTERMIT
7L3	1.380	1.592	.212	Y		INTERMIT
7M1	0.961	1.071	.110	N	46.7%	N
7M2	1.111	1.248	.137	N	50.5%	N
7M3	1.228	1.384	.156	N	52.7%	N
7N1	1.011	1.123	.113	N	47.0%	N
7N2	1.155	1.299	.144	N	51.2%	N
7N3	1.280	1.444	.164	N	53.2%	N
701	1.072	1.202	.130	N	49.4%	N
702	1.216	1.370	.154	N	52.1%	N
703	1.345	1.519	.152	N	54.1%	N

Table H-A (c)

7P1	1.166	1.311	.146	N 51.2%	N
7P2	1.311	1.479	.169	N 53.6%	N
7P3	1.445	1.628	.184	N 53.1%	N

Materal : 1/4"(6.35mm) 2219-T87 Aluminum (7A-7H)
1/4"(6.35mm) A36 Mild Steel (7I-7P)

QORIG = Power obsorbed by workpiece.

QM = Latent power of workpiece.

QSQS = Conduction loss in workpiece (= QORIG-QM).

These values are calculated by the model

Table H-B

CALCULATION COMPARED WITH EXPERIMENT

Estimating whether keyhole can be formed

ID#	CALCULATION					EXPERIMENT RESULTS				
	QSQS (kW)	QORIG (kW)	QM (kW)	Keyhole? (Y/N)		Weld width Crown Root		Weld height Crown Root		Bead Appearance
8A	1.103	1.184	.089	N	85.7 %	9.86	*	1.24	*	PP,N
8B	1.101	1.180	.070	N	85.2 %	9.45	*	1.30	*	PP,N
8C	1.105	1.135	.080	N	85.9 %	9.40	*	1.31	*	PP,N
8D	1.103	1.183	.080	N	85.6 %	9.41	*	1.08	*	PP,N
8E	1.103	1.183	.080	N	85.6 %	9.58	*	1.52	*	PP,N
8F	0.935	0.982	.046	N	61.6 %	5.74	*	1.70	*	PP,N
8G	1.164	1.362	.198	Y		10.03	*	1.14	0.75	PP,PT,N
8H	0.979	1.084	.105	N	76.1%	9.00	*	1.25	*	PP,N
8I	0.976	1.081	.105	N	75.8%	8.38	*	1.85	*	PP,D
8J	0.977	1.082	.105	N	75.9%	9.80	*	1.17	*	PP,D
8K	0.977	1.082	.105	N	75.9%	9.32	*	1.02	*	PP,D
8L	0.972	1.078	.104	N	76.5%	8.78	*	1.30	*	PP,N
8M	0.889	0.973	.084	N	67.4%	7.87	*	1.11	*	PP,N
8N	1.059	1.182	.123	N	87.0%	8.28	*	*	*	PP,D

Materal : 1/4"(6.35mm) 2219-T87 Aluminum (8A-8G)
1/4"(6.35mm) A36 Mild Steel (8H-8N)

QORIG = Power obsorbed by workpiece.

QM = Latent power of workpiece.

QSQS = Conduction loss in workpiece (= QORIG-QM).

These values are calculated by the model

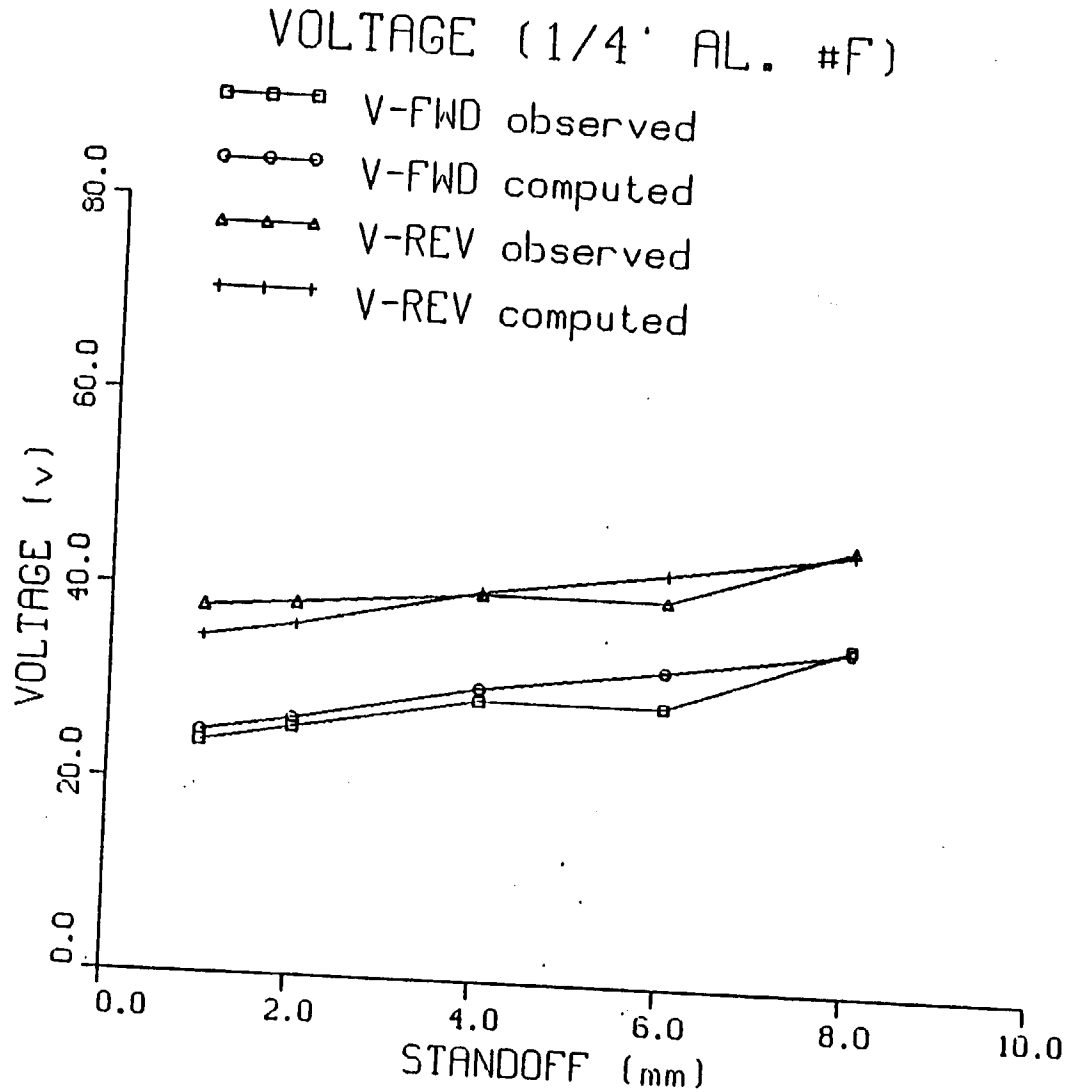
VOLTAGE (1/4' AL. #F)
V-FWD observed
V-FWD computed
V-REV observed
V-REV computed
VOLTAGE (v)
80.0
60.0
40.0
20.0
0.0
0.0
2.0
4.0
6.0
8.0
10.0
STANDOFF (mm)

Fig. H-1

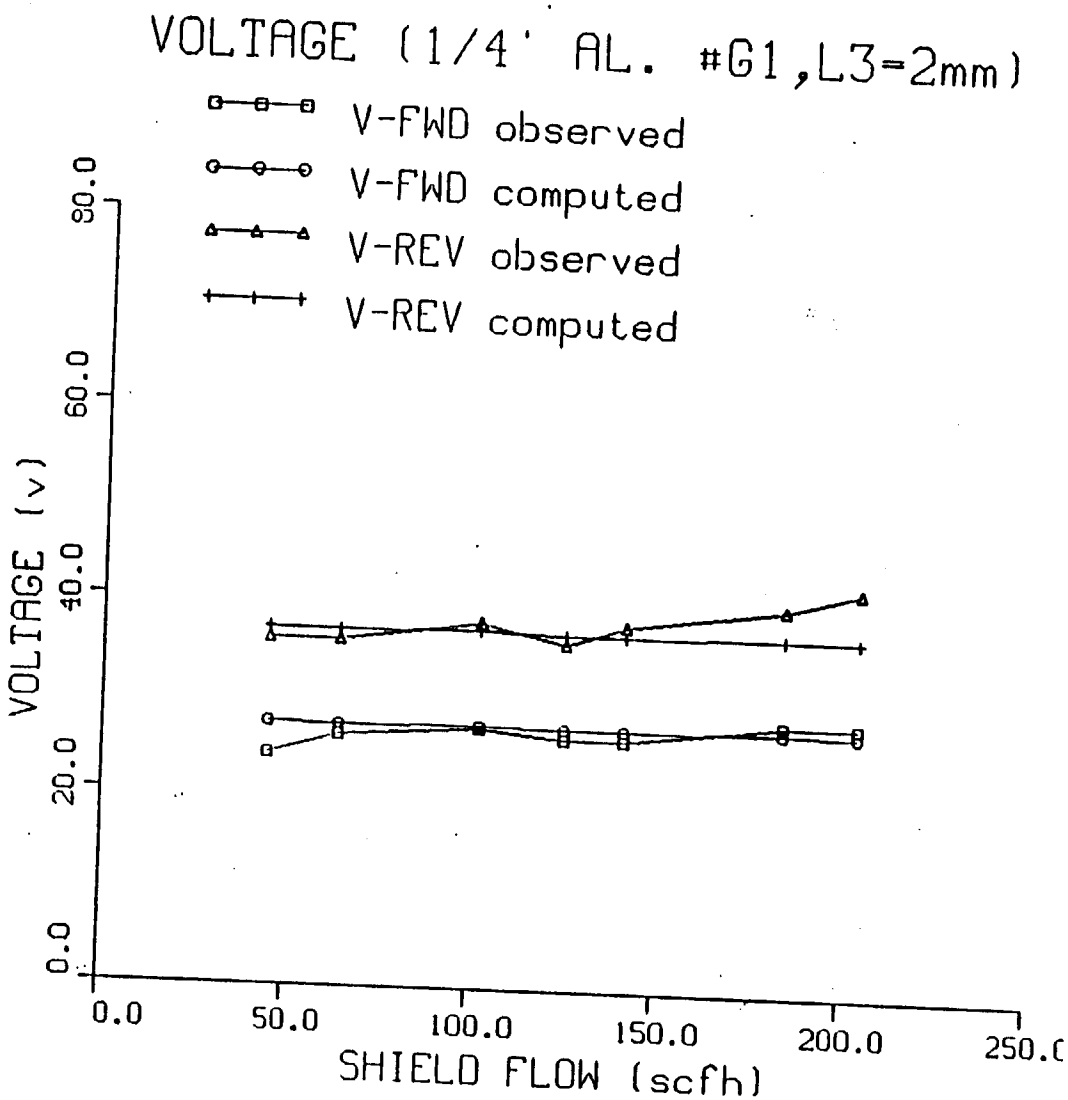
VOLTAGE (1/4' AL. #G1,L3=2mm)
V-FWD observed
V-FWD computed
V-REV observed
V-REV computed
VOLTAGE (v)
80.0
60.0
40.0
20.0
0.0
0.0
50.0
100.0
150.0
200.0
250.0
SHIELD FLOW (scfh)

Fig. H-2

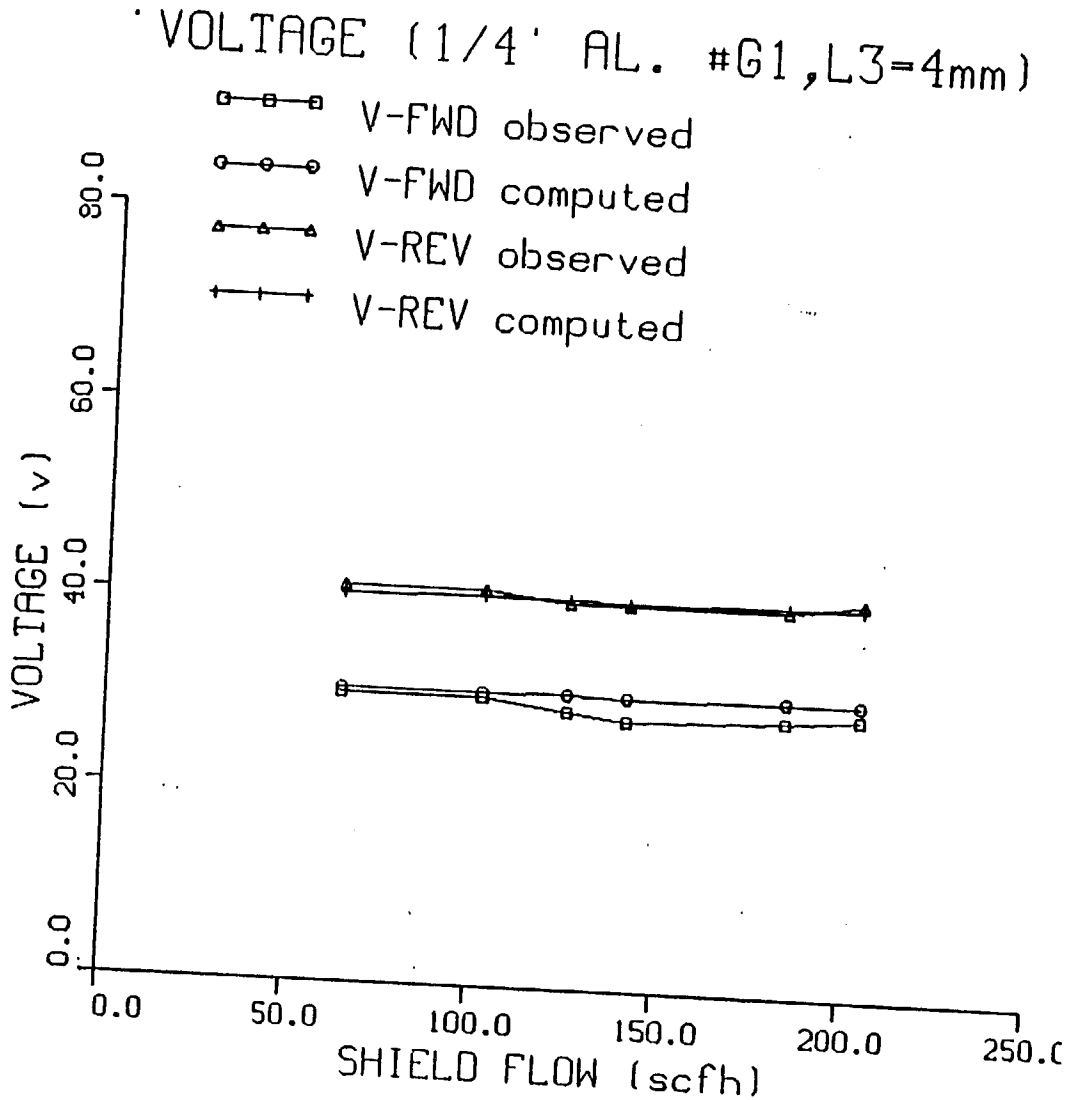
VOLTAGE (1/4' AL. #G1,L3=4mm)
V-FWD observed
V-FWD computed
V-REV observed
V-REV computed
VOLTAGE (v)
80.0
60.0
40.0
20.0
0.0
0.0
50.0
100.0
150.0
200.0
250.0
SHIELD FLOW (scfh)

Fig. H-3

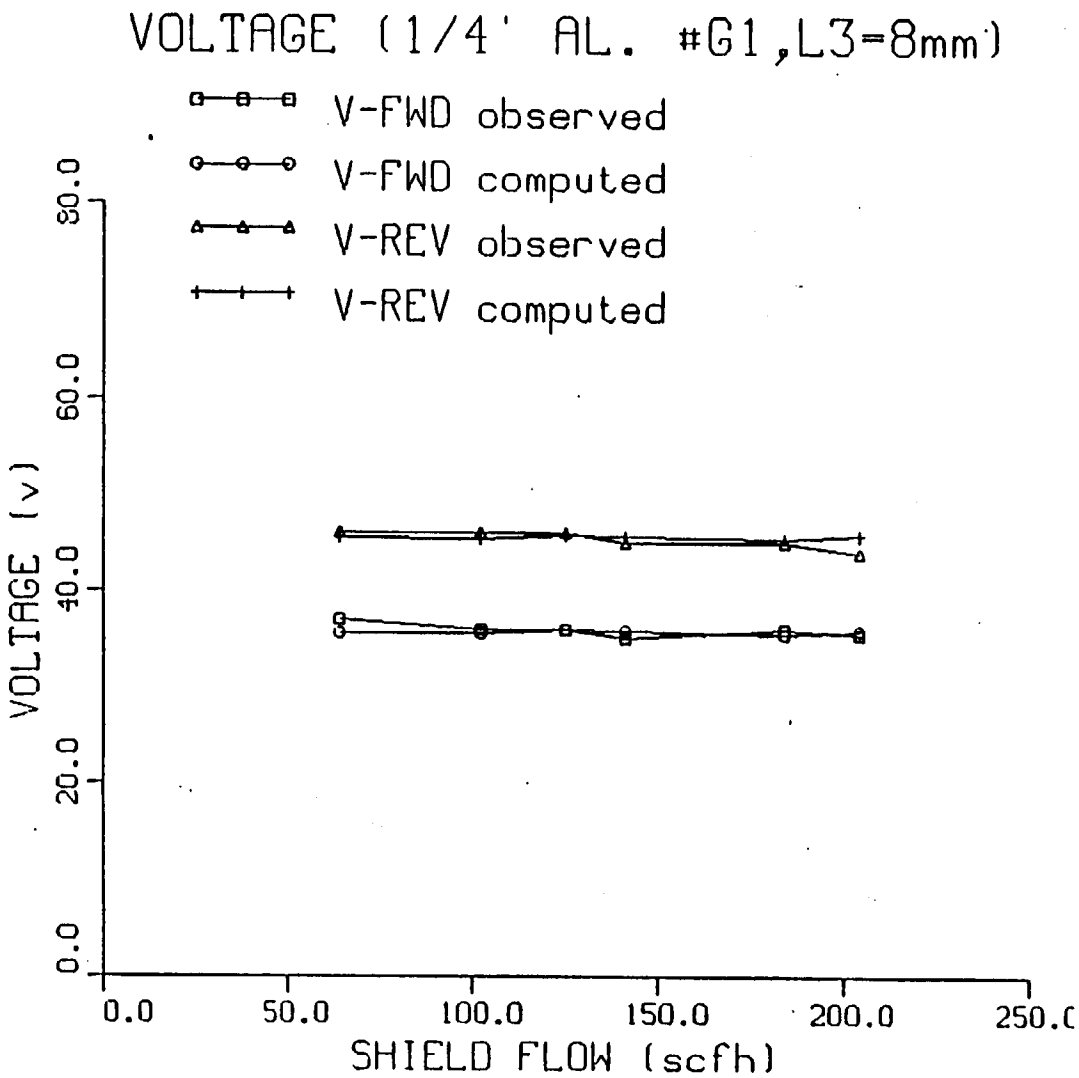
VOLTAGE (1/4' AL. #G1,L3=8mm)
V-FWD observed
V-FWD computed
V-REV observed
V-REV computed
VOLTAGE (v)
80.0
60.0
40.0
20.0
0.0
0.0
50.0
100.0
150.0
200.0
250.0
SHIELD FLOW (scfh)

Fig H-4

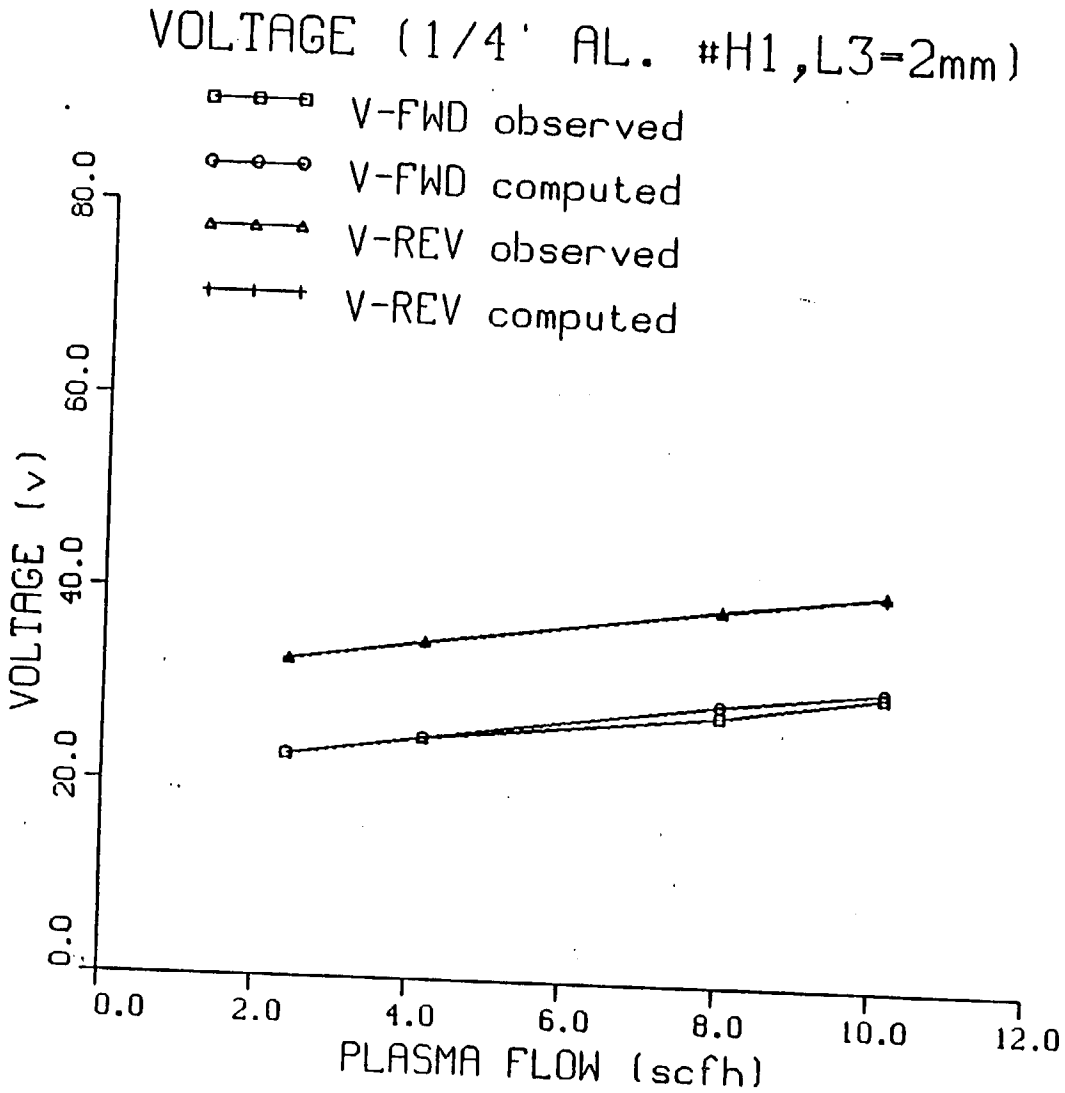
VOLTAGE (1/4' AL. #H1,L3=2mm)
V-FWD observed
V-FWD computed
V-REV observed
V-REV computed
VOLTAGE (v)
80.0
60.0
40.0
20.0
0.0
0.0
2.0
4.0
6.0
8.0
10.0
12.0
PLASMA FLOW (scfh)

Fig. H-5

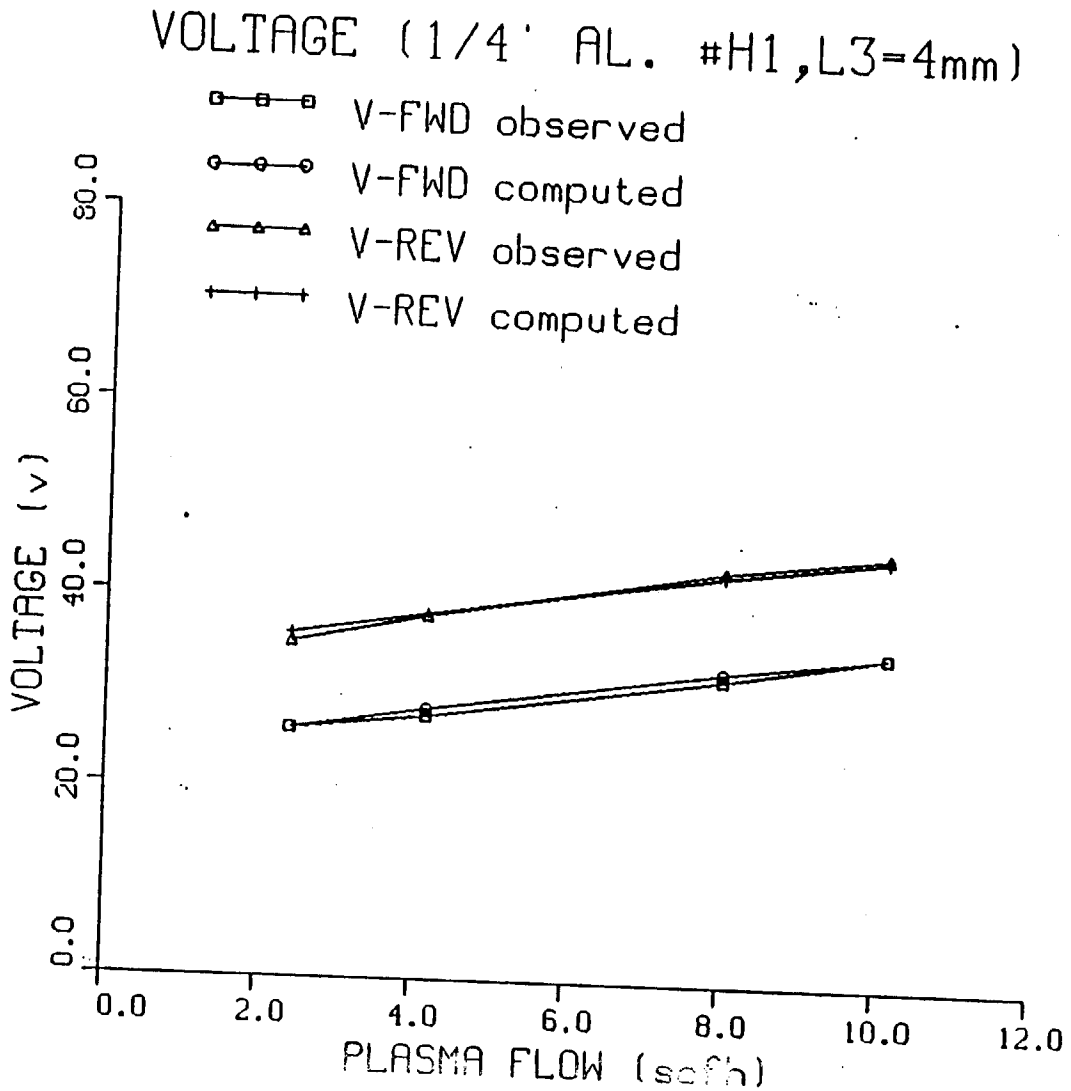
VOLTAGE (1/4' AL. #H1,L3=4mm)
V-FWD observed
V-FWD computed
V-REV observed
V-REV computed
VOLTAGE (v)
80.0
60.0
40.0
20.0
0.0
0.0
2.0
4.0
6.0
8.0
10.0
12.0
PLASMA FLOW (scfh)

Fig. H-6

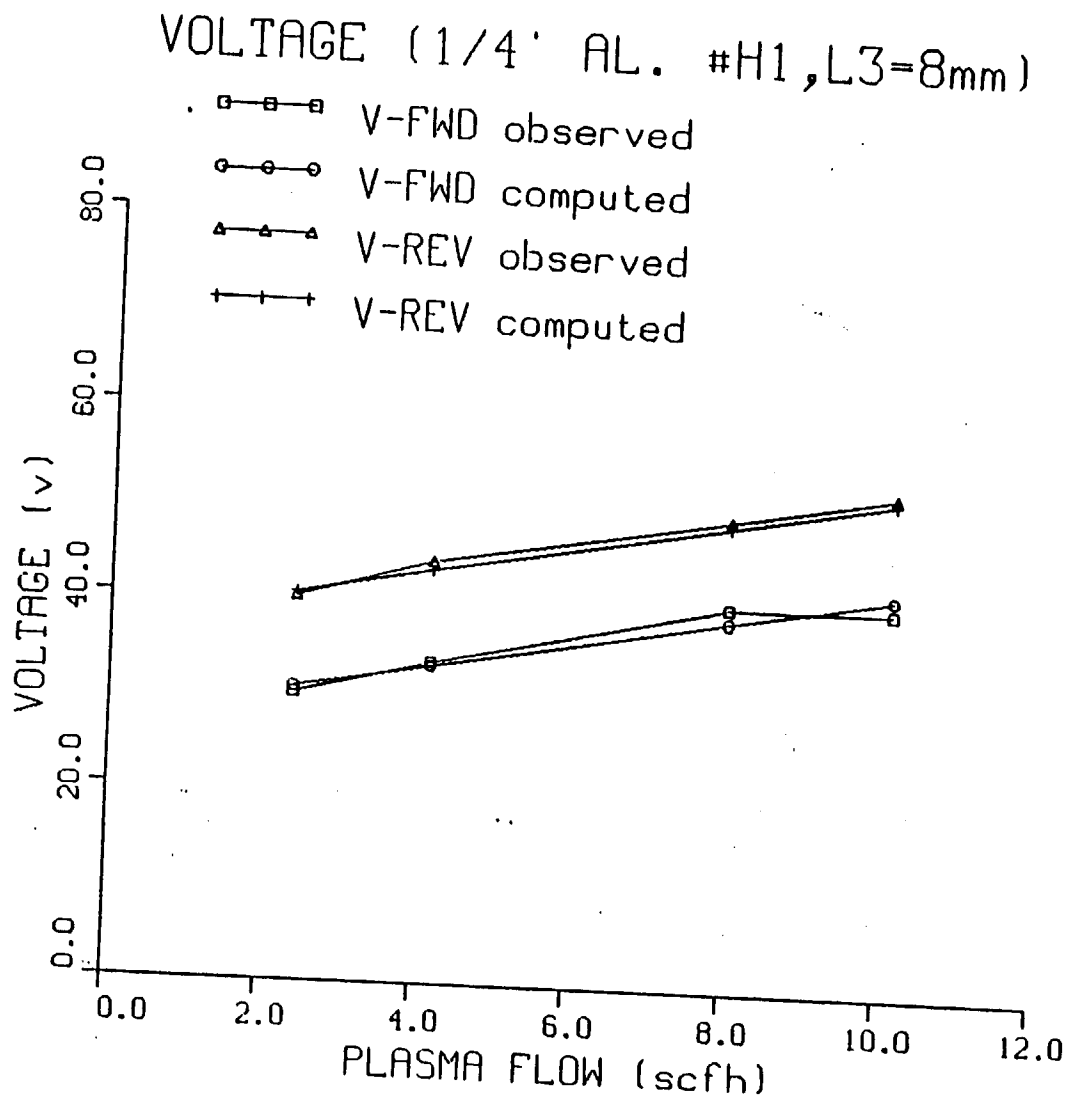
VOLTAGE (1/4' AL. #H1,L3=8mm)
V-FWD observed
V-FWD computed
V-REV observed
V-REV computed
VOLTAGE (v)
80.0
60.0
40.0
20.0
0.0
0.0
2.0
4.0
6.0
8.0
10.0
12.0
PLASMA FLOW (scfh)

Fig. H-7

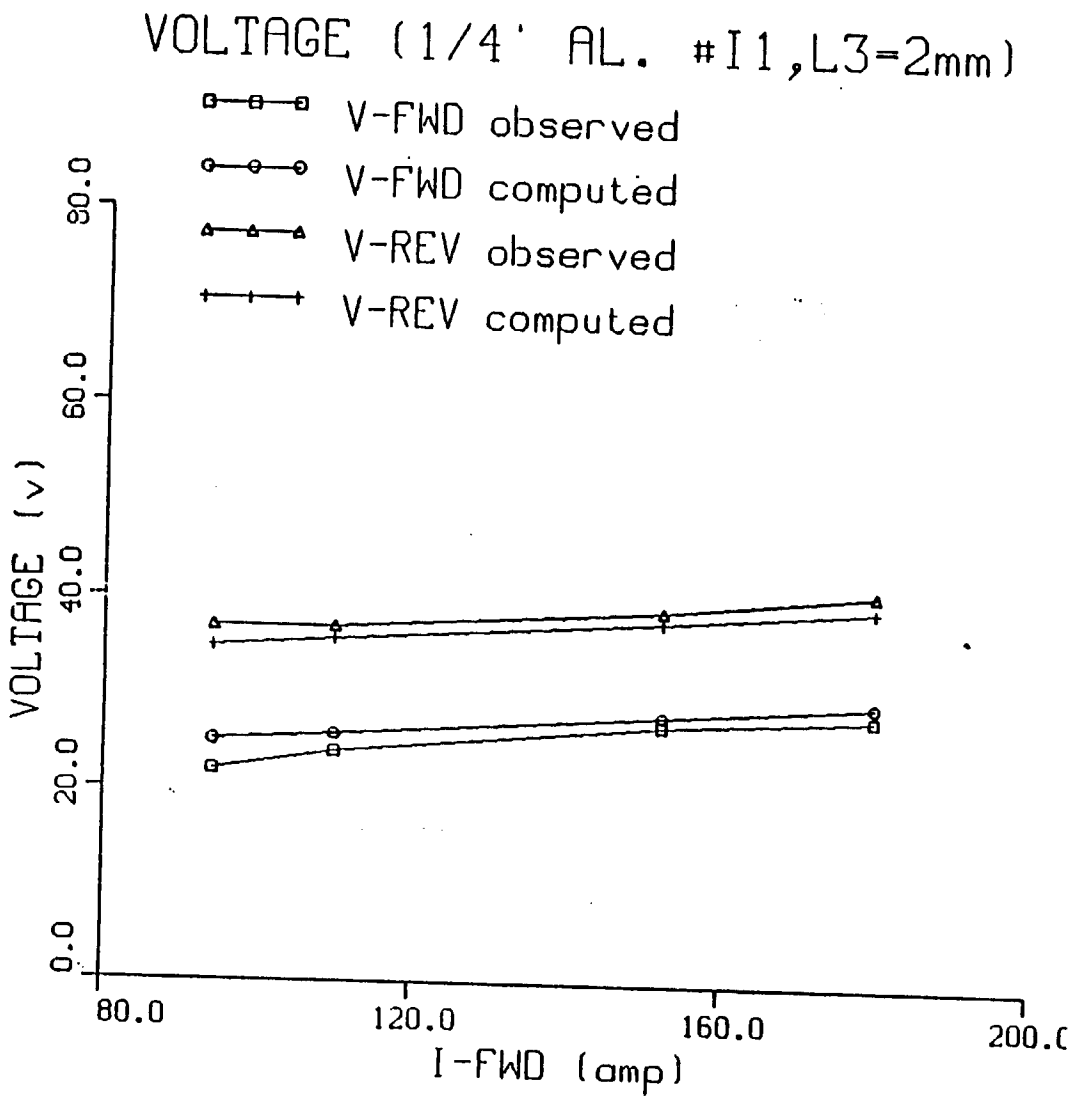
VOLTAGE (1/4' AL. #I1,L3=2mm)
V-FWD observed
V-FWD computed
V-REV observed
V-REV computed
VOLTAGE (v)
80.0
60.0
40.0
20.0
0.0
80.0
120.0
160.0
200.0
I-FWD (amp)

Cut

Fig. H-8

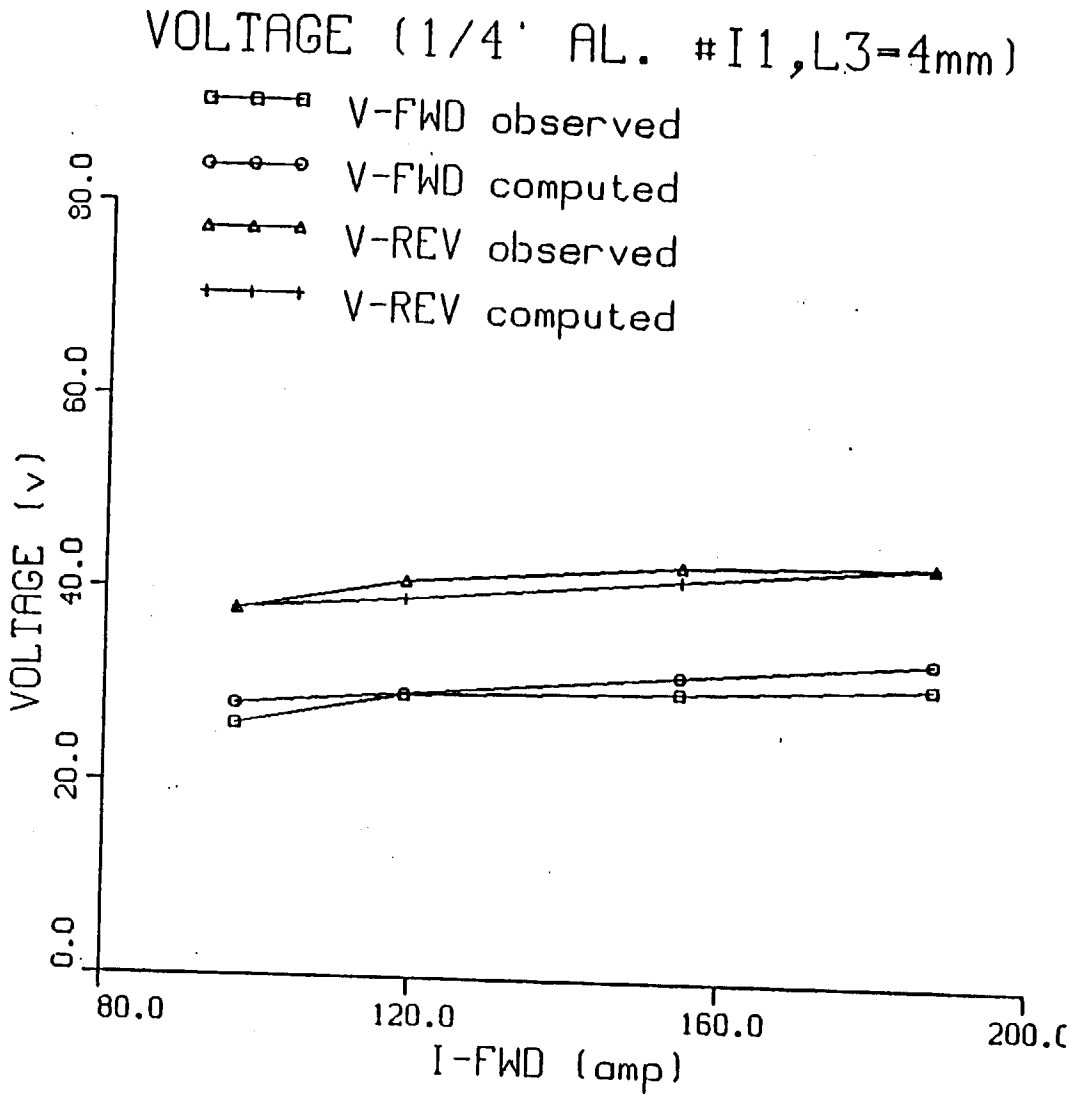
VOLTAGE (1/4' AL. #I1,L3=4mm)
V-FWD observed
V-FWD computed
V-REV observed
V-REV computed
VOLTAGE (v)
0.0
20.0
40.0
60.0
80.0
80.0
120.0
160.0
200.0
I-FWD (amp)

Cut

Fig. H-9

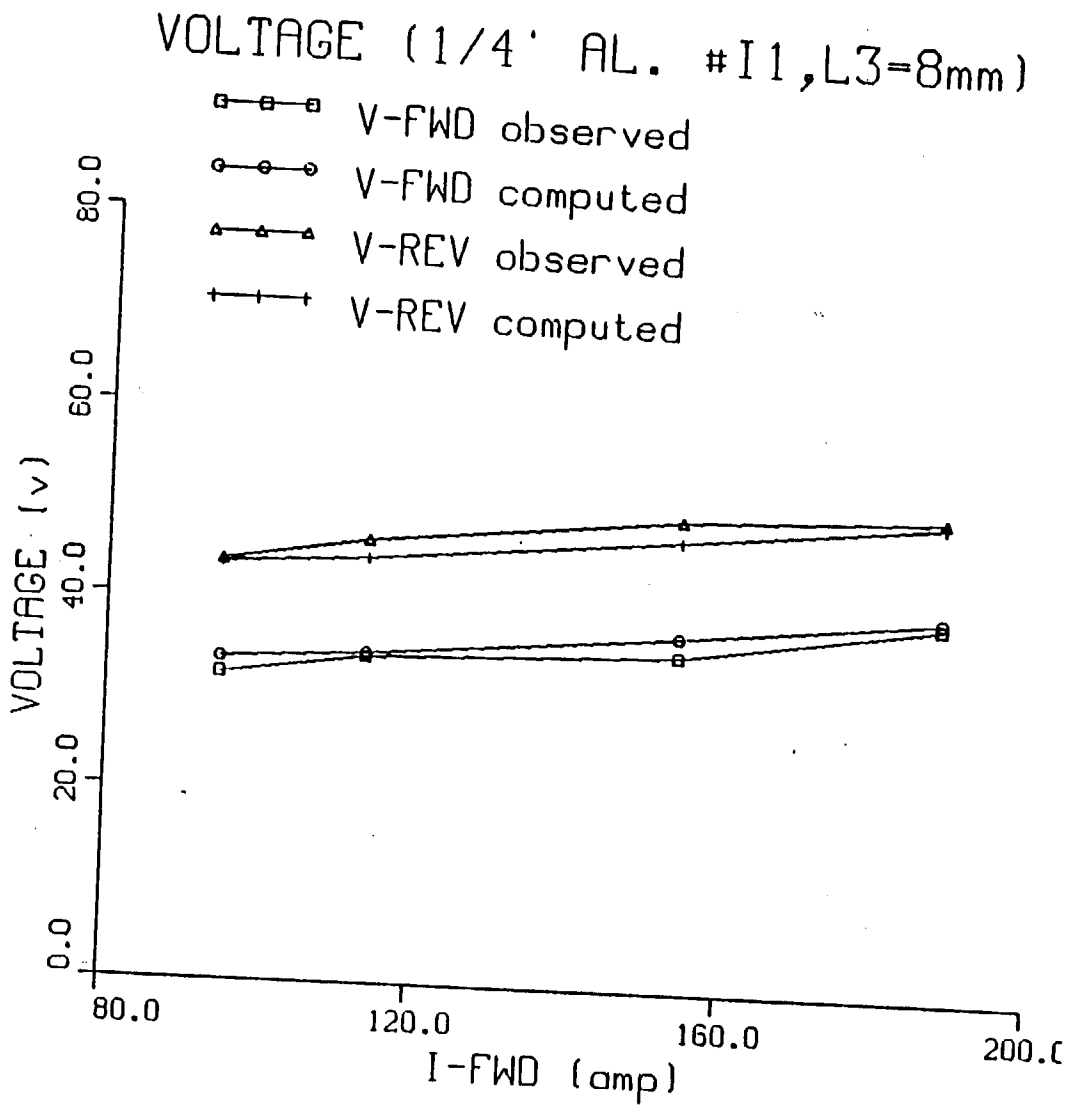
VOLTAGE (1/4' AL. #I1,L3=8mm)
V-FWD observed
V-FWD computed
V-REV observed
V-REV computed
VOLTAGE (v)
80.0
60.0
40.0
20.0
0.0
80.0
120.0
160.0
200.0
I-FWD (amp)

Fig. H-10

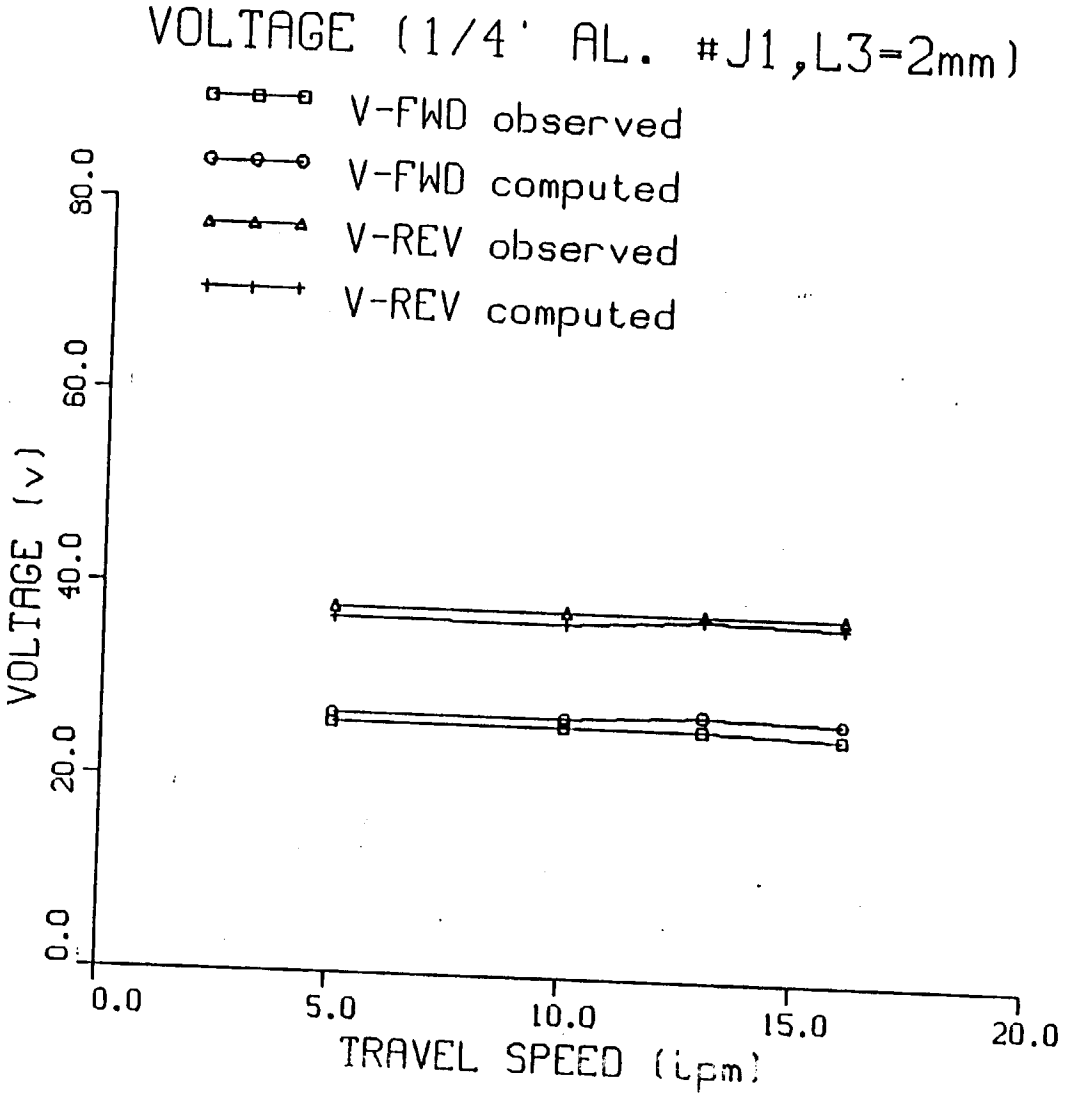
VOLTAGE (1/4' AL. #J1,L3=2mm)
V-FWD observed
V-FWD computed
V-REV observed
V-REV computed
VOLTAGE (v)
80.0
60.0
40.0
20.0
0.0
0.0
5.0
10.0
15.0
20.0
TRAVEL SPEED (ipm)

Fig. H-11

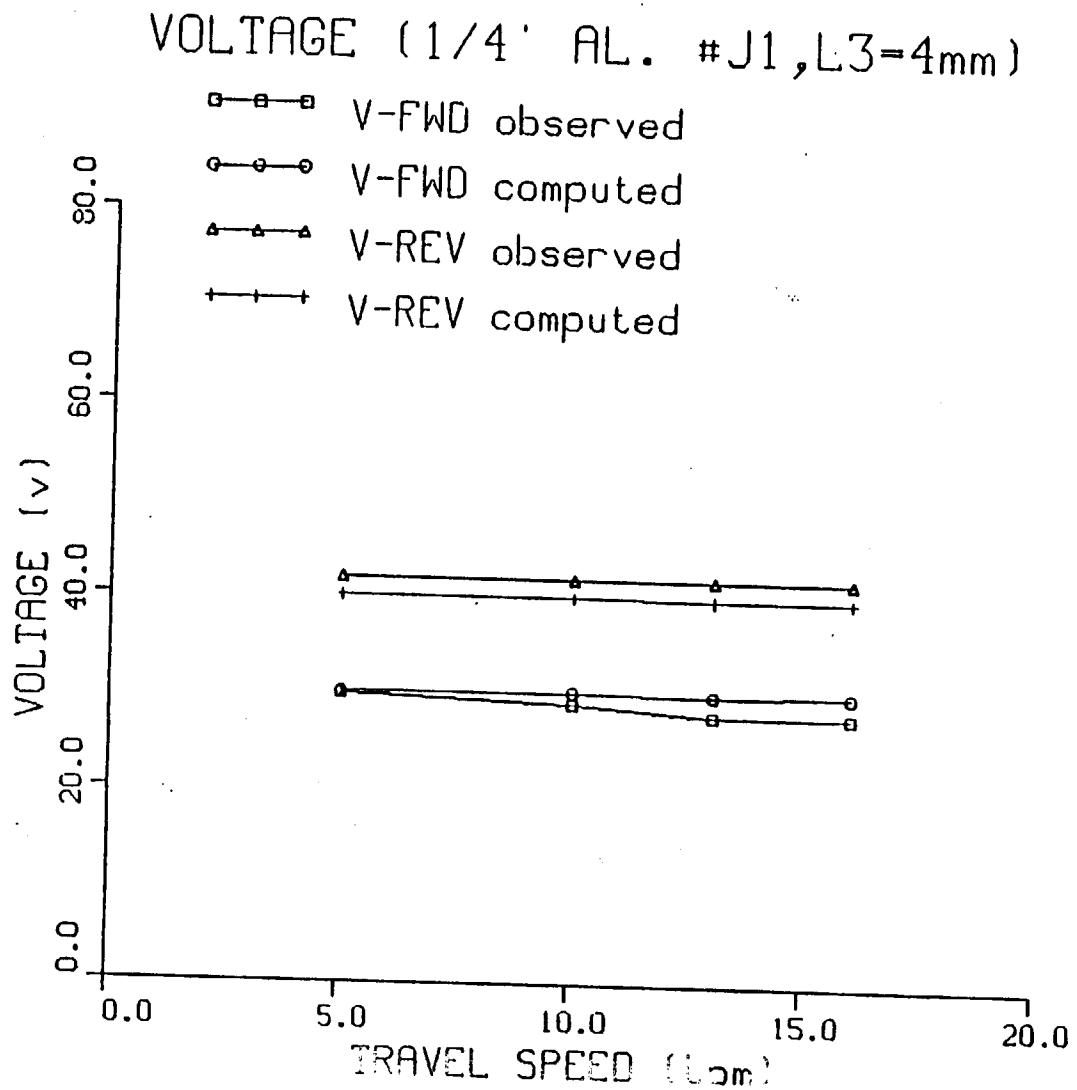

Fig. H-12

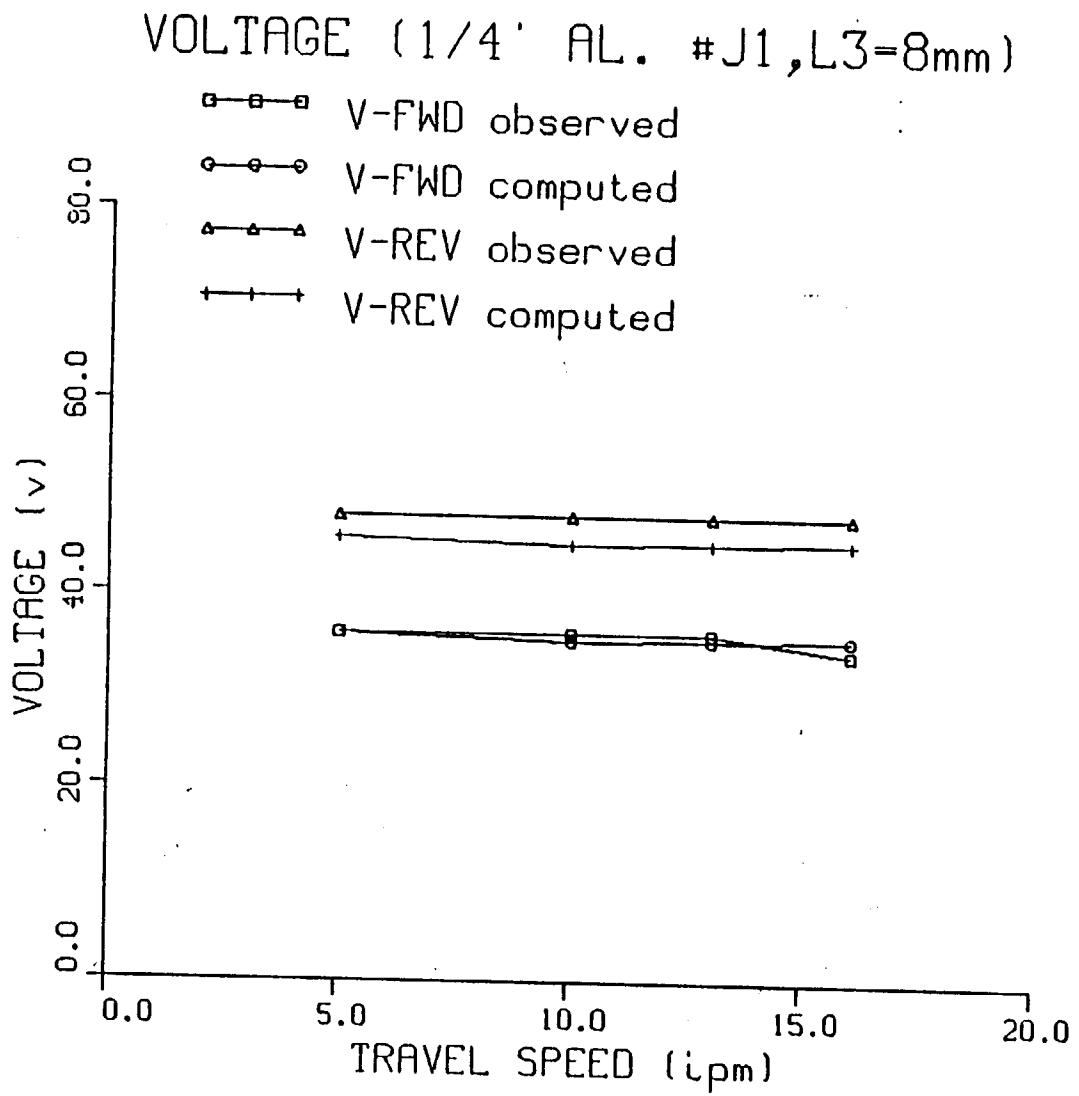

RC
U
LU

Fig. H-13

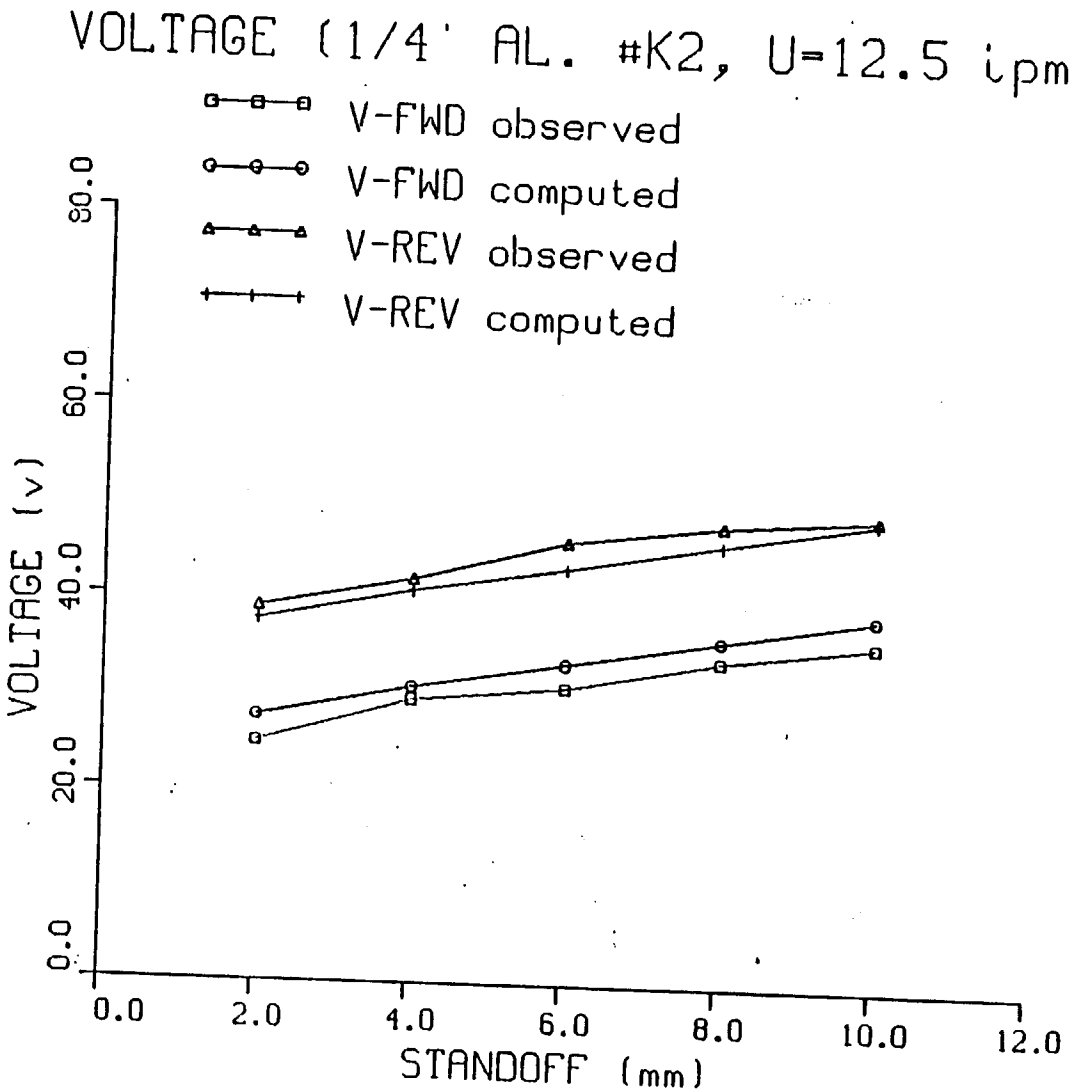
VOLTAGE (1/4' AL. #K2, U=12.5 ipm)
V-FWD observed
V-FWD computed
V-REV observed
V-REV computed
VOLTAGE (v)
80.0
60.0
40.0
20.0
0.0
0.0
2.0
4.0
6.0
8.0
10.0
12.0
STANDOFF (mm)

Fig. H-14

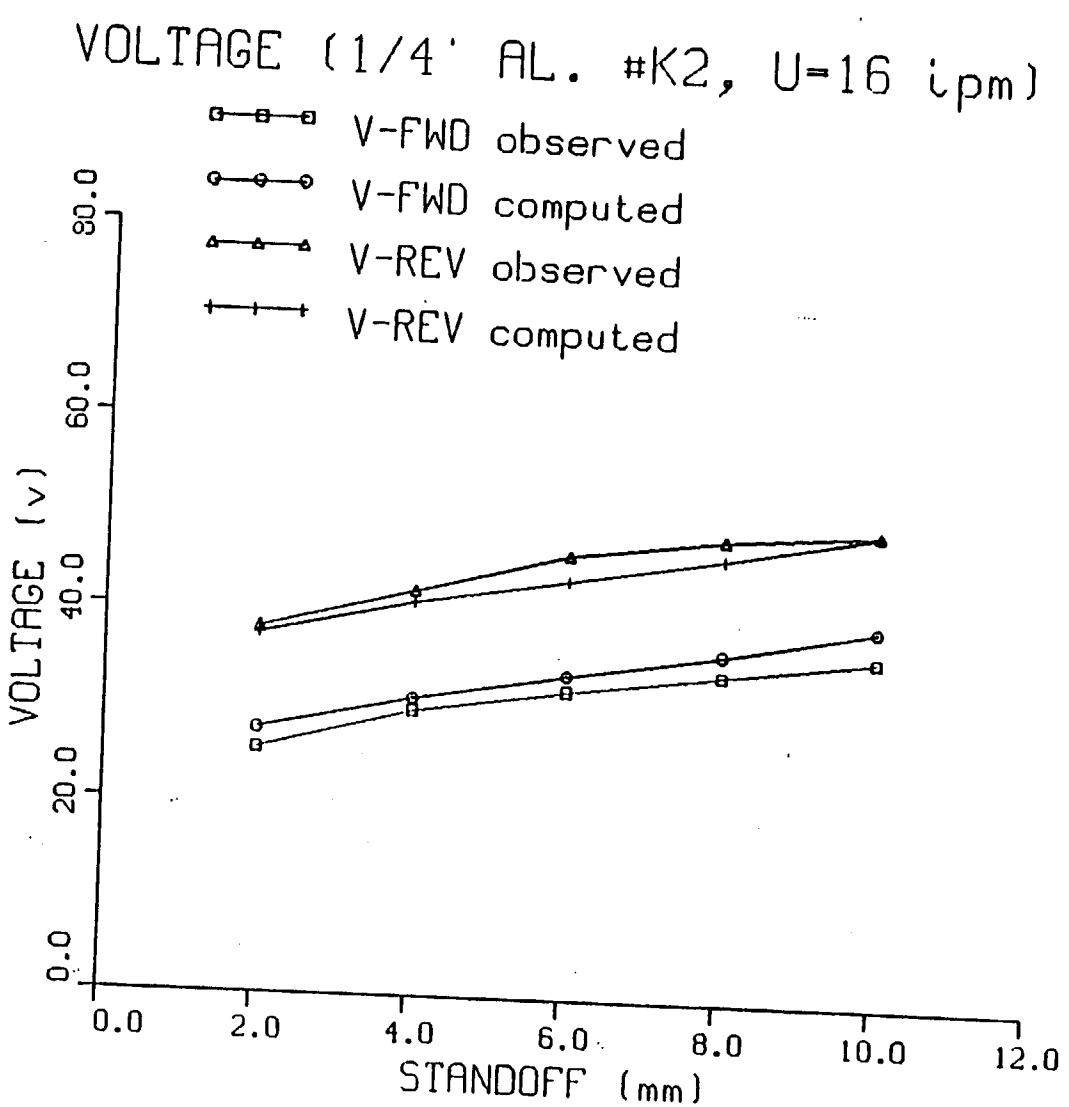
VOLTAGE (1/4' AL. #K2, U=16 ipm)
V-FWD observed
V-FWD computed
V-REV observed
V-REV computed
VOLTAGE (v)
80.0
60.0
40.0
20.0
0.0
0.0
2.0
4.0
6.0
8.0
10.0
12.0
STANDOFF (mm)

Fig. H-15

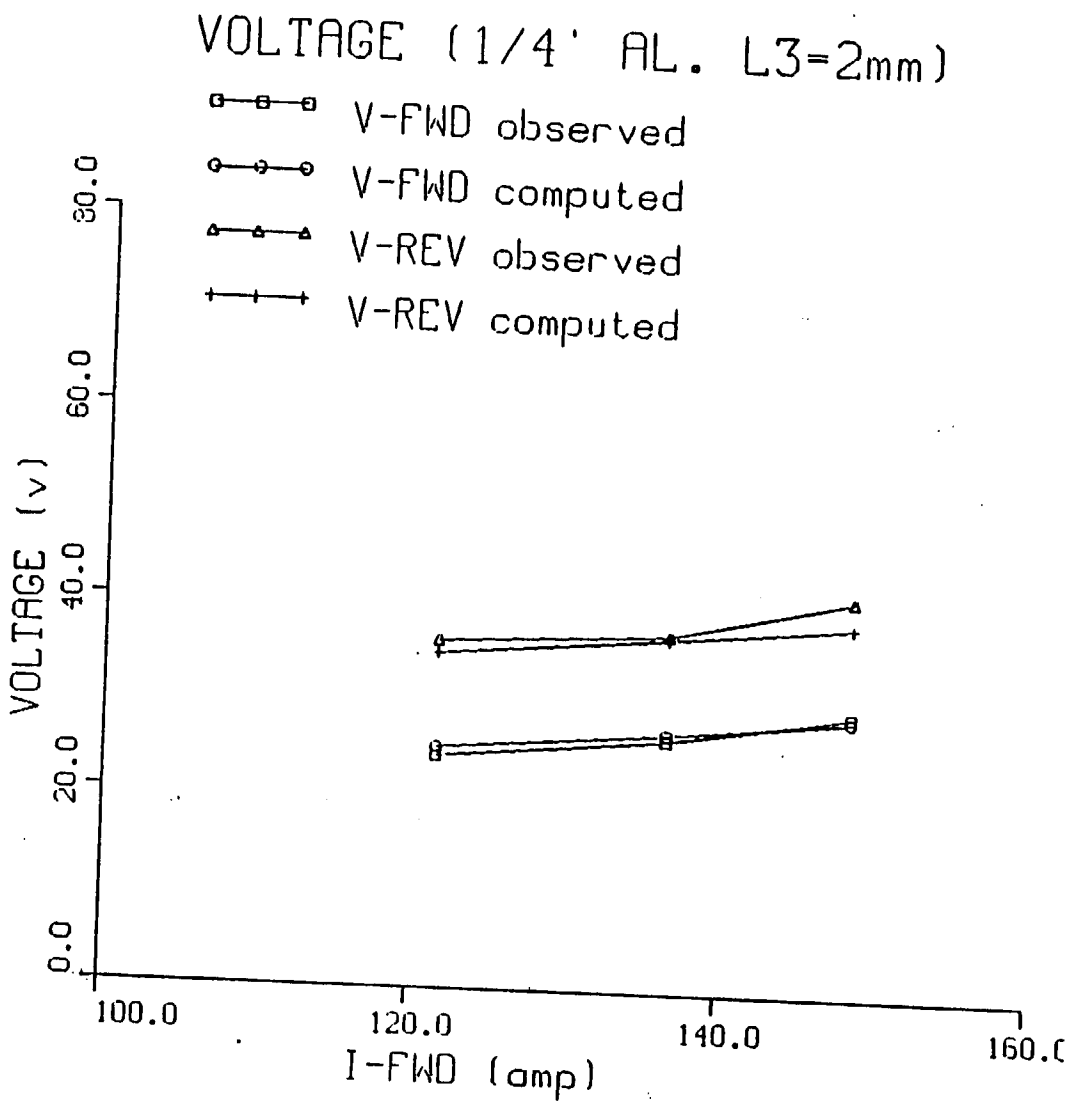
VOLTAGE (1/4' AL. L3=2mm)
V-FWD observed
V-FWD computed
V-REV observed
V-REV computed
0101
0102
0103
VOLTAGE (v)
0.0
20.0
40.0
60.0
80.0
100.0
120.0
140.0
160.0
I-FWD (amp)

Fig. H-16

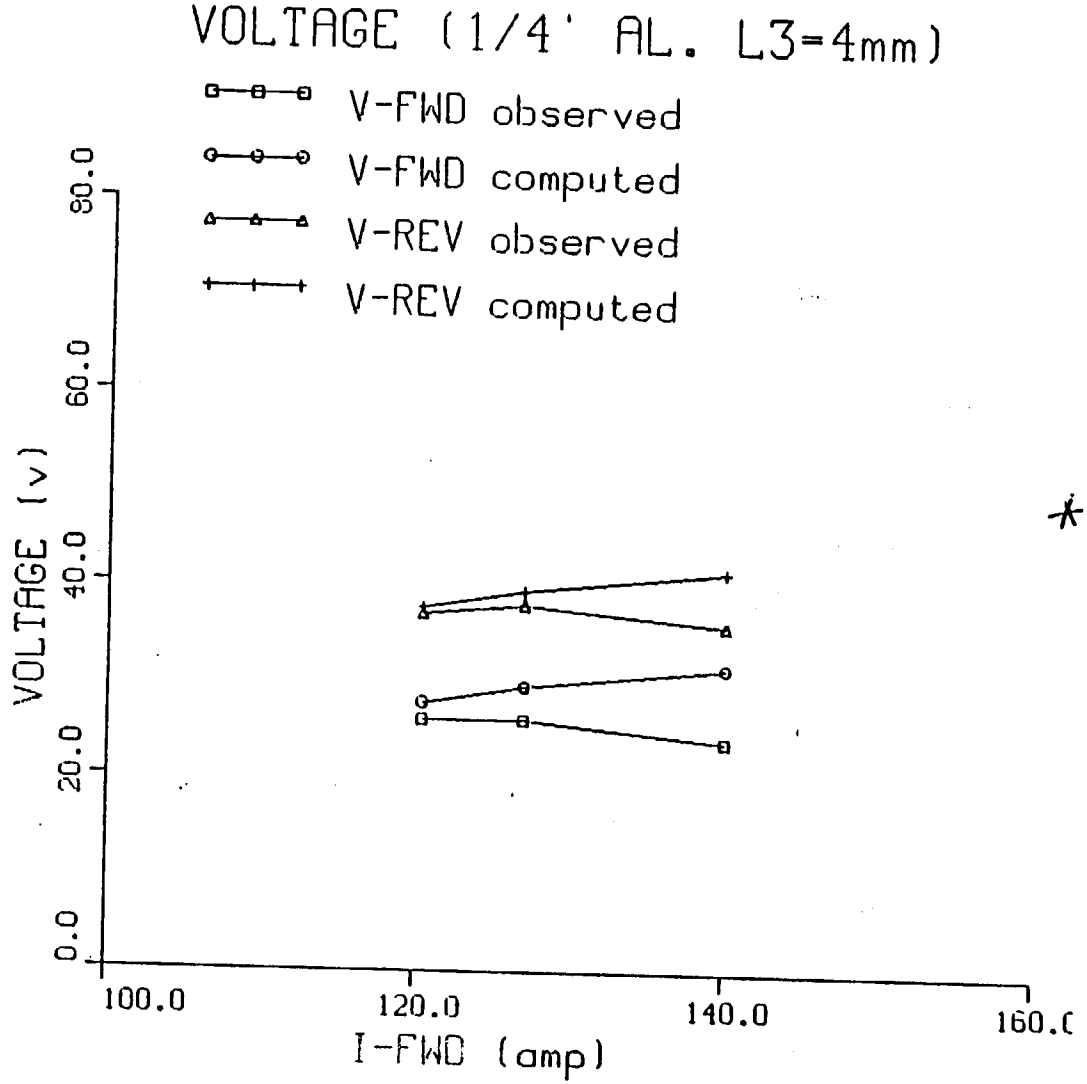

* Bad strip chart

Fig. H-1

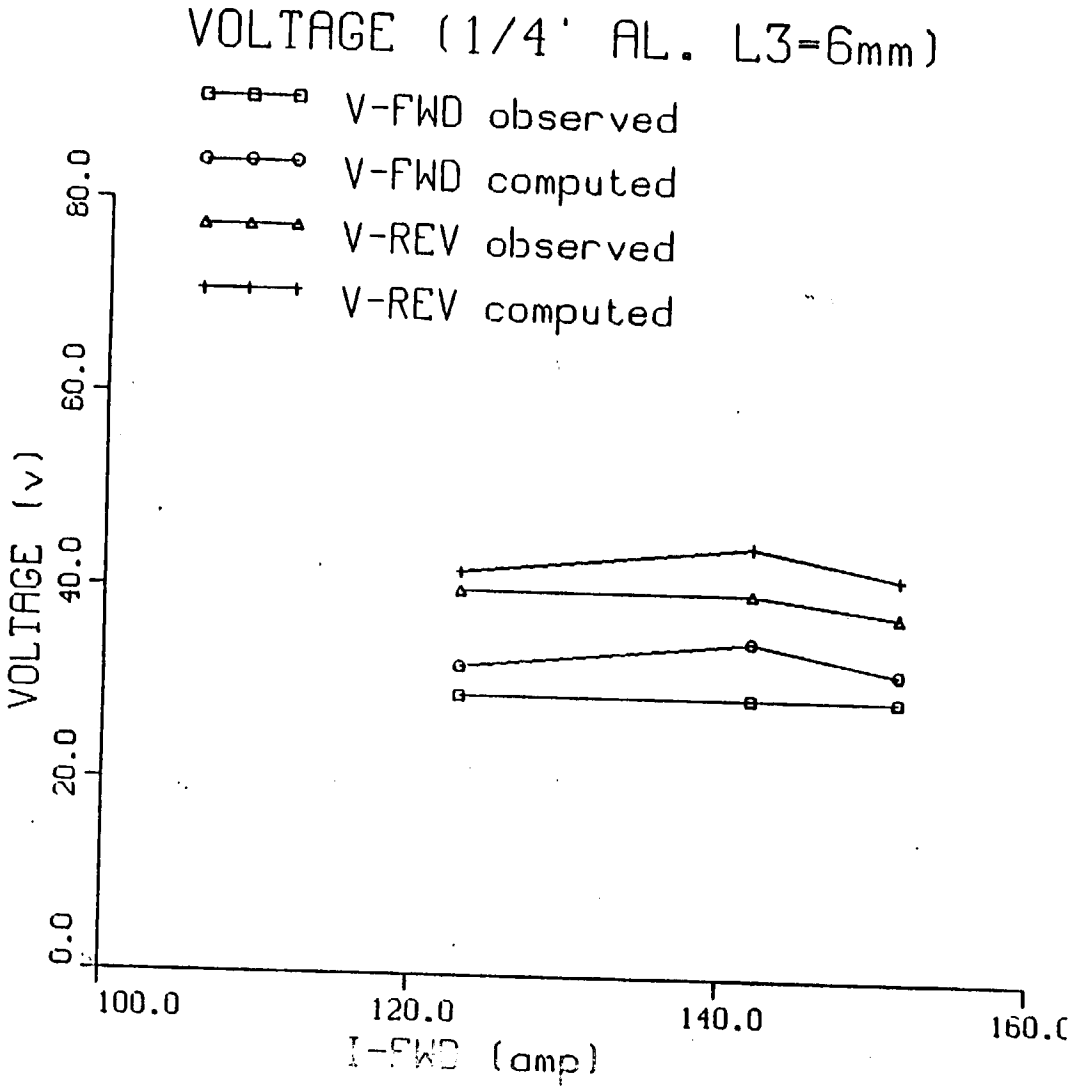

0107-2
0108
0109

RU

Fig. 5-15

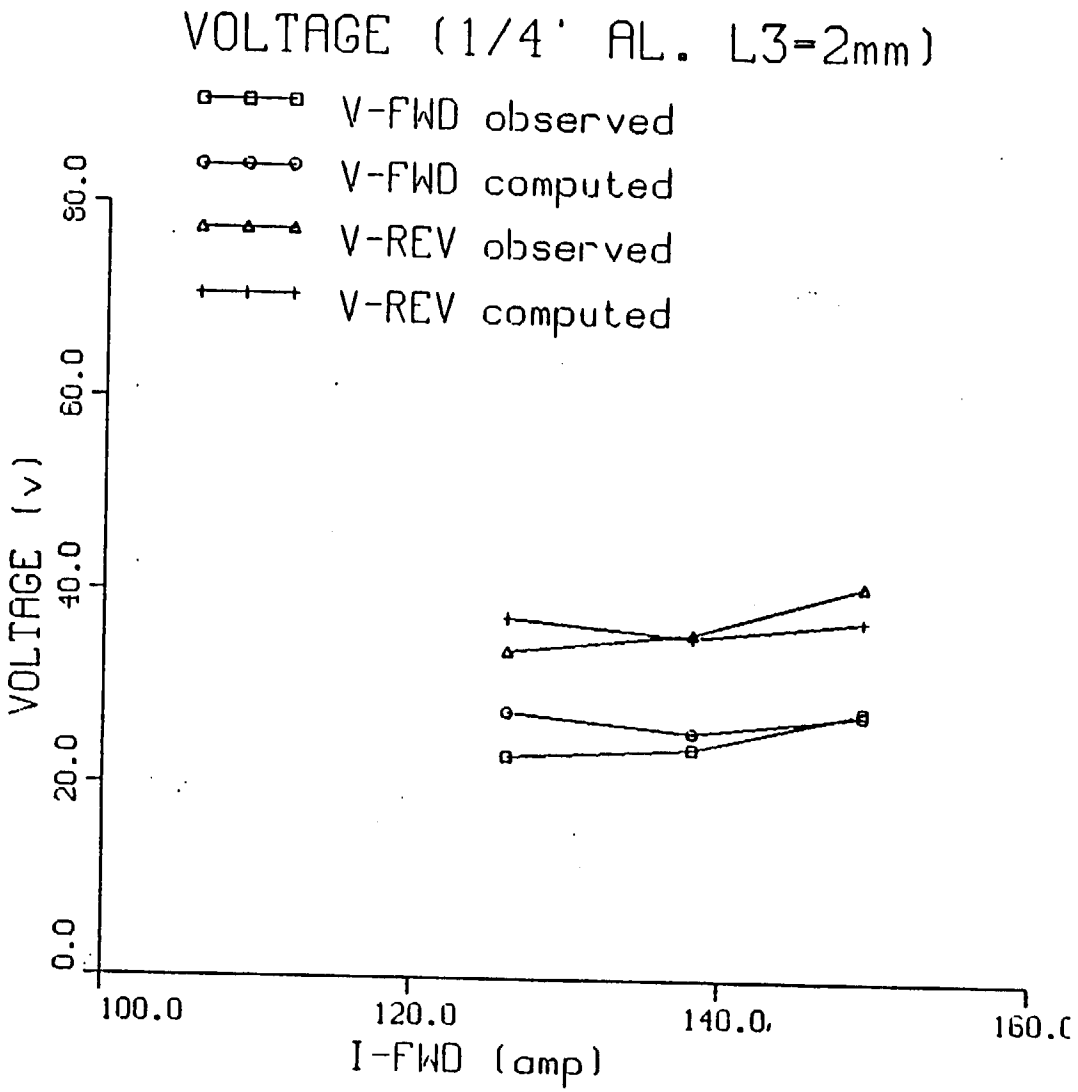

0110-2

0111-2

0112

XU

ED

Fig. H-19

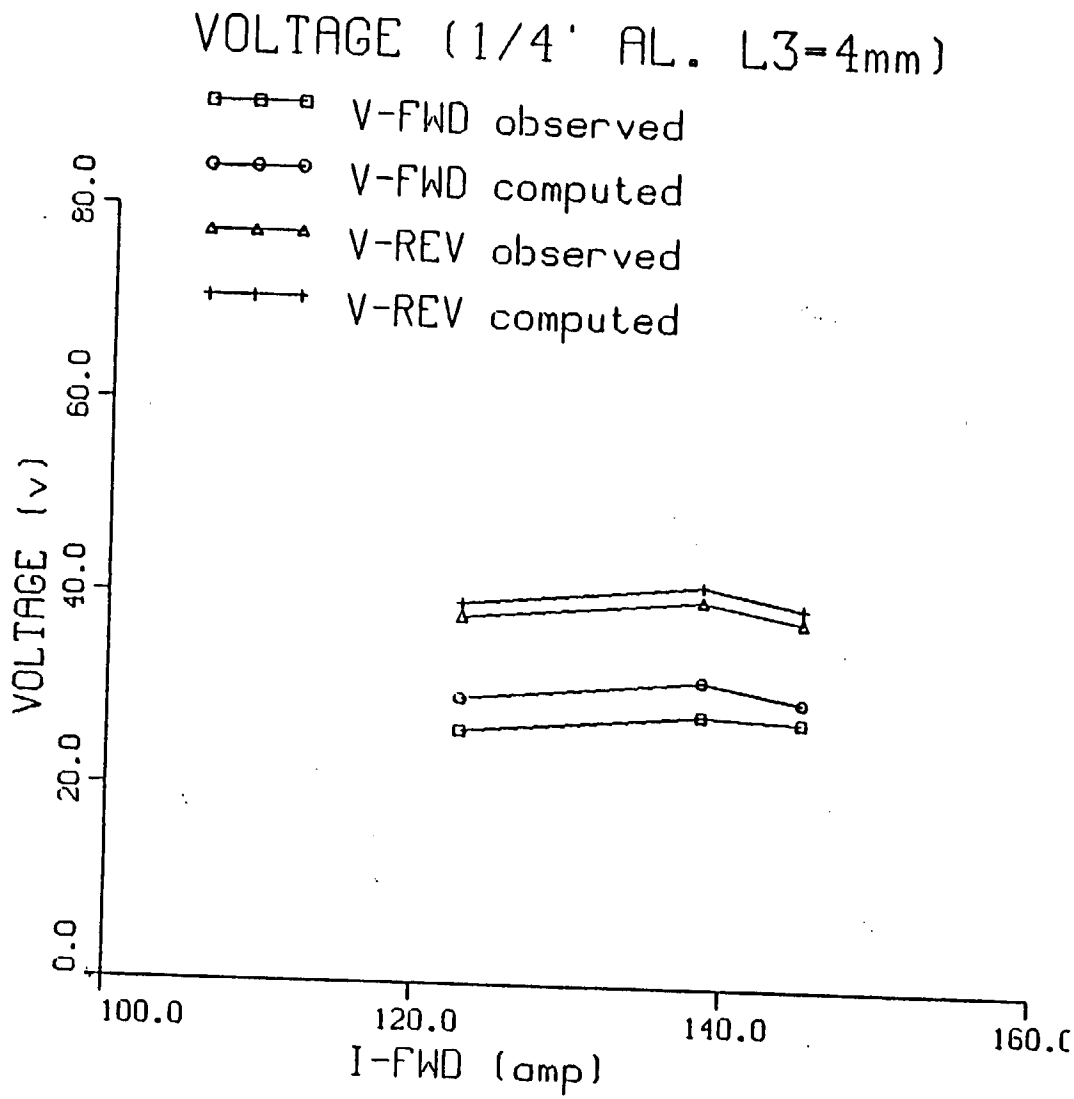

0113-2
0114-2
0115

RU
LU

Fig. H-20

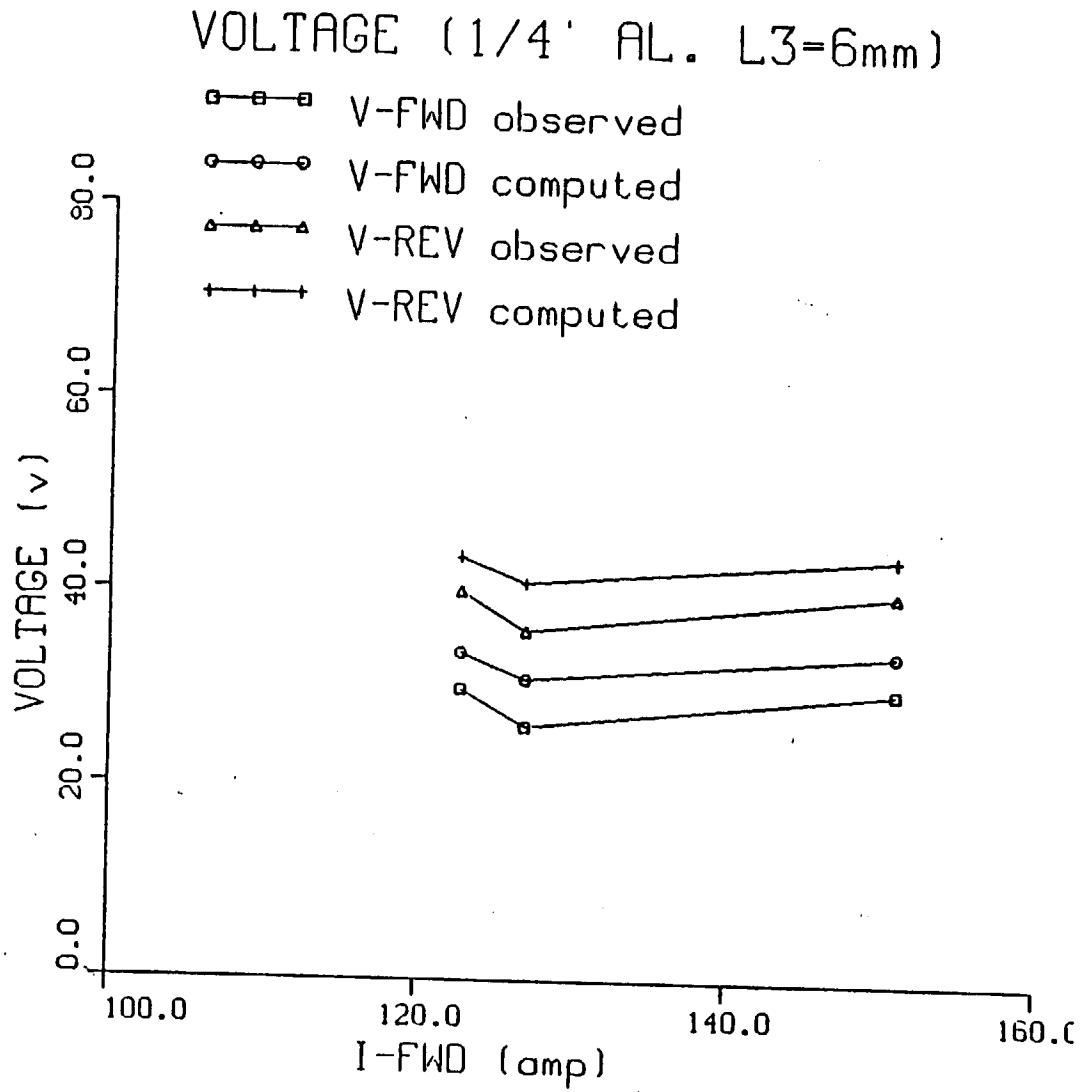

0116
0117-3
0118

* Bad strip chart

Fig. H-21

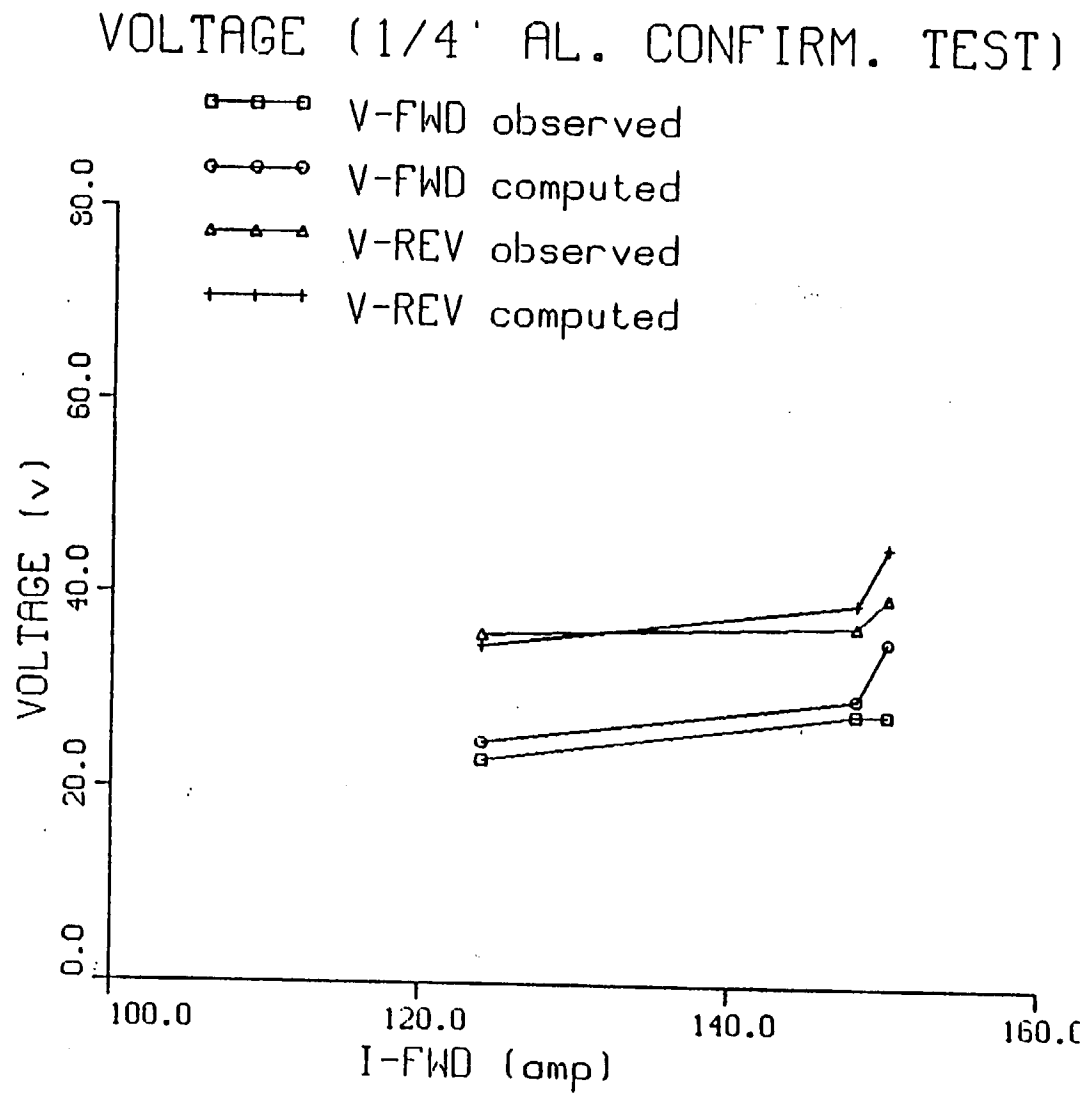

0126
0119-A
0123

ED

Fig. H-22

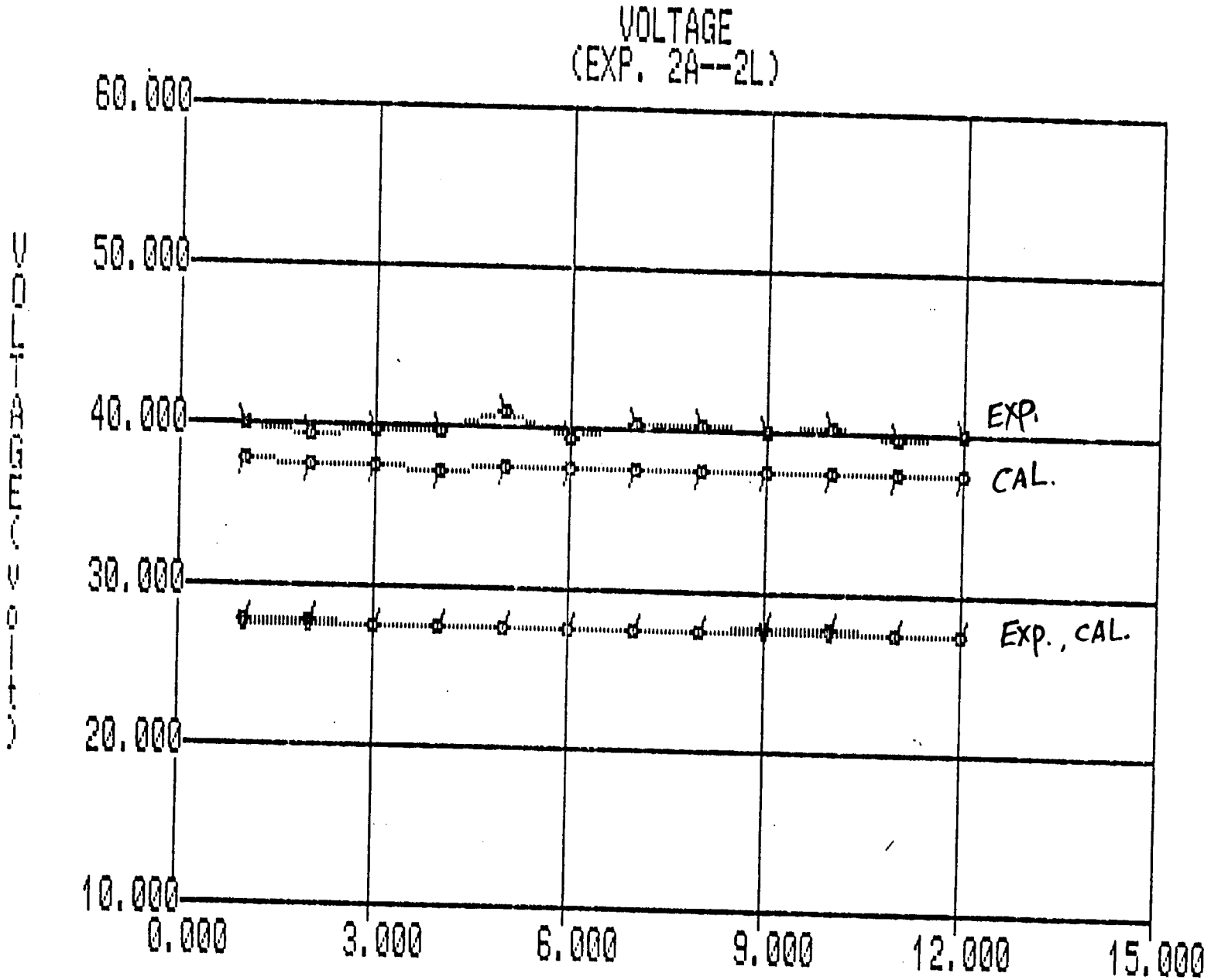
VOLTAGE
(EXP. 2A--2L)
60.000
50.000
40.000
30.000
20.000
10.000
0.000
3.000
6.000
9.000
12.000
15.000
EXP.
CAL.
EXP., CAL.

Fig. H-23

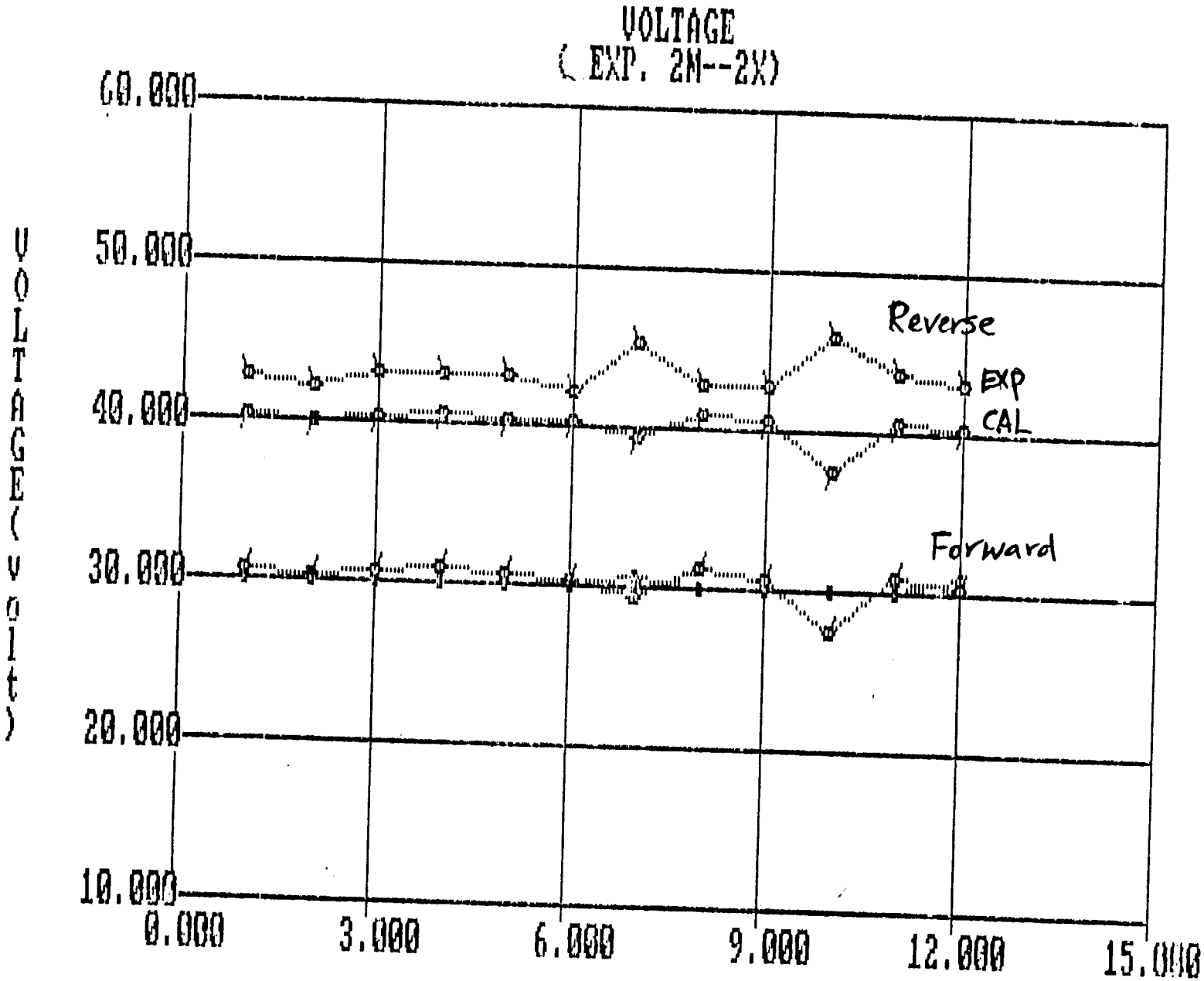
VOLTAGE
(EXP. 2N--2X)
60.000
50.000
40.000
30.000
20.000
10.000
VOLTAGE(volt)
Reverse
EXP
CAL
Forward
0.000
3.000
6.000
9.000
12.000
15.000

Fig. H-24

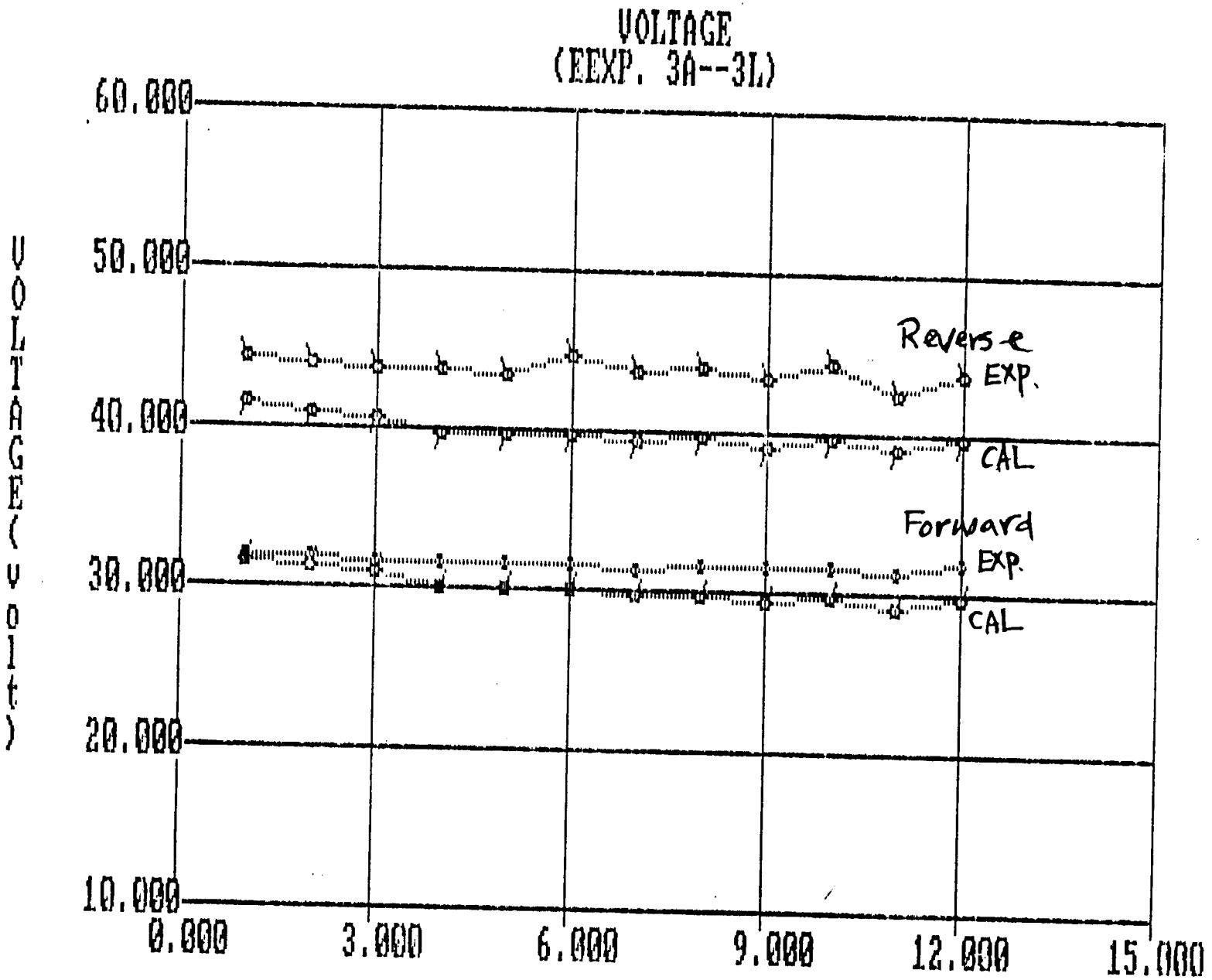
VOLTAGE
(EEXP. 3A--3L)
VOLTAGE(volt)
60.000
50.000
40.000
30.000
20.000
10.000
0.000
3.000
6.000
9.000
12.000
15.000
Reverse
EXP.
CAL
Forward
EXP.
CAL

Fig. H-25

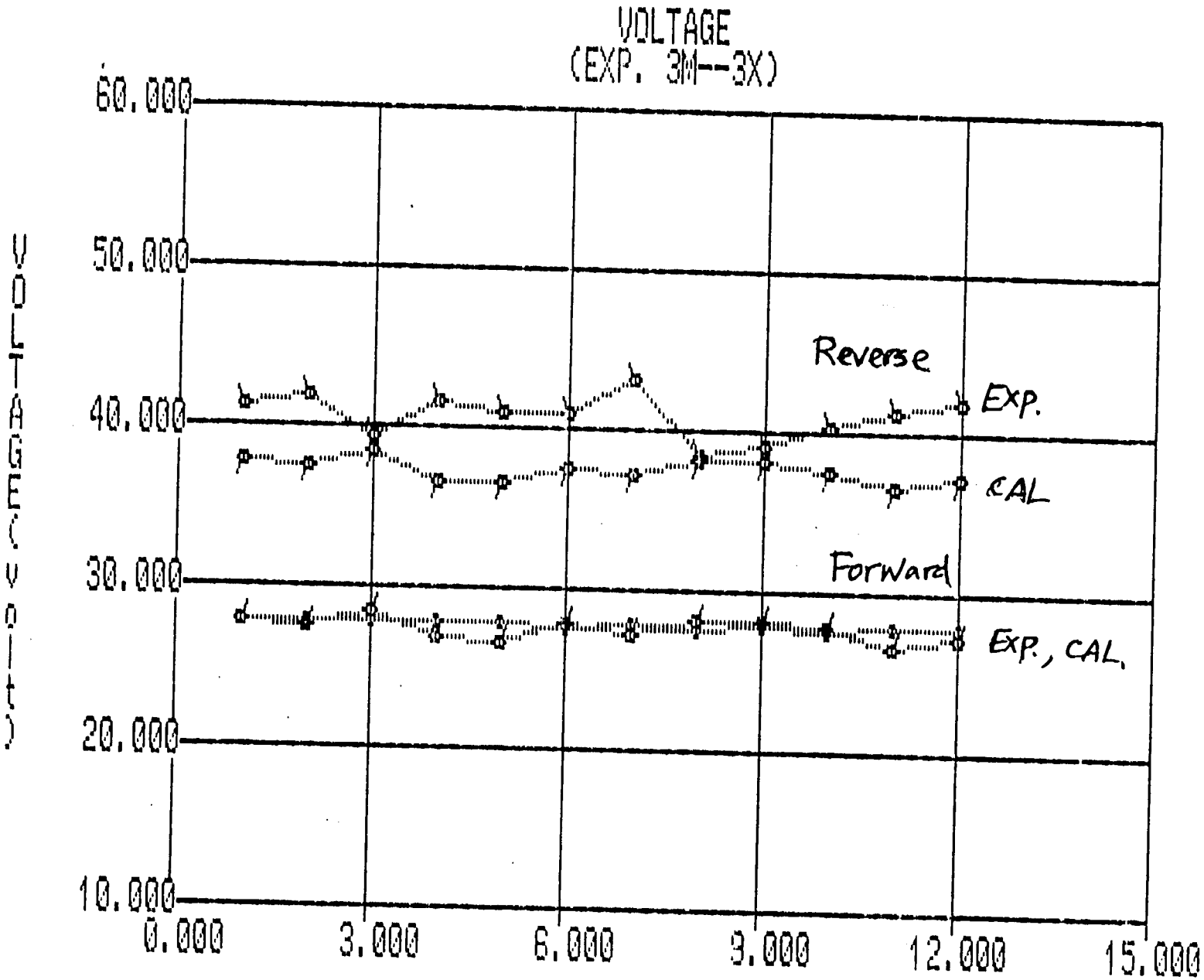
VOLTAGE
(EXP. 3M--3X)
60.000
50.000
40.000
30.000
20.000
10.000
VOLTAGE(volt)
0.000
3.000
6.000
9.000
12.000
15.000
Reverse
EXP.
CAL
Forward
EXP., CAL.

Fig. H-26

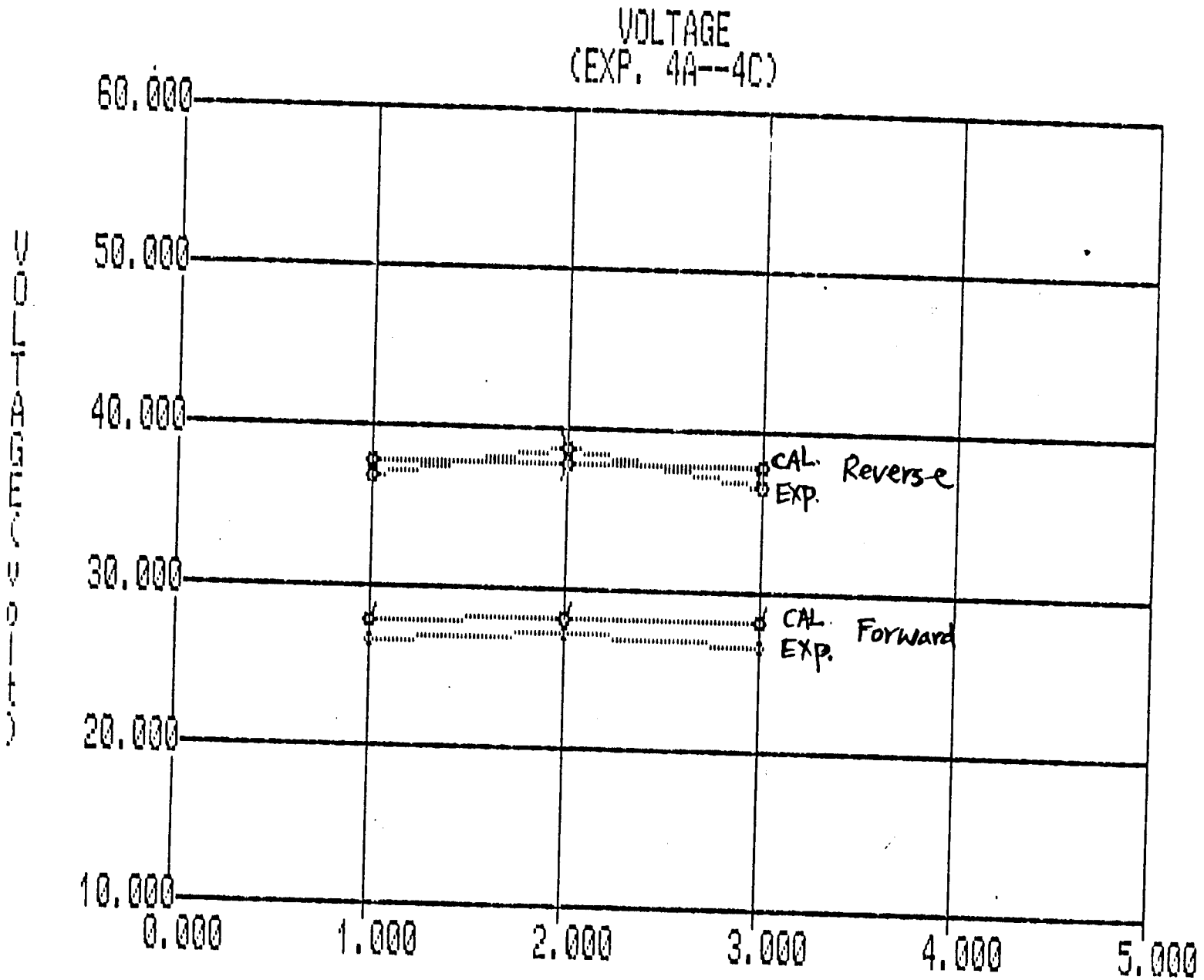
VOLTAGE
(EXP. 4A--4C)
VOLTAGE (volts)
60.000
50.000
40.000
30.000
20.000
10.000
0.000
1.000
2.000
3.000
4.000
5.000
CAL.
EXP.
Reverse
CAL.
EXP.
Forward

Fig. H-27

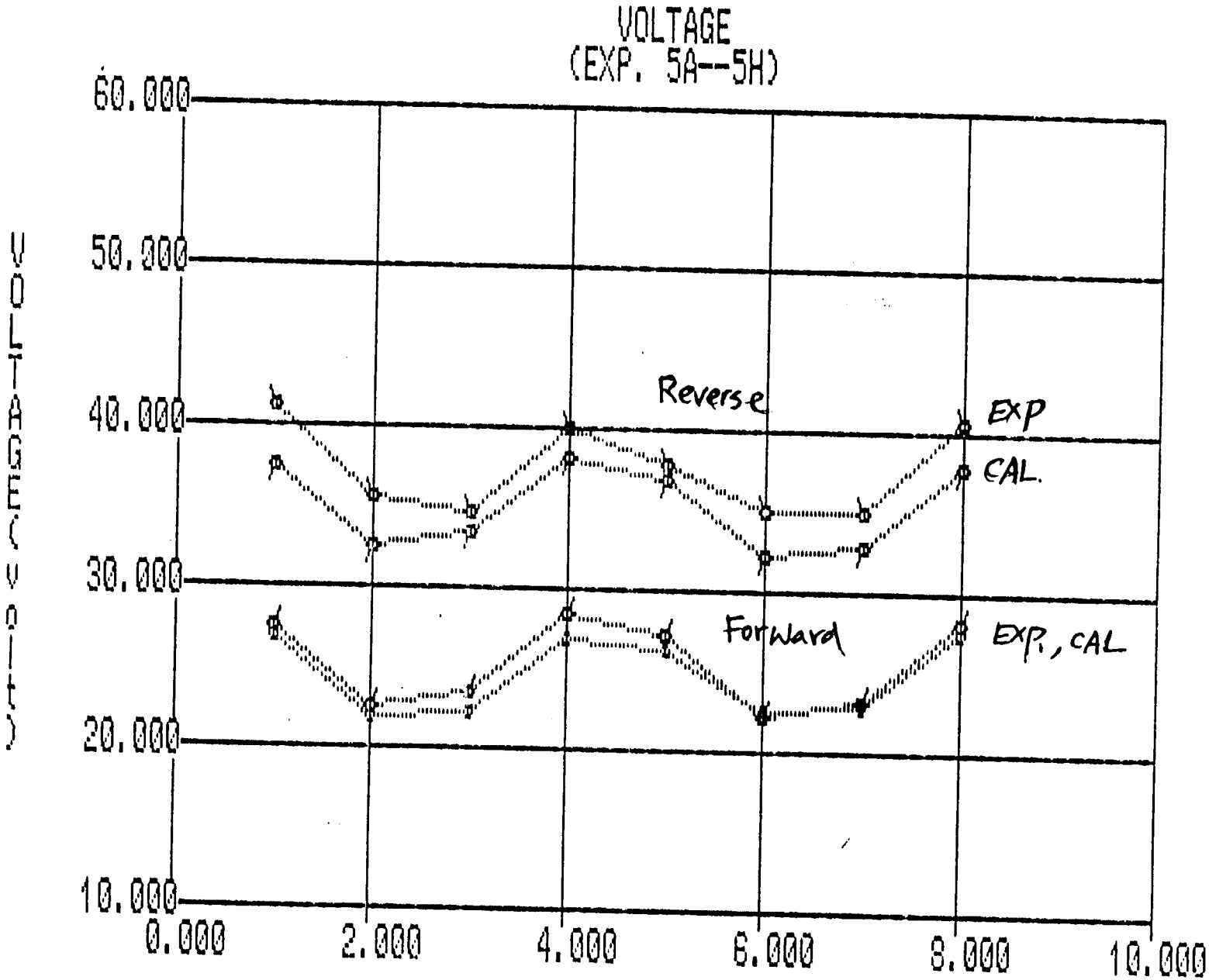
VOLTAGE
(EXP. 5A--5H)
60.000
50.000
40.000
30.000
20.000
10.000
VOLTAGE (V)
0.000
2.000
4.000
6.000
8.000
10.000
Reverse
EXP
CAL.
Forward
EXP., CAL

Fig. H-28

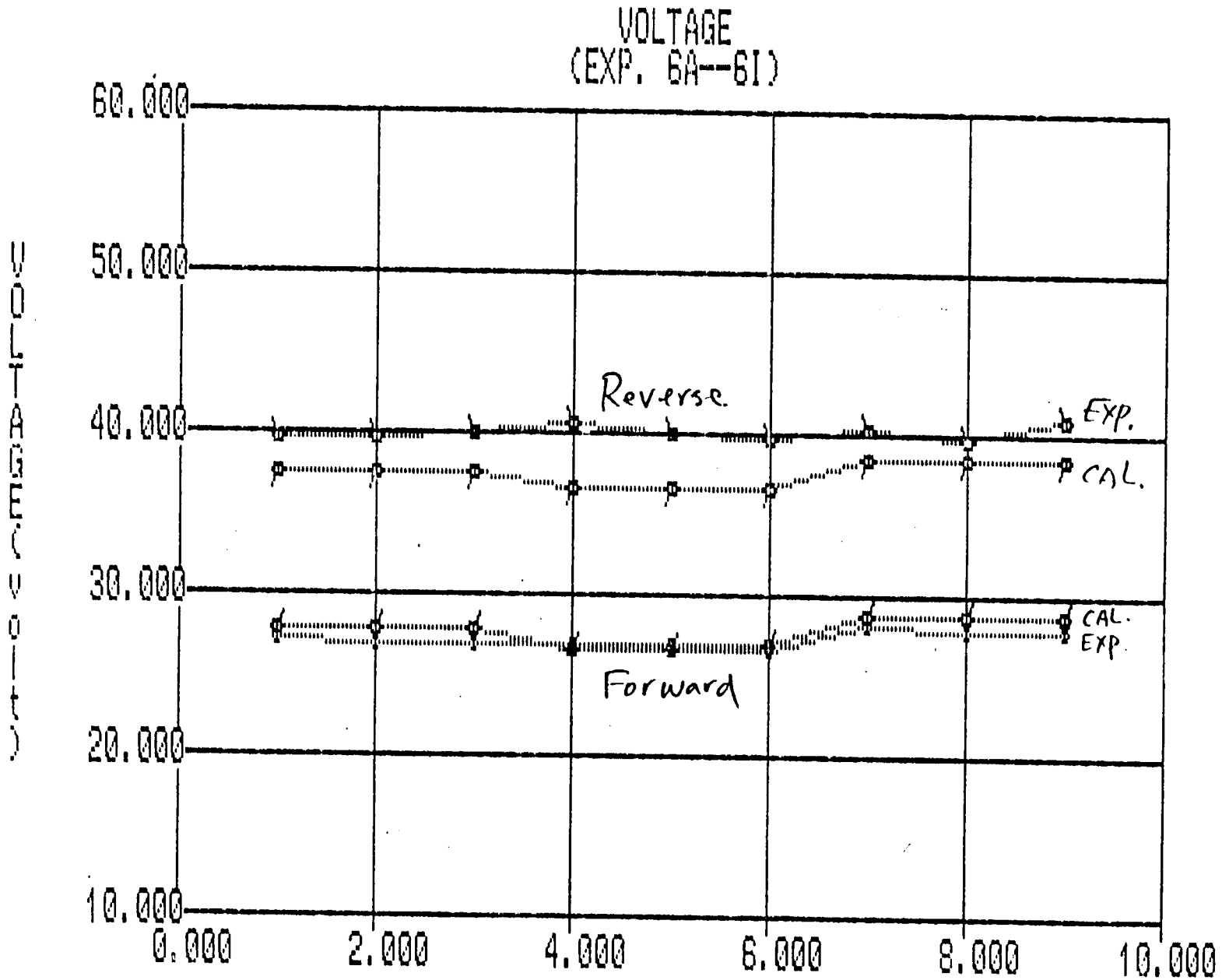
VOLTAGE
(EXP. 6A--6I)
60.000
50.000
40.000
30.000
20.000
10.000
VOLTAGE(volts)
Reverse
EXP.
CAL.
CAL.
EXP.
Forward
0.000
2.000
4.000
6.000
8.000
10.000

Fig. H-29

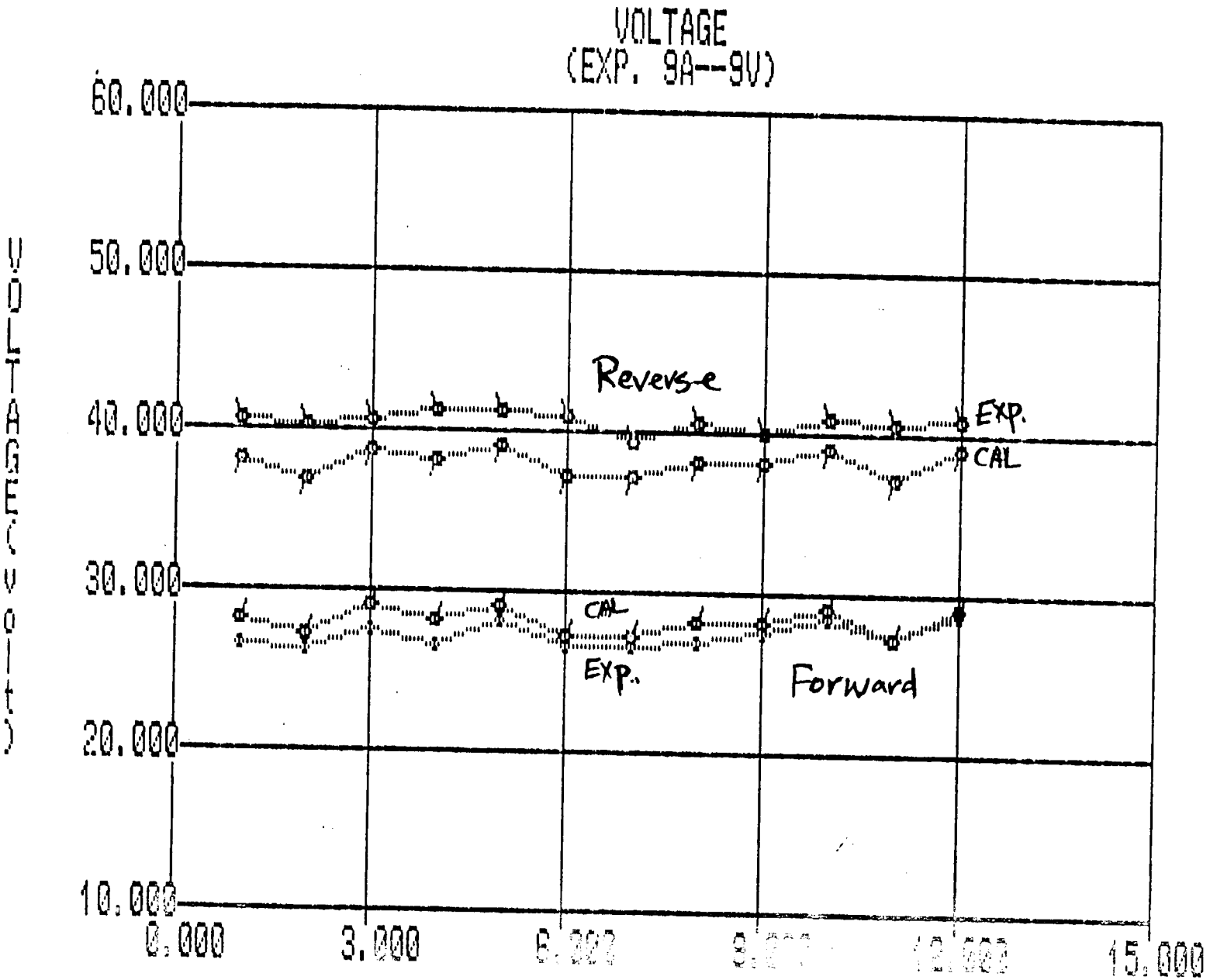
VOLTAGE
(EXP. 9A--9V)
60.000
50.000
40.000
30.000
20.000
10.000
0.000
3.000
15.000
VOLTAGE(volts)
Revers-e
EXP.
CAL
CAL
EXP.
Forward

Fig. H-30

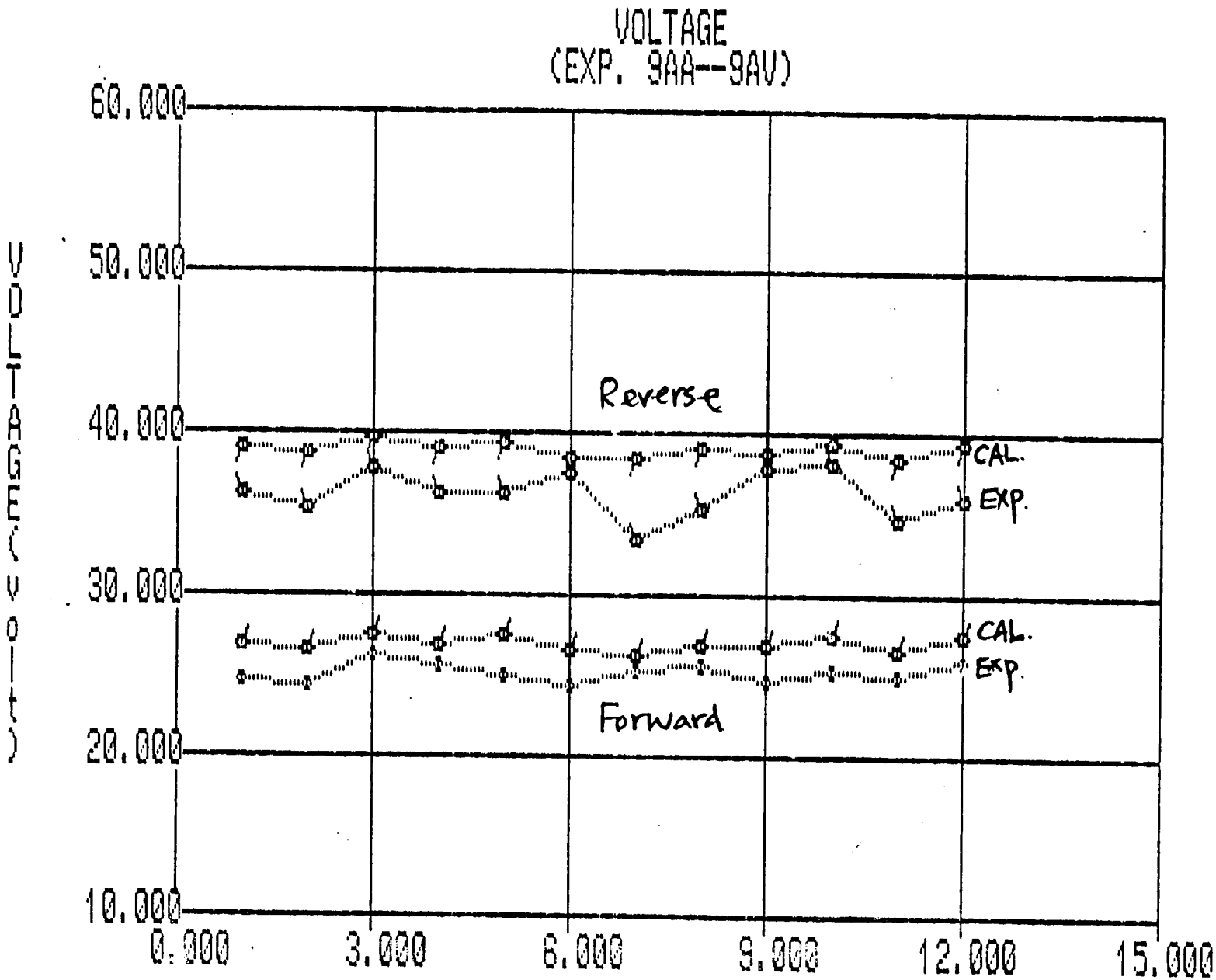
VOLTAGE
(EXP. 9AA--9AV)
60.000
50.000
40.000
30.000
20.000
10.000
VOLTAGE(volts)
Reverse
CAL.
EXP.
CAL.
EXP.
Forward
0.000
3.000
6.000
9.000
12.000
15.000

Fig. H-31

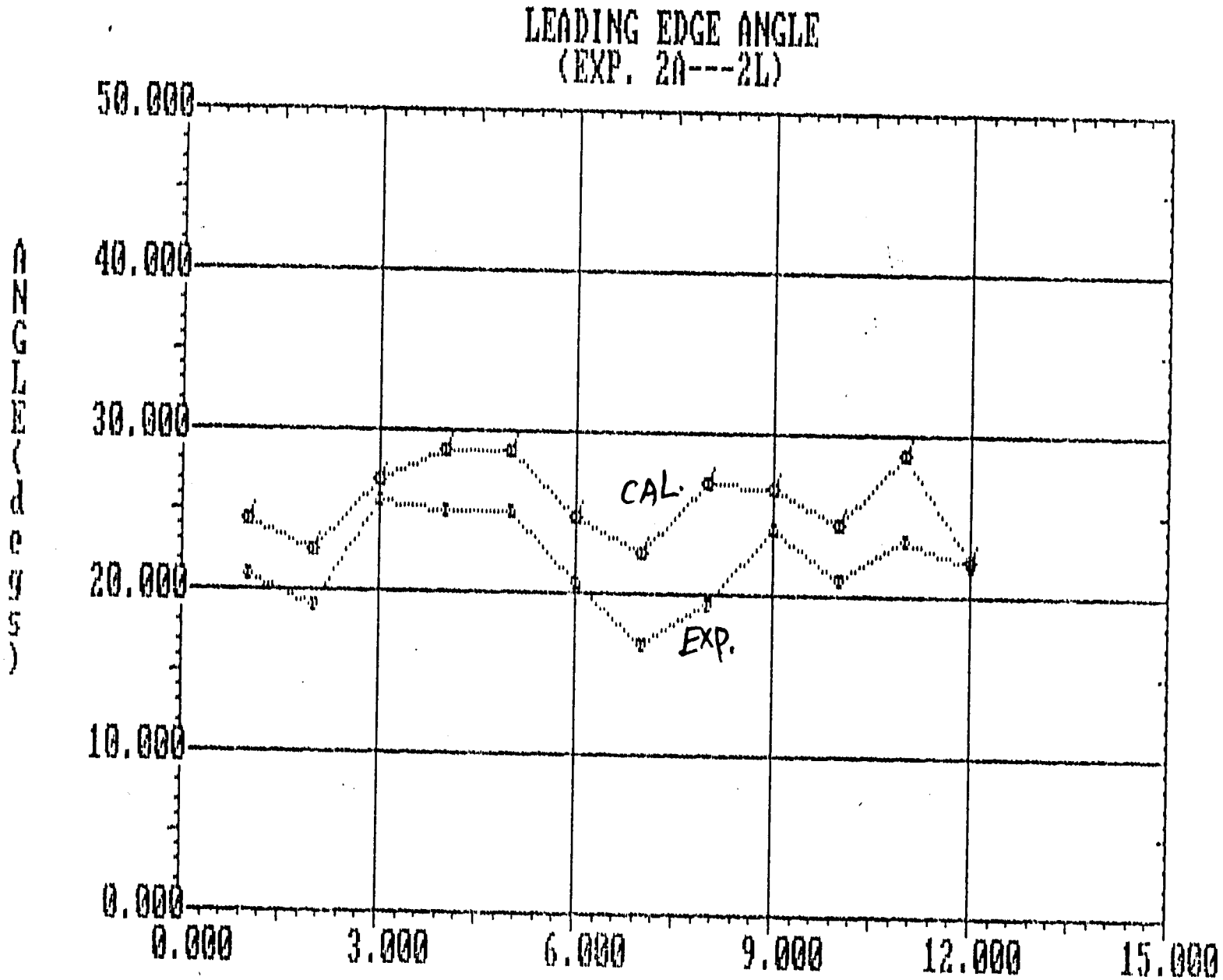
LEADING EDGE ANGLE
(EXP. 2A---2L)
ANGLE(deg)
50.000
40.000
30.000
20.000
10.000
0.000
0.000
3.000
6.000
9.000
12.000
15.000
CAL.
EXP.

Fig. H-32

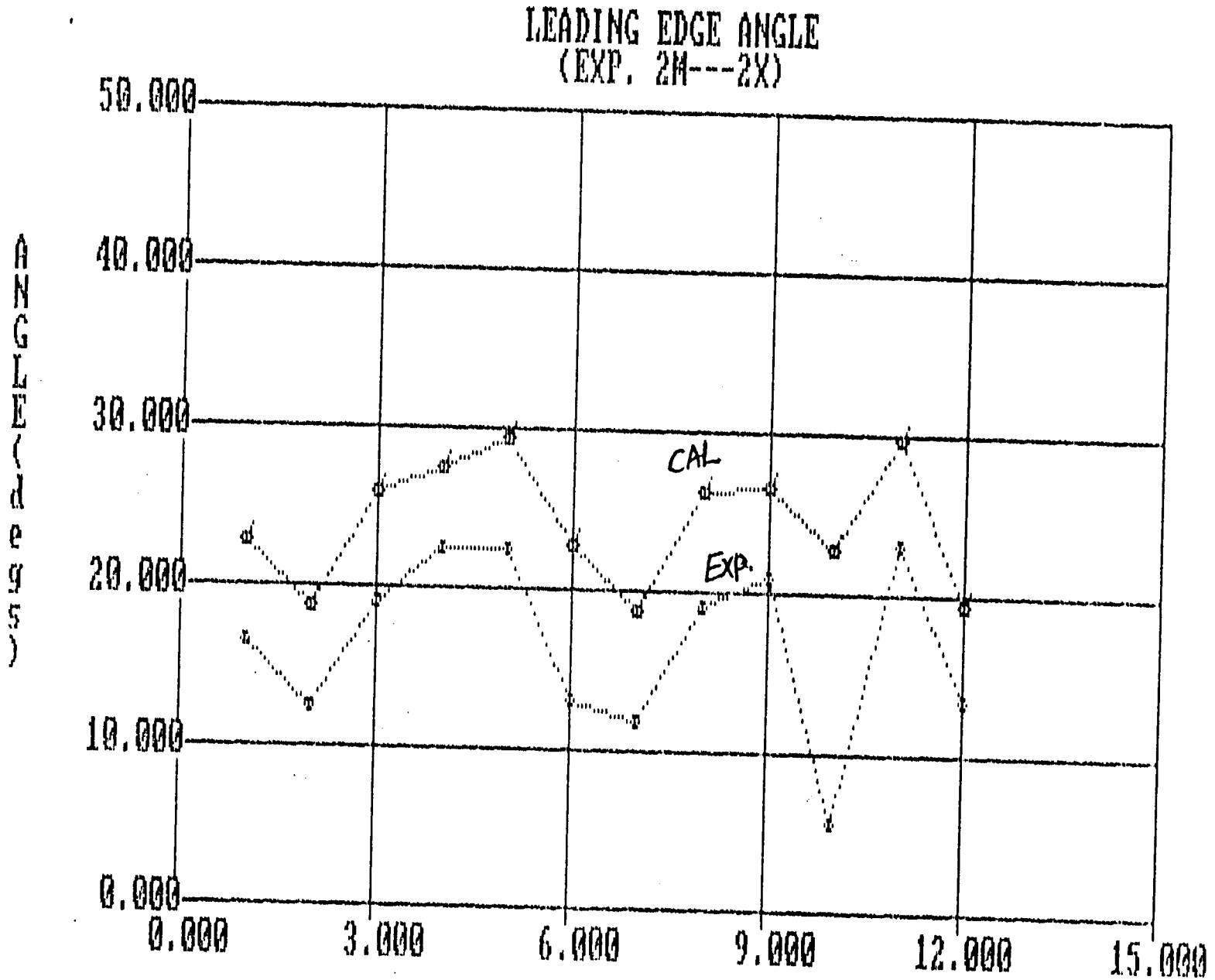
LEADING EDGE ANGLE
(EXP. 2M---2X)
ANGLE(deg)
50.000
40.000
30.000
20.000
10.000
0.000
0.000
3.000
6.000
9.000
12.000
15.000
CAL
EXP.

Fig. H-33

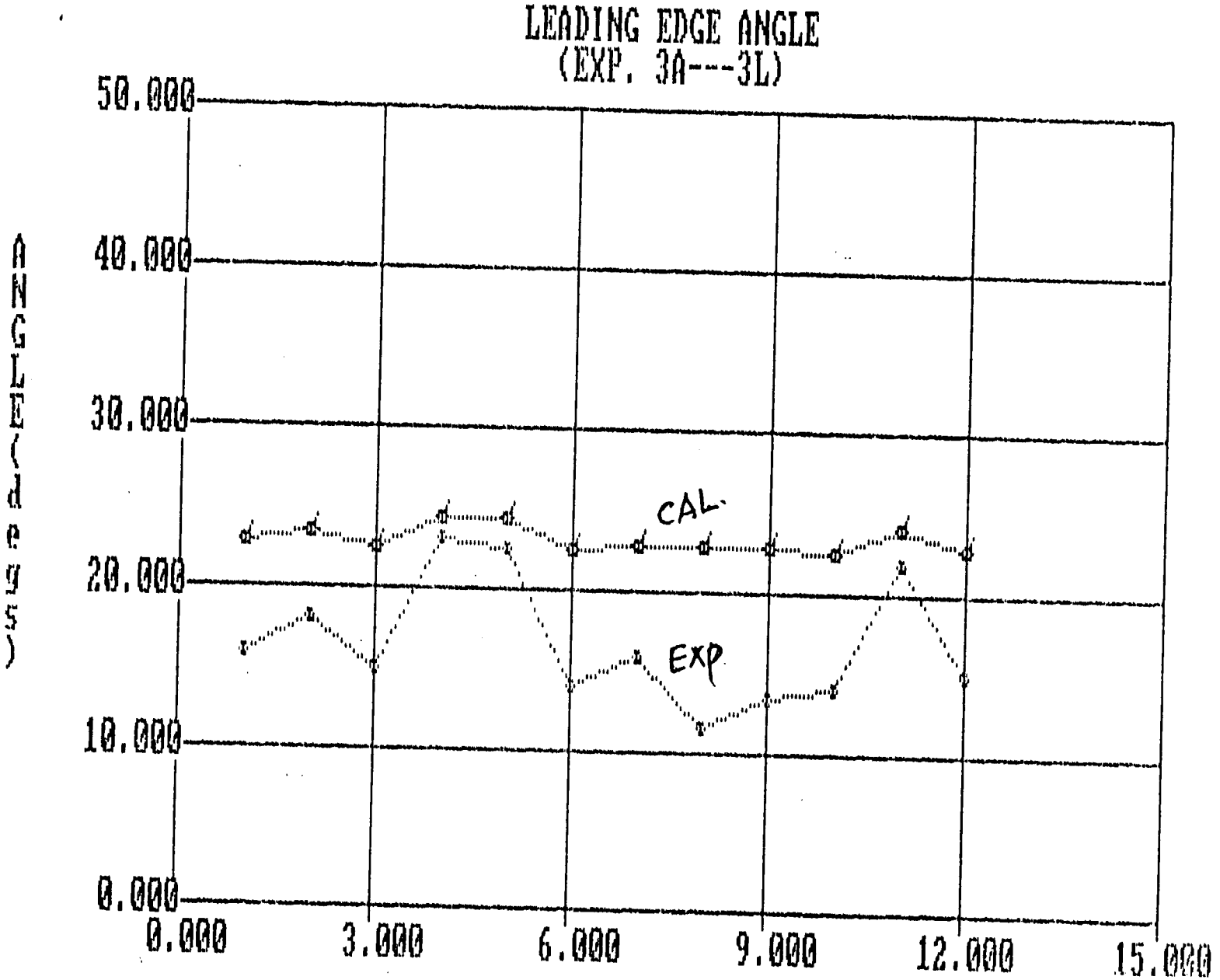
LEADING EDGE ANGLE
(EXP. 3A---3L)
ANGLE(deg)
50.000
40.000
30.000
20.000
10.000
0.000
0.000
3.000
6.000
9.000
12.000
15.000
CAL.
EXP

Fig. H-34

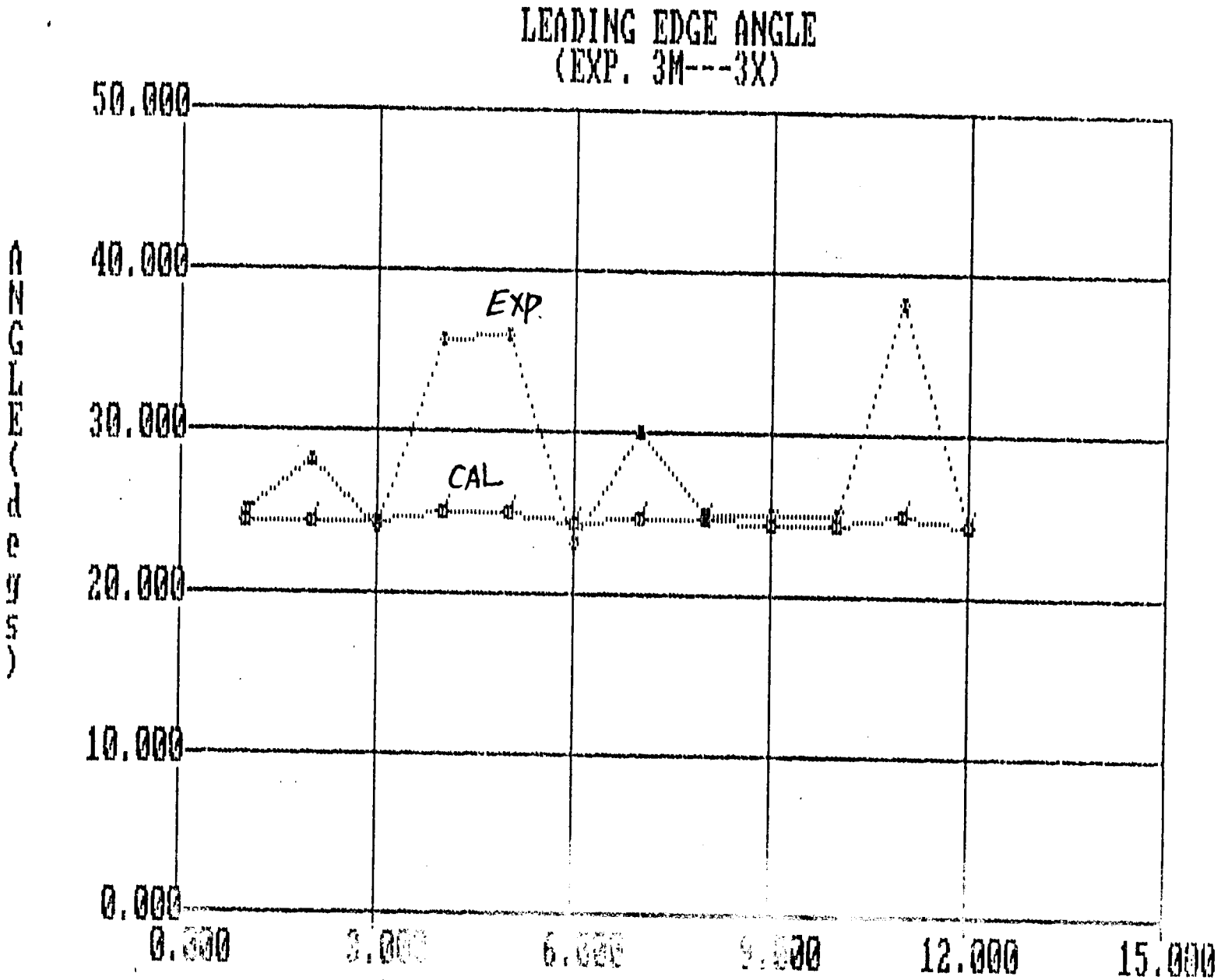

Fig. H-35

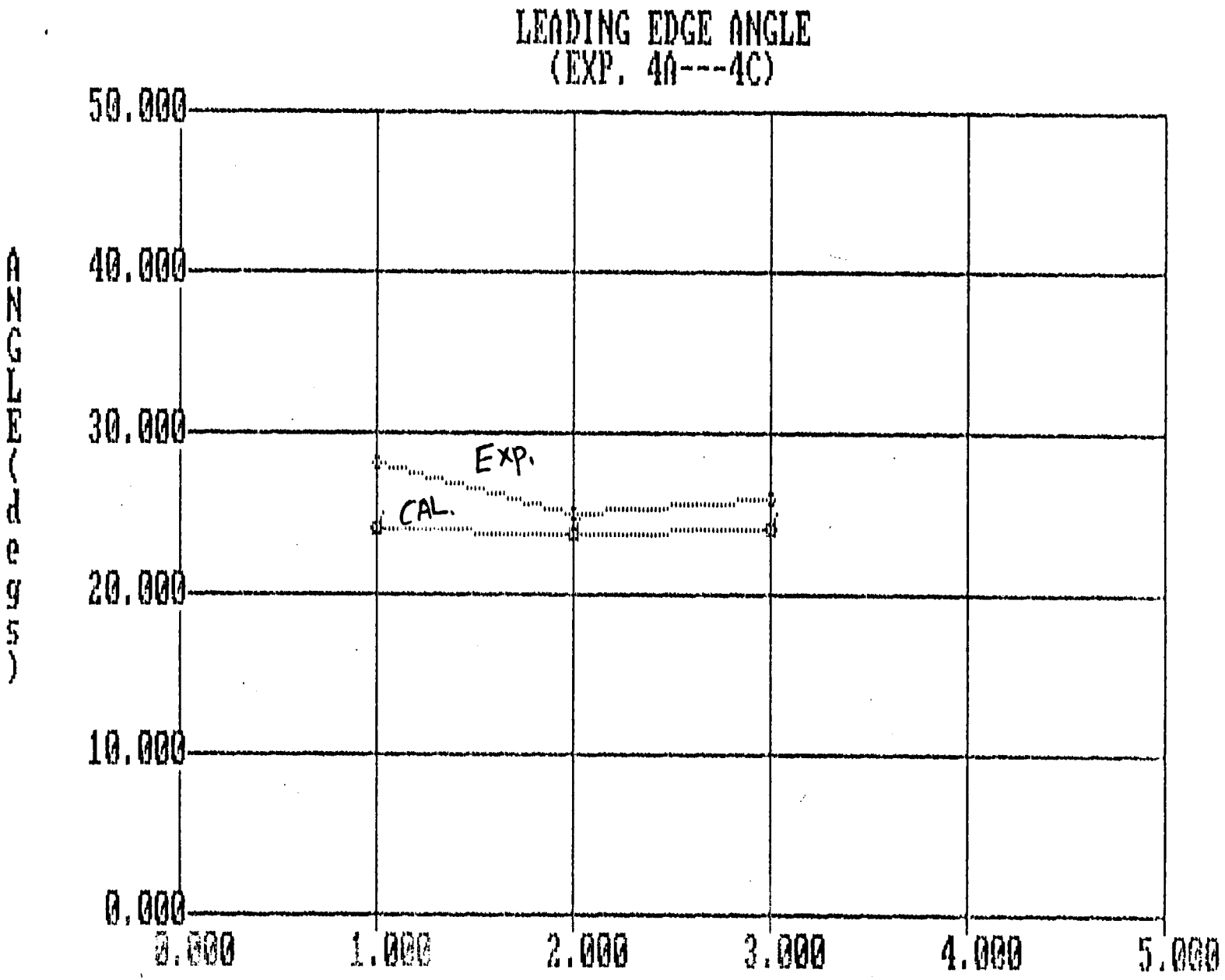
LEADING EDGE ANGLE
(EXP. 4A---4C)
ANGLE(degs)
50.000
40.000
30.000
20.000
10.000
0.000
0.000
1.000
2.000
3.000
4.000
5.000
EXP.
CAL.

Fig. H-36

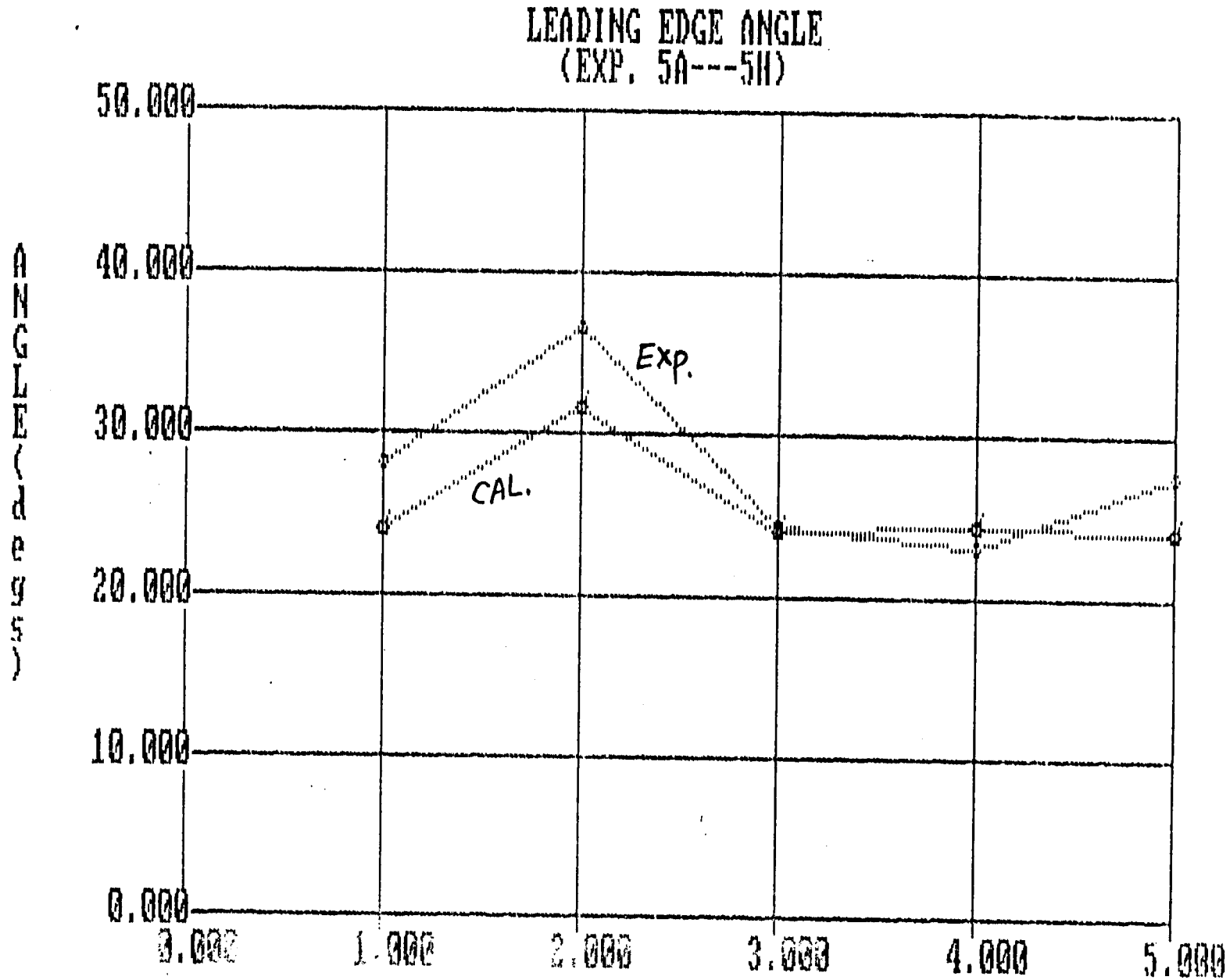
LEADING EDGE ANGLE
(EXP. 5A---5H)
ANGLE(degree)
50.000
40.000
30.000
20.000
10.000
0.000
Exp.
CAL.
1.000
2.000
3.000
4.000
5.000

Fig. H-37

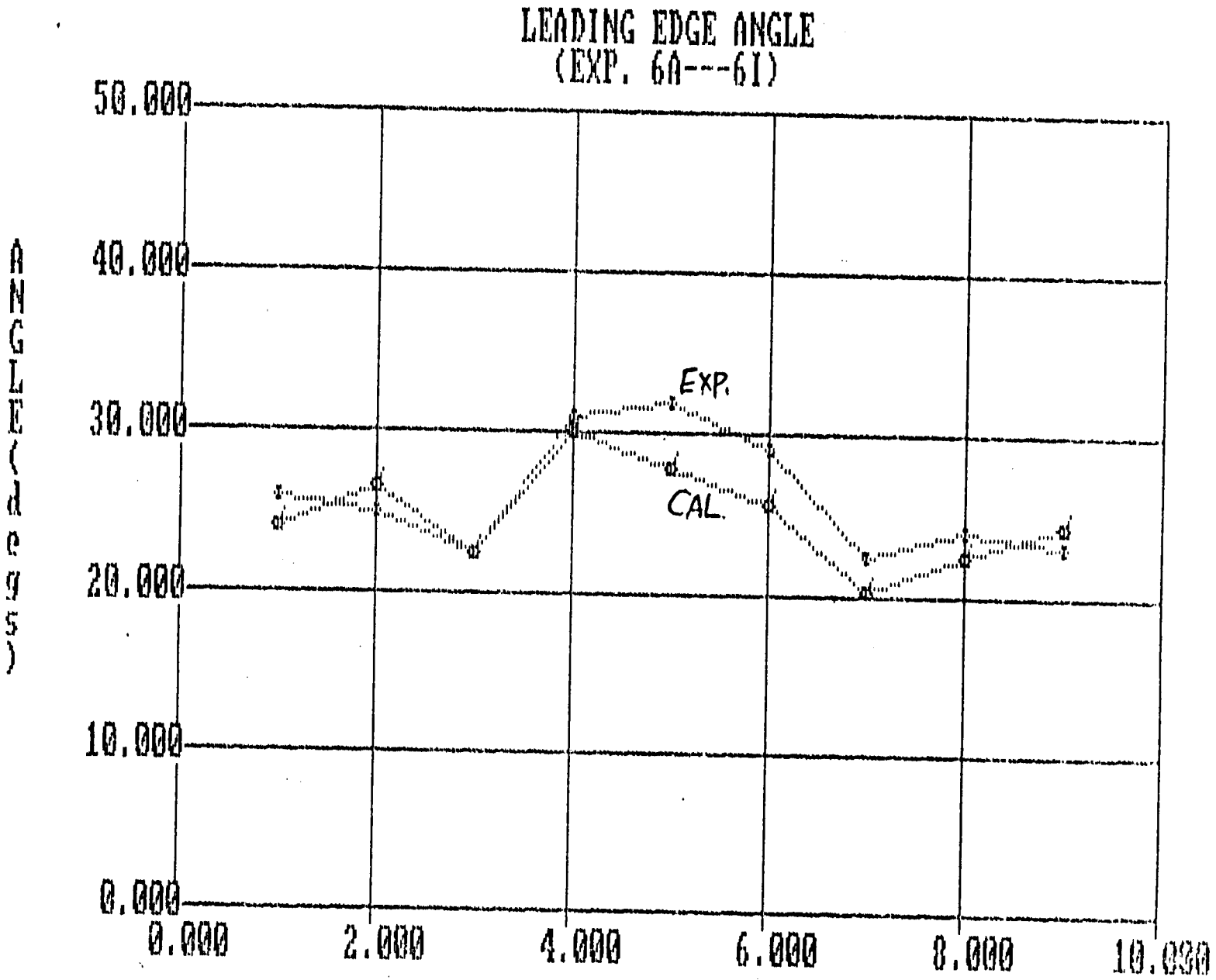
LEADING EDGE ANGLE
(EXP. 6A---6I)
ANGLE(degs)
50.000
40.000
30.000
20.000
10.000
0.000
0.000
2.000
4.000
6.000
8.000
10.000
EXP.
CAL.

Fig. H-38

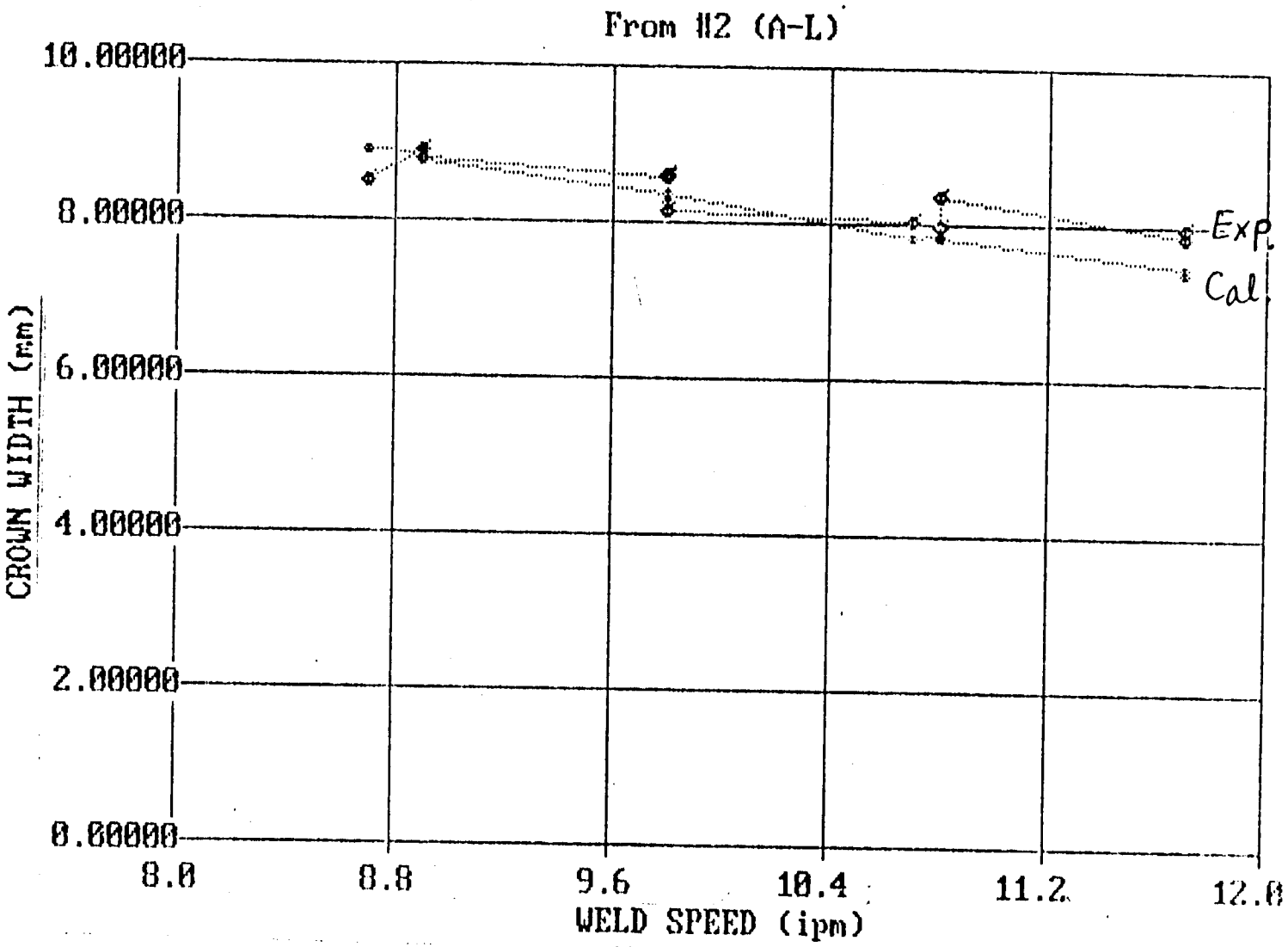
From 112 (A-L)
10.00000
8.00000
6.00000
4.00000
2.00000
0.00000
CROWN WIDTH (mm)
8.0
8.8
9.6
10.4
11.2
12.0
WELD SPEED (ipm)
Exp.
Cal.

Fig. H-39

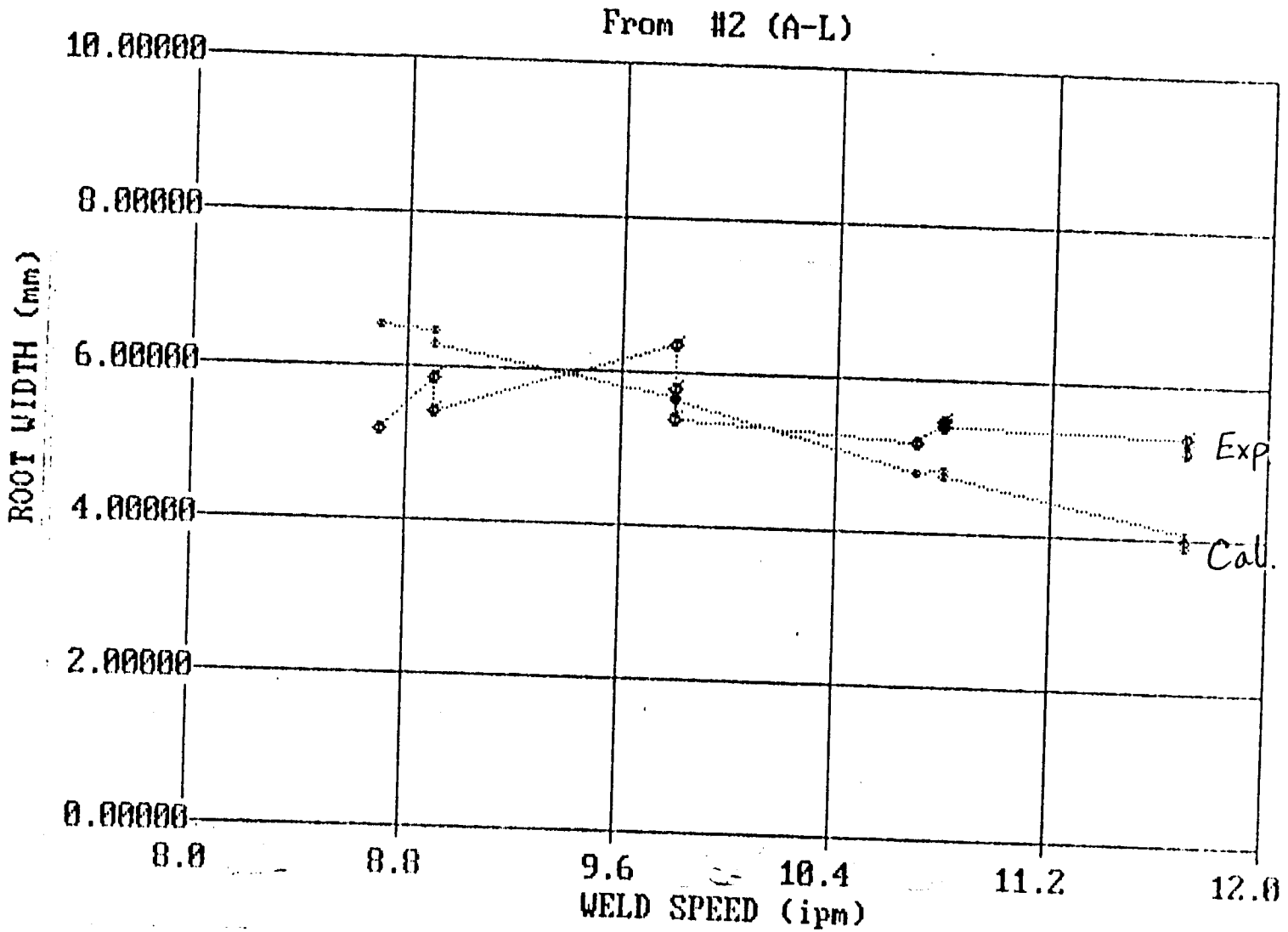
From #2 (A-L)
10.00000
8.00000
6.00000
4.00000
2.00000
0.00000
ROOT WIDTH (mm)
8.0
8.8
9.6
10.4
11.2
12.0
WELD SPEED (ipm)
Exp
Cal.

Fig. H-40

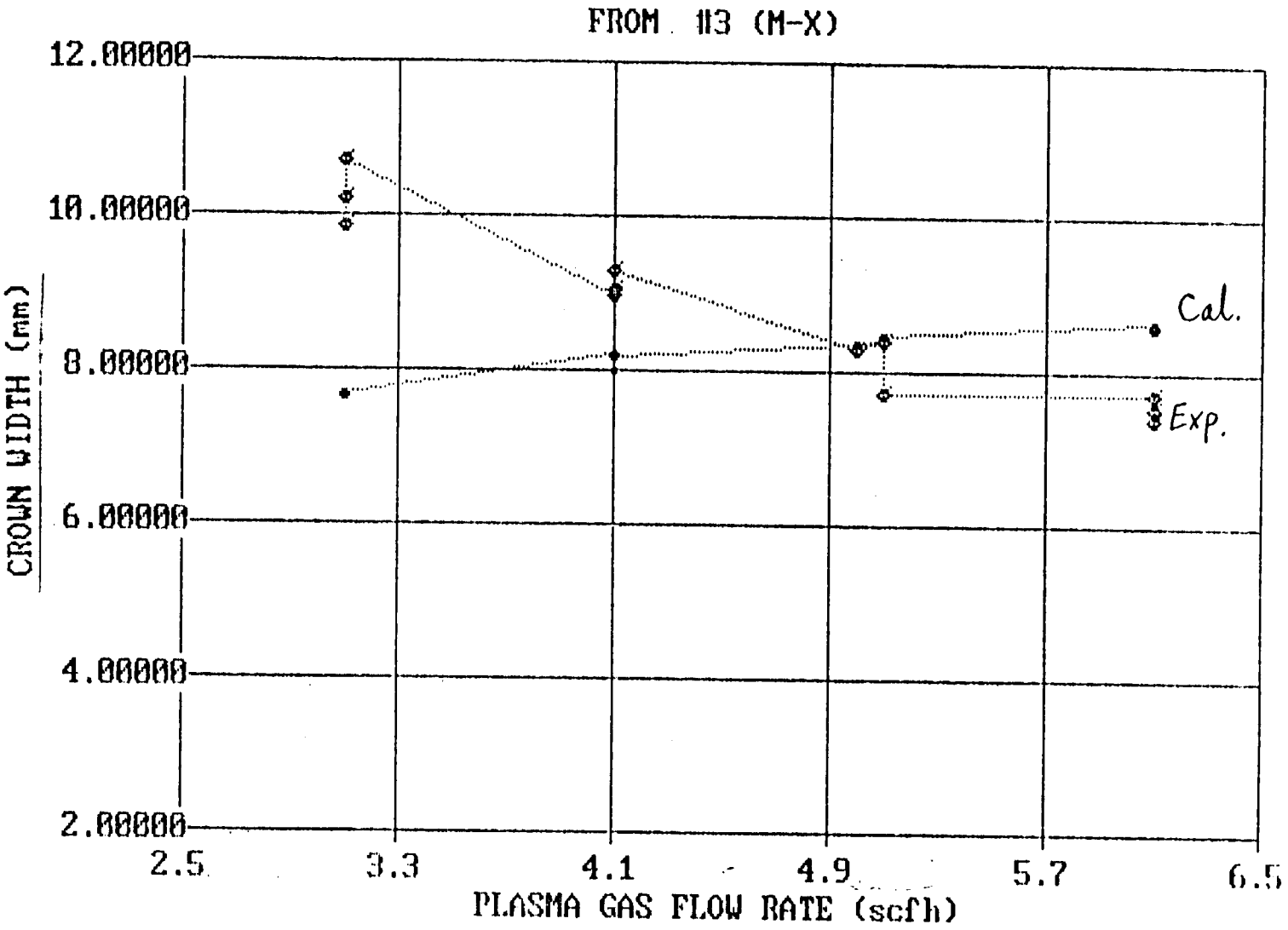
FROM 113 (M-X)
12.00000
10.00000
8.00000
6.00000
4.00000
2.00000
CROWN WIDTH (mm)
Cal.
Exp.
2.5
3.3
4.1
4.9
5.7
6.5
PLASMA GAS FLOW RATE (scfh)

Fig. H-41

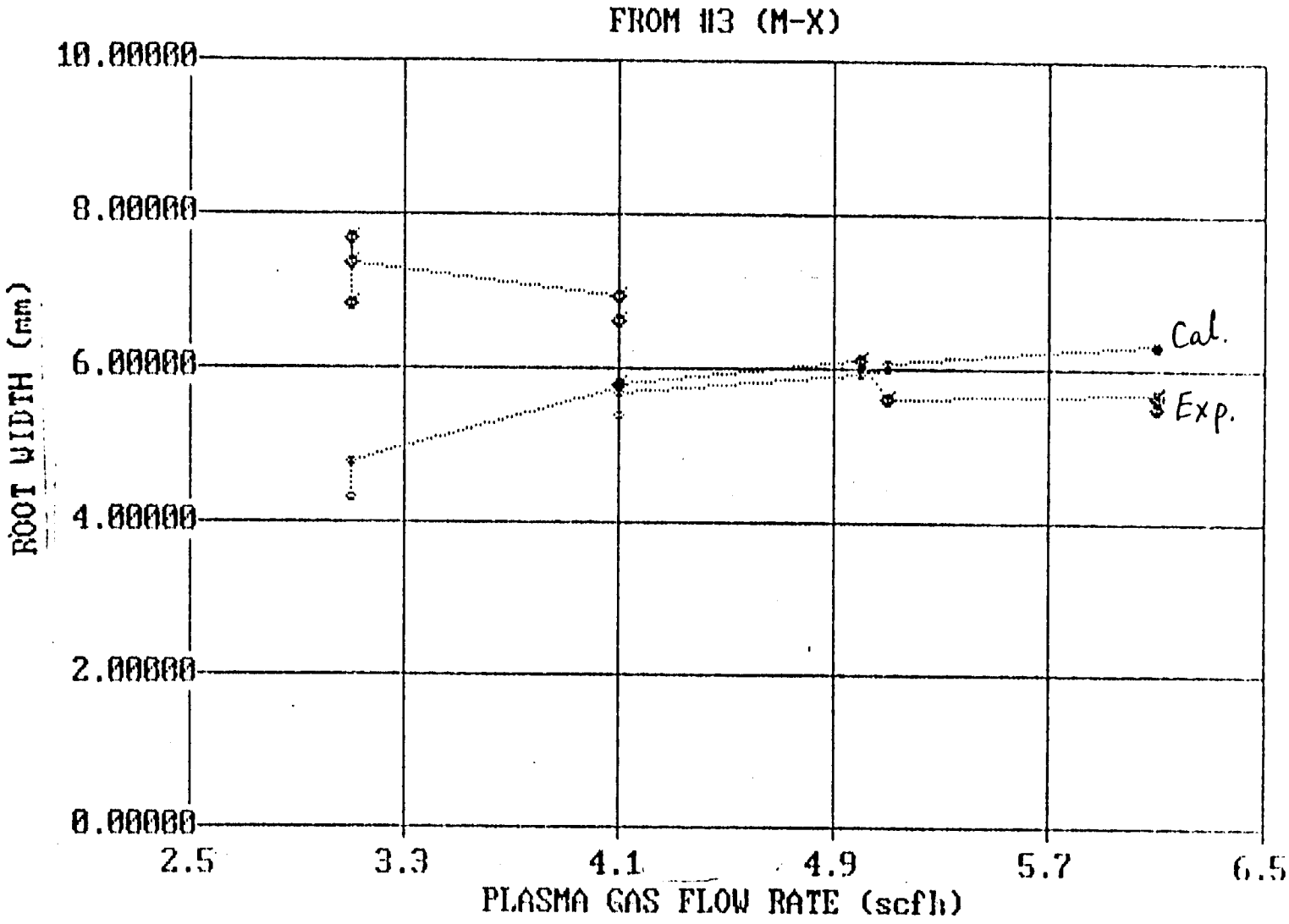
FROM 113 (M-X)
10.00000
8.00000
6.00000
4.00000
2.00000
0.00000
ROOT WIDTH (mm)
2.5
3.3
4.1
4.9
5.7
6.5
PLASMA GAS FLOW RATE (scfh)
Cal.
Exp.

Fig. H-42

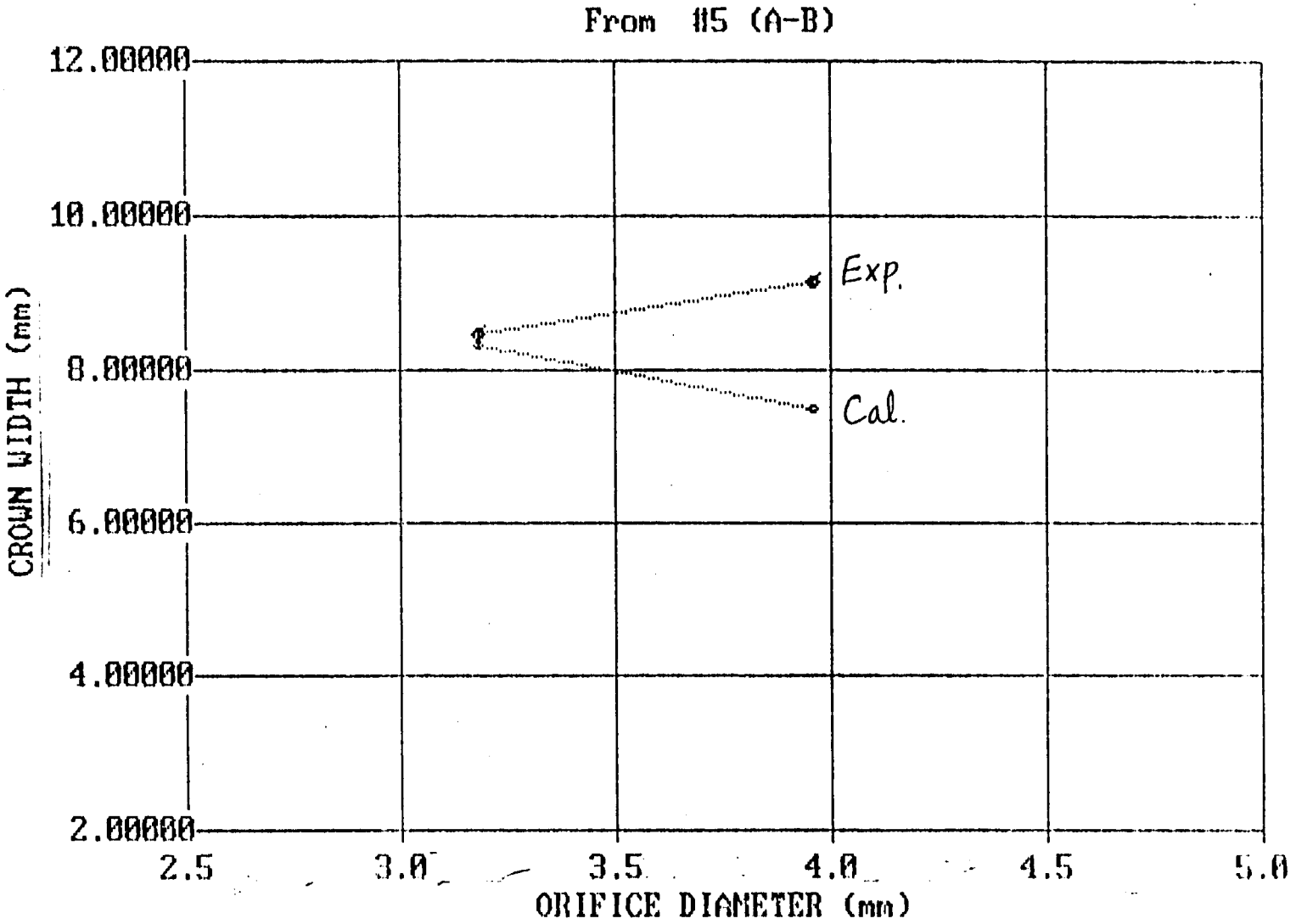
From 115 (A-B)
12.00000
10.00000
8.00000
6.00000
4.00000
2.00000
CROWN WIDTH (mm)
Exp.
Cal.
2.5
3.0
3.5
4.0
4.5
5.0
ORIFICE DIAMETER (mm)

Fig. H-43

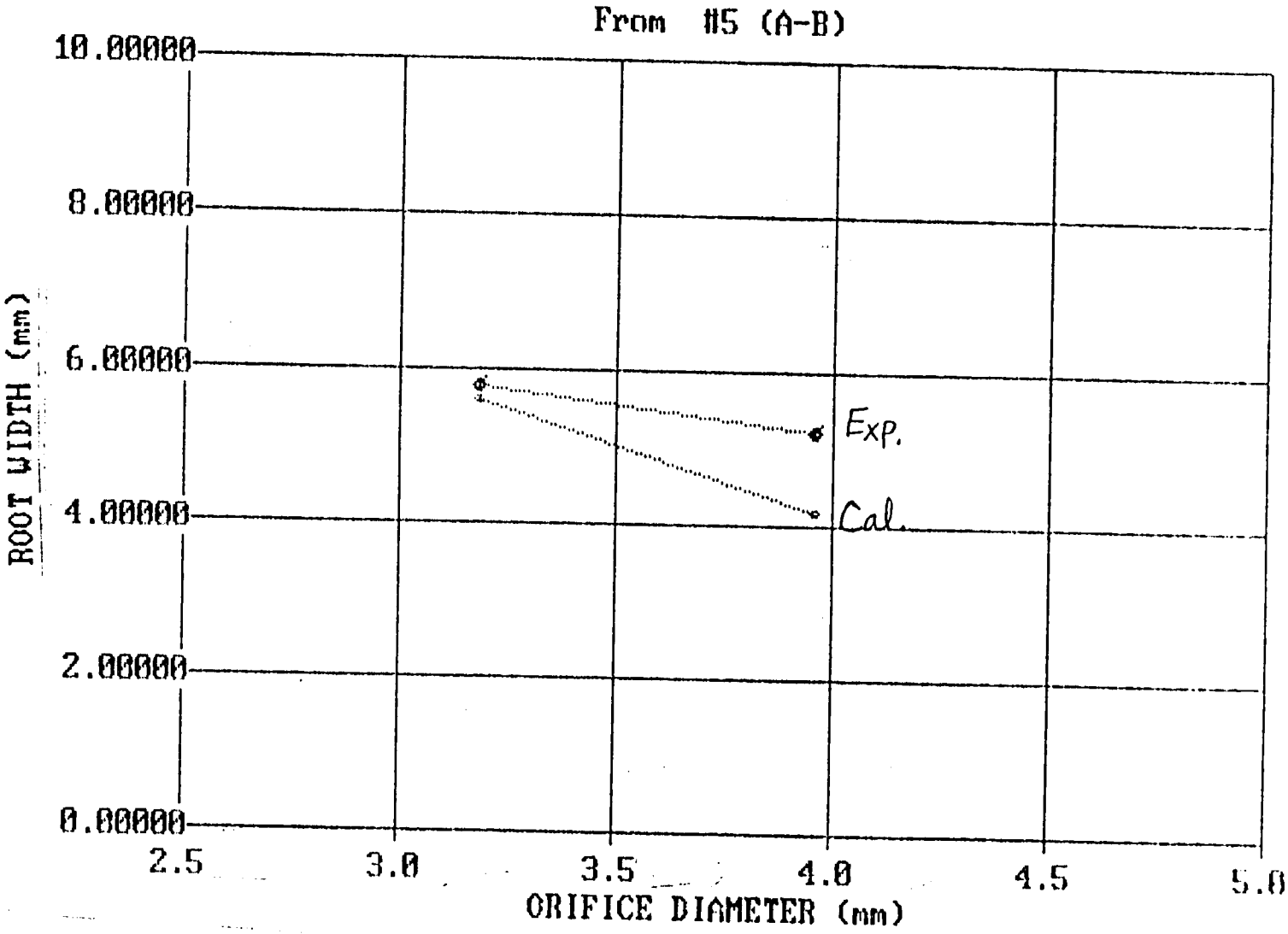
From #5 (A-B)
10.00000
8.00000
6.00000
4.00000
2.00000
0.00000
ROOT WIDTH (mm)
2.5
3.0
3.5
4.0
4.5
5.0
ORIFICE DIAMETER (mm)
Exp.
Cal.

Fig. H-44

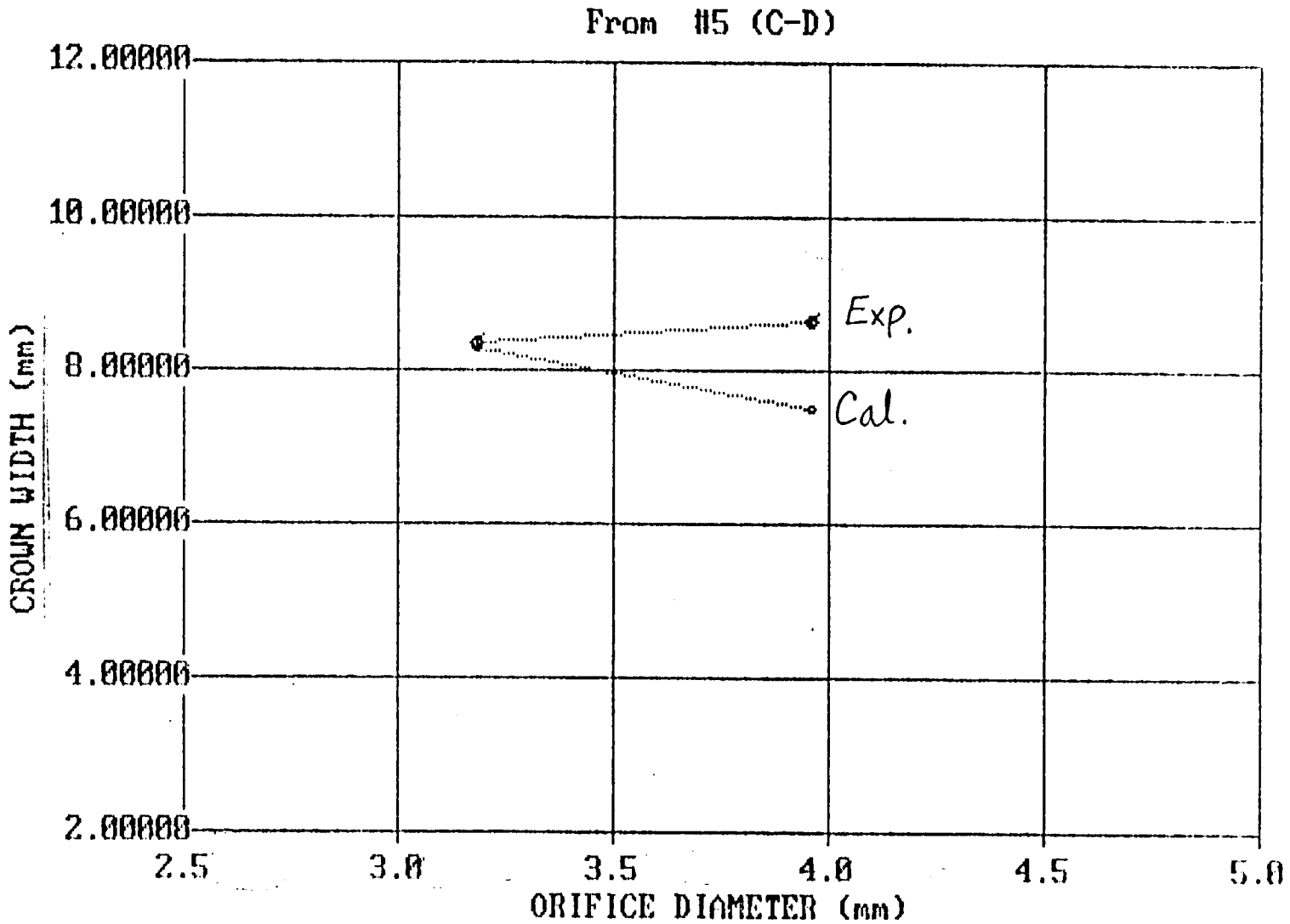
From #5 (C-D)
12.00000
10.00000
8.00000
6.00000
4.00000
2.00000
CROWN WIDTH (mm)
Exp.
Cal.
2.5
3.0
3.5
4.0
4.5
5.0
ORIFICE DIAMETER (mm)

Fig. H-45

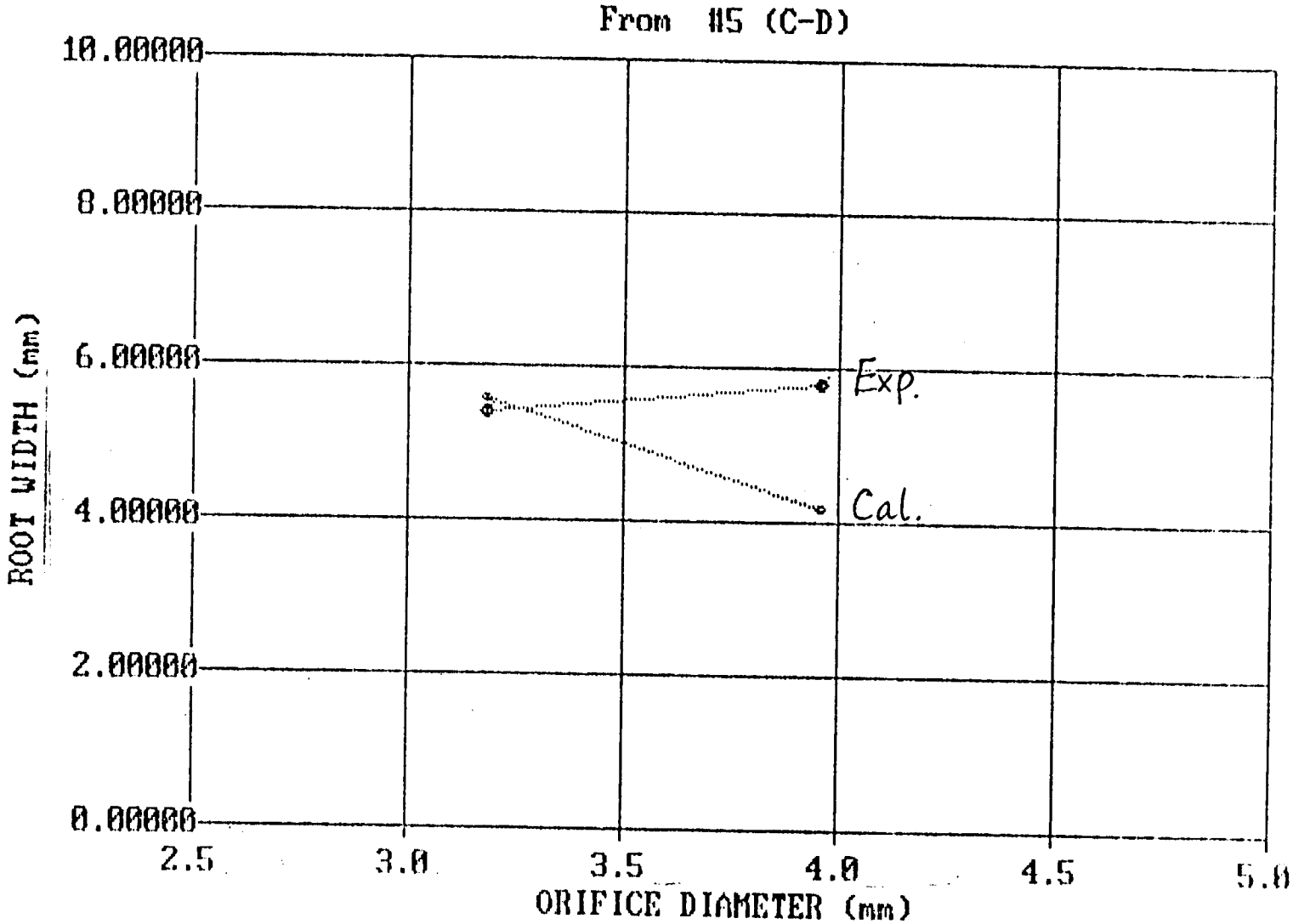
From 115 (C-D)
10.00000
8.00000
6.00000
4.00000
2.00000
0.00000
ROOT WIDTH (mm)
Exp.
Cal.
2.5
3.0
3.5
4.0
4.5
5.0
ORIFICE DIAMETER (mm)

Fig. H-46

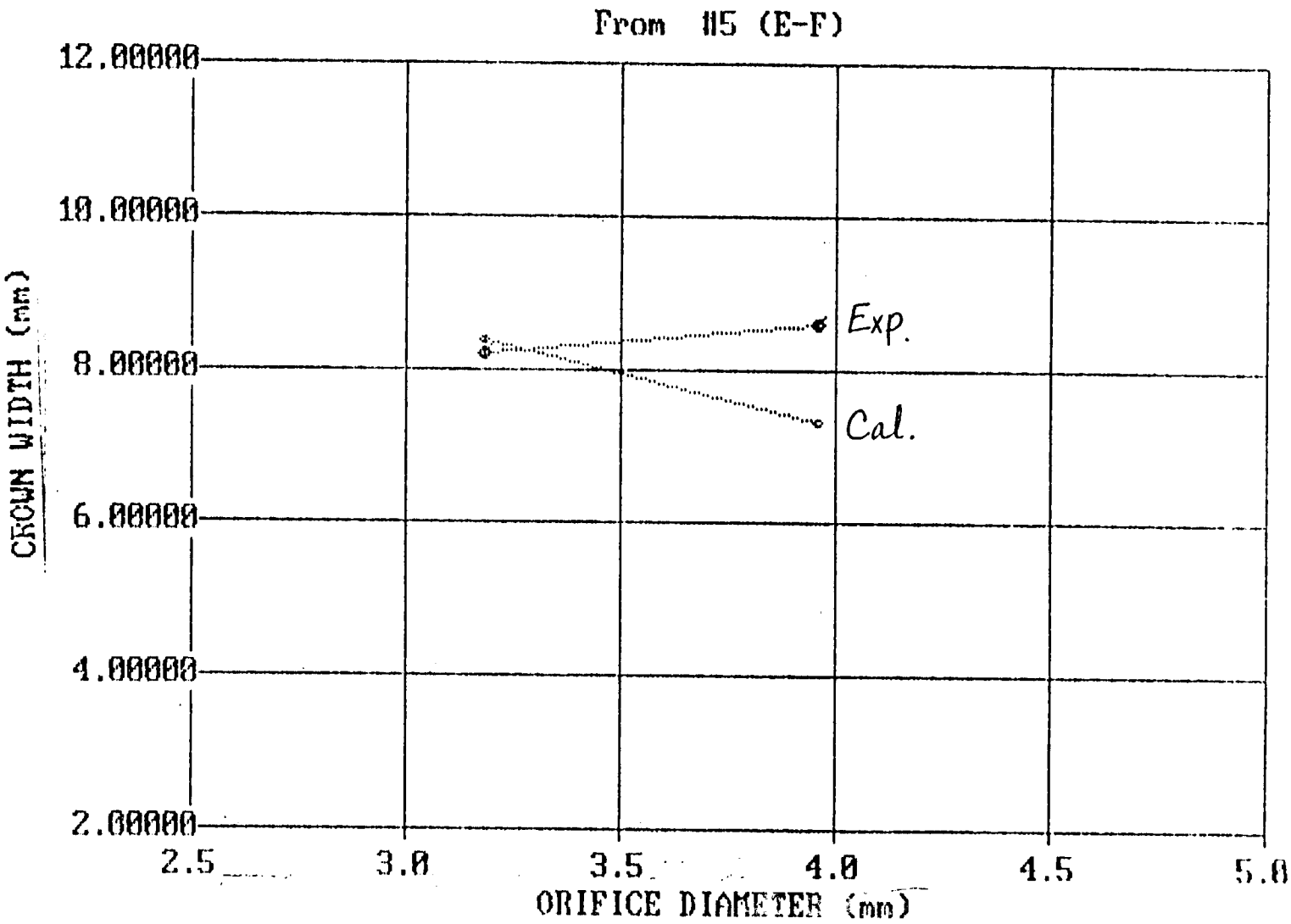
From 115 (E-F)
12.00000
10.00000
8.00000
6.00000
4.00000
2.00000
CROWN WIDTH (mm)
Exp.
Cal.
2.5
3.0
3.5
4.0
4.5
5.0
ORIFICE DIAMETER (mm)

Fig. H-47

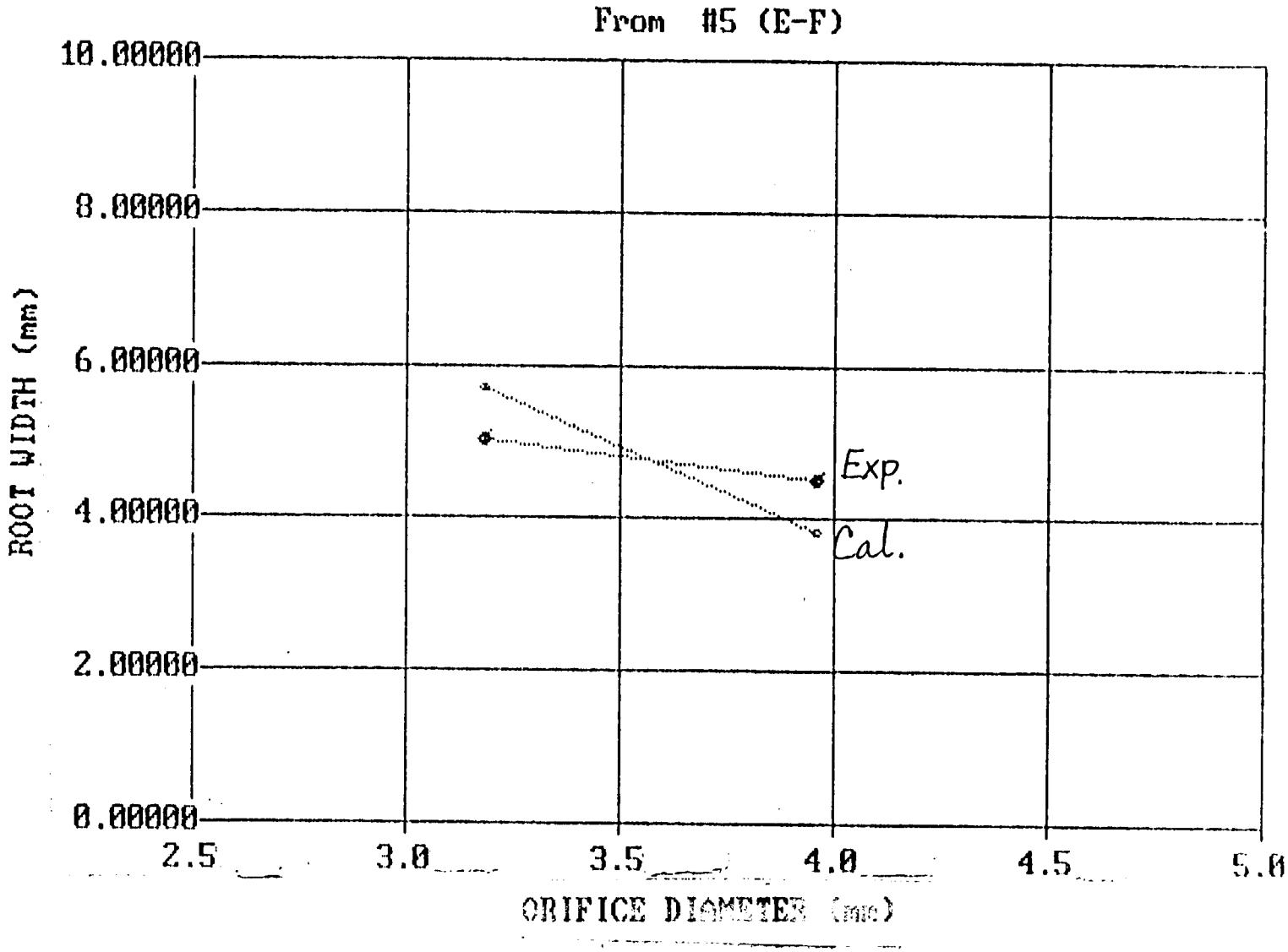

Fig. 4-48

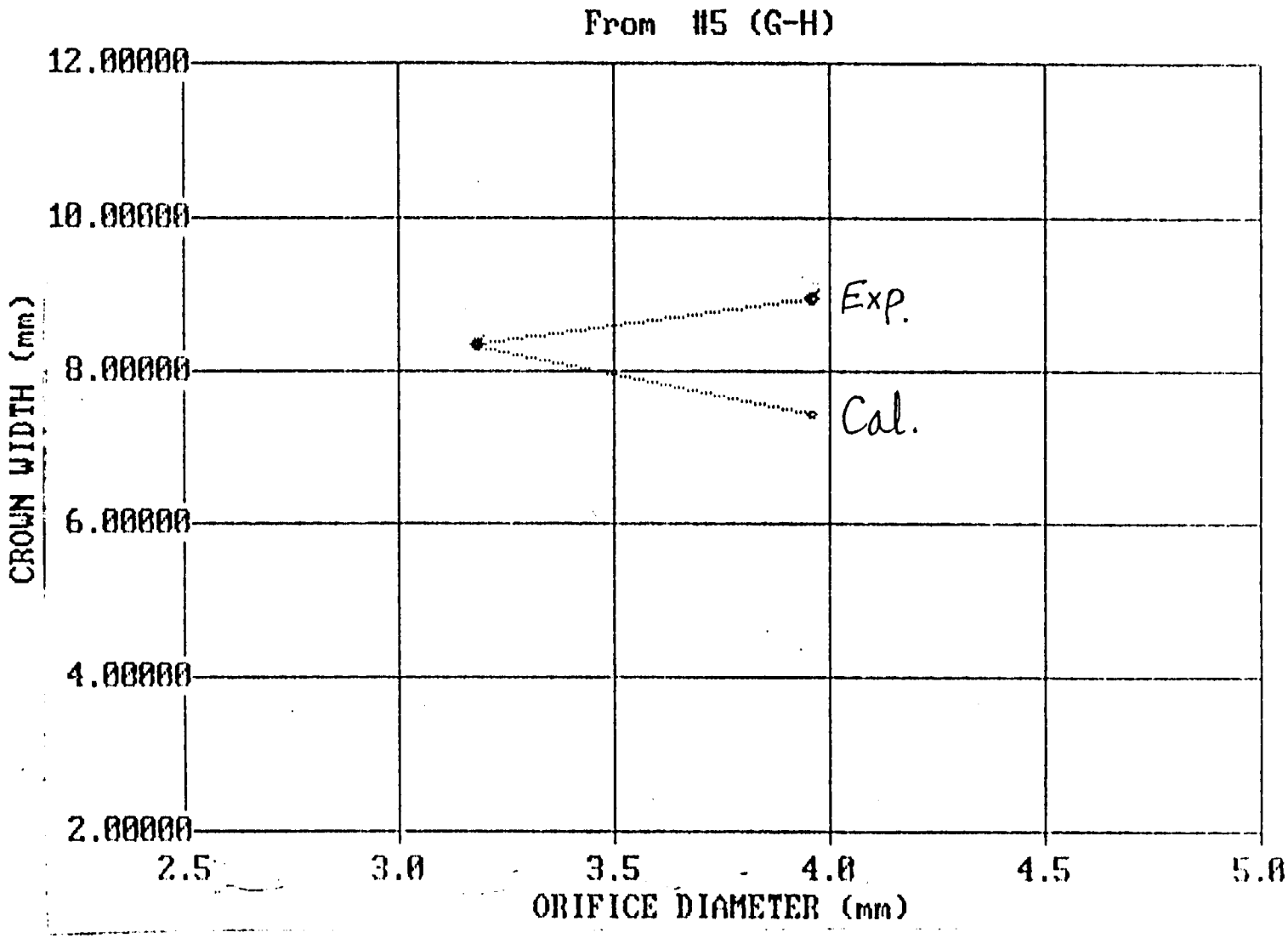
From 115 (G-H)
12.00000
10.00000
8.00000
6.00000
4.00000
2.00000
CROWN WIDTH (mm)
Exp.
Cal.
2.5
3.0
3.5
4.0
4.5
5.0
ORIFICE DIAMETER (mm)

Fig. H-49

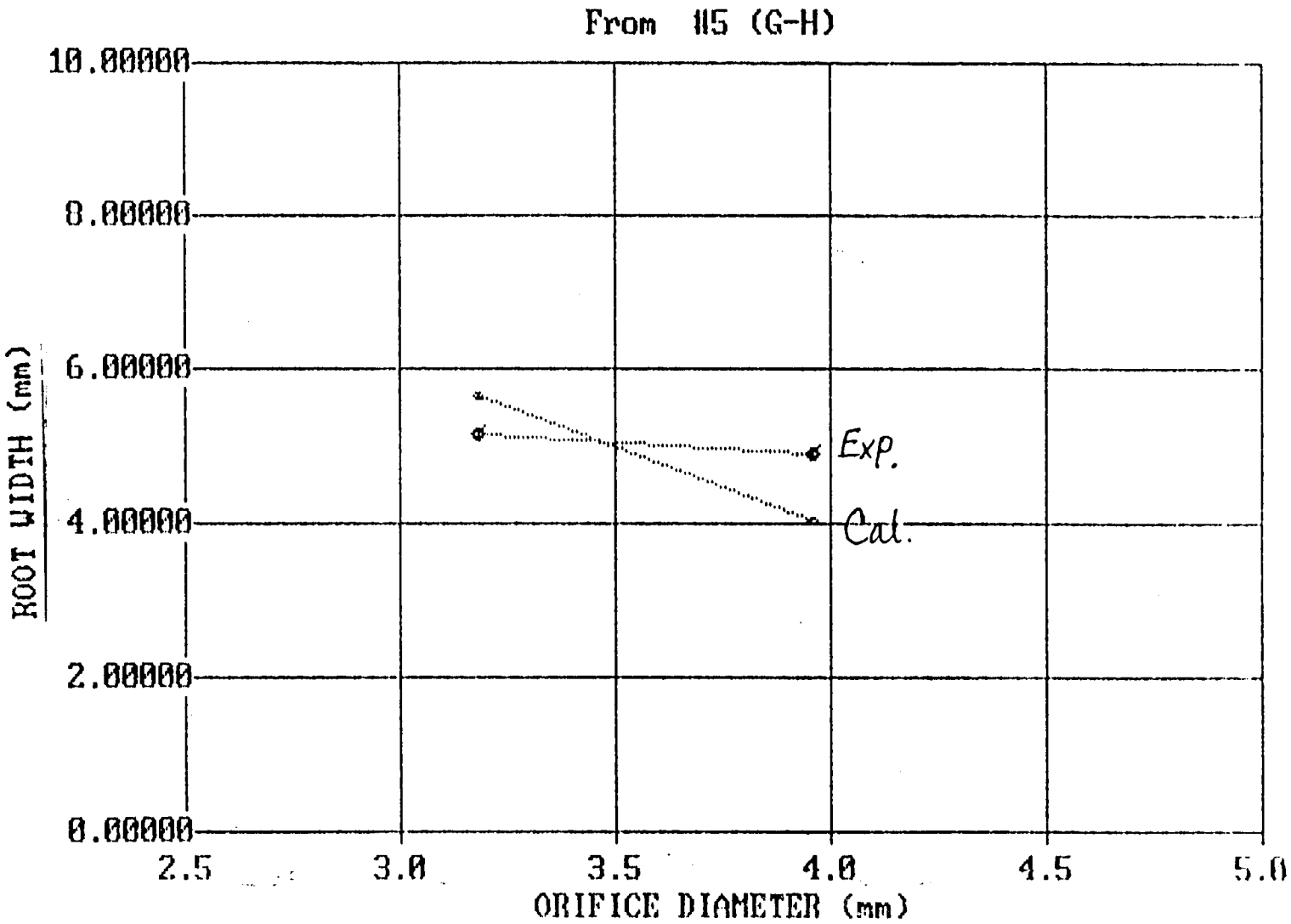
From 115 (G-H)
10.00000
8.00000
6.00000
4.00000
2.00000
0.00000
ROOT WIDTH (mm)
2.5
3.0
3.5
4.0
4.5
5.0
ORIFICE DIAMETER (mm)
Exp.
Cal.

Fig. H-50

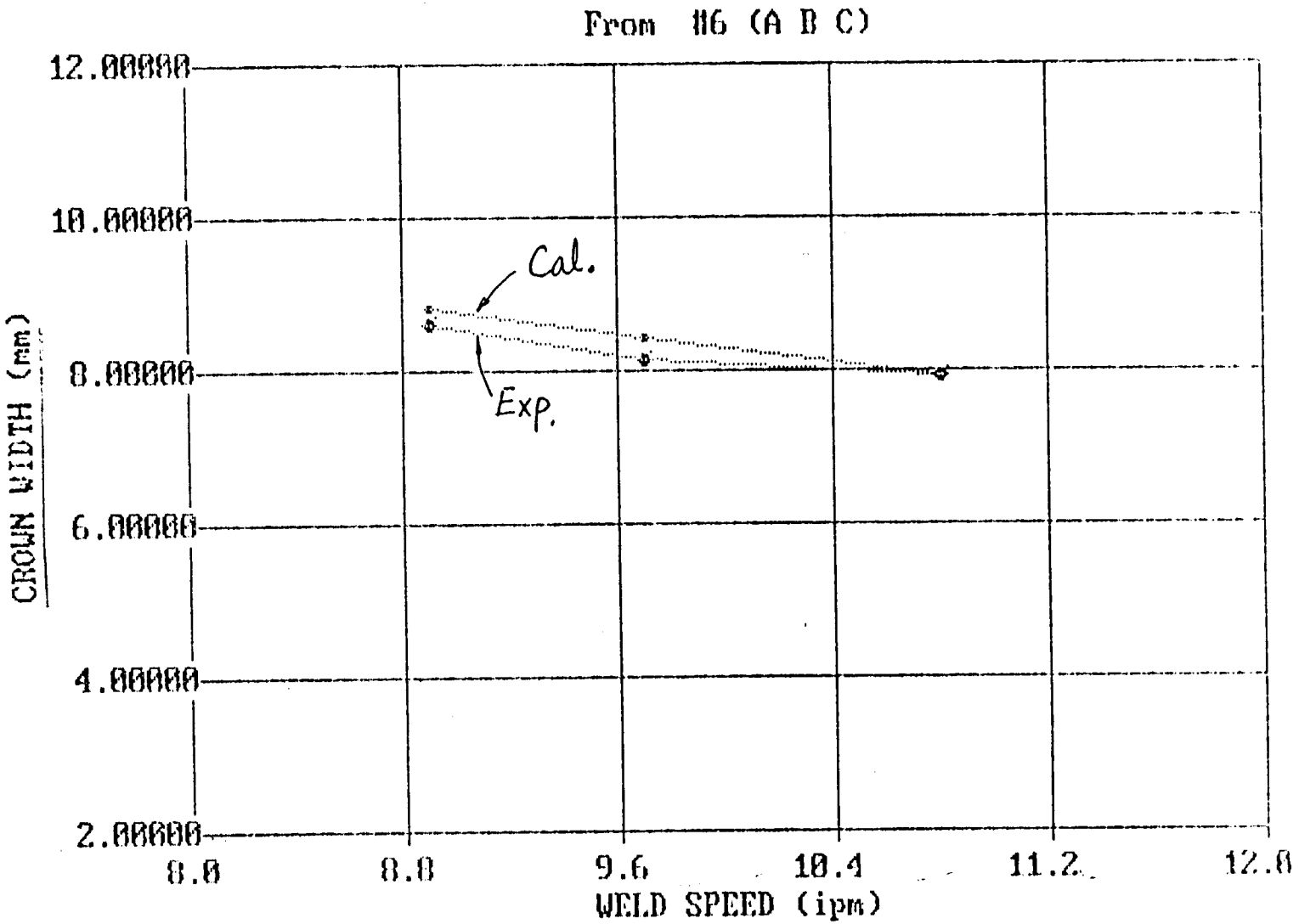
From 116 (A B C)
12.00000
10.00000
8.00000
6.00000
4.00000
2.00000
CROWN WIDTH (mm)
Cal.
Exp.
8.0
8.8
9.6
10.4
11.2
12.0
WELD SPEED (ipm)

Fig. H-51

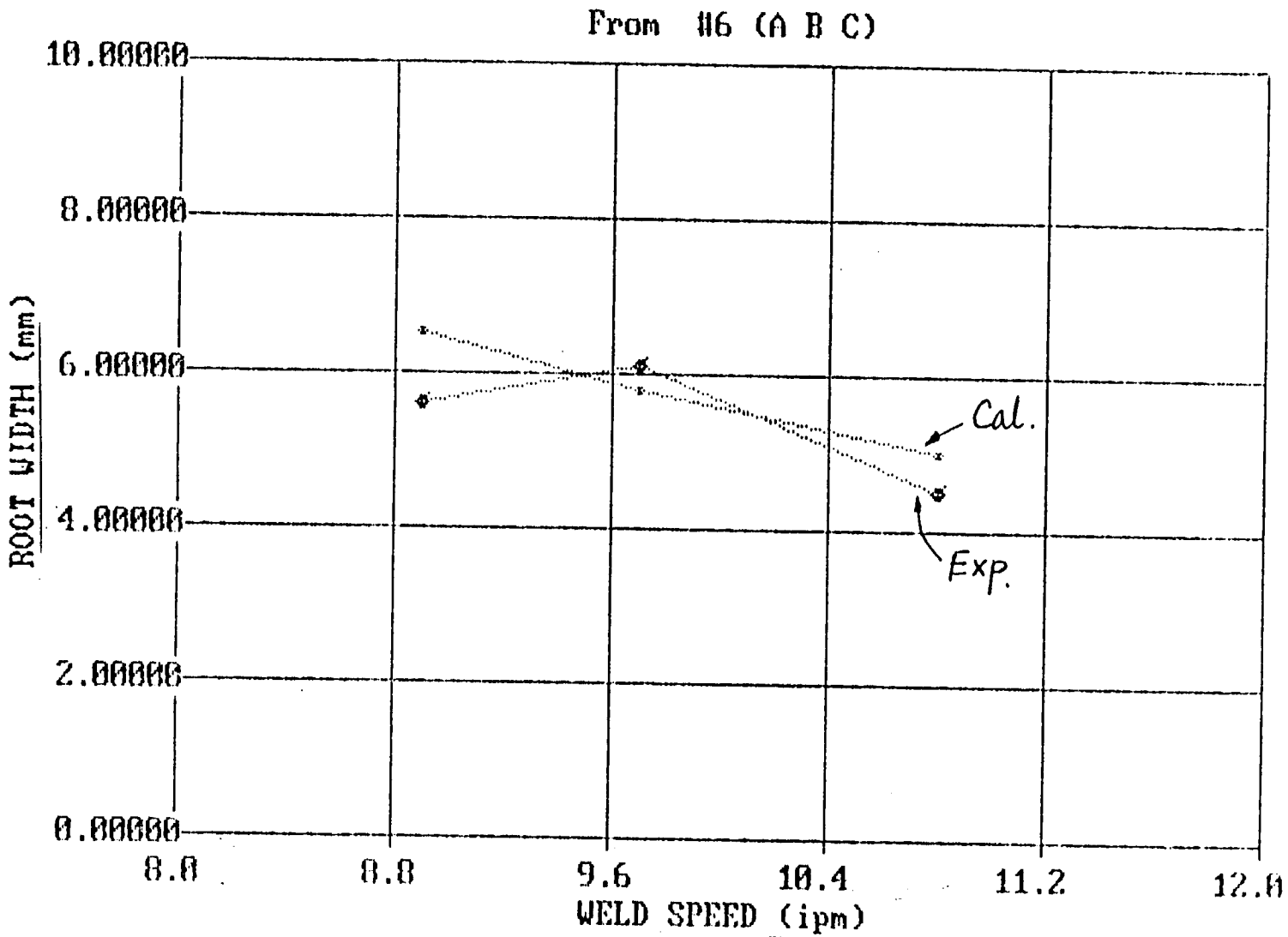
From #6 (A B C)
10.00000
8.00000
6.00000
4.00000
2.00000
0.00000
ROOT WIDTH (mm)
8.0
8.8
9.6
10.4
11.2
12.0
WELD SPEED (ipm)
Cal.
Exp.

Fig. H-52

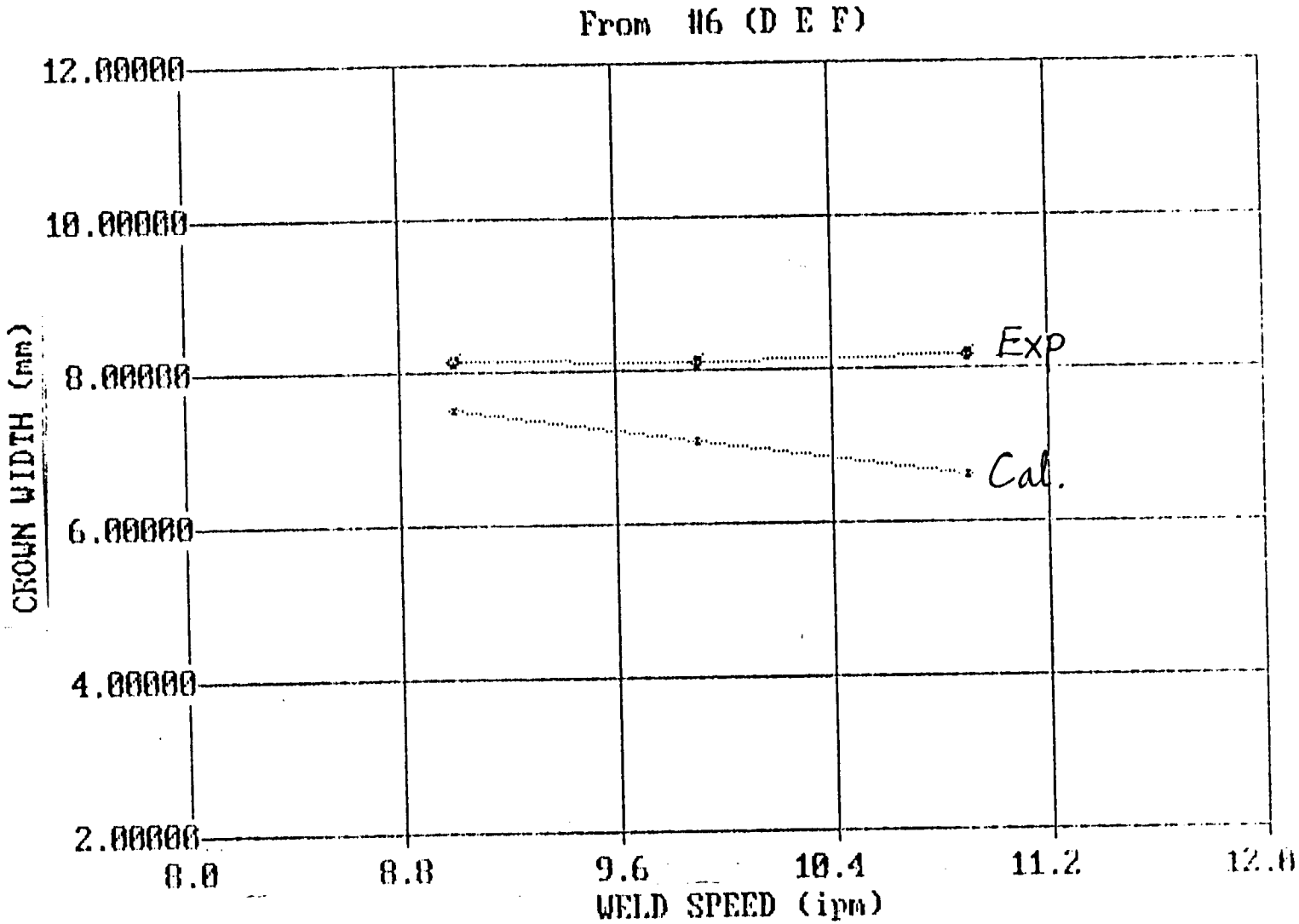
From H6 (D E F)
12.00000
10.00000
8.00000
6.00000
4.00000
2.00000
CROWN WIDTH (mm)
Exp
Cal.
8.0
8.8
9.6
10.4
11.2
12.0
WELD SPEED (ipm)

Fig. H-53

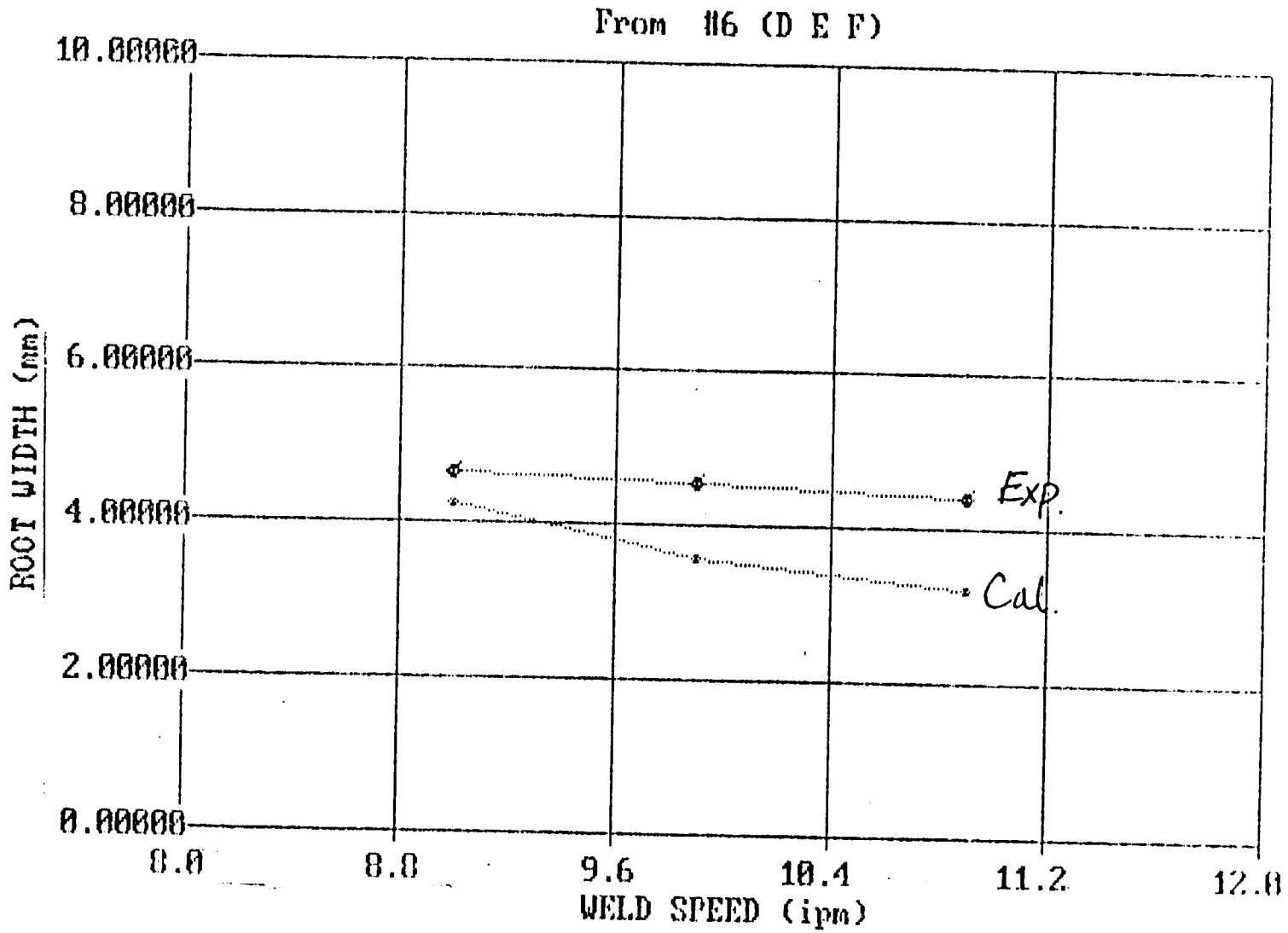
From 116 (D E F)
10.00000
8.00000
6.00000
4.00000
2.00000
0.00000
ROOT WIDTH (mm)
8.0
8.8
9.6
10.4
11.2
12.0
WELD SPEED (ipm)
Exp.
Cal.

Fig. H-34

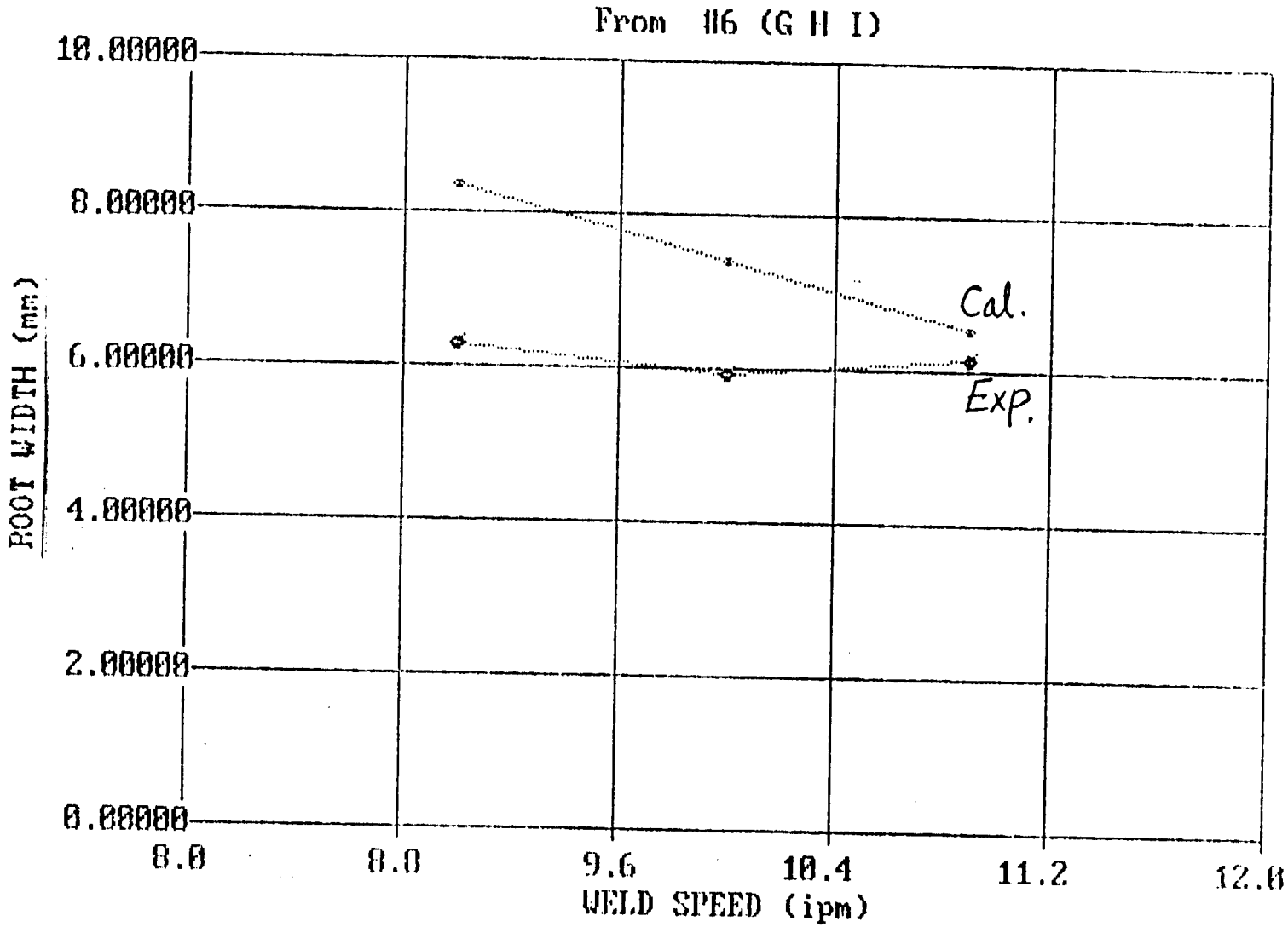
From 116 (G H I)
10.00000
8.00000
6.00000
4.00000
2.00000
0.00000
ROOT WIDTH (mm)
Cal.
Exp.
8.0
8.8
9.6
10.4
11.2
12.0
WELD SPEED (ipm)

Fig. H-55

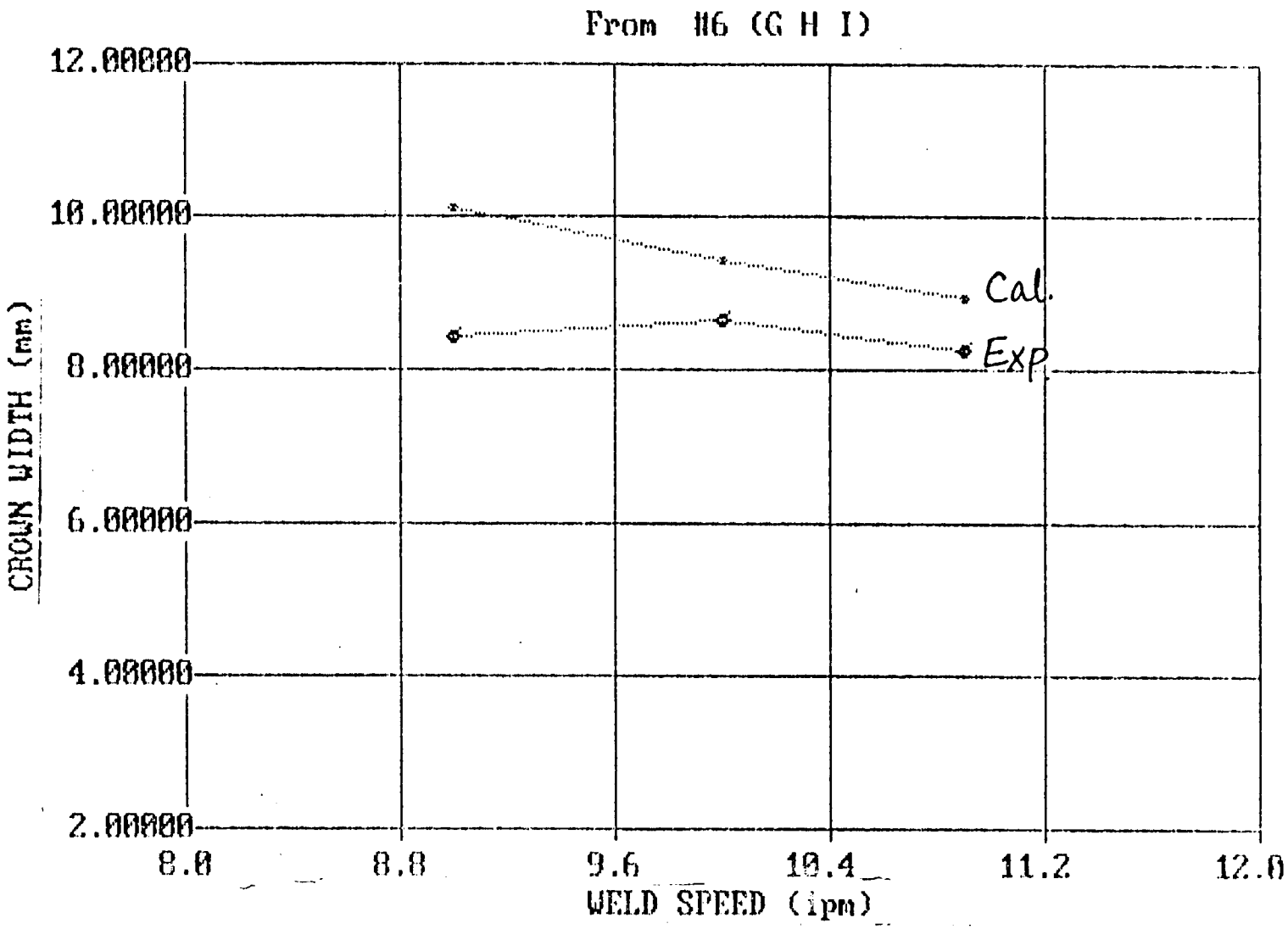
From #6 (G H I)
12.00000
10.00000
8.00000
6.00000
4.00000
2.00000
CROWN WIDTH (mm)
Cal.
Exp.
8.0
8.8
9.6
10.4
11.2
12.0
WELD SPEED (ipm)

Fig. H-56

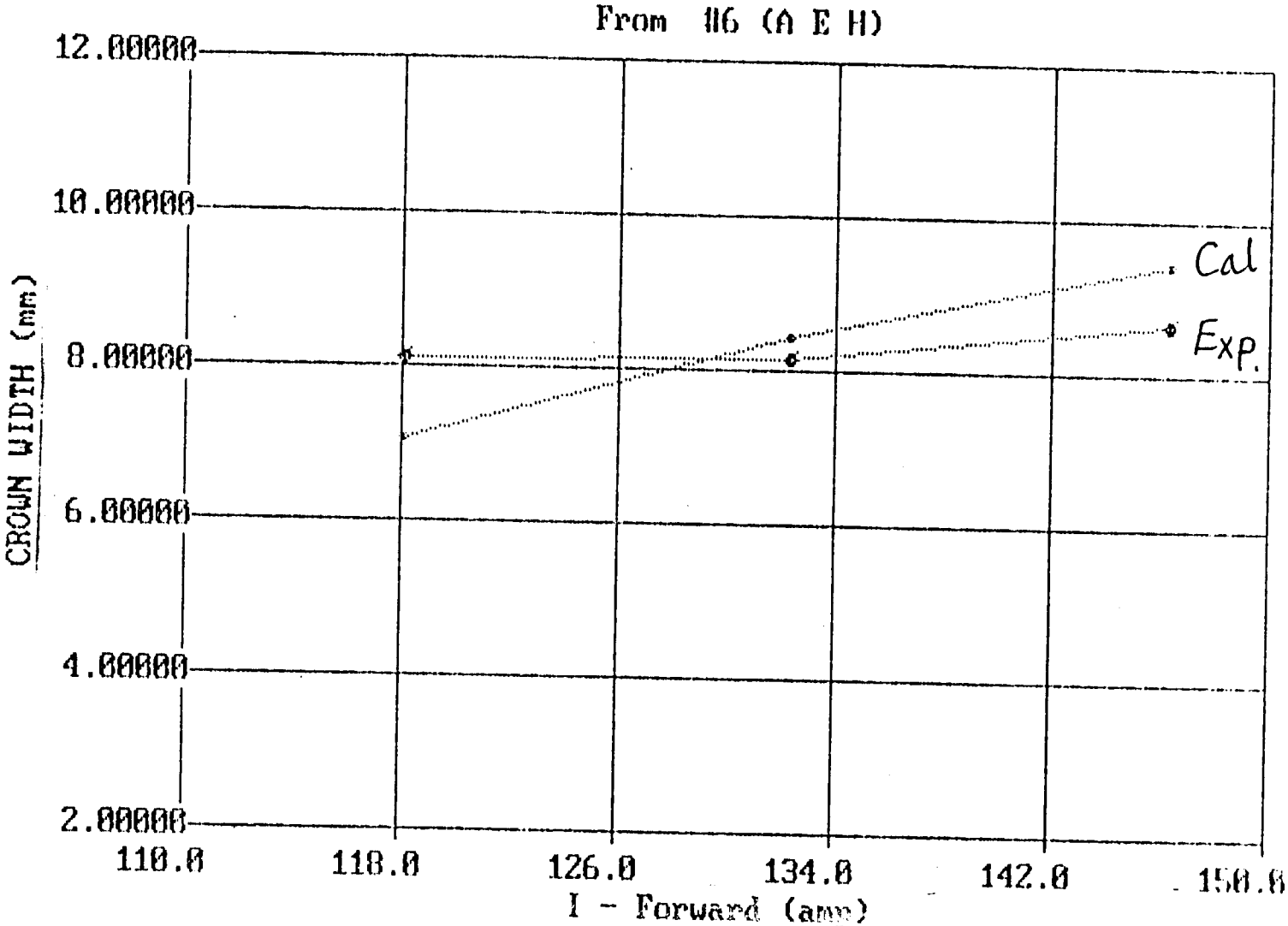
From 116 (A E H)
12.00000
10.00000
8.00000
6.00000
4.00000
2.00000
CROWN WIDTH (mm)
Cal
Exp.
110.0
118.0
126.0
134.0
142.0
150.0
I - Forward (amp)

Fig. A-3

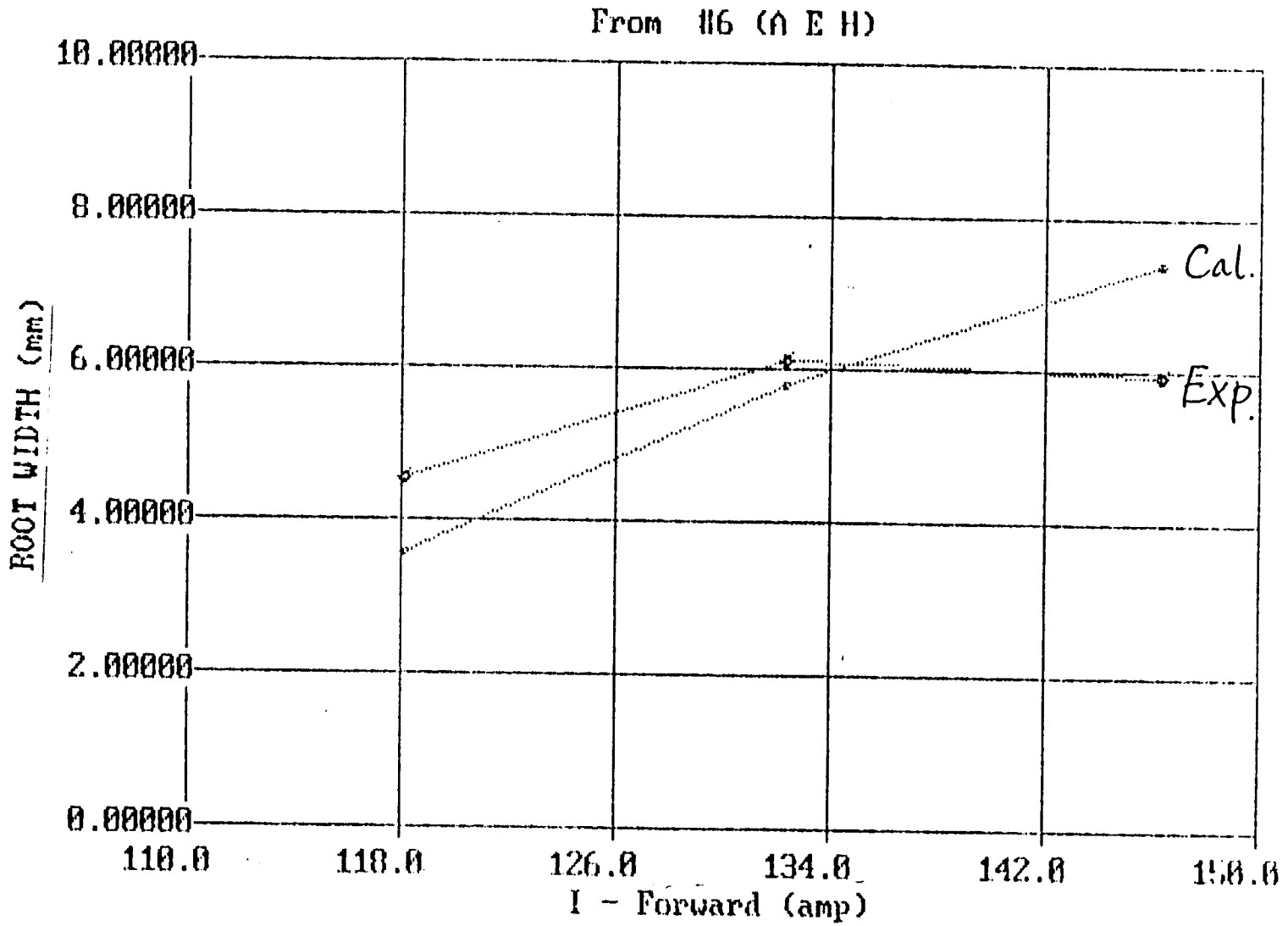
From 116 (A E H)
10.00000
8.00000
6.00000
4.00000
2.00000
0.00000
ROOT WIDTH (mm)
Cal.
Exp.
110.0
118.0
126.0
134.0
142.0
150.0
I - Forward (amp)

Fig. H-58

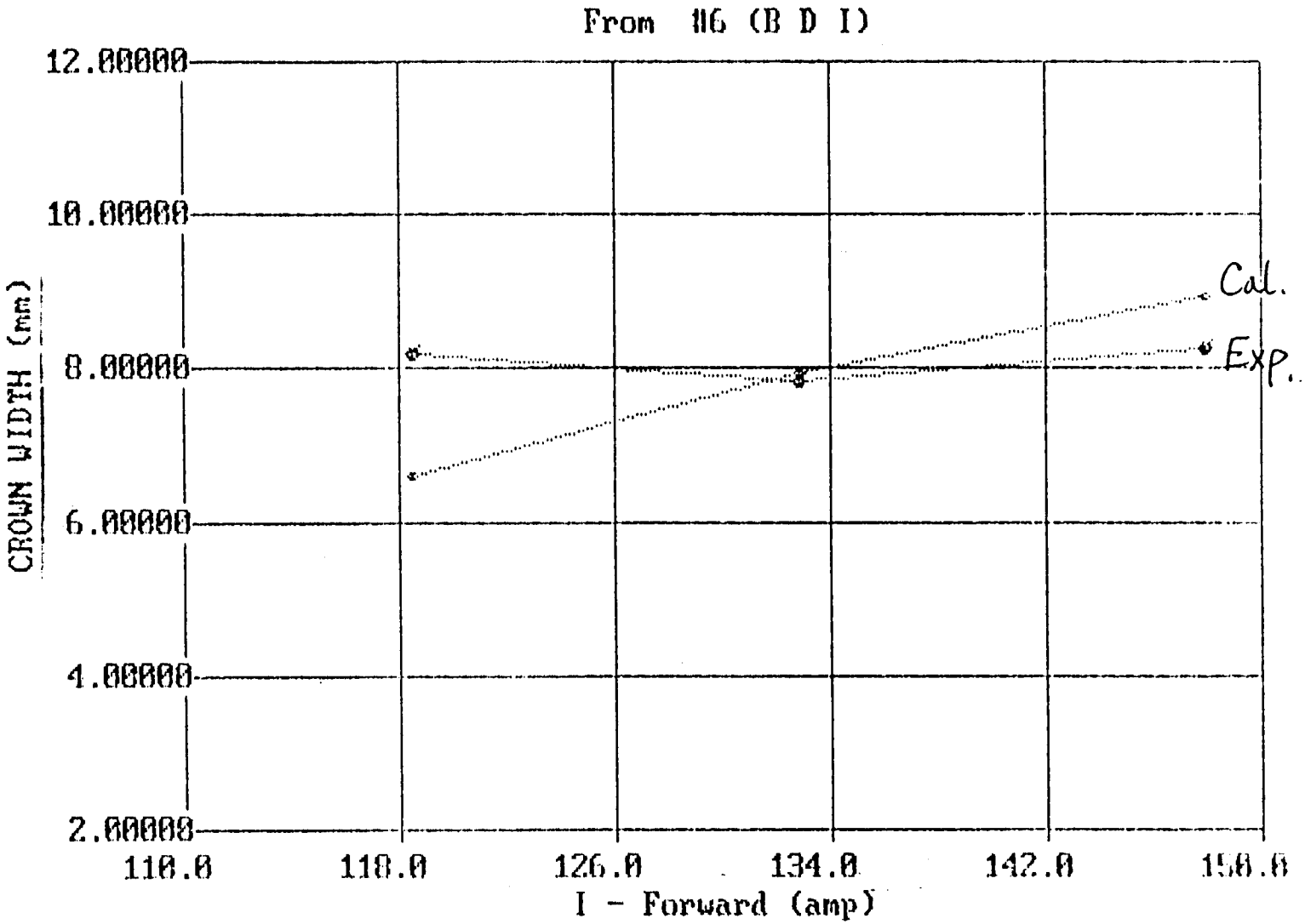
From 116 (B D I)
12.00000
10.00000
8.00000
6.00000
4.00000
2.00000
CROWN WIDTH (mm)
110.0
118.0
126.0
134.0
142.0
150.0
I - Forward (amp)
Cal.
Exp.

Fig. H-59

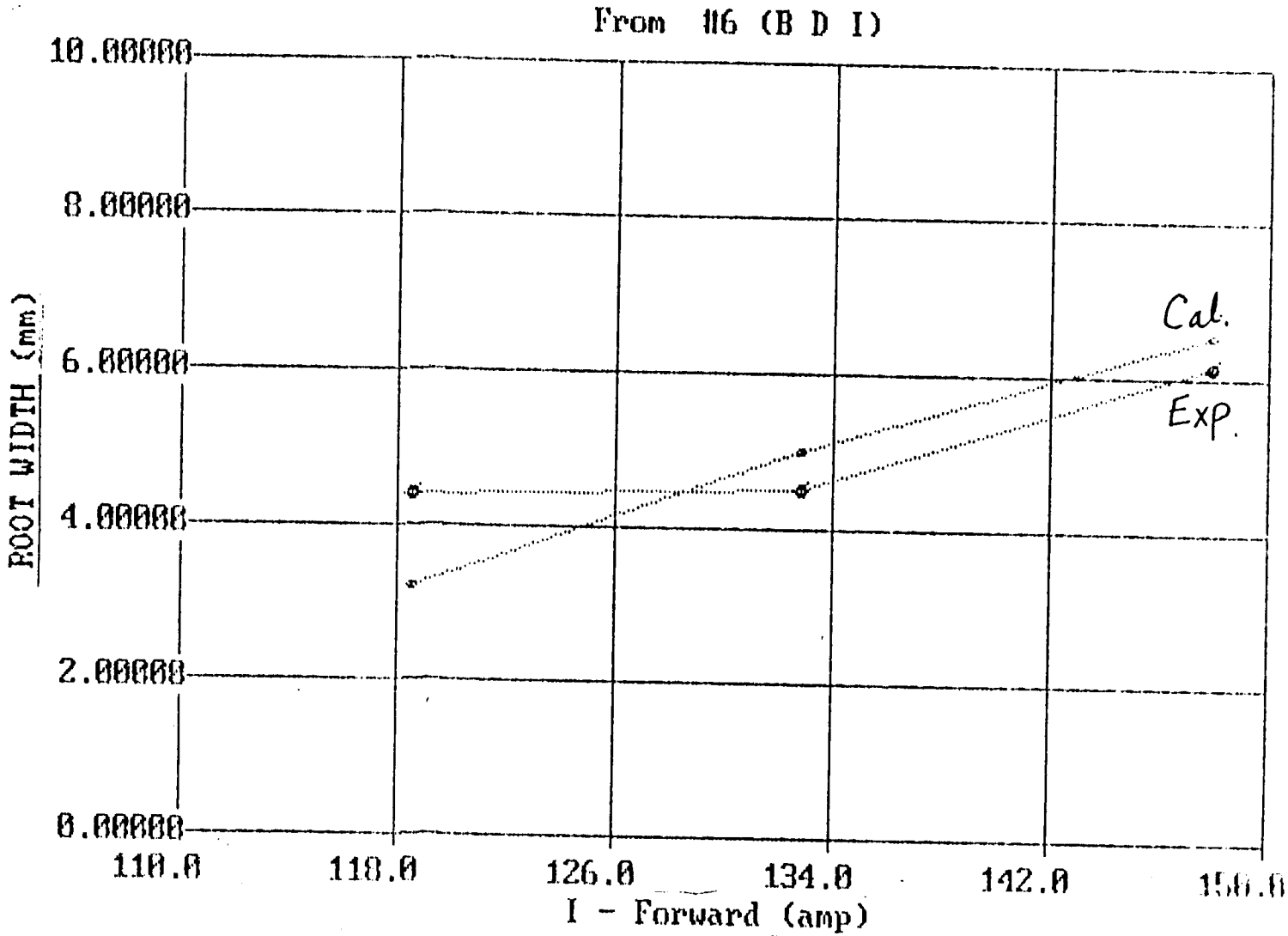
From 116 (B D I)
10.00000
8.00000
6.00000
4.00000
2.00000
0.00000
ROOT WIDTH (mm)
Cal.
Exp.
110.0
118.0
126.0
134.0
142.0
150.0
I - Forward (amp)

Fig. H-60

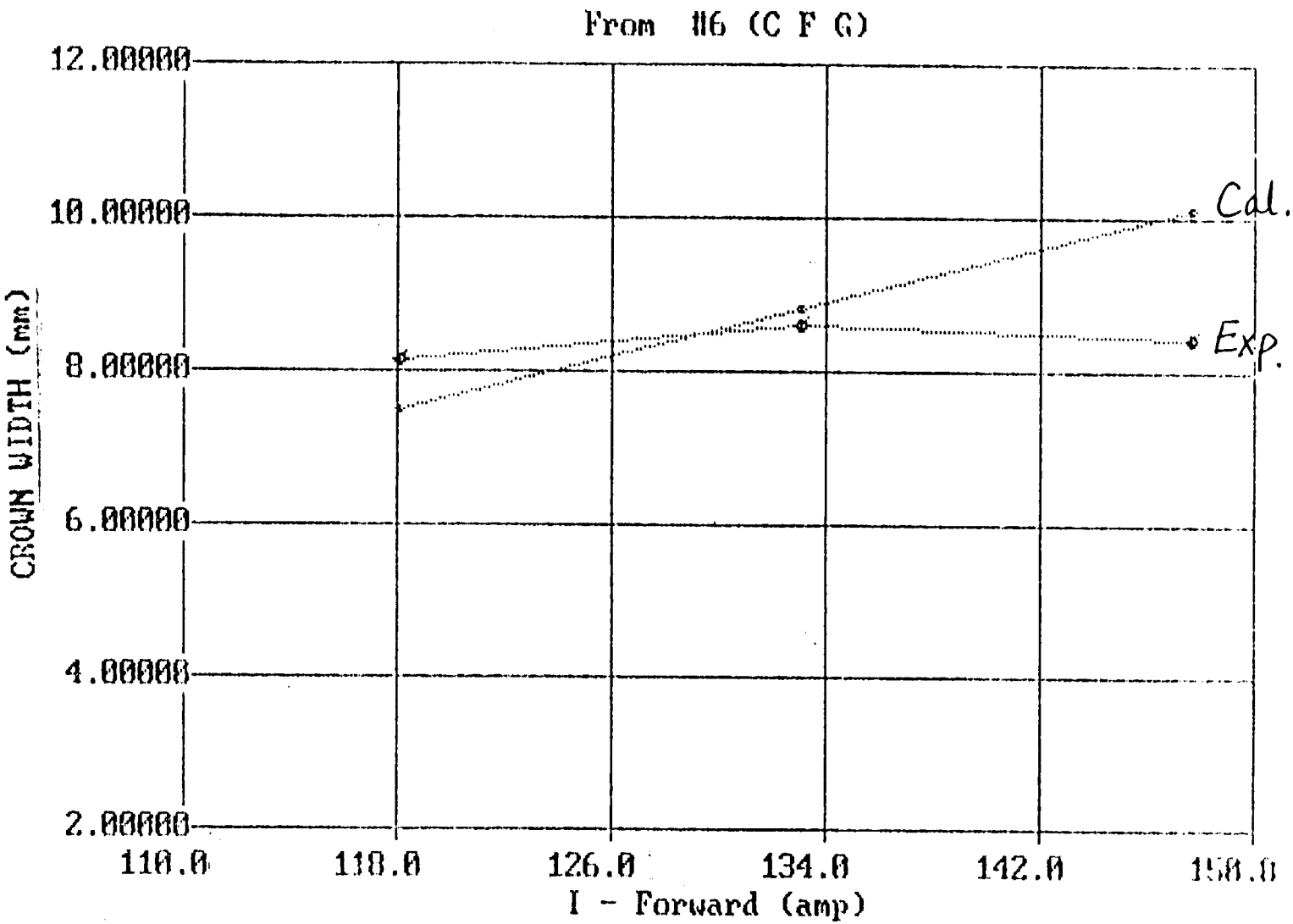
From 116 (C F G)
12.00000
10.00000
8.00000
6.00000
4.00000
2.00000
CROWN WIDTH (mm)
110.0
118.0
126.0
134.0
142.0
150.0
I - Forward (amp)
Cal.
Exp.

Fig. H-61

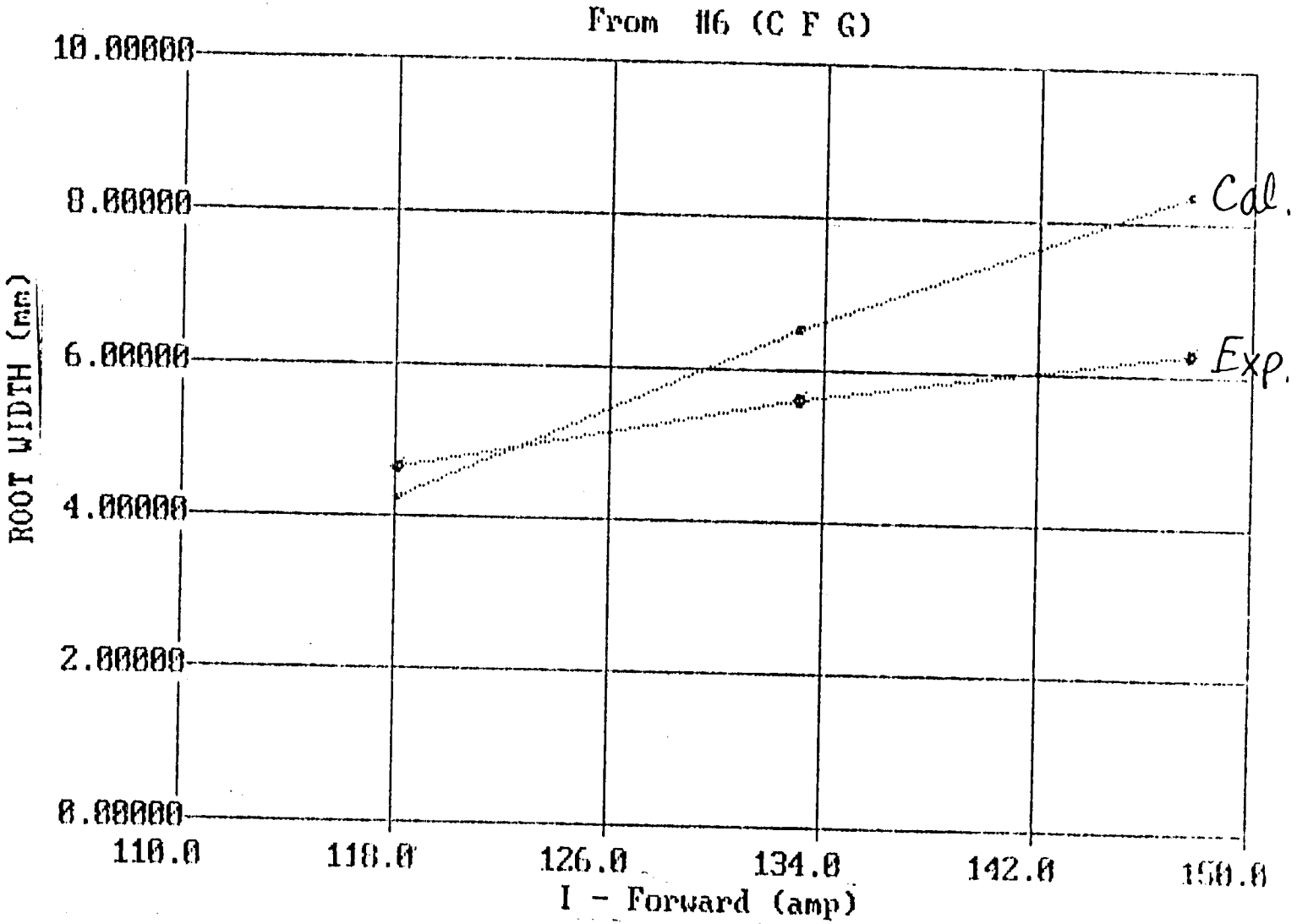
From 116 (C F G)
10.00000
8.00000
6.00000
4.00000
2.00000
0.00000
ROOT WIDTH (mm)
110.0
118.0
126.0
134.0
142.0
150.0
I - Forward (amp)
Cal.
Exp.

Fig. H-62

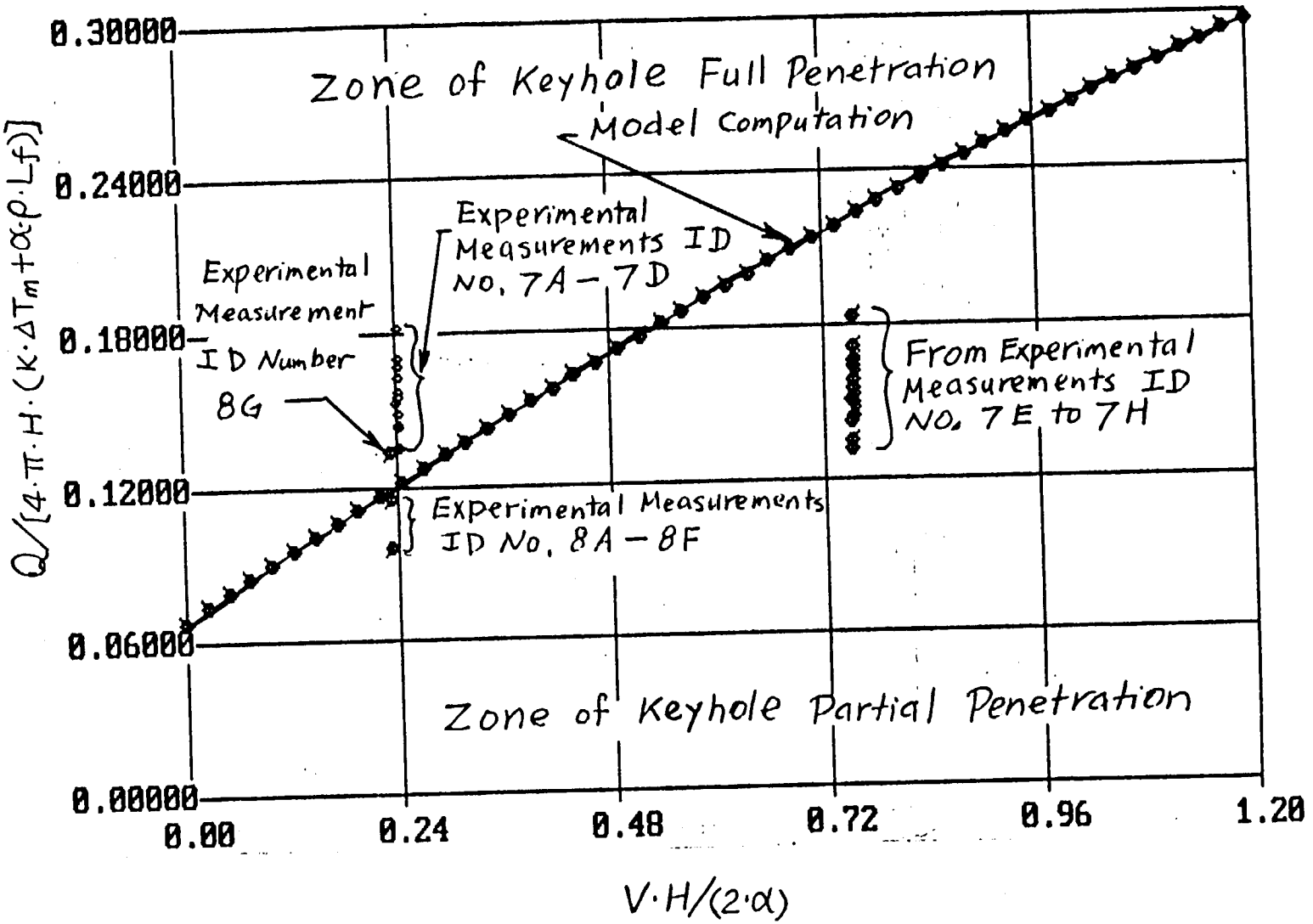
0.30000
0.24000
0.18000
0.12000
0.06000
0.00000
0.00
0.24
0.48
0.72
0.96
1.20
Q/[4·π·H·(K·ΔTm+α·ρ·Lf)]
V·H/(2·α)
Zone of Keyhole Full Penetration
Model Computation
Experimental Measurements ID No. 7A – 7D
Experimental Measurement ID Number 8G
From Experimental Measurements ID No. 7E to 7H
Experimental Measurements ID No. 8A – 8F
Zone of Keyhole Partial Penetration

Fig. H-63

NASA
National Aeronautical and Space Agency

Report Document Page

1. Report No.	2. Government Accession No.	3. Recipient's Catalog No.

4. Title and Subtitle

UAH Mathematical Model of the Variable Polarity Plasma Arc Welding System Calculation

5. Report Due

6. Performing Organization Code

University of Alabama in Huntsville

7. Author(s)

R. J. Hung

8. Performing Organization Report No.

10. Work Unit No.

9. Performing Organization Name and Address

University of Alabama in Huntsville
Huntsville, Alabama 35899

11. Contract or Grant No.

NAS8-38609 Delivery Order No. 34

12. Sponsoring Agency Name and Address

National Aeronautics and Space Administration
Washington, D.C. 20546-001
Marshall Space Flight Center, AL 35812

13. Type of report and Period covered

Final Report

14. Sponsoring Agency Code

15. Supplementary Notes

16.Abstract

Significant advantages of Variable Polarity Plasma Arc (VPPA) welding process include faster welding, fewer reparis, less joint preparation, reduced weldment distortion, and absence of porosity. In this report, a mathematical model is have been compared with the experimental obeservation accomplished by the GDI team.

17. Key Words (Suggested by Author(s))	18. Distribution Statement
Welding Process, Plasma Arc Welding, Variable Polarity Plasma Arc Welding, Space Fabrication	

19. Security Class. (of this report)	20. Security Class. (of this page)	21. No. of pages	22. Price
Unclassified	Unclassified		

NASA FORM 1626 OCT 86